THE UNIVERSITY
of EDINBURGH

The Role of Activation of Microglia in Neurodegenerative Prion Disease

James Vincenti

2014

THE UNIVERSITY *of* EDINBURGH

A thesis submitted in partial fulfilment of the requirements of The University of Edinburgh for the degree of Doctor of Philosophy (PhD.) by Research.

This programme of PhD. by research was funded by the Biotechnology and Biological Sciences Research Council and carried out in the Neurobiology Division, The Roslin Institute and R(D)SVS, The University of Edinburgh.

Declaration

I declare that this thesis has been completed entirely by myself and that the work presented herein is my own. All experiments were designed and carried out by myself, in collaboration with my supervisors. No part of this thesis has, or will be, submitted for any other degree, diploma or qualification.

James Vincenti. 2014

Acknowledgements

Supervisors

Dr. Enrico Cancellotti:	Primary Supervisor until 2012.
Prof. Tom Freeman:	Secondary Supervisor from 2013.
Prof. Jean Manson OBE:	Secondary then Primary Supervisor from 2012.
Prof. Stephen Bishop:	Temporary supervisor while Enrico was absent.
Dr Karen Brown:	Temporary supervisor while Enrico was absent.

Thesis Committee

Dr. Andreas Langling

Prof. Karen Horsburgh

I cannot thank my supervisors and committee members enough for their help, support, and perhaps above all, patience in guiding me through my PhD. It was an especially hard time for Enrico who became gravely ill and took the difficult decision to return home to Italy to convalesce. He was greatly missed by all within the division and I wish him all the best for the future.

Neurobiology Division

I wish to thank all those in my laboratory group and wider division. There really are too many to list but I was in constant receipt of kind advice and all important constructive criticism throughout my PhD.

Ark Genomics (now Edinburgh Genomics) & Roslin Genetics and Genomics Division

Mr Richard Talbot

Miss Chieko Kontaini

Miss Alison Downing

Mrs Karen Troup

Pathology Services (Vacuolation Scoring & Section Cutting)

Mrs Aileen Boyle

Mrs Gillian McGregor

Mrs Sandra Mack

Ms Dawn Drummond

BALBcJ$^{Fms\text{-}EGFP/-}$ Mice

Prof. David Hume

Dr Dave Sester

Dr Kristin Sauter

Mice Care & Inoculations (Wallace Annex)

Mrs Rebecca Hogan

Mr Kris Hogan

Special Mentions (Alphabetical Order)

Dr Debbie Brown:	For taking the time and trouble to teach me many of the techniques used in the laboratory.
Ms Jacque Brown:	Autism Scotland Mentor who helped me considerably in understanding social dynamics.
Miss Claire Davies:	For teaching me free-floating IHC and for being a great friend.
Dr David Donaldson:	For taking the time to listen to me and always offer friendly advice, especially on the subject of office politics.
Mr Bob Flemming:	For considerable help and advice with FACS & Bioimaging.
Mrs Dot Kisielewski:	For taking the time and trouble to teach me many of the techniques used in the laboratory.

Dr Barry McColl:	For advice on immunology and developing a reliable microglia RNA isolation technique.
Ms Lynesay McKay:	Flow Cytometry Key Account Manager at Miltenyi Biotec who personally trained me to use Miltenyi equipment and offered friendly advice on experimental set-up.
Dr Lita Murphy:	For taking me under her wing and offering invaluable help and support with my data analysis.
Mrs Kathleen Renault:	For helping me develop a reliable microglia RNA isolation technique and for being a great friend.
Mrs Kathy Smith:	My specific learning difficulties advisor without who I simply would not have completed my PhD.

Family

The unconditional love and support of my parents is immeasurable and needless to say I would never have reached this stage in life, let alone my PhD, without their care. I also wish to thank Miss Rachael Blenkinsop, without her support I would never have finished further education or this PhD.

Abbreviations

Note: Mouse gene nomenclature shown below in describing transcript abbreviation e.g. *Inf-γ*. The mouse protein nomenclature (INF-γ) or human gene nomenclature (*INF-γ*) should be regarded as interchangeable for the purposes of referencing the full name when using this table.

APC	Allophycocyanin
BSA	Bovine serum albumen
CCR	CC-chemokine receptor
CD	Cluster of Differentiation
CNS	Central nervous system
Csf-1	Colony stimulating factor-1
ddH_2O	Double distilled H_2O
DMEM	Dulbecco's modified eagle medium
DNA	Deoxynucleic acid
EGFP	Enhanced Green Fluorescent Protein
FACS	Fluorescence-activated cell sorting
Gfap	Glial fibrillary acidic protein
GO	Gene Ontology
HBSS	Hanks balanced salt solution
i.c.	Intracerebral (injection route)
i.p.	Intraperitoneal (injection route)
IL	Interleukin
Inf-g	Interferon gamma
LPS	Lipopolysaccharide
Ly6C	Lymphocyte antigen 6 complex
MHC	Major histocompatibility complex
MPTP	1-Methyl-4- Phenyl-1,2,3,6-Tetrahydropyridine
mRNA	Messenger Ribonucleic acid

NfkB	Nuclear factor of kappa light polypeptide gene enhancer in B cells
OCT	Optimum cutting temperature (freezing compound)
PE	Phycoerythrin
QUIN	Quinolinic acid
RIN	Ribonucleic acid integrity value (Agilent unit of quality)
RNA	Ribonucleic acid
SAM	Significance analysis of microarrays
Spi1	Spleen proviral integration oncogene
Tgfb1	Transforming growth factor *beta-1*
TLR	Toll-like receptor
Tnf-a	Tumour necrosis factor-alpha
w/v	Weight per volume

Thesis Abstract

Prion diseases are a group of fatal neurodegenerative protein-misfolding diseases. Microglia, the resident myeloid cells found within the brain, have been shown to demonstrate a reactive morphology during the disease process with conflicting evidence for both a neurotoxic and neuroprotective role. The studies presented here aimed to investigate the role of microglia activation using transcriptomic and morphological analysis of prion disease in mice.

Initially, the host immune response to prion disease was explored using a publically available mouse prion disease dataset. Re-analysis of this dataset was performed using BioLayout *Express*^{3D}; a novel software tool that supports the visualisation and clustering of correlation networks. Disease-associated genes up-regulated during the later stages of infection were present in two main clusters. The cellular origin of these genes was explored by examining their expression in a dataset comprised of pure populations of cells. This demonstrated that the primary cluster of up-regulated transcripts encompassed genes expressed mainly by microglia and to a lesser extent astrocytes and neurons. The secondary cluster comprised almost exclusively of interferon response genes. The conclusions of these analyses were different from those of the original study that suggested disease-associated genes were primarily neuronal in origin.

Mouse models of prion disease were established by infecting a novel line of BALB/cJ inbred mice, expressing EGFP under control of a myeloid specific *Csf1r* promoter, with the 79A prion strain. Quantification of the morphological changes of EGFP expressing microglia suggested the cells accumulated in the medulla at sites of early misfolded protein deposition with minimal change in their overall appearance. An activated microglia morphology was not observed until protein deposition was extensive. Isolation of EGFP expressing microglia was performed for transcriptome analysis. The vast majority of disease associated genes demonstrated increased expression at the onset of clinical symptoms. The gene list was found to be highly enriched for genes

associated with an innate immune response regulated by the NFκB signalling cascade. Also highly enriched were processes associated with protein translation, energy production and stress response. These data suggest a high metabolic load is burdened by proliferating microglia; and as part of a response which is strikingly more pro-inflammatory in nature than has previously been attributed to the microglia phenotype within prion disease.

As an active contributor to normal homeostasis, microglia are more than just innate immune surveillance and are now considered an integral component in both the healthy and diseased brain. The ramifications of activation toward the microglia phenotype shown here will have direct and potentially cytotoxic influence on neighbouring microglia and other brain cell types implying microglia as major contributors to the neurotoxic environment found within the CNS during prion disease. Furthermore the identification of genes associated with metabolism offer many intriguing possibilities for manipulating the activity of microglia in pre-clinical therapeutic intervention.

Thesis Table of Contents

Thesis Figures, Tables and Appendices

1 Introduction

1.1 Prion Disease

1.1.1 Protein-Misfolding Diseases

A neurodegenerative disease, as the name implies, demonstrates a loss of neuronal cells and eventual loss of brain function. Neuronal loss can prove fatal; presumably as the capacity for maintaining normal bodily homeostasis crosses a threshold which cannot be reversed. Other important hallmarks of a number of neurodegenerative diseases include accumulation of misfolded protein as intracellular tangles and extracellular plaques. Such is the degree of protein accumulation that the illnesses are often classed as protein-misfolding diseases. Prion diseases are a group of invariably fatal protein-misfolding neurodegenerative diseases which, uniquely, are transmissible between hosts (Pattison *et al.*, 1959, Zlotnik and Rennie, 1962, Zlotnik and Rennie, 1965, Brotherston *et al.*, 1968). The diseases can be found in numerous mammalian species including Creutzfeldt-Jakob Disease in humans, Bovine Spongiform Encephalopathy in cattle, Chronic Wasting Disease in deer and Scrapie in sheep and goats (Table 1-1).

1.1.2 Natural and Experimental Hosts

The earliest recording of a prion disease in the United kingdom under the name 'Scrapie', a name that continues to this day, was attributed to a flock of cross-bred Cheviot and Leicester sheep in a farm near Yetholm within the Scottish Borders in 1853 (Stockman, 1913). The disease had been known, albeit often incorrectly categorised, under different names for many centuries (Appendix 8-1). The more recent widespread epidemic of Bovine Spongiform Encephalopathy in cattle was first detected in 1987 by Wells *et al.* (1987). Infected animals presented with abnormal behaviour, exhibited hypersensitive anxiety, progressive ataxia and resulted in the death of over 100,000 cattle. Bovine Spongiform Encephalopathy was confirmed to have infected humans, presenting as New-Variant Creutzfeldt-Jakob Disease using

experimental mouse models where both human and cattle forms presented with the same pathology in mice (Bruce *et al.*, 1994, Bruce *et al.*, 1997). Interestingly the first identified bovine case was in a zoological Nyala (*Trugeluphus ungasi*), an African ruminant belonging to the sub-family *bovinae* of the family *Bovidae* in a wildlife park (Jeffrey and Wells, 1988). This case was followed a year later by the infection, in the same wildlife park, of a Gemsbok antelope (*Oryx guzellu*), again a member of the *Bovidae* family, and crucially there was no contact between the two animals. The origin of the disease was presumed to be ingestion of 'meat and bone meal' animal feed produced from infected animals (Wilesmith *et al.*, 1988, Wilesmith *et al.*, 1991). Widespread ban of this type of feed coincided with the reduction in new cases.

Other prion diseases have been shown to be directly infectious, including Chronic Wasting Disease and Scrapie, with little evidence to determine the source of infection. Scrapie was shown to be infectious between sheep following carefully controlled trials in the 1940s (Gordon *et al.*, 1940, Greig, 1940). Under experimental conditions Scrapie was revealed to be transmissible from sheep to goats (Chelle, 1942, Pattison *et al.*, 1959, Pattison and Millson, 1961, Brotherston *et al.*, 1968). There has never been a case of human infection by Scrapie although there is some tentative evidence that non-human primates are susceptible following oral ingestion of Scrapie infected hamster or mouse brain (Gibbs and Gajdusek, 1972, Gibbs *et al.*, 1980). Chronic Wasting Disease is highly contagious within cervid populations (Miller *et al.*, 2004). The disease was identified as a prion disease in 1980 (Williams and Young, 1980) and is widespread in both free-ranging and captive cervid populations in North America. The contact between humans and both wild and captive cervid populations is frequent, particularly within the hunting fraternity, yet the natural host of Chronic Wasting Disease has remained within cervids with no reported natural transmission to other mammals. The inability of prion diseases to easily adapt to another species is termed the species barrier. The barrier presents as both the failure to infect another species by a natural (oral) route, (Figure 1-1) or if infection does

transmit there is evidence of adaptation through the shorter incubation periods of subsequent passages (Bruce *et al.*, 1994).

Table 1-1: Prion diseases found in mammalian species and the causes currently agreed upon by general consensus.

Disease	Species	Cause
Scrapie	Sheep, Goats	Maternal and horizontal transmission of infection.
Bovine Spongiform Encephalopathy (BSE)	Cattle	Ingestion of infected 'meat and bone meal' in animal feed
Chronic Wasting Disease (CWD)	Deer, Elk, Moose	Unknown. Suspected to be horizontal transmission
Transmissible Mink Encephalopathy (TME)	Mink	Unknown. Suspected to be ingestion of infected 'meat and bone meal' in animal feed
Feline Spongiform Encephalopathy	Domestic and captive zoological cats	Ingestion of (Bovine Spongiform encephalopathy) infected meat
Sporadic Creutzfeldt-Jacob Disease (sCJD)	Human	Unknown. Suspected de-novo generation of misfolded protein
Familial Creutzfeldt-Jacob Disease (fCJD)	Human	Germline mutation within the *PRNP* gene
Iatrogenic Creutzfeldt-Jacob Disease (iCJD)	Human	Exposure to (Creutzfeldt-Jacob Disease) contaminated surgical equipment and tissue grafts.
Variant Creutzfeldt-Jacob Disease (vCJD)	Human	Ingestion of (Bovine Spongiform encephalopathy) infected meat
Kuru	Human	Ritual cannibalism of infected meat
Gerstmann-Straussler-Scheinker Syndrome	Human	Germline mutation within the *PRNP* gene
Fatal Familial Insomnia	Human	Germline mutation within the *PRNP* gene
Atypical Scrapie	Sheep	Unknown. Suspected to be genotypes associated with resistance to classical Scrapie
Bovine "Amyloidotic" Spongiform Encephalopathy (BASE or Atypical BSE)	Cattle	Unknown. Suspected de-novo generation of misfolded protein.
Exotic Ungulate Encephalopathy (EUE)	Nyala and greater kudu	Ingestion of infected 'meat and bone meal' in animal feed.

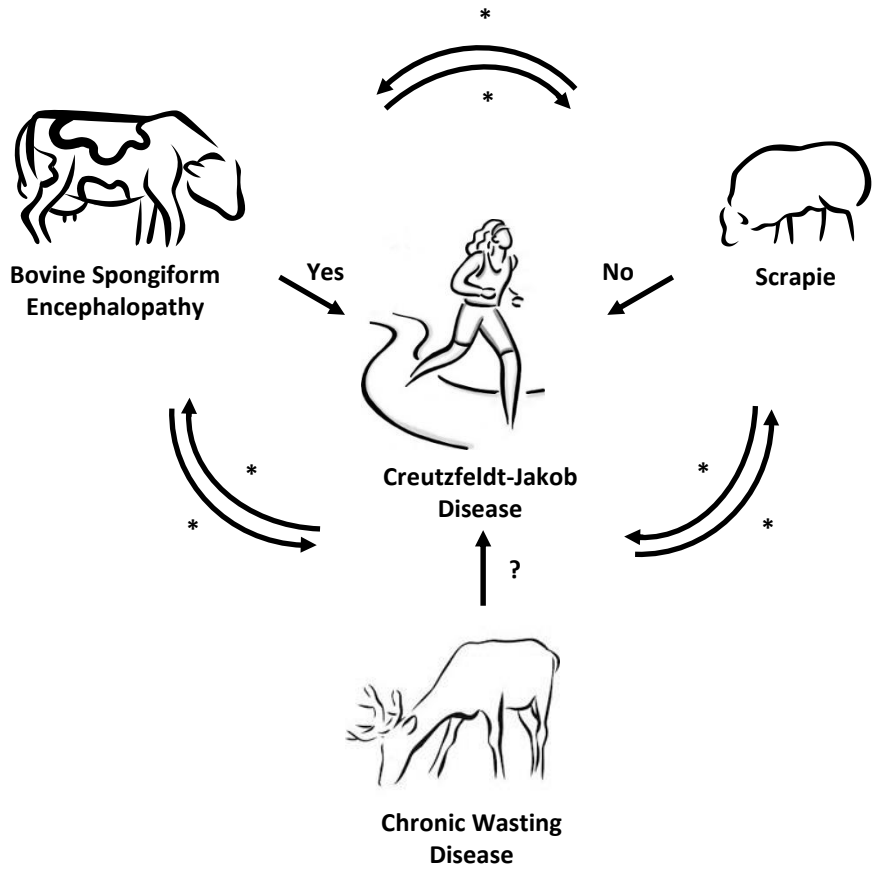

Figure 1-1: Species barriers to natural (oral) routes of infection. Bovine spongiform encephalopathy is orally transmissible to humans and presents as Variant Creutzfeldt-Jakob Disease. Despite the long term presence of sheep Scrapie in commercial flocks, and the prevalence of human contact with cervids suffering from Chronic Wasting Disease, there has been no evidence for transmission of these diseases to humans.

*: Under laboratory conditions, using an artificial intracerebral route, transmission is possible (Raymond *et al.*, 2000, Hamir *et al.*, 2004, Concepcion *et al.*, 2005, Hamir *et al.*, 2005, Kong *et al.*, 2005, Hamir *et al.*, 2006, Hamir *et al.*, 2007, Dagleish *et al.*, 2008, Greenlee *et al.*, 2011, Greenlee *et al.*, 2012, Konold *et al.*, 2013).

1.1.3 The Infectious Agent

The infectious agent for prion disease was initially proposed to be a 'slow virus' (Cho and Greig, 1975, Cho, 1976), a term first utilised in describing Maedi-visna infection of sheep by the Icelandic physician Dr Bjorn Sigurdsson (Sigurdsson *et al.*, 1957, Sigurdsson and Palsson, 1958). The considerably long incubation period and, following evidence gained from serial passage in both sheep and mice, the clearly replicating nature of the agent lent the disease well to the slow virus concept. Attempts to isolate the infectious agent, and more importantly associated nucleic acids, proved difficult (Alper *et al.*, 1967). Attempts to isolate nucleic acids using caesium chloride resulted in considerable loss of infectivity in the nucleic acid fraction (Mould *et al.*, 1965, Adams *et al.*, 1969). However investigations into the size of the infectious agent revealed that at only 150 Kilo Daltons (KDa) the agent was in the realm of a viroid (Alper *et al.*, 1966). Considering the complex nature of the disease (it would require more than a few nucleobases) and that the agent was resistant to nucleic acid-damaging levels of ultraviolet radiation (Alper *et al.*, 1967), the presence of nucleic acids in the agent was questioned. Ultimately it was evidence that the application of ultraviolet light revealed a transparency to nucleic acid blocking wavelengths (Latarjet *et al.*, 1970) that seriously challenged a viral origin for the agent. Further experiments revealed tentative evidence to suggest a link between the agent and plasma membrane (Hunter *et al.*, 1971, Millson *et al.*, 1971). The removal of nucleic acids from infected plasma membrane preparations did not result in loss of infectivity (Kimberlin *et al.*, 1971a).

As part of efforts to separate the infectious agent from membrane preparations it was noted that treatment of preparations with proteases, denaturing detergents and lowered pH dramatically reduced infectivity (Hunter and Millson, 1967, Hunter *et al.*, 1969, Kimberlin *et al.*, 1971a). This lead to suggestions that the coding and replication nature of the agent might be contained within basic (Pattison and Jones, 1967) or glycoproteins (Gibbons and Hunter, 1967, Lewin, 1972) with strong arguments for an endogenous and erroneously folded protein put forward that

would explain both the spontaneous and transmissible nature of the agent (Griffith, 1967). In the early 1980s it was noted in the lab of Stanley Pruisner (NIH San Francisco) that infectivity titre correlated with a partially protease resistant protein of 27-30 KDa in size when migrated on a sodium dodecyl sulphate polyacrylamide gel (Bolton *et al.*, 1982). This work was immortalised in 1982 when published as the Proteinaceous Infectious agent, abbreviated to Prion (Prusiner, 1982). The structural protein component of the infectious fraction was later designated as the Prion Protein or PrP (McKinley *et al.*, 1983). The hypothesis proposed by Griffith (1967) was for a host origin for the replicative agent. A cellular gene was found to encode the PrP 27-30 kDa protein (Oesch *et al.*, 1985) with the complete PrP gene (*Prnp*) identified shortly after (Basler *et al.*, 1986, Sparkes *et al.*, 1986). Further evidence implicating PrP as the replicative agent was that *Prnp* knockout mice were shown to be resistant to infection (Büeler *et al.*, 1993).

Stanley Prusiner was later awarded the 1997 Nobel Prize in Physiology, or Medicine, for coining the prion hypothesis which states that endogenous host PrP^{C} sialoglycoprotein refolds from the normal and predominantly α-helical form (Baldwin *et al.*, 1994) to a β-pleated sheet containing form (PrP^{Sc}) which is also the disease causing agent. The conversion is mediated by the presence of PrP^{Sc} acting as a template (Nguyen *et al.*, 1995b). Gradually more of the cellular PrP^{C} is requisitioned and changed into the abnormal isoform which accumulates within the brain as deposits. Evidence for the template mediated conversion was shown within cell-free *in-vitro* conversion assays (Kocisko *et al.*, 1994, Saborio *et al.*, 2001). To encompass the many different strains of disease, considered to be a confounding factor for a protein-only agent, it was proposed that although the primary sequence of PrP^{Sc} was identical the protein could exhibit many different biologically active conformations (Stahl *et al.*, 1993, Prusiner, 1998, Tremblay *et al.*, 2004). A comparable system of prion protein-only mediation of phenotypic properties was also shown to exist within both experimental and wild yeast strains within the laboratory of Susan Lindquist (Patino *et al.*, 1996, True and Lindquist, 2000, Halfmann *et al.*, 2012). The generation

of purified recombinant mis-folded prion protein provided further evidence for the strain encoding properties of a self-replicating infectious protein that could induce a strain-specific disease within mice (Legname *et al.*, 2004, Legname *et al.*, 2005, Wang *et al.*, 2010). The specificity of template refolding was demonstrated used purified synthetic protease sensitive PrP^{Sc} at the first passage and then harvested prions for the second passage (Colby *et al.*, 2010). Both passages induced neurodegeneration and yielded solely protease sensitive PrP^{Sc}. The absolute requirement for a template 'seed' of PrP^{Sc} to initiate misfolding of a batch of PrP^{C} further supported the specificity of template misfolding (Cosseddu *et al.*, 2011).

Opponents to the non-Mendelian theory of inheritance that the prion only hypothesis would imply proposed the Virino hypothesis. Whereby a small quantity of nucleic acid or additional cellular co-factors were contained within and protected by the prion protein isomer (Dickinson and Outram, 1988). Attempts to counter the Virino hypothesis, and confirm a protein-only agent, led to experiments generating recombinant PrP^{Sc} with a complete absence of cellular co-factors, even going so far as to ensure the procedures were carried out in a laboratory that had seen no prior use of prion protein. The subsequent passaging in mice revealed the lack of obligatory requirement for any additional co-factors to generate a robust, albeit lengthy, prion disease (Kim *et al.*, 2010, Makarava *et al.*, 2010, Wang *et al.*, 2012). The requirement for co-factors has not been fully laid to rest with *in-vivo* experiments demonstrating the enhanced re-folding and accelerated disease properties in the presence of RNA and lipid co-factors (Deleault *et al.*, 2007, Timmes *et al.*, 2013).

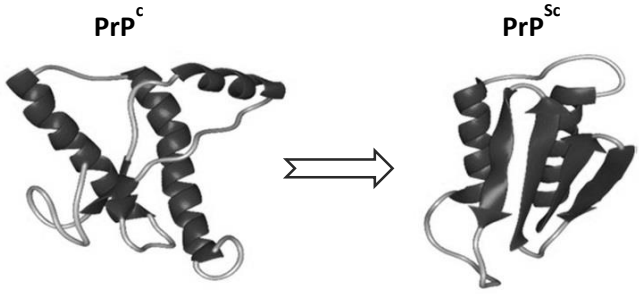

Figure 1-2: The prion hypothesis postulates the template folding of PrP^{C} into the misfolded, partially protease resistant, and disease-information (coding) containing PrP^{Sc} isoform.

The connection of the *Prnp* gene with the prion protein was not the first time the gene had been associated with prion disease. The gene was first identified in mice as important for controlling the incubation length of experimental Scrapie and was named the Scrapie Incubation (*Sinc*) gene (Dickinson and Mackay, 1964, Dickinson *et al.*, 1968). Two alleles; $Sinc^{s7}$ and $Sinc^{p7}$ were identified in mice which depending upon the encoded genotype resulted in a short or long incubation period respectively. Such was the control of the alleles that a combined infection of two very different Scrapie strains into groups of mice with different alleles would result in a reversal of which prion strain dominated the disease pathogenesis (Dickinson and Meikle, 1971). Later work confirmed *Sinc* and *PrnP* were the same gene (Moore *et al.*, 1998) but with *PrnP* already prevalent in the literature the original work by Dickinson has unfortunately been overshadowed and $Sinc^{s7}$ and $Sinc^{p7}$ remain known as $PrnP^{a}$ and $Prnp^{b}$.

The genotype of *Prnp* forms part of the species barrier affect with evidence for homophilic preference between the PrP^{Sc} containing inoculum and the host PrP^{C} (Scott *et al.,* Race *et al.*, 1995). In addition to inhibiting infection across species, the genotype of *Prnp* also imparts on the susceptibility of infection within a species and

is exemplified by the impact of sheep genotype on the susceptibility to Scrapie (Hunter *et al.*, 1997a, Hunter *et al.*, 1997b, Dawson *et al.*, 1998). Such was the impact that attempts to control Scrapie through selective breeding of resistant genotypes were conducted in 2001 through the National Scrapie Plan of Great Britain implemented by the Department for Environment, Food & Rural Affairs.

Other than a strong association with plasma membrane though a glycosyl phosphatidylinositol anchor (Naslavsky *et al.*, 1997, Agostini *et al.*, 2013), the actual role of *Prnp* and the encoded protein PrP^{C} remains unknown with normal neonatal development and no apparent anatomical alteration occurring if the gene is knocked out (Büeler *et al.*, 1993, Manson *et al.*, 1994a). At the cellular level the number of mitochondria is reduced (Miele *et al.*, 2002) linking the association of the protein with the cellular response to oxidative stress (Brown *et al.*, 1999a). Neuronal circuits are altered (Collinge *et al.*, 1994, Colling *et al.*, 1997) and behavioural changes are also apparent with impairment to circadian sleep patterns (Tobler *et al.*, 1996).

1.1.4 Prion Strains

It is known that interaction between the strain and host *Prnp* genotype (Bruce *et al.*, 1991, Carlson *et al.*, 1994) glycosylation status (Kascsak *et al.*, 1985, DeArmond *et al.*, 1994, DeArmond *et al.*, 1997, Somerville *et al.*, 1997, Cancellotti *et al.*, 2010), availability of host PrP (Manson *et al.*, 1994b) and protease sensitivity of the misfolded isomer (Safar *et al.*, 1998) all influence disease pathology and susceptibility. Disease phenotype can be further compounded by the ability to have an infection by more than one prion strain, first shown with competition between the 22C and 22A strains (Dickinson *et al.*, 1972).

An infectious isolate is only considered a pure strain when the outcome is a stable and unique disease. The stability of prion strains is such that even when a species barrier is crossed, the adapted form of the disease will present with a potentially new but nonetheless unique and consistent pathology (Pattison, 1966, Sisó *et al.*, 2012).

This is only possible once a strain is highly purified following successive mouse infections using low titre (cloned). That said, it is still possible for some strains to be separated further using a highly selective host environment (Mahal *et al.*, 2010). This implies these strains remain a heterogeneous conglomerate of multiple prion agents and is a topic classed under the 'quazi-species' affect, a term first conceived by the German biophysicist and Nobel Prize in Chemistry winner Manfred Eigen (Eigen and Schuster, 1977) and associated with prion strains by Weissmann *et al.* (2011).

Natural Scrapie is readily transmissible into laboratory mice and isolation of Scrapie infected material from serially passaged mice of different genetic backgrounds has yielded a number of murine-adapted experimental Scrapie isolates. These isolates demonstrate variation in the magnitude and localisation of vacuolation, mis-folded protein deposition and marked differences in the length of the incubation period (Bruce, 2003).

1.1.5 Effect of Host Age

Infected neonatal mice were shown to either survive or demonstrate a significantly longer incubation period than the equivalent titre in postnatal mouse pups (Outram *et al.*, 1973). Prion disease infection was shown to first replicate in lymphoid tissue (Eklund *et al.*, 1967) and the incomplete development of this tissue in neonatal mice hindered successful infection. Replication within lymph tissue was later shown to specifically require the scavenging uptake and replication of infectious material by mesenchymal follicular dendritic cells (Fraser *et al.*, 1996, Brown *et al.*, 1999b). When mice reach over 400 days old at the point of injection there is once again a noticeable impact on disease infection. As part of the healthy aging process the loss of the splenic margin zones and the corresponding reduction in follicular dendritic cell uptake has a marked influence on whether the disease reaches clinical stage or remains sub-clinical (Brown *et al.*, 2009, Brown *et al.*, 2011).

1.1.6 Effect of Route of Infection

The speed of infectious uptake into the central nervous system is determined in the main by the concentration of available infectious material. Following injection, and regardless of route, dissemination of infectious material rapidly occurs to tissues throughout the body (Millson *et al.*, 1979) with a higher rate of loss in titre observed with an intraperitoneal route than an intracerebral route (Kimberlin and Walker, 1978). Accordingly the infectivity titre of an inoculum is lower when using a peripheral route. This is further compounded by the complexity of the peripheral mechanisms of replication in the lymphoid tissues (Kimberlin and Walker, 1979, Brown *et al.*, 2009, Brown *et al.*, 2011). Thus use of an intracerebral route, effectively flooding the brain with a considerable quantity of infectious material, produces a much shorter overall disease incubation period.

However the increase in incubation period in a peripheral route is not simply due to a lower titre of available infectious material. The neural phases of replication, classed as the time from first detection of protein deposition in the central nervous system to clinical onset, is actually quicker in a peripheral route (Kimberlin and Walker, 1986, Langevin *et al.*, 2011); conclusions born from the examination of many thousands of infected mice. This almost counterintuitive situation is rationalised when it is considered that prion disease pathogenesis in the brain is restricted to certain neuroanatomical pathways (Fraser and Dickinson, 1968, Kimberlin and Walker, 1980, Kimberlin *et al.*, 1983, Scott *et al.*, 1992). This can be observed in detail following an intraspinal route of infection where the requirements for extra-neuronal replication are bypassed, yet still requiring entry into the brain along nerve pathways. The neural phase of replication is initiated from the outset, thereby reducing the time required for replication phase in the brain, resulting in the shortest incubation period of all the possible routes of infection (Kimberlin *et al.*, 1987).

The restriction of disease pathogenesis to neuroanatomical pathways means the regional distribution of lesions and PrP deposition specific to a strain/host

combination is typically conserved regardless of route of inoculation (Kimberlin *et al.*, 1971b, Kimberlin and Walker, 1980). This is fortuitous as the disruption of the blood brain barrier in an intracerebral injection (Millson *et al.*, 1979) initiates both an intracerebral and an systemic infection simultaneously. The latter, due to the time required for movement into the central nervous system, lags significantly behind the pathogenesis already taking place in the brain yet both end up with the same, overlapping, pattern of misfolded protein deposition.

1.1.7 Effect of Host Gender

The impact of gender on experimental mouse-adapted prion disease pathogenesis is restricted to differences in incubation period. Very large collections of data performed in a wide variety of mouse strains from inoculations spanning decades show that there is a small increase in the incubation period in male mice (Kimberlin, 1976, Kimberlin and Walker, 1978, McLean and Bostock, 2000). The differences were not always statistically significant and in most cases the difference was only a few days. No gender differences have been observed with regional targeting and severity of lesions, misfolded protein deposition, neuronal loss and levels of endogenous PrP^C expression (Akhtar *et al.*, 2011). Interestingly the gender difference in incubation period is most pronounced following a peripheral route. The increase in body size of male mice, and resulting reduction in the infectious titre already exaggerated by further loss with a peripheral route, is therefore a possible explanation. There has also been tentative evidence to suggest that androgens influence incubation period in male mice following experiments in castrated mice (Loeuillet *et al.*, 2010). Within the healthy mouse brain the number of microglia are observed to be approximately 20% less in male mice than females (Mouton *et al.*, 2002), with female sex steroids shown to be marked inhibitors of microglia activation (Drew and Chavis, 2000, Saravia *et al.*, 2007). Castration is also known to affect the peripheral immune function of male mice by inducing a reduction in mature peripheral T cells and alterations to basal splenic B cell activation (Viselli *et al.*, 1995). The gender differences in incubation period seen by Loeuillet *et al.* (2010) were confined to a peripheral route;

Therefore requiring a fully functioning peripheral immune system. The impact on lymphoid tissue function, and more specifically the uptake of infectious Scrapie agent, following castration has yet to be investigated.

1.1.8 Defining the events in protein misfolding diseases

The highly reproducible characteristics of mouse-adapted Scrapie strains make them an ideal model for studying neurodegenerative disease. The neuronal loss, build-up of a misfolded host protein and, most importantly, the invariably fatal outcome match that observed in human neurodegenerative diseases.

The association with a misfolded protein is similar in many respects to other neurodegenerative diseases including Alzheimer's Disease (DeArmond, 1993) and there has been considerable effort in recent years to further investigate the amyloidal properties of the misfolded proteins found in other neurodegenerative diseases. The overriding consensus is that initiation of misfolding from very small initial quantities; termed 'seeding', and the spread of misfolded protein from cell to cell within the host demonstrate overlapping properties to prion protein propagation (Bolmont *et al.*, 2007, Desplats *et al.*, 2009, Stohr *et al.*, 2012, Duran-Aniotz *et al.*, 2013, Guo and Lee, 2013, Dujardin *et al.*, 2014). There is no evidence to suggest the other non-prion protein diseases are transmissible from host to host but there has been work to suggest isolates of amyloid from other protein misfolding diseases demonstrate distinct pathogenic properties that could be described as prion-like strains (Kayed *et al.*, 2010, Guo *et al.*, 2013, Gath *et al.*, 2014, Pinotsi *et al.*, 2014, Stohr *et al.*, 2014, Watts *et al.*, 2014).

Of particular relevance to this project is that many of the human neurodegenerative diseases including Alzheimer's Disease, Parkinson's Disease and Creutzfeldt-Jakob Disease demonstrate activation of microglia (McGeer *et al.*, 1993, Guiroy *et al.*, 1994, Eitzen *et al.*, 1998, McGeer and McGeer, 1999, McGeer and McGeer, 2008, Abutbul *et al.*, 2012), a pathological feature also replicated in experimental mouse-adapted

prion disease (Williams *et al.*, 1994). The injection of infectious prion material into a wild type mouse ensures the exact starting point of the disease is identified. Considering the proteinaceous seeding potential of many neurodegenerative misfolded host proteins, the exact determination of the start, of what would otherwise be a de-novo occurrence, is an advantage unique to prion disease (Jucker and Walker, 2013). The middle and end stages are then clearly defined allowing for the time course of events during disease pathogenesis to be documented in chronological order. Uninfected mice, kept separate from prion infected mice, do not develop disease and provide healthy control animals in which there is only one experimental variable to consider. Conversely the use of complex transgenic manipulation required to develop other neurodegeneration diseases in mice, including Alzheimer's Disease, creates many variables and an uncertain disease starting point.

1.2 Microglia

Whilst the neuron has been subject to the majority of research into protein misfolding diseases, other cells such as microglia have also been suggested as important players by demonstrating microgliosis throughout the infectious process (Williams *et al.*, 1994). Microglia are distributed fairly evenly, with a slight bias of location in the grey matter, and at an estimated 3.5 $x10^6$ cells comprise approximately 10% of all cells found in the adult mouse brain (Lawson *et al.*, 1990). Unique to the central nervous system, microglia are of haematopoietic stem cell origin and, as will be discussed in this chapter, form an intrinsic part of the multicellular central nervous system far beyond merely operating as the principal resident innate immune cell.

1.2.1 Origin of Microglia

Microglia were recognised as a visually distinct type of neuroglia with rod-shaped nuclei almost simultaneously by Robertson (1900) and Nissl (1899) using platinum deposition and basic dyes respectively. Prior to this, the blanket term 'neuroglia' was given to all non-nerve interstitial cells within the brain (Virchow, 1846, Virchow, 1858). In particular it was noted by Dr Fraz Nissl that his newly discovered "Stäbchenzellen" or 'Rod-cells' had the ability to scavenge dying neurons during trauma. The action of phagocytosis by rod-cells, and their acknowledgement as a separate type of neuroglia, was not widely accepted with many leading neurologists of the time attributing the observations to an unfamiliarity with the nervous system (Cerletti, 1902, Cerletti, 1903, Cerletti, 1905, Noda, 1921). It was not until the studies by Penfield (1925) on diseased brains, inflicted with glioma, was the phagocytic activity found to be restricted to the rod shaped cells, arresting all doubt that this cellular activity took place within the brain. The debate on how neuroglia were to be characterised was finally concluded in the 1930's following the pioneering work by Pio del Río-Hortaga in which the three glia cell types were identified; and continue to

be known as microglia, astrocytes and oligodendrocytes (Río-Hortega, 1920, Río-Hortega, 1921, Rio-Hortega, 1932).

Microglia progenitors were initially proposed to be present in both the embryonic and adult mouse brain following identification of a highly prolific cell type that rapidly differentiated under culture into cells specific for myeloid markers (Alliot *et al.*, 1991). The progenitors were later suggested to originate in the yolk-sac from day 8 of mouse embryo development and continue to proliferate and differentiate into the adult microglia population by late gestation (Alliot *et al.*, 1999, Kierdorf *et al.*, 2013). In *Csf-1*r-deficient mice, microglia fail to develop correctly and this state of affairs was found to be maintained throughout the life of the animal despite uninterrupted numbers of circulating monocytes (Ginhoux *et al.*, 2010). Fate mapping with sophisticated fluorescent reporter mice also demonstrated how microglia progenitors present in the yolk-sac entered the embryo proper via the newly circulating blood system on embryonic day 9 (E9) and specifically contributed to microglia and not to other circulating myeloid cells (Ginhoux *et al.*, 2010). Further work using complex transgenic mice then traced the progenitors as leaving the yolk-sac on E9 as an intermediate stage expressing Cd45 but not Cc3cr1, F4/80 or Cd115 before entering the structures, that later develop into the brain on E10.5, as immature macrophages expressing $Cd45^{+}$, $Cc3cr1^{+}$ $F4/80^{+}$ and $Cd115^{+}$ (Neumann and Wekerle, 2013). Immediately after birth microglia proliferate rapidly generating the numbers and distribution that will then persist for life (Alliot *et al.*, 1999). It is still not known if the rapid replication is entirely sourced from the resident microglia population or in part from influx of circulating myeloid cells but evidence would suggest that by E13.5 the mouse blood brain barrier is fully developed prior to the blood-borne circulation of monocytes (Daneman *et al.*, 2010).

1.2.2 Origin and Maturation of Monocytes

The embryonic entry into the brain of specific hematopoietic progenitors is unique to microglia and very different to the formation of other tissue myeloid populations. It

is prudent to next describe the processes of peripheral tissue macrophage formation as the necessity of inflammation and the actions of epithelium drive this process, and both have an impact on the turnover of the resident microglia population.

Macrophages are represented in nearly every tissue type and display considerable, yet highly conserved, heterogeneity in resting phenotype dependent upon the microenvironment in which the cell resides (Figure 1-3). Differing levels of burden of immune surveillance in any given tissue require resting macrophage function and appearance to be adapted to suit. Few cells in as complex an environment as an adult body can be considered to be stand-alone and the macrophage is no exception with homeostatic function in a multi-cell type microenvironment equally as important as immune surveillance.

The macrophage, meaning 'big eater' was largely identified following on from the work of Nobel prize winner Ilya Metchinkov in describing the uptake and subsequent destruction of microorganisms by mono-nucleated cells circulating within blood (Mechnikov, 1908). The process of macrophage formation initially starts with a series of precursor cells derived from haematopoietic stem cell lineage in the bone marrow. The result of this process (leukopoiesis) is the monocyte cell population found in the blood stream, and now known to be those identified with use of aniline dyes by Metchinkov. Monocytes are themselves divided into sub-populations, by expression levels, of lymphocyte antigen 6 complex (Ly6C) (Jutila *et al.*, 1988, Kennedy and Abkowitz, 1998) and the associated retention of CC-chemokine receptors (CCR) 7, CCR8 and CCR2 (Sunderkötter *et al.*, 2004).

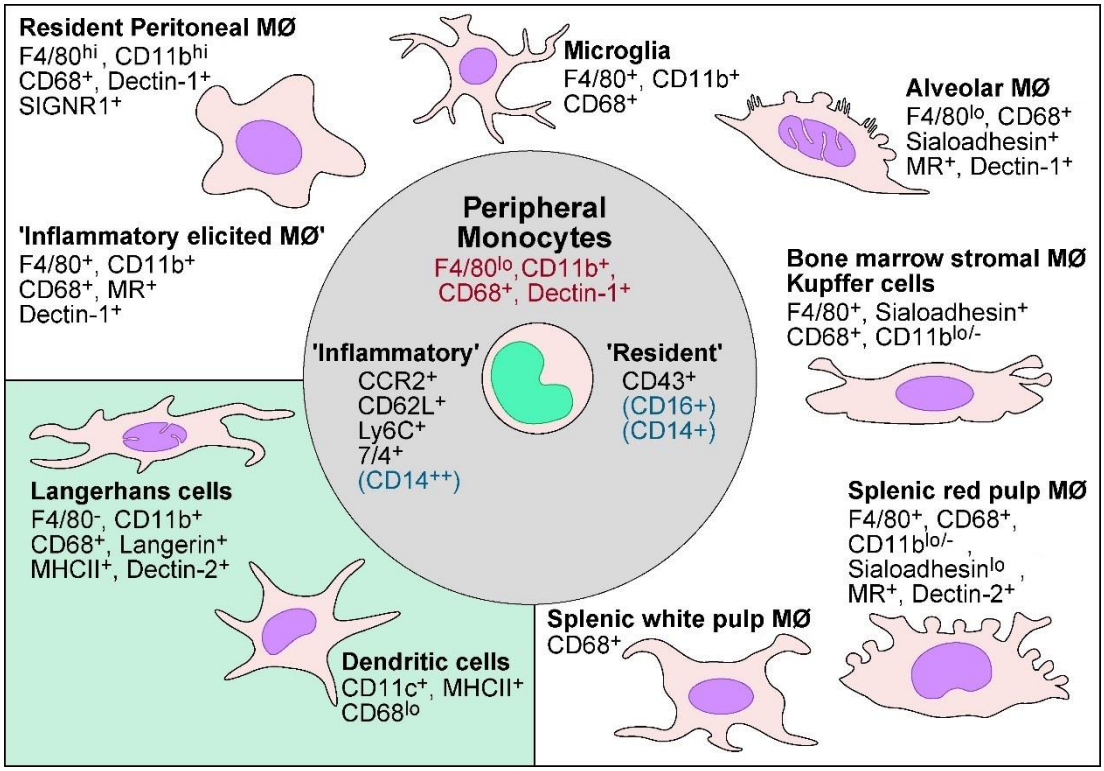

Figure 1-3: Tissue macrophage variants and phenotypic surface marker expression. Highly dependent upon the tissue type in which a monocyte takes up residence; resident macrophages display a remarkable variation in appearance. Figure source: (Taylor *et al.*, 2005).

All newly formed monocytes express high levels of LY6C and are chemotactically attracted to sites of inflammation where they mature into inflammatory macrophages in an effort to return the tissue to normal homeostasis (Geissmann *et al.*, 2003). It is now known that the blood-borne cells Metchinkov observed were in fact $LY6C^{Hi}$ inflammatory monocytes; cells able to respond to inflammatory signals and thus demonstrate a weak phagocytic ability. Monocytes that remain in general circulation gradually lose Ly6C expression along with the retention of CCR7, CCR8 and CCR2 (Geissmann *et al.*, 2003) and would appear to gain the glycoprotein Cluster of Differentiation 16 (CD16) (Passlick *et al.*, 1989) and the fractalkine receptor CX3CR1 (Ancuta *et al.*, 2003). The resulting $LY6C^{Lo}/CD16^{Hi}/CX3CR1^{Hi}$ monocyte populations

are presumed to be lost from the blood through fractalkine mediated migration into vascular endothelium (Ancuta *et al.*, 2003, Auffray *et al.*, 2007, Nahrendorf *et al.*, 2007) and form the resident and wound-healing macrophage populations represented in nearly every tissue type.

Resident non-inflamed tissue macrophages suddenly finding themselves in an acute site of inflammation, and those derived from LY6C^{Hi} inflammatory monocytes in response to inflammatory signals, react to their local microenvironment at an innate level when activated by both interferon gamma (INFg), a cytokine released by natural killer cells in response to exogenous molecules, and tumour necrosis factor (TNF) released by macrophages in response to Toll-like receptor (TLR) ligation with exogenous molecules. The result is an increase in the production of reactive oxygen species and the ability to degrade exogenous intracellular material (Hibbs, 2002). This is in addition to production of further TNF and interleukins that stimulate natural killers to express more INF-g and recruit neutrophils and T-helper cells to the site of inflammation (Annunziato *et al.*, 2012).

1.2.3 Resident Ramified Population Turnover

The resident microglia population is highly stable and efforts to determine if such stability is the result of a resident or a peripheral contribution have led to experiments performed in both healthy and diseased brain scenarios. The questions posed of the resident population can be broken down into two areas of research, the maintenance of the healthy ramified pool and the circumstances surrounding the apparent increase in numbers during microgliosis.

The immunoactive nature of the blood brain barrier in regulating monocyte transmigration into the parenchymal perivascular spaces (Piccio *et al.*, 2002, Kovac *et al.*, 2011) would suggest that from E13.5 onwards resident microglia in the healthy brain comprise a self-sufficient population. Healthy microglia turnover has been shown, using [3H]thymidine incorporation and autoradiography, to be 20 fold slower

than all other tissue macrophage populations with only 0.05% of the microglia population at any given time undergoing mitosis (Lawson *et al.*, 1992).

There is limited evidence to determine the exact contribution of monocyte crossover to the healthy resident microglia population although the mechanisms certainly exist for monocytes to enter the healthy adult brain. Without disruption of the blood brain barrier a very slow crossover has been shown with detection in the parenchyma of < 10 cells per 1 $x10^6$ fluorescently labelled monocytes injected into the blood stream after a period of 24 hours (Wu *et al.*, 2006). The influx is most likely to be mature $LY6C^{Lo}/CX3CR1^{+}$ monocytes for which inflammation mediated crossover is not necessarily required. The specific detection of $LY6C^{Lo}$ $CX3CR1^{+}$ monocytes using transgenic mice expressing red fluorescent protein tagged CCR2 (CCR2-RFP), combined with green fluorescent protein tagged CX3CR1, has allowed this population of cells to be distinguished from the resident microglia population (Saederup *et al.*, 2010). This type of experiment has shown that infiltration by CCR2-RFP expressing, and therefore $LY6C^{Hi}$, monocytes in the healthy brain is negligible.

Far greater numbers of monocytes have been shown to rapidly enter the brain and replace missing microglia following the use of transgenic thymidine kinase expression under the control of the *Cd11b* allele (*Cd11b-HSVTK*) to specifically elicit widespread microglia 'suicide' (Varvel *et al.*, 2012). Importantly the study by Varvel *et al.* (2012) reported the surviving resident microglia remained ramified and did not exhibit any sign of activation although the same was not true of the astrocytes population. The exclusion of $LY6C^{lo}/CX3CR1^{+}$ from the inflamed brain would suggest that in situations of mass depletion, microglia are replaced by $LY6C^{Hi}$ inflammatory monocytes (Mildner *et al.*, 2007, Saederup *et al.*, 2010).

An alternative explanation has been offered that missing microglia are replenished through resident mitotic potential. This has been elegantly shown, and in the absence of inflammation, by the work of Parkhurst *et al.* (2013) using mice expressing

tamoxifen-inducible Cre recombinase under the control of the CX3CR1 promoter and a red fluorescent combination reporter. Following administration of tamoxifen, the resident microglia population remained exclusively recombined long after tamoxifen had dissipated and with no evidence for the non-recombined cell influx observed in peripheral tissues. The use of elegant parabiotic experiments in which the circulatory systems of two healthy mice were co-joined, one of which expressed myeloid transgenic reporters, also demonstrated extremely low contribution from circulating progenitors and that upon entry the cells maintained a strict line of lineage differentiation into microglia only (Massengale *et al.*, 2005). Recent work has also uncovered evidence that following microglia depletion the rapidly proliferating cells which replenish the population express nestin, a marker of stem lineage, and were devoid of the microglia specific marker allograft inflammatory factor 1 (AIF1) suggesting a microglia progenitor resides in the adult brain (Elmore *et al.*, 2014). Widespread depletion of microglia has therefore been instrumental in determining the ability of monocytes to enter the brain. Overall it would therefore seem that while monocyte influx can contribute to turnover of the resident microglia when inflammation is present, the population in the healthy brain is largely self-sufficient.

1.2.4 Perivascular Microglia

Occupying the parenchymal perivascular regions, the perivascular microglia present with a higher turn-over rate with a steady contribution from influx of circulating myeloid precursors (Hickey and Kimura, 1988). Both perivascular and intermediately located juxtavascular (Lassmann *et al.*, 1991) populations demonstrate rapid activation and expression of myeloid inflammatory surface receptors (Vass and Lassmann, 1990) indicating that similar to the resident parenchymal microglia, the contributing circulating myeloid precursors are indistinguishable in their function once matured. Also as per parenchymal microglia; perivascular microglia intrinsically communicate with other cells and respond with a localised and highly specific activation state (Serrats *et al.*, 2010). Indeed the maturation of myeloid precursors into a perivascular microglia phenotype is not possible out with the multicellular

brain microenvironment (Tanaka *et al.*, 1993). Although perivascular populations can be identified by expression of specific markers (Galea *et al.*, 2005) it is accepted terminology that the perivascular populations are considered microglia subtypes separated only by location and not appearance (Gehrmann *et al.*, 1995).

1.2.5 Population Dynamics during Microgliosis

Microgliosis is the term used to describe both the visual change in appearance and the increase in population size observable when microglia become activated. Much debate surrounds whether the apparent increase in microglial numbers observed during microgliosis is due to influx of circulating monocytes or though the mitotic potential of resident microglia and both arguments will be discussed in this section.

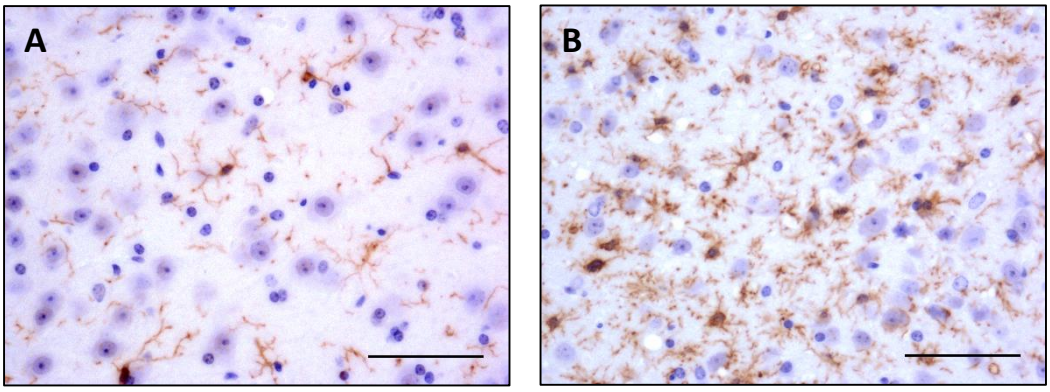

Figure 1-4: Microglial morphological response. **A:** resting microglia in the healthy brain display a small central soma with delicate processes extending out into the parenchyma. **B:** Conversely activated microglia have enlarged somas with shorter thicker processes. The cell density also increases through recruitment and/or division. Scale bars equate to 50 µm. Murine microglia in the thalamus stained with anti-Allograft inflammatory factor 1.

The minimal contribution of circulating LY6C^{lo}/CX3CR1^{+} monocytes to the resident microglia pool during normal turnover is the result of limited expression of chemoattractants in the healthy brain (Section 1.2.3). By contrast the brain in situations of acute and chronic trauma is, as evidenced by activated microglia and astrocytes, a source of inflammatory cytokines and chemokines. The conditions are therefore favourable for the influx of LY6C^{Hi} inflammatory monocytes (Section 1.2.2) and studies utilising re-constitution with transgenic reporters in situations of chronic neurodegeneration reported a high level of contribution from reconstituted cells to the resident population Two notable studies that have adopted transgenic reporters are those by Williams *et al.* (1995) and Priller *et al.* (2006). The former utilised XX-XY chimeric reporter mice in which irradiated C57BL/6J female mice were reconstituted with bone marrow derived from C57BL/6J male mice. A combination of immunohistochemistry and detection of the Y-chromosome by in-situ hybridisation revealed that prion infected mice chimeric mice demonstrated recruitment of peripheral Y-probe positive myeloid derived cells. Furthermore no difference in visible morphology could be attributed between host microglia and those containing a Y-chromosome. The use of XX-XY chimerism elegantly allowed host and reconstituted microglia to be distinguished and the study concluded that the overall low-level recruitment of monocytes was independent of both lesion severity and incubation length. The maximum level of chimerism gained within the experiment was 33% and by ensuing that a considerable proportion of the original host microglia were intact the study were able to conclude that the recruitment of peripheral myeloid cells was not a critical part of the disease process.

By contrast a significantly higher proportion of peripheral bone marrow-derived derived microglia were observed in the study by Priller *et al.* (2006). This study utilised a green fluorescent protein tagged bone morrow reconstitution reporter system and found that, although the total number of microglia in prion infected brain remained constant, the number of reporter cells comprised just over half of the population. Furthermore bone marrow derived cells were recruited early on in the

disease process suggesting a constant turnover throughout the incubation period. Although the use of lethal irradiation has been defended by the studies that utilised the method, typically by control measurements including checking the stability of the host microglia population as part pf the aging process and blood brain barrier integrity through detection of Immunoglobulin G extravasation (Priller *et al.*, 2006) there remains the generation of a non-physiological condition.

Parabiotic experiments co-joining the circulatory systems of two mice during both acute and chronic neuroinflammation following irradiation that, crucially, left microglia and the blood brain barrier intact, established that in a physiologically correct situation no circulating monocytes cross over into the brain (Ajami *et al.*, 2007). Importantly, further experiments by Ajami *et al.* (2007) revealed that significant monocyte influx took place if a healthy mouse subjected to lethal peripheral irradiation with a head shield was rescued with bone marrow reconstitution. The act of lethally irradiating mice to deplete myeloid cells followed by reconstitution with a bone-marrow donation induces a non-physiological state with possible persistence of hematopoietic cells and progenitors normally found in bone marrow remaining in circulation (Mildner *et al.*, 2007). Others have also shown how the significant monocyte influx associated with cranial irradiation contributes directly to the resident microglial population in efforts to mediate irradiation induced inflammation (Burrell *et al.*, 2012) Consequently it would seem that lethal irradiation and/or bone marrow reconstitution are actually necessary for crossover of circulating monocytes bringing the interpretation of previous experiments using these techniques to quantify circulating progenitor contribution to resident microglia into question (Ransohoff, 2007). Most studies since this seminal work now take the precaution to shield the head during irradiation to allow for the spontaneous infiltration of monocytes to be reported in a more normal pathological state.

The exception to most neurodegenerative diseases would appear to be artificially induced experimental autoimmune encephalomyelitis in which monocytes can cross a physiologically intact blood brain barrier (Ransohoff, 2011). Using transgenic CCR2

and CX3CR1 knockout mice, expressing red and green fluorescent tags respectively, demonstrated that inflammatory LY6C^{Hi}/CCR2^{+} monocytes increase the morphological activation of all resident microglia during experimental autoimmune encephalomyelitis (Saederup *et al.*, 2010). Indeed the progression of experimental autoimmune encephalomyelitis can actually be halted by using CCR2 knockout mice to inhibit recruitment of LY6C^{Hi}/CCR2^{+} monocytes into the brain implying these cells are crucial to the ongoing pathology, even if, after resolution of the acute phase, all undergo apoptosis leaving only resident cells to persist (Ajami *et al.*, 2011).

The contribution in acute injury is more complex with conflicting reports existing for the contribution of LY6C^{Hi} inflammatory monocytes to the increase in microglia observed during acute microgliosis. Efforts to reconstitute circulating monocytes following depletion of circulating progenitors with injected clodronate-encapsulated liposomes, a method that results in minimal lasting inflammation, found the bulk of replicating microglia to be resident in origin (Ladeby *et al.*, 2005). Conversely, reconstitution following lethal irradiation revealed considerably more LY6C^{Hi} monocytes contributed to the resident pool (Getts *et al.*, 2008). The difference between the levels of LY6C^{Hi} monocyte influx might be attributed to changes in the immunoactive state of both the brain parenchyma and vascular epithelium.

There is some data to support the crossover of infiltrating cells back into the blood circulation as antigen presentation cells following active phagocytosis of debris in localised acute lesions (Joly *et al.*, 2009) and that interleukin 10 expressing anti-inflammatory macrophages, derived from infiltrating cells, are necessary for acute lesion recovery and are recruited by involvement of the adaptive immune system (Shechter *et al.*, 2009). The involvement of the adaptive immune system in neurodegenerative diseases is still little understood although the recruitment of T-cells into the brain parenchyma is known (Lewicki *et al.*, 2003) with further evidence to suggest partial protection is afforded by their presence (Klein *et al.*, 2005, Iken *et al.*, 2011, Clarkson *et al.*, 2012).

1.2.6 Acute Inflammatory Activation

Resident resting microglia continuously sample the surrounding microenvironment with highly mobile actin rich protrusions for which motility is regulated by purinergic receptors (Capani *et al.*, 2001, Boucsein *et al.*, 2003, Davalos *et al.*, 2005, Haynes *et al.*, 2006, Franke *et al.*, 2007). Even in the resting state microglia demonstrate broad regional differences in morphology (Lawson *et al.*, 1990) through adaptations to local architecture (section 1.2.4). Microglia are incredibly sensitive to any perturbations within their immediate environment and respond rapidly to any insult with increased process motility and physical migration to the affected area (Davalos *et al.*, 2005, Nimmerjahn *et al.*, 2005, Kozai *et al.*, 2012). Such is the sensitivity of microglia that Nimmerjahn *et al.* (2005) found the heat generated from scraping a scalpel blade across mouse skull to thin down the bone for *in-vivo* multi-photon imaging was, if not performed gently enough, sufficient to aggravate underlying microglia in the cortex (Hughes, 2012).

Microglia express a wide variety of scavenging, Toll-like, Nod-like receptors and receptors for advanced glycation end products (RAGE) to detect the presence of damage-associated molecular patterns (DAMPS) including ATP, nucleotides, oxidised lipids, and DNA histones released by dead and dying cells (reviewed extensively in Bianchi, 2007). Also included within the spectrum of acute detection, primarily by toll-like receptors, is the detection of pathogen-associated molecular patterns (PAMPS). PAMPS, as the name implies, initiate the response to pathogens and foreign bodies. The detection of PAMPs and DAMPs by microglia initiates the MAP kinase, $p21^{ras}$ and the NF-KB pathways leading to amplification of microglia activation (Lander *et al.*, 1997, Basta *et al.*, 2002).

The full activation of microglia in acute damage is kept at bay though the action of constitutively expressed inhibitory membrane bound neuronal ligands including the chemokine CX3CL1 (Boehme *et al.*, 2000, Hughes *et al.*, 2002, Cardona *et al.*, 2006b,

Liang *et al.*, 2009) and the glycoproteins CD200 and CD47 (Hoek *et al.*, 2000, Jenmalm *et al.*, 2006, Gitik *et al.*, 2011). Where neurons are functioning correctly these inhibitory ligands bind to corresponding receptors on microglia and keep the full activation of microglia under tight feedback control. The release of inflammatory cytokines and oxidative products is quickly suppressed to limit the collateral damage to surrounding neurons (Nahrendorf *et al.*, 2007, Clausen *et al.*, 2008, Hines *et al.*, 2009, Shechter *et al.*, 2009). Even when phagocytising damaged and apoptotic neurons in the otherwise healthy brain, microglia demonstrate a remarkably down-regulated phenotype (Takahashi *et al.*, 2005, Sierra *et al.*, 2010) in a process that has been termed 'phagoptosis' (Brown and Neher, 2012). The phagocytosis of dying cells and debris is a well-known function of microglia during the resolution of inflammation (Neumann *et al.*, 2008, Neumann *et al.*, 2009). The relatively silent removal of otherwise viable neurons by phagoptosis is also seen as a core component of neurodegeneration (Fricker *et al.*, 2012).

Traditionally, macrophage differentiation in response to INF-g and corresponding antagonists Interleukin (IL) 4 and IL-13, released by T-helper-1 and T-helper-2 cells, (Mosmann and Coffman, 1989, Sallusto and Lanzavecchia, 2009) is thought to result in two distinct phenotypes: classical M1 and alternative M2 (Mantovani *et al.*, 2007, Martinez *et al.*, 2009, Varin and Gordon, 2009). There is also some controversy over a third macrophage subtype splitting categorisation into classical, regulatory and wound-healing phenotypes (Mosser, 2003, Mosser and Edwards, 2008). As the resident myeloid immune cell in the central nervous system the classifications of classical and alternative activation have been applied to microglia, particularly as microglia are able to express a wide variety of macrophage associated cytokines (Table 1-2). Experiments performed in situations of acute central nervous system damage revealed the presence of classically activated M1 microglia, immediately following an acute lesion, resulted in significant neuronal loss (Boutin et al., 2001, Kigerl et al., 2009). Alternatively activated microglia, associated with neuro-regeneration are present in the minority. This situation rapidly resolves as the ratio

reverses and normal homeostasis is restored. Those cells that could be described as demonstrating a classically activated phenotype, associated with neuronal loss, outnumber those displaying an alternatively activated phenotype associated with neuro-regeneration (Kigerl *et al.*, 2009, Varin and Gordon, 2009). Gradually this situation resolves as the ratio reverses and normal homeostasis is restored.

Table 1-2: The main macrophage-like cytokine and chemokine repertoire expressed by microglia (Adapted from Raivich *et al.*, 1999).

Abbreviation	Name
IL-1a/1b	interleukin-1α/1β
IL-3	interleukin-3
IL-6	interleukin-6
IL-8	interleukin-8
IL-10	interleukin-10
IL-12	interleukin-12
IL-15	interleukin-15
IL-18./IGIF	interleukin-18/interferon-γ inducing factor
M-CSF	macrophage-colony stimulating factor
TGFB	transforming growth factor β
TGFA	transforming growth factor α
GROA	growth regulated oncogene α
MCP-1	monocyte chemoattractant protein-1
MIP-1a/Mip-1b	macrophage inflammatory protein-1α/1β
MIP-2	macrophage inflammatory protein-2
RANTES	regulated on activation, normal T cell expressed and secreted

1.2.7 Chronic Activation in Neurodegenerative Diseases

Neurodegenerative diseases typically involve chronic microglial activation that lasts throughout the disease process. The protracted timescale of the diseases introduces the potential for changes in inflammatory triggers to occur in the central nervous system as the disease progresses. The activation of microglia during chronic inflammations is therefore considerably more complex. Indeed it is now considered likely that microglia in chronic diseases do not conform to the M1 and M2 profiles

and instead demonstrate a considerable degree of plasticity (Figure 1-5) with unique phenotypes at any given point in time determined by changes in the immediate microenvironment (Streit *et al.*, 1988, Perry *et al.*, 2010).

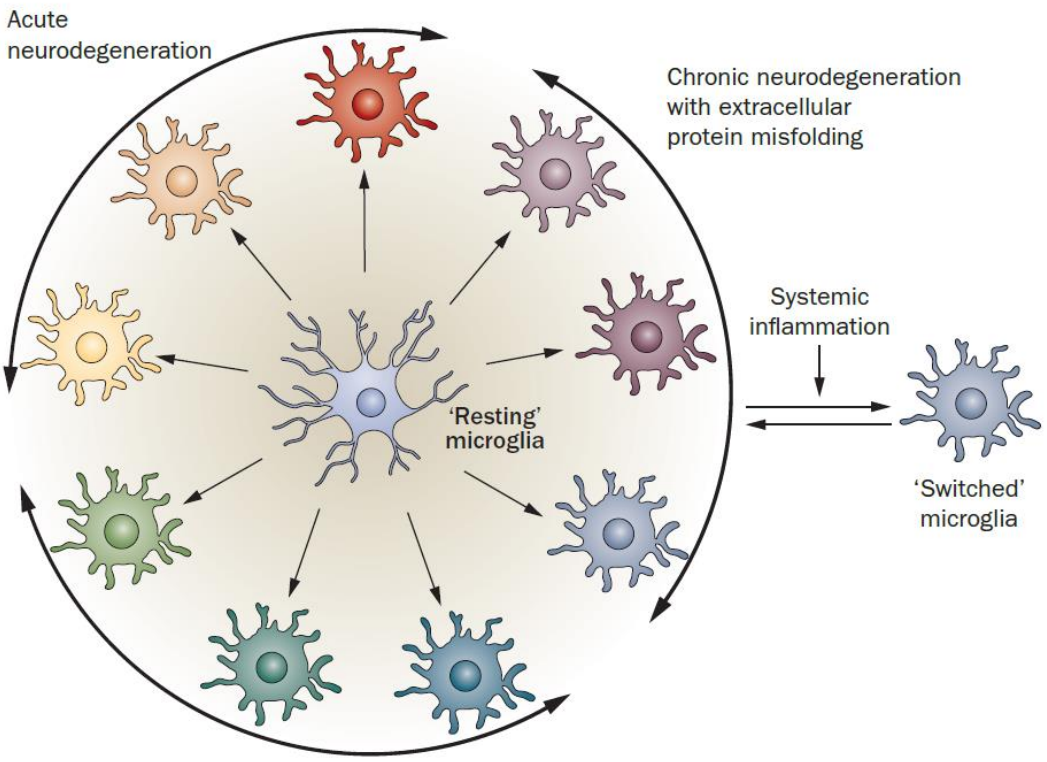

Figure 1-5: Microglial activation plasticity. Any perturbations to the immediate microenvironment surrounding microglia initiates an immediate but unique response governed by many factors including the type of insult, host age, and overall host (systemic) inflammatory state. The latter has the capacity to influence microglial activation phenotype from outside of the central nervous system. It is therefore important to consider the differences in host condition, and the corresponding downstream effect on microglia activation phenotype, when comparing an experimental host population with a heterogeneous human population. Image courtesy of Perry *et al.* (2010).

Chronic protein misfolding neurodegenerative diseases affect large areas of the brain and microglial activation is seen on a wider scale. The recruitment of microglia has been associated with the deposition of amyloid precursor protein (APP) plaques in APP transgenic mice where numbers of microglia are proportional to amyloid plaque size (Stalder *et al.*, 1999, Bolmont *et al.*, 2008). Involvement of microglia with plaques is thought not to be direct engulfment of amyloid but an intricate, and little understood, interaction with surrounding cells and filaments on the outer edges of the plaque (Stalder *et al.*, 2001, Hughes *et al.*, 2010, Cramer *et al.*, 2012).

Activated microglia impart a cytotoxic environment through expression of soluble pro-inflammatory products including IL-1β, IL-6, tumour-necrosis factor-α (TNF-a), and multiple reactive oxygen species (Boje and Arora, 1992, Benzing *et al.*, 1999, Cox *et al.*, 2013). The long term effects of chronic activation and the role a cytotoxic pro-inflammatory saturated environment are not well known. Prion disease models are one of the few models that successfully replicate both misfolded protein deposition and neuronal loss and in this group of diseases neurons appear not to die though toxin or damage mediated necrosis but through caspase-mediated apoptosis (Giese *et al.*, 1995, Lucassen *et al.*, 1995, Jamieson *et al.*, 2001, Siso *et al.*, 2002). The presence of progressive autophagy has also been suggested as part of this process (Boellaard *et al.*, 1991, Xue *et al.*, 1999, Sikorska *et al.*, 2004, Xu *et al.*, 2012). The clearance of apoptotic cells by myeloid cells involves the ligation of thrombospondin-1 on the apoptotic cell surface with CD36 and $\alpha_V\beta_3$ receptors on the phagocyte as part of the self-recognition process (Brown *et al.*, 2002). Binding with thrombospondin-1 induces a reduction in pro-inflammatory TNF-a, and a marked increase in expression of anti-inflammatory transforming growth factor-β1 (TGF-b1) and IL10 (Voll *et al.*, 1997, Freire-de-Lima *et al.*, 2000). Murine models of prion disease have been described as being dominated by an increase in expression of TGF-β1 (Cunningham *et al.*, 2002, Boche *et al.*, 2006). The resulting downstream anti-inflammatory profile induced by increasing levels of TGF-b1, has led to the widespread adoption of the term ‘atypical inflammation’ when describing microglia

phenotype in neurodegenerative diseases (Fadok *et al.*, 1998, Baker *et al.*, 1999, Walsh *et al.*, 2001, Cunningham *et al.*, 2002, Perry *et al.*, 2002, Baker and Manuelidis, 2003).

The multifunctional cytokine TGF-β1 is evident throughout the disease process where, although it has no impact on the deposition of misfolded protein, it is involved in supressing microglia activation through inhibiting translation (Lodge and Sriram, 1996, Abutbul *et al.*, 2012). The cytokine is also heavily involved in maintenance of endothelium basement membrane and the blood brain barrier (Cunningham *et al.*, 2002, Garcia *et al.*, 2004). TGF-β1 is known to act in concert with Glial Cell Line-Derived Neurotrophic Factors (GDNF), further members of the transforming growth factor superfamily, to impart a neurotrophic potential on neurons (Krieglstein *et al.*, 1998, Schober *et al.*, 1999, Peterziel *et al.*, 2002). GDNFs are now recognised as beneficial to the survival of dopaminergic neurons in Parkinson's Disease (Grathwohl *et al.*, 2009, Ramaswamy *et al.*, 2009, Patel *et al.*, 2013, Tereshchenko *et al.*, 2014). Care however needs to be applied in describing the neurotrophic function of transforming growth factors within the context of microglia in neurodegenerative diseases. Microglia express and bind with a wide variety of neurotrophic factors (Elkabes *et al.*, 1996). Although the presence of these factors are known to increase in murine prion models of neurodegenerative disease (Lee *et al.*, 2006), the modulatory effect on microglia activation following ligation of neurotrophic factors to microglia-bound receptors is not universal throughout the brain (Elkabes *et al.*, 1996, Boscia *et al.*, 2009). There is also some *in-vitro* data hinting at an increase in nitric oxide, T-a and the phagocytic response in the presence of transforming growth factors (Wang *et al.*, 2013, Zlotnik and Spittau, 2014).

Microglia have the mechanism in place to elicit a cytotoxic action on other cells and this has been comprehensively demonstrated using *in-vitro* co-cultures through detection of reactive oxygen species following activation of microglia by lipopolysaccharide (LPS), Interferon-gamma (INF-g), amyloid-β or the prion protein

amino acid 106-126 peptide sequence (Colton and Gilbert, 1987, Boje and Arora, 1992, Meda *et al.*, 1995, Peyrin *et al.*, 1999). To date there is no evidence for actual neuronal toxic activity *in-vivo* where the added complications of a multicellular environment and multi-functional immunomodulators restrict the ability to form definite conclusions (Jeong *et al.*, 2010).

Pioneering work investigating the response of microglia in the regenerative environment, induced by sub lethal motor neuron axotomy, revealed microglia to express a wide range of immunomodulators including the adhesive and migration associated protein thrombospondin (Moller *et al.*, 1996, Schiefer *et al.*, 1999). Crucially thrombospondin is also associated with immature microglia during CNS development and is an aid to axon growth (Chamak *et al.*, 1994, Chamak *et al.*, 1995). Also observed were major histocompatibility complex (MHC) Class I antigens (Streit *et al.*, 1989b) which upon further investigation into the proximal location of microglia to sites of neuronal repair led to the conclusion that activated microglia expression might also have a role in both initial synaptic loss and subsequent neuron regeneration (Kreutzberg *et al.*, 1989, Streit *et al.*, 1989c).

Within *in-vivo* mouse models of neurodegenerative disease the earliest indications of neuronal stress are the loss of synapses, termed 'synaptic stripping' (Gray *et al.*, 2009, Hilton *et al.*, 2013, Siskova *et al.*, 2013). The accumulation of misfolded protein is not thought to directly interfere with synaptic vesicle transport (Asuni *et al.*, 2008) but by interfering with lipid raft located transmembrane proteins (Jeffrey *et al.*, 1997, Siso *et al.*, 2002, Bouzamondo-Bernstein *et al.*, 2004, Ishikura *et al.*, 2005, Inoue *et al.*, 2009, Godsave *et al.*, 2013, Vargas *et al.*, 2014). Co-cultures of neurons and microglia in the presence of a PrP 106-126 peptide sequence has shown microglia will engulf damaged neurons (Brown *et al.*, 1996, Bate *et al.*, 2001) and that this is dependent upon for CD14 mediated contact (Bate *et al.*, 2005). Gene expression studies have also revealed interruptions to the otherwise neurotrophic actions of N-methyl-D-aspartic acid receptor signalling (Liu *et al.*, 2007, Majer *et al.*, 2012).

With a clearer understanding of the vital roles microglia perform in the brain as part of a tightly regulated multi-cellular system, combined with a better understanding of the non-physiological conditions that can impact on the microglia population (see section 1.2.5), it is perhaps not surprising that recent investigations have observed minimal contribution from circulating monocytes during neurodegenerative mouse-adapted prion disease (Gomez-Nicola *et al.*, 2014). The resident population is, for the most part, self-maintained. It is interesting to note that past evidence for removal of anti-inflammatory IL-10 and the corresponding acceleration in disease progression and severity (Thackray *et al.*, 2004) was previously dismissed in the literature with the aforementioned consensus for an 'atypical' anti-inflammatory phenotype. What the data indicated was that pro-inflammatory modulators were a key driving force and recent work has once again shown how microglia activation is regulated by the *Spi1* transcription factor initiating a strong IL34-driven differentiation into a pro-inflammatory phenotype (Gomez-Nicola *et al.*, 2013), and that ablation of microglia proliferation and pro-inflammatory activity considerably slows down neuronal damage (Gomez-Nicola *et al.*, 2013, Sakai *et al.*, 2013, Song *et al.*, 2013). Microglia activation by the JAK-STAT signalling pathway, and resulting expression of pro-inflammatory products, has been shown to be regulated by non-coding MicroRNA 146a (Saba *et al.*, 2012) and overall activation requires perturbation of neuronal inhibitory signalling (Riemer *et al.*, 2008, Fuhrmann *et al.*, 2010, Xie *et al.*, 2013) providing evidence that the complex and tight control over inflammation seen in the healthy brain is maintained during chronic disease.

The large numbers of activated microglia all releasing inflammatory modulators has the potential to induce a self-perpetuating cycle maintaining high levels of microglial activation; termed reactive-microgliosis. This can be elegantly observed within the 1-Methyl-4- Phenyl-1,2,3,6-Tetrahydropyridine (MPTP) toxin model of selective dopaminergic neuron loss (Langston *et al.*, 1983). The strong link between MPTP toxin and microglial activation is well known (Wu *et al.*, 2003) and, importantly, neuro-inflammation continues to take place long after any remaining MPTP toxin has

been cleared from the system (Langston *et al.*, 1999, McGeer *et al.*, 2003). Reactive-microgliosis is also observable under conditions of Wallerian degeneration, where the separation of the axon from the cell soma has been initiated. Microglial activation is rapid following separation (Lawson *et al.*, 1994) yet following resolution the microglia remain activated with an anti-inflammatory phenotype that can persist for years (Palin *et al.*, 2008).

Tachyphylaxis, the increasing tolerance to a stimulant, is not an uncommon response displayed by *in-vitro* macrophage cultures. While *in-vitro* does not always match the *in-vivo* environment, tachyphylaxis is a factor to be considered in the conditions of long term chronic activation, particularly if that tolerance is toward anti-inflammatory signalling. Microglia cultured *in-vitro* have been shown to express numerous pro-inflammatory cytokines in response to 24 hour exposure to the cytotoxic prion protein amino acid 106-126 peptide sequence (Peyrin *et al.*, 1999). Interestingly there is a marked reduction in tumour necrosis factor-α following prolonged exposure (Zhou *et al.*, 2008) suggesting a level of tolerance has been reached. The persistence of microglia activation during reactive microgliosis has been suggested to be a form of "innate immune memory" (Perry *et al.*, 2010) although it is not known if this is an advantageous adaption. A more subtle form of chronic activation can however be studied in situations of 'priming' both from systemic signalling and the effects of senescence.

1.2.8 Microglia Priming and Senescence

The sensitivity of microglia to even the smallest perturbation within their immediate microenvironment mean microglia also responded to local signals with an origin from outside of the central nervous system. At the broadest level, microglia are a key part of 'cytokine-induced sickness behaviour' whereby the host will demonstrate fever, malaise, anorexia and seek solitude during the acute phase reaction to pathogenic infection. The evolutionary significance of this well-defined set of physiological and behavioural actions is to make the host inhospitable for pathogen survival, enhance

the normal immune response and, through seeking solitude, minimise further spread of the disease (Miller, 1964, Kluger, 1979, Hart, 1988, Dantzer, 2001). The release of pro-inflammatory cytokines in the brain parenchyma during sickness behaviour including IL1β, TNF-a and nitric oxide synthase have been extensively documented with specific contributions made towards sickness behaviour upon recombinant inoculation and/or infection by LPS determined for each (Ban *et al.*, 1992, Kent *et al.*, 1992, Gatti and Bartfai, 1993, Laye *et al.*, 1994, Buttini and Boddeke, 1995, Quan *et al.*, 1999, Thomson *et al.*, 2014). Importantly morphology can be observed to be independent of cytokine expression for the release of pro-inflammatory cytokines during the acute phase reaction to pathogenic infection is by ramified microglia and indicating activation toward a more amoeboid appearance is kept at bay (van Dam *et al.*, 1992, Van Dam *et al.*, 1995).

The sensitivity of microglia to peripheral inflammation can result in excessive production of pro-inflammatory cytokines if microglia are pre 'primed' from an underlying chronic neurodegenerative condition afflicting the brain. Such a secondary peripheral insult has the potential to 'switch' the current predominant down-regulated anti-inflammatory microglia phenotype, found in most neurodegenerative diseases, to a more neurotoxic pro-inflammatory phenotype (Palin *et al.*, 2008, Murray *et al.*, 2011). This has been demonstrated in experimental mouse-adapted prion disease in which the combined sources of inflammation pertaining from both the periphery and the brain yielded a considerable increase in expression of cytokines and accelerated disease pathogenesis (Combrinck *et al.*, 2002, Cunningham *et al.*, 2005b, Cunningham *et al.*, 2009, Field *et al.*, 2010, Murray *et al.*, 2012). Studies in transgenic mouse models of Alzheimer's Disease and Parkinson's Disease also show an increase in pro-inflammatory response upon acute systemic insult with LPS (Sly *et al.*, 2001, Kitazawa *et al.*, 2005, Pott Godoy *et al.*, 2008). The importance of combined brain and peripheral insult is particularly relevant in lengthy chronic neurodegenerative diseases where the presence of

multiple co-morbidities are a real possibility, particularly in human diseases where the incubation period can be many years (Drake *et al.*, 2011, Thaler *et al.*, 2012).

The impact of systemic inflammation in the aged brain also results in exaggerated innate inflammation initiated and maintained by microglia. Microglia residing in this aged environment adopt a phenotype with increased expression of pro-inflammatory MHC Class II antigen, TNF-a, IL1b and IL-6 (Perry *et al.*, 1993, Sierra *et al.*, 2007, Kohman *et al.*, 2013). Shorter less complex processes are also visible presumably indicative of a state of permanent 'priming' (Streit *et al.*, 2004, Sierra *et al.*, 2007). There is also a marked increase in inflammation induced by gradual neuronal and glial cell loss by apoptosis and associated microglia activation (Lee *et al.*, 2000, Schuitemaker *et al.*, 2012, Gao *et al.*, 2013). Isolated cultured microglia demonstrate a similar aged phenotype indicating microglia are subject to, and respond to, their own age related changes and not just to the condition of surrounding cells (Sierra *et al.*, 2007, Caldeira *et al.*, 2014). There is also a marked reduction in surface expression of the CX3CR1 fractalkine receptor signifying loss of inhibitory support from neurons (see section 1.2.6) as a possible cause of priming (Wynne *et al.*, 2010). Impact on mitotic potential through analysis of telomeres revealed a progressive reduction in telomere length both *in-vivo* and *in-vitro* by senescent microglia (Flanary *et al.*, 2007). Despite this, actively replicating and pre-primed aged microglia *in-vivo* show increased basal telomerase activity partly mitigating telomere length (Flanary and Streit, 2005, Conde and Streit, 2006). The rate of proliferation of aged microglia in response to injury is also greater (Conde and Streit, 2006) as is the basal expression of certain anti-inflammatory cytokines including TGFβ1 and IL-10 suggesting a certain level of inherent counteraction to the rising levels of inflammation within the parenchyma (Sierra *et al.*, 2007).

Senescent microglia respond to systemic inflammation with a phenotype strikingly similar to that seen in neurodegenerative diseases (Godbout *et al.*, 2005, Dilger and Johnson, 2008, Murray *et al.*, 2012) . Indeed the increased basal levels of pro-

inflammatory cytokines released by senescent microglia have been suggested as a cause of age-related neurodegeneration (Benzing *et al.*, 1999, Riemer *et al.*, 2004).

1.2.9 Involvement in Neurodevelopment, Neurogenesis and Repair

The brain is not a one cell-type centric environment and shows evidence of multicellular interactions and regulation. Regulation of microglia immune response by neuronal inhibitory signals has been discussed (1.2.6); however microglia extend their interaction with neurons and other glial cells in activities that are not necessarily associated with immune function.

Microglia progenitors enter the embryonic region that will later develop into the brain as a distinct group of cells with a hematopoietic origin (see section 1.2.1). Why these cells should enter this region so early in development, prior to other resident tissue myeloid populations, led to investigations into determining if the cells have a role in correct neurodevelopment. Evidence from *in-vivo* knockout studies in which microglia were ablated using spleen proviral integration oncogene (*Spi1*) and colony stimulating factor-1 (*Csf-1*), both recruitment factors, strongly supported the requirement of primitive yolk-sac derived microglia as critical for correct neurovascular development. The developing brain does not have an intrinsic vascular system and relies entirely on angiogenesis (Vasudevan *et al.*, 2008). Hematopoietic cell lineages failed to develop correctly without angiogenesis stimulating factors (Scott *et al.*, 1994, Kubota *et al.*, 2009). Furthermore microglia knockout resulted in a significant reduction in brain vascular structure complexity, thereby indicating a strong role for these cells in angiogenesis (McKercher *et al.*, 1996, Kubota *et al.*, 2009). Microglia have also been implemented in the regulation of post-natal angiogenesis by governing the suppression of branching (Stefater *et al.*, 2011) and the absence of microglia *in-vivo* and *in-vitro* from neuronal precursors negatively impacts neurogenesis, proliferation and the bias of stem cell differentiation into astrocyte or oligodendrocyte precursors (Antony *et al.*, 2011, Shigemoto-Mogami *et al.*, 2014).

Interfering with microglia function after vascular development has shown microglia to be critical for correct motor function. The use of *Tgfb1* knockout mice to gradually ablate microglia in in the embryo from E14.5, until the almost complete ablation by postnatal day 160, resulted in severe motor coordination abnormalities and weight loss (Butovsky *et al.*, 2014). Crucially it was noted by Butovsky *et al.* (2014) that there was a steady influx of $LY6C^{hi}/CD11b^{+}$ circulating progenitors that replaced the postnatal resident population of microglia. These were immunologically active but did not correct lost motor function or display the same gene expression profile as the original microglia. Indeed infiltrating inflammatory monocytes would appear to be detrimental to homeostatic vascularisation (Li *et al.*, 2012).

The development of postnatal synaptic connections requires microglia for initiation of dendritic spine formation and synapse formation through IL-10 mediated stimulation (Lim *et al.*, 2013). The modulation of synapses in the postnatal developing brain also requires continual pruning by microglia for correct neuronal circuit maturation, and ablation of microglia to limit pruning has been shown to yield persistent electrophysiological hallmarks of immature brain circuitry (Paolicelli *et al.*, 2011, Rogers *et al.*, 2011) and even perturbations to sexual differentiation (Levi *et al.*, 1998, Minghetti and Levi, 1998, Lenz *et al.*, 2013).

The mass caspase-mediated programmed cell death of immature neurons is critical for the correct formation of neuronal architecture, leaving behind the bulk of neurons and connections that will be retained for life. The apoptotic process is driven competitively by starvation of nerve growth factors (Martin *et al.*, 1988, Cattaneo and McKay, 1990) and microglia engulf the dead and dying cells and processes. Critically, microglia are not just reacting to the presence of apoptotic cells but are drivers of the process with selective killing of immature neurons through targeted respiratory burst activity (Marín-Teva *et al.*, 2004, Cunningham *et al.*, 2013).

The capacity for the adult brain to renew neurons is limited and the primary reason for the tight regulation of inflammation to minimise damage. A secondary side effect of Inflammation is inhibition of neurogenesis (Ekdahl *et al.*, 2003, Goshen *et al.*, 2007, Perez-Asensio *et al.*, 2013). Inflammation inhibited neurogenesis is therefore a contributing factor to the overall neuronal loss seen in neurodegenerative diseases (Kiyota *et al.*, 2010) and efforts to block pro-inflammatory, or enhance anti-inflammatory inflammation, at least partially restored adult neurogenesis (Monje *et al.*, 2003, Kiyota *et al.*, 2012, Mouihate, 2014). Microglia, as considerable contributors to soluble inflammatory immunomodulators, are therefore involved in regulating neurogenesis and can enhance cell renewal and repair when the activation phenotype is biased toward the resolution of inflammation (London *et al.*, 2011, Zhang *et al.*, 2014).

Resident ramified microglia also have a direct influence on both the maintenance and differentiation of neural stem cell populations (Zhu *et al.*, 2008, Bachstetter *et al.*, 2011, Vinet *et al.*, 2012). It is important to note that these resting microglia display no visible morphological indication of activation. There has recently been considerable research in investigating the interaction between ramified microglia and other cells in the adult healthy brain and the role microglia play in normal neuronal function and the most striking evidence to date for microglia involvement with neuronal function in the healthy brain is work performed by Tremblay *et al.* (2010) and Chen *et al.* (2014). This seminal *in-vivo* work by Tremblay *et al.* (2010) witnessed microglia dynamically altering their interaction with newly formed and transient synapses in response to visual sensory stimuli and directly influenced dendritic spine plasticity. Ablation of microglia has since revealed the vital role microglia play in modulating the increase in hippocampal neurogenesis in response to exercise (Vukovic *et al.*, 2012), the lack of which is known to correlate with the decline in activity of neuronal precursor cells (Blackmore *et al.*, 2009, Blackmore *et al.*, 2012). Highly detailed 3D ultrastructure analysis of microglia using 3D electron microscopy was used by Chen *et al.* (2014) to determine that microglia are intrinsically involved

in regulating the neuroprotective and anti-apoptotic response of neurons in the adult brain by actively displacing inhibitory synapses. Microglia interaction with synapses is made by actin cytoskeletal rich processes of which even the finest are highly mobile (Tasker *et al.*, 2012) and the length of time contact is made is directly related to synapse excitatory levels (Wake *et al.*, 2009).

Not all synapses are shared with microglia during homeostasis and at any one time approximately 6% of synapses have microglia interaction and then by only 30% of the available processes on an individual microglia (Tremblay *et al.*, 2010). Although the term 'quad-partite' synapse has been coined in describing such interaction (Schafer *et al.*, 2013) it is not perhaps as prevalent as the 'tri-partite' complex between astrocytes and neuronal synapses found ubiquitously throughout the brain and necessary for neurotransmitter recycling and correct synapse function (Araque *et al.*, 1998, Sykova, 2004, Pascual *et al.*, 2005).

1.3 The Transcriptomic Revolution

The ability to capture the entire profile of genetic mechanisms in a tissue sample at once offers many advantages in determining expression levels and sequencing, not least cost and time, over previous gene-by-gene methods including quantitative real time polymerase chain reaction and gene knockout studies. The ability to investigate the entire gene expression profile was made possible by the whole genome sequencing of target organisms. Microarrays were developed as a surface chip upon which are attached DNA probe sequences corresponding to multiple genes in the target organism (Fodor *et al.*, 1991). Target RNA is reverse transcribed into tagged complimentary DNA (cDNA) sequences and washed over the chip surface to hybridise with the corresponding probe sequences on the chip surface, whereby annealing is quantified using the tagged cDNA (Nguyen *et al.*, 1995a, Schena *et al.*, 1995, Lashkari *et al.*, 1997). Initially used as an aid to sequencing, the application of microarrays for determining differential gene expression on a large scale was rapidly adopted (Schena *et al.*, 1996, Duggan *et al.*, 1999). The main issues of reproducibility, sensitivity and specificity have been addressed, and much data has been made freely available, to the point that confidence in the accuracy of the technology for expression studies is high within the scientific community (Brazma *et al.*, 2001, Barrett and Edgar, 2006, Shi *et al.*, 2006, Barrett *et al.*, 2007, Parkinson *et al.*, 2007, Shi *et al.*, 2008, Shi *et al.*, 2010).

1.3.1 Cluster Based Analysis

Cluster analysis is a multivariate technique that is frequently adopted when there is little knowledge of the overall dynamics taking place within the sample. The technique investigates the similarity between all the samples, termed *n*-dimensional vectors, within a population to yield an answer based upon the grouping together of similar entities. Within the context of gene expression differential this is accomplished through calculation of the correlation distance by determining whether any two *n*-dimensional vectors increase or decrease in the same way (Butte and

Kohane, 2000). False significance is a hazard of this type of multiple-testing architecture whereby outliers can have a pronounced effect on measured distances throughout the sample. Normalisation of the data is therefore key prior to starting analysis although multiple resampling to adjust the *p*-value or confidence of the clustering is typically applied (Westfall, 1993) and includes techniques such as 'bootstrapping' (Felsenstein, 1985, Zharkikh and Li, 1995) and 'permutation' (Edgington, 1964) to ensure some 'goodness-of-fit' measurement. To gain a better understanding of the biological significance within a cluster network the weighting of similarities between samples is typically applied whereby the weight of the link signifies the strength of the connection (Zhang and Horvath, 2005).

BioLayout *Express*^{3D} (The Roslin Institute & R(D)SVS, Easter Bush, UK) network analysis software provides a cluster based approach to systems biology analysis of gene expression by generating a three dimensional network graph where nodes, representing individual genes, are connected to each other based upon their co-expression with other genes throughout the entire sample (Freeman *et al.*, 2007, Theocharidis *et al.*, 2009). The software has the ability to accommodate very large datasets and automatically calculates the Pearson correlation matrix, edge weighing and *p*-value confidence. The threshold matrix cut-off above which relationships are plotted is user defined thus allowing the number of calculations for similarities between samples, and the resulting clustering complexity, to be controlled. Graphs are produced in a three dimensional environment that efficiently removes the requirement to manipulate the layout as a compromise between logic and aesthetics in an effort to fit the data with the confines of a given space. BioLayout *Express*^{3D} negates the necessity of identification of gene origin to explain potential contribution within the network. A gene is clustered in a three dimensional neighbourhood with other genes sharing a similar expression both in intensity and, if part of a serial analysis, time of expression. BioLayout *Express*^{3D} therefore provides a visual and unbiased instrument for identification of a gene both in terms of shared origin with other genes and expression differentiation.

1.4 Thesis Aims

The aim of this thesis was to use mouse-adapted Scrapie prion disease as an *in-vivo* model of neurodegeneration to determine the role of microglia during neurodegenerative disease development. Microglia are crucial for healthy homeostatic function and recent research has uncovered the intricate nature of microglia interaction with other cells in the central nervous system and the impact this has on neurodegenerative diseases. Furthermore microglia are not the only source of immunomodulators and other cells found in the brain can also impart a marked influence on the surrounding environment (Sheng *et al.*, 1997, Schultz *et al.*, 2004, Norden *et al.*, 2014). The current literature portrays microglia in neurodegenerative diseases as down-regulated or 'atypical' in their overall response. Separating the specific microglial contribution towards the overall immune signature seen in neurodegenerative diseases has not yet been performed.

The first part of this thesis explored the inflammatory response found within mouse-adapted prion disease using previously published total brain transcriptome data. This was analysed using the novel cluster-based analysis tool BioLayout *Express*^{3D} which confirmed the majority of differential expression was microglial in origin. A consistent microglial signal occurred regardless of the length of disease incubation period, disease severity or mouse background and increased in strength as the disease progressed. A considerable number of genes could not be attributed to any one cell type and it was not possible to further separate the signal indicative of an extremely high degree of co-expression by microglia and the other cell types found in the brain. A mouse model of prion disease was then characterised using a novel strain of mice in which microglia were tagged with a ubiquitously-expressed green fluorescent protein transgene. Following confirmation that the transgene and fluorescent protein made no impact to disease the specific areas of microglial activity were then determined.

The second half of the thesis covers time course mouse experiments in which morphological changes made by microglia in response to prion disease were quantified using the green fluorescent protein and image analysis software. The aim was to determine if microglia are significant contributors towards a neurotoxic environment resulting from disruptions to normal homeostasis. Using the same time points as the preceding experiments the final results chapter reports on the successful isolation of adult microglia from infected mice and the analysis of their transcriptome using BioLayout *Express*^{3D}. This allowed for determination of the specific response of microglia in prion disease.

2 Re-analysis of the Brain Transcriptome of Multiple Mouse Strains Infected with Multiple Strains of Prion Disease.

2.1 Introduction

This chapter describes the re-analysis of a previously published microarray dataset using the novel biological network analysis tool BioLayout *Express*^{3D} (Freeman *et al.*, 2007). In 2009 a large scale prion disease study made by Hwang *et al.* (2009) argued to have identified a core set of disease associated markers shared by many different prion disease pathologies. The data was freely available (http://prion.systemsbiology.net) to download thereby facilitating re-analysis and reinterpretation. By choosing to reanalyse a previously published dataset this chapter was able to determine the disease associated signature associated with murine-adapted prion disease in both wild type and *Prnp* transgenic mice and determine the overall contribution of microglia within the signal.

The original study identified a glial cell response as part of the developing pathology but the proportion of genes associated with an immunological response was felt not to be in accordance with other studies in which neuroinflammation was noted (Brown *et al.*, 2003, Riemer *et al.*, 2004, Brown *et al.*, 2005). The study by Hwang *et al.* (2009) focused on the contribution of toxic prion replication within neuronal lipid rafts. Furthermore the explanation for the presence of lysosome markers and cytoskeletal processing was attributed to neuronal prion protein processing. In part, this prompted this re-analysis using BioLayout *Express*^{3D} to better determine gene origin as it was felt that many of those genes attributed to be neuronal in origin could equally be associated with the innate immune system.

The study of Hwang *et al.* (2009) described how pathological differences of prion disease are not due to inherent properties of any given strain and that differences in incubation time and severity are due to specific interactions between the individual host and prion strain. Accordingly two prion inoculates were utilised; Rocky

Mountain Laboratory (RML) derived from a mixture of mouse adapted Drowsy goat Scrapie strains (Dickinson, 1976), and 301V derived as a pure strain from Bovine Spongiform Encephalopathy (BSE) adapted to mice (Bruce *et al.*, 2002), were chosen for their marked differences in incubation time and pathological hallmarks within a single inbred mouse strain. These were inoculated into C57Bl/6 strains homozygous for either *a* and *b* alleles of *Prnp* and FVB/NCr (FVB) homozygous for the '*a*' allele. The generation of a heterozygous strain for *Prnp,* by crossing FVB.1290*Prnp*^{tm1Zrch} with FVB mice, expressed a reduced PrP^{C} level and accordingly demonstrated a dramatic increase in the incubation period but not intensity of the disease (Manson *et al.*, 1994b). By direct contrast the study adopted (FVB-Tg(PrP-A)4053 indicator mice (Tg4053) over-expressing the *Prnp a* allele >30 times over normal levels (Carlson *et al.*, 1994) in which incubation times are considerably shorter.

It becomes increasingly difficult to distinguish general disease damage from prion-specific response at the later stages of the incubation period and in particular just prior to terminal disease (Booth *et al.*, 2004). The importance of time points early on in disease pathogenesis is paramount and unfortunately few studies have this broad number of time points taken during the earlier events of prion disease. It was in this area of contention in which the study by Hwang *et al*., had significant power over all other RNA analysis studies courtesy of the sheer number of serial investigative points throughout disease progression in multiple mouse and prion strain combinations.

Finally, the data were freely available (http://prion.systemsbiology.net) to download thereby facilitating re-analysis and reinterpretation. By choosing to reanalyse a previously published dataset this chapter was able to determine the disease-associated signature associated with murine-adapted prion disease in both wild type and *Prnp* transgenic mice and determine the overall contribution of microglia within the signal.

2.2 Methodology

2.2.1 Origins of Data: Mouse Inoculations by Hwang et al., (2009)

Using a systems biology approach, Hwang *et al*., (2009) adopted a multiple host/strain combination study to generate eight prion/mouse strain combinations (summarised in Table 2-1). Their aim was to ascertain the differentially expressed genes (DEGs) involved in prion disease pathogenesis regardless of individual host and prion strain combinations. Mice were inoculated by an intracerebral (i.c) route at 5 weeks with either 10 µl of 10% RML or 301V infected mouse brain material. Mice inoculated with normal brain homogenate acted as age and genotype matched controls to eliminate perturbations resulting from both inoculation and the effects of ageing. Three mice from each group were harvested at 1, 2 or 4 week intervals depending upon the length of incubation period to provide 8 - 10 samples across the entire incubation range.

The group felt that pathological differences of TSE disease are not due to inherent properties of any given strain and reflected that differences in incubation time and severity are due to specific interactions between the individual host and TSE strain. Accordingly two TSE strains; RML derived from mouse adapted Drowsy goat Scrapie strains (Dickinson, 1976), and 301V derived from mouse adapted BSE (Bruce *et al.*, 2002), were chosen for their marked differences in incubation time and pathological hallmarks within a single inbred mouse strain. These were inoculated (summarised in Table 2-1) into C57Bl/6 strains homozygous for either *a* and *b* alleles of *Prnp*, FVB/NCr (FVB) homozygous for the '*a'* allele. The generation of a heterozygous strain for *Prnp,* by crossing FVB.1290*Prnp*^{tm1Zrch} with FVB mice, expressing a reduced PrP^{C} level and accordingly demonstrate a dramatic increase in the incubation period but not intensity of the disease(Manson *et al.*, 1994b). By direct contrast the study adopted (FVB-Tg(PrP-A)4053 indicator mice (Tg4053) over-expressing the *Prnp a* allele >30 times over normal wild type levels (Carlson *et al.*, 1994) in which incubation times are considerably shorter.

Table 2-1: Number of microarrays arranged by murine and prion strains as utilised in the original study by Hwang et al., (2009). The aim was to generate murine disease encompassing multiple differing phenotypes in an effort to identify the core differentially expressed genes shared by all combinations.

Mouse Strain	*Prnp* genotype	*Prion Strain*	*Incubation (Weeks)*	*N° of Time Points*	*N° of Infected Arrays*	*N° of Control Arrays*
C57BL/6J	*a/a*	RML	23	12	31	45
C57BL/6J	*a/a*	301V	41	10	25	
C57BL/6.I-1	*b/b*	RML	52	11	27	39
C57BL/6.I-1	*b/b*	301V	18	9	27	
FVB/NCr	*a/a*	RML	22	11	33	34
FVB-Tg(PrP-A) 4053	> 30*a*	RML	8	8	24	22
(FVBxFVB.129*Prnp*^{tm1Zrch}) F1	*a/0*	RML	56	14	32	33
FVB x FVB.129*Prnp*^{tm1Zrch}	*0/0*	RML	51	7	22	24

Table 2-2: Number of microarrays arranged by murine and prion strains incorporated in this re-analysis following global background quality control. A total of 32 arrays failed this process and were not investigated any further.

Mouse Strain	*Prion Strain*	*Incubation (Weeks)*	*N° of Time Points*	*N° of Infected Arrays*	*N° of Control Arrays*	*Mean N° of Arrays per Group*
C57BL/6J	RML	23	12	27	38	2.50 ± 0.27 SE
C57BL/6J	301V	41	10	25		2.29 ± 0.19 SE
C57BL/6.I-1	RML	52	11	25	34	2.36 ± 0.20 SE
C57BL/6.I-1	301V	18	9	27		2.50 ± 0.22 SE
FVB/NCr	RML	22	11	29	34	3.00 ± 0.00 SE
FVB-Tg(PrP-A) 4053	RML	8	8	22	20	2.41 ± 0.23 SE
(FVBxFVB.129*Prnp*^{tm1Zrch}) F1	RML	56	14	31	31	2.68 ± 0.22 SE
FVB x FVB.129*Prnp*^{tm1Zrch}	RML	51	7	20	23	2.50 ± 0.27 SE

2.2.2 Data Handling for Re-analysis

Formatting and analysis of the datasets used in this study were processed as per the pipeline in Figure 2-1.

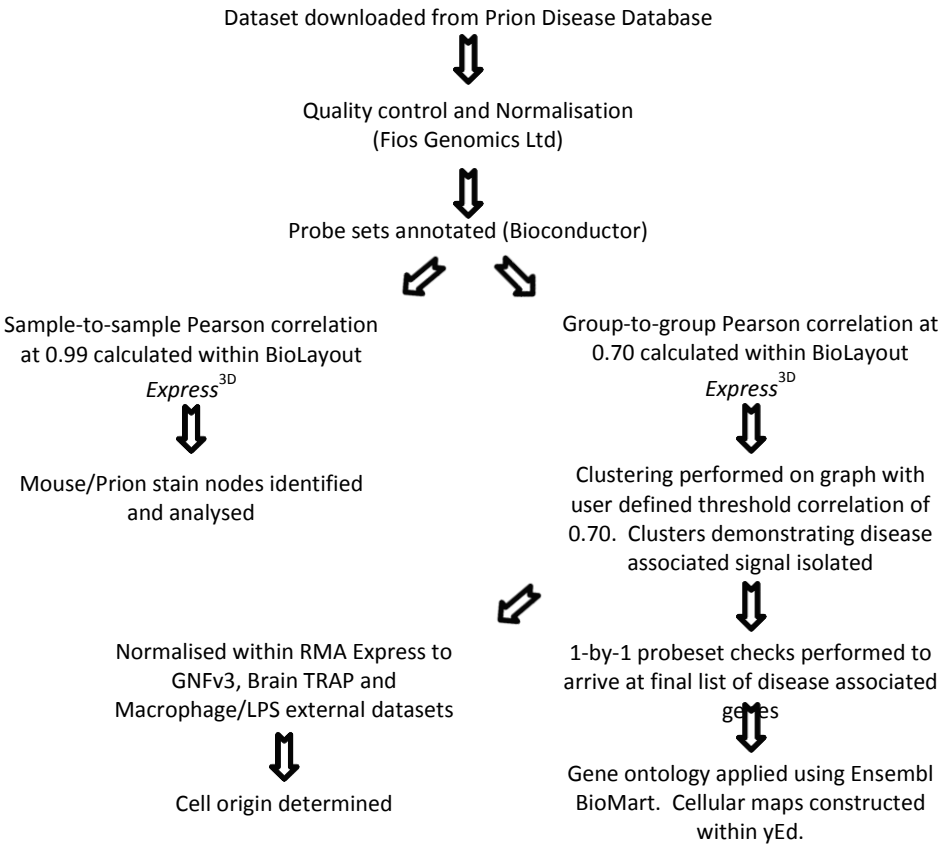

Figure 2-1: Analysis workflow pipeline.

Quality Control and Normalisation

The Affymetrix microarray data assembled from the time course inoculations of mouse strains C57BL/6J, C57BL/6I, FVB/NCr, FVB-Tg(PrP-A)4053, (FVB x FVB.129-*Prnp*^{tm1Zrch}) F1 and FVB.129-*Prnp*^{tm1Zrch} with RML and 301V were downloaded as 418 .CEL files from the Prion Disease Database (Gehlenborg *et al.*, 2009).

Quality control on downloaded raw .CEL data was performed independently by Fios Genomics Ltd (Edinburgh, Scotland) using the ArrayQualityMetrics package available from Bioconductor (http://www.bioconductor.org). To identify outlier arrays, those which demonstrate significant variations generated during labelling, hybridization and scanning; a system scoring was performed on each chip based upon evaluation of MA-plot, boxplot, heatmap, relative log expression (RLE) and spatial distribution of log-intensity (Kauffmann *et al.*, 2009) metrics. A chip was considered an outlier and removed from the dataset if it failed on one or more metrics. Quality control removed 32 microarrays leaving 386 as the final data set for re-analysis (Table 2-2). The loss of arrays yielding an overall mean average of 2.5 ± 0.08 SE arrays per time point and thus did not affect the overall balance of the dataset. Following global background quality control, normalisation of individual data sets generated from .CEL files was undertaken using the Robust Multiarray Average (RMA) expression measure (Irizarry *et al.*, 2003). The RMA Express program (http://rmaexpress.bmbolstad.com) is a stand-alone graphic user interface that operates as a quintile normalization technique to reduced gene-to-gene variation. The aim is to set the distribution of probe intensities the same for each array in the dataset (Bolstad *et al.*, 2003). The remaining perturbation between arrays is of biological significance and not an artefact of intensity variation.

Normalised data was saved as an '.expression' file and Affymetrix chip probe set identifications were annotated using the latest Affymetrix Mouse Genome 430 2.0 Array annotation available from Bioconductor (http://www.bioconductor.org) including global gene name, function, pathway if known and a unique identifier

comprising probeset ID concatenated to gene symbol. Samples were ordered in terms of the strain of mouse/prion agent and the relative incubation period from which the brain sample was derived.

2.2.2.1 Sample-to-Sample Data Analysis

Normalised data was loaded into BioLayout *Express*^{3D} with the matrix threshold cut-off set at 0.99; set at this high value to visualise the differences in correlation that were not present at < 0.98. Here nodes were assigned to classes corresponding to animal background, uninfected control group (regardless of strain) and prion infected groups subdivided into a gradient representation of the serial time points across the disease pathology.

2.2.2.2 Group-to-Group Data Analysis: Selection of Genes of Interest

With a Pearson correlation matrix cut-off threshold set to r = 0.7 within the user interface of BioLayout *Express*^{3D}, the annotated .expression files were loaded into BioLayout *Express*^{3D} and pairwise correlations were calculated for each probeset on the array against all other probesets ($P^2/2$ pairwise calculations, where P is the number of probesets) and values of $r \geq 0.7$ were saved as a binary '.pearson' file for future analysis.

BioLayout *Express*^{3D} correlation threshold was set at 0.75 to limit the number of edges to a manageable number and allow for visualisation of biological relationships that demonstrate a statistically significant perturbation in correlation. This formed a highly structured graph consisting of nodes (probesets) connected by edges of expression correlation.

To identify groups of co-expressed genes, clustering of the graph was performed using the graph based Markov clustering (MCL) algorithm (Dongen, 2000) which has been designed to function with weighted or non-weighed graphs. The algorithm

operates on the principle of generating artificial paths through the data from which Markov stochastic matrices apply the mathematical results of the random walks directly to the graph. Using the expression viewer it is possible to observe the expression of probe sets in each cluster and identify those demonstrating biological interest.

2.2.2.3 Expression Analysis

The expression profile of each cluster was viewed, as a mean, in the class viewer function within BioLayout *Express*^{3D}. 9 clusters (here on termed 'clusters of interest') were identified as differentially expressed during disease. Annotations for each of these clusters was isolated into a new expression file generating a new graph of 671 probesets demonstrating differential expression in response to prion disease.

Disease association was viewed within BioLayout *Express*^{3D}. Probesets with a poor profile in which the expression profile was not sharp or had a considerable amount of signal noise were removed. Probeset duplicates were removed by keeping only the expression profile with the highest difference in expression. This left a dataset comprising 492 genes in which there was high degree of user confidence.

2.2.3 Ontological Analysis

2.2.3.1 Ensembl Biomart Derived Functional Ontology

Functional ontology was determined by uploading the Affymetrix chip ID of the disease associated genes to the online Ensembl Biomart data mining tool (ensembl.org/biomart) using the *Mus musculus* genes dataset (Ensembl Genes 66). Filters were applied restricting results to the Affymetrix 430 2.0 chip probe sets. To increase accuracy for correct selection of function, filters for gene ontology evidence code, domain and name were applied with experimental evidence codes preferred.

2.2.3.2 Known and Predicted Protein-Protein Interactions

The 492 disease associated genes were uploaded as a multiple sequence to the online Search Tool for the Retrieval of Interacting Genes/Proteins (STRING) (http://string-db.org)(Jensen *et al.*, 2009) and predicted associations attributed to *Mus musculus*. Within the network view, edges were restricted to evidence based prediction for co-expression, experimental and database determined interactions. Clustering was performed dynamically by initiating the relaxation feature to force nodes to adopt a distance proportional to the STRING global score. Grouping based on shared co-interaction was performed using the inbuilt MCL function with an inflation value of 2.0.

2.2.3.3 Cell Origin: Normalisation with the Cultured Macrophage, Mouse Brain RNA Trap and GNFv3 Mouse Tissue Datasets

Cell origin was determined with reference to external datasets derived from purified central nervous system cells found in the GNFv3 (Su *et al.*, 2002, Wu *et al.*, 2009) and mouse brain RNA TRAP datasets (Doyle *et al.*, 2008, Heiman *et al.*, 2008). Also Included were datasets derived from serial macrophage cultures subjected to lipopolysaccharide (LPS) bacterial endotoxin (Lattin *et al.*, 2008). The LPS datasets were included to allow for labelling of those genes associated with activation of the innate immune system. The strong inflammatory reaction by macrophages to LPS is well characterised and involves the majority of cellular inflammatory mechanisms (Ulevitch and Tobias, 1995).

Mouse brain cell type data from the external datasets were loaded into the '.expression' file for the genes demonstrating differential expression in response to prion disease. Overlaps between Affymetrix chip probeset identifications were filtered to both confirm the validity of using the external datasets and identify the required .CEL files.

The chosen .CEL files data for both the external datasets and the Prion Disease Database derived genes datasets were then loaded into the RMA Express (http://rmaexpress.bmbolstad.com) GUI program and the former normalised to match the previously normalised Prion Disease Database derived genes of interest. Following normalisation the genes demonstrating differential expression in response to prion disease were then identified from the normalised GNFv3 mouse tissue dataset through chipset annotation. These genes were then incorporated into the '.expression' file to allow for a direct comparison to be made on the origin of expression profile with a known cell type in the brain.

2.3 Results

2.3.1 Sample to Sample

Sample-to-sample graph analysed in BioLayout *Express*^{3D} with a matrix cut-off threshold set to 0.99 generating an organised graph with a divide based upon mouse background (Figure 2-2A). The matrix threshold determines which nodes are incorporated into the graph. This was based on whether they correlate to other data within the dataset above the set threshold. Nodes would only be incorporated if they satisfied this user set level and at 0.99 the threshold matrix is sufficiently high for this to be independent of differential expression and produce a graph comprising nodes with only extremely high correlation with others. No divide was observable at a threshold of 0.98 in which all nodes were found to be correlating with each other.

Each mouse/prion combination was assigned a different colour incorporating both infected and normal brain controls. The number of nodes dropped to 378 joined by 17853 edges, a result of the matrix filter set to display only the high correlation relationships between chipsets. The lower divide contained solely the C57BL strains inoculated with both RML and 301V whilst the upper encompassed the remaining strains inoculated with RML alone hinting at a slight variation in the host immune response specific to C57BL mice.

The lack of a significant change in differential expression when all infected and uninfected source nodes were highlighted in one colour prompted a need to determine if there was a difference when the infected nodes were coloured corresponding to their time of capture within the disease incubation periods. To achieve this each infected serial time point was given a scaled colour ranging from white at disease initiation then changing through increasing darkening shades of yellow, orange and finally ending with red at terminal disease (Figure 2-2B). An outward pattern in the infected datasets could be observed as signifying a reduction

in correlation, and consequently an increase in difference, between earlier and later stages of disease progression.

The nodes for both infected and uninfected samples were then assessed according to animal background and each given a new colour; red for infected and white for controls (Figure 2-2C). The distribution of nodes analysed according to mouse background can be visualised as forming loose clusters with a degree of overlap in the centre of each divide. The difference in correlation between infected and control nodes was not immediately obvious. Interestingly, the lack of discernible pattern between nodes derived from infected brains and those from control animals suggested that the perturbation to gene expression in the developing pathology in prion disease is not particularly strong. The exception was the B4053 PrP^C overexpressing mice in which disease is very rapid. In the B4053 strain a clear difference could be determined between nodes from infected and those from an uninfected source hinting at a much greater impact on differential disease expression.

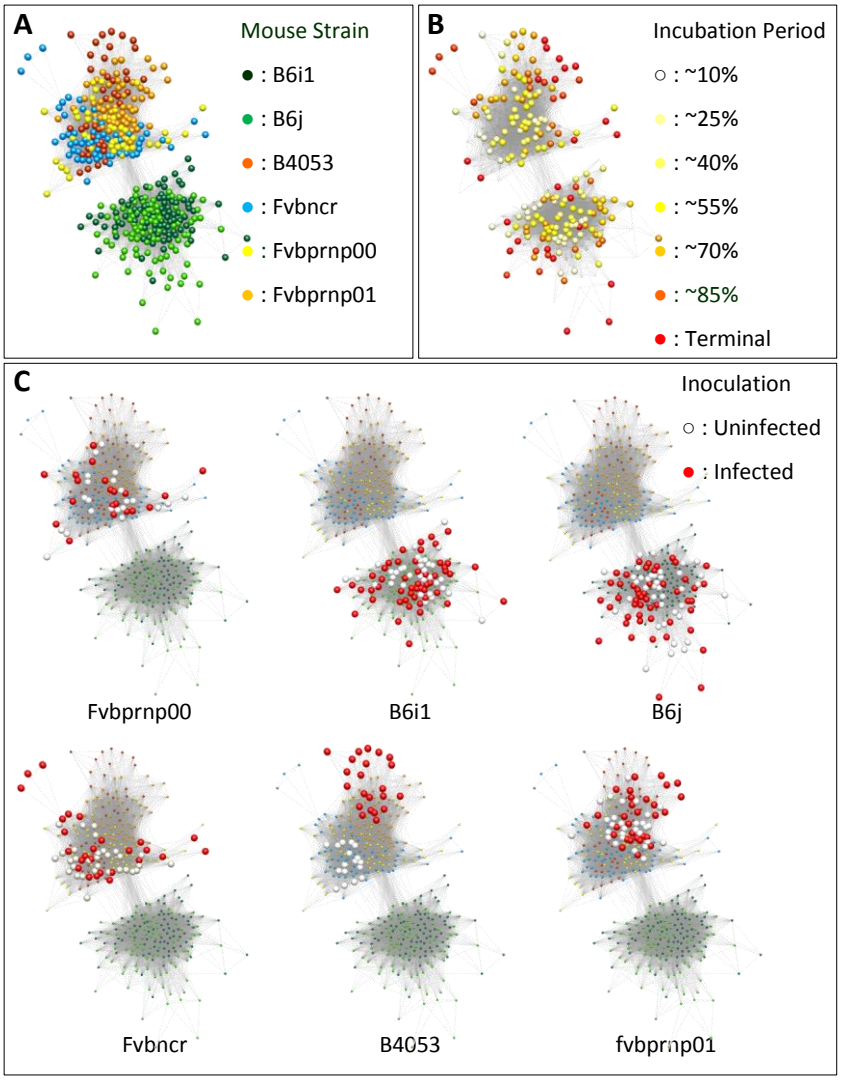

Figure 2-2: Global array sample-to-sample graphs revealed differences between prion infected and uninfected controls to be subtle. **A:** A threshold matrix cut-off set at >0.98 was required to visualise any difference between strains. Stains based on the BL/6 mouse background form a distinct cluster to the lower half of the graph. **B:** As disease progressed the datasets dissociate from both neighbours and earlier disease time points and migrate toward the outer edges of the cluster (from white to red). This reflected the slight reduction in correlation between nodes caused by a progressive increase in difference. **C:** Subtlety of differences in arrays induced by disease also evident when comparing infected and uninfected arrays for each strain. Note difference bought about potentially by the rapid and severe pathology in the PrP^{C} overexpressing B4053 mouse strain.

2.3.2 Group-to-Group: Genes of Interest

Transcript level prion infected microarray data within BioLayout *Express*^{3D} at a correlation threshold of 0.70 produced a highly organised graph comprising 21,550 nodes joined by 1,253,332 edges. A threshold of 0.70 was adopted as the difference in correlation at group (probeset) level was greater than sample (array) level and at group level produced a highly organised graph which allowed for visualisation of biological relationships. The graph was grouped by MCL into 416 clusters comprising 14253 nodes with the remaining 7297 assigned as 'no class'; the latter indicative of no correlation with other nodes in the graph at the designated correlation threshold. The clusters each represent probesets which have a high degree of correlation of expression and hence share a biological relationship. The expression profile of each cluster was viewed, as a mean, in the class viewer function within BioLayout *Express*^{3D}. Seven clusters comprising 692 probesets in close proximity to each other demonstrated a disease associated change in expression (Figure 2-3A). Out of the 333 genes identified in the original study by Hwang *et* al., (2009), 321 were taken through to the group-to-group graph at a correlation threshold of 0.70. These also predominantly resided in the same location. There were more outlying nodes with little correlation to the rest (Figure 2-3B). Note also that some of these were 'no-class' nodes and as such do not appear in Figure 2-3A.

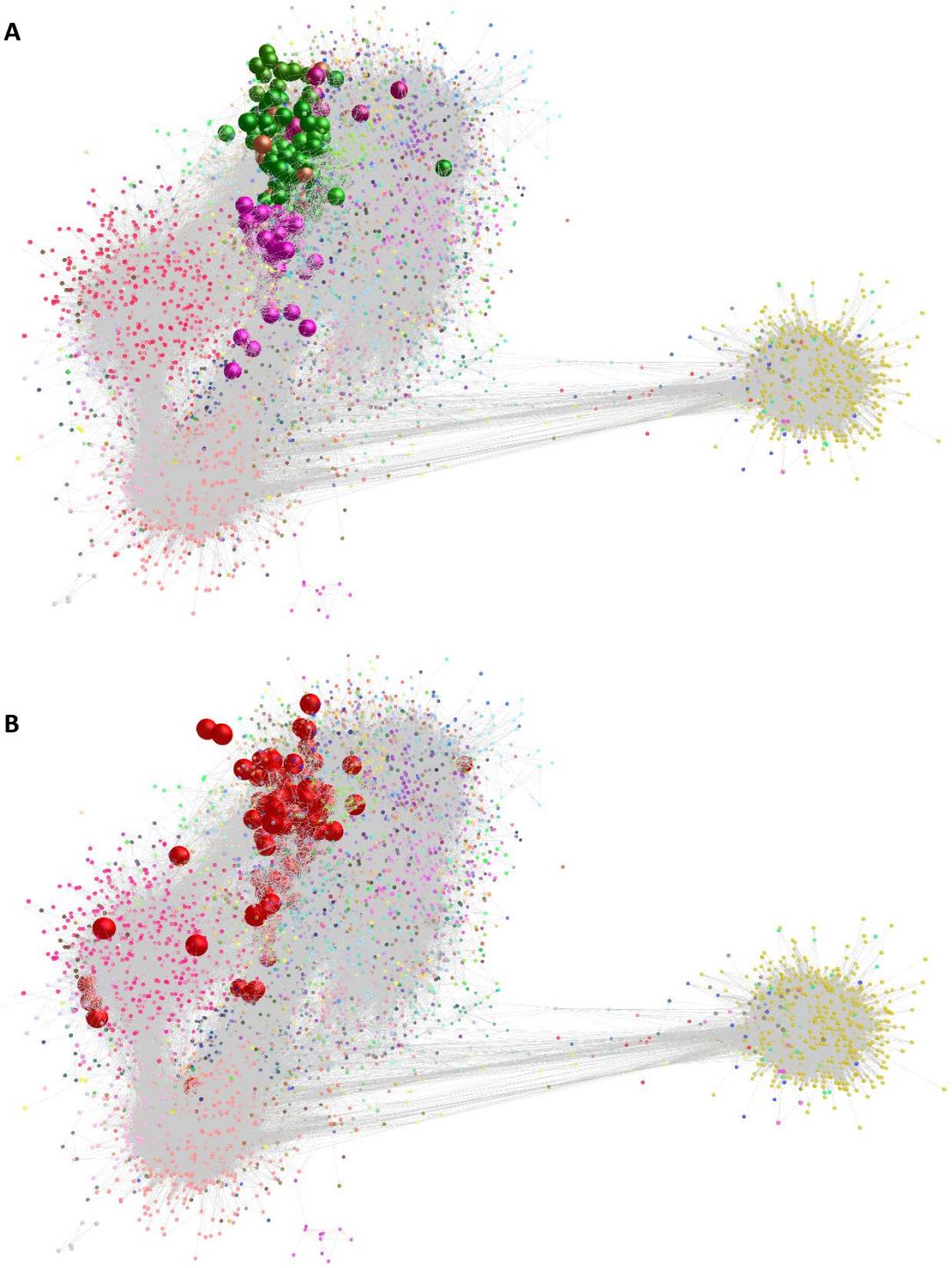

Figure 2-3: BioLayout *Express*^{3D} generated transcript-to-transcript clustered graph of total brain data obtained from all serial mouse/prion combinations. **A:** Comprising 142531 nodes (no-class nodes removed) and clustered by MCL revealed 416 highly organised clusters, each assigned a random colour, representing genes sharing a high degree of co-expression. Enlarged nodes represent the 692 nodes with an expression pattern indicative of disease association and in close proximity to each other indicative of a high degree of correlation. Note the purple nodes showing lower correlation towards the primary green cluster. **B**: Red nodes are the disease associated genes identified by Hwang *et* al., (2009) of which 321 are incorporated into the graph at a correlation threshold of .70.

Following removal of probeset duplicates the final number of disease associated genes identified in this study was 492. Visualising the 492 genes within BioLayout *Express*^{3D} with a correlation threshold set at 0.75 revealed a tightly grouped graph organised into 2 main clusters by MCL (Figure 2-4A). A threshold of 0.75 enabled the majority of the biologically significant data to be incorporated in the graph and allow for visualisation of biological relationships.

Clustering the differentially expressed genes identified by Hwang *et al*., (2009), at the same correlation threshold of 0.75, produced a graph of 321 nodes. This was also organised into 2 main clusters (Figure 2-4B). 21 nodes were not assigned to a class and correspond to the outliers seen in Figure 2-3B. In total 205 of the genes identified by the original study were taken through with this re-analysis. All genes followed a similar expression profile with an increase in expression starting at approximately 50% of the incubation period (Figure 2-4C). There was an expression bias of the secondary cluster towards BL/6 mouse strains.

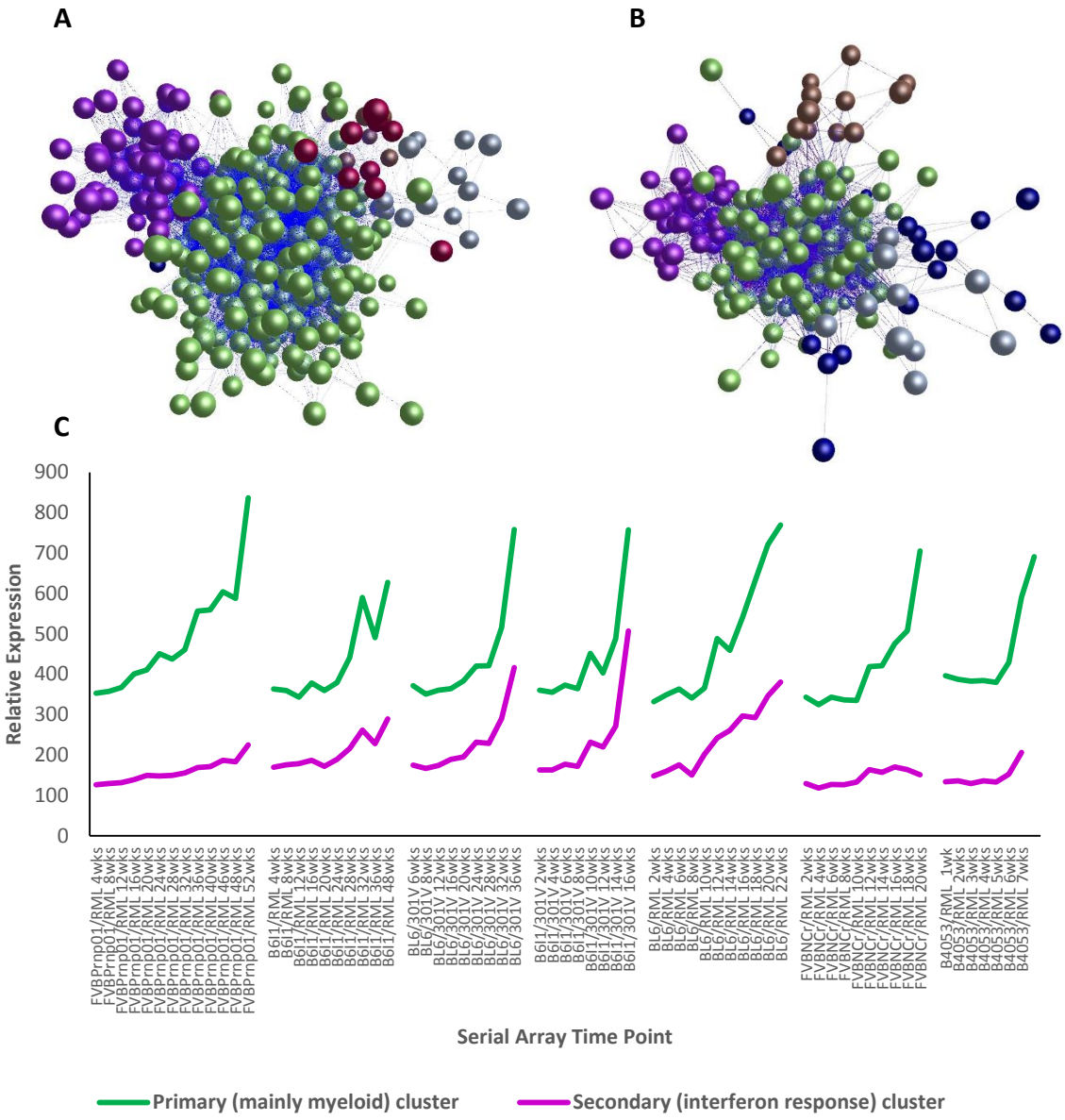

Figure 2-4: BioLayout *Express*^{3D} generated graphs at a correlation threshold of 0.75 from genes demonstrating a disease associated signal. **A:** The final list of 492 genes was organised into 2 main clusters by MCL with the primary cluster (green) comprising 410 nodes joined by 29339 edges indicating a high degree of co-expression between genes. The secondary cluster (purple) comprised 67 nodes and 1453 edges. **B**: Clustering the genes found in the original analysis by Hwang *et al.*, (2009) revealed 21 nodes (dark blue) that are not assigned to a cluster by MCL. The majority of the others (of which 205 are included in this re-analysis) are also grouped within two main clusters. **C:** Early up-regulation of disease signature at approx. 50% of incubation period. As a mean expression profile for all genes in the primary cluster, there is a very similar disease signature for all genes in all mouse/prion combinations. Expression for the secondary, mainly interferon response genes, is predominantly expressed higher in the BL/6 mouse strains.

2.3.3 Group-to-Group: Exploring the Graph.

Out of 416 clusters within the large group-to-group graph only 9 demonstrated a disease associated signal. These were determined following individual cluster-by-cluster checks of the expression signature within BioLayout Express3D for a profile that convincingly changed with disease pathogenesis. Those clusters that contained profiles that were unconvincing collectively comprised fully 97% of the available infected brain data. Ontological analysis within FuncAssociate was performed on the top 5 largest clusters to determine why these clusters were formed and what they comprised (Figure 2-5).

The largest (yellow), cluster 1, was unique as it showed the least correlation with the main graph and resided as a singular, but highly correlated, cluster some distance away on the periphery. The cluster comprised overwhelmingly of random metabolic genes although there was a small but highly enriched component for epithelium-associated keratin filaments. Considering the majority were not related to a specific function, the lack of correlation with the main graph was most likely influenced by differences in chip intensity or a batch effect.

The remaining clusters had relatively low levels of expression and an invariable profile with no evidence of association with the disease process. The formation of clusters by MCL within BioLayout Express3D is dependent upon a degree of shared co-expression between multiple gene nodes. Slight differences in what amounts to a majority of random metabolic genes in these clusters would suggest partial specialisation and enrichment statistics of 2, 4 and 5 indicate an association with organelle membrane, ribosome location and dendrite protection respectively. Both clusters 2 and 5 also included enrichment for nitrogen metabolism.

Cluster 57 was not one of the largest clusters but was included here to portray the effects of intermittent hybridisation. Cluster 57 was found to be highly enriched for hormone binding and contained probesets associated with the pituitary gland. Due

to the location of the gland it is entirely feasible for the gland to be variably collected during the procedure of brain removal due to human error and this would explain the entire absence of pituitary gland probesets on some arrays but not others. The variable inclusion is particularly striking in this dataset where, using RML infected BL/6 mice as an example, the genes are found only in 5, 7 and 9 weeks and absent from all other time points. The cluster therefore appears as a separate component in the graph with no correlation to the main dataset and was excluded from the dataset at an early stage

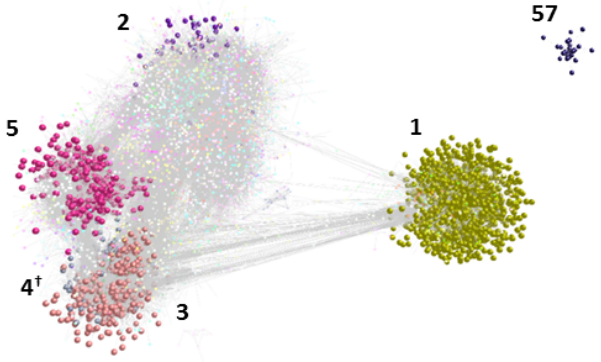

Cluster	Expression Profile (RML/BL6 Shown)	Gene N°	GO Enrichment (% of Gene N°)	*P* Value
1	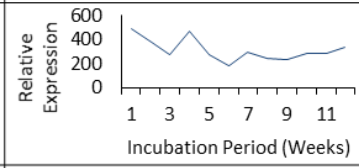	2604	• 0.6% Keratin filament*	6.2×10^{-7}
2	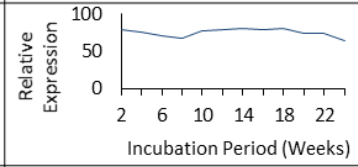	2237	• 10.9% Mitochondrion • 9.3% Organelle membrane • 22.6% Nitrogen metabolism	1.7×10^{-21} 2.2×10^{-19} 1.8×10^{-8}
3	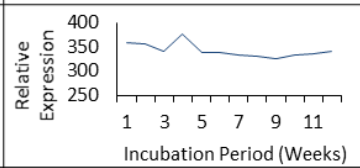	701	• Not Enriched	N/A
4	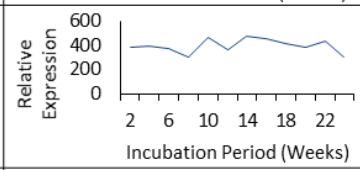	653	• 28.4% Localization • 14.7% Ribonucleotide binding	1.3×10^{-18} 1.7×10^{-14}
5	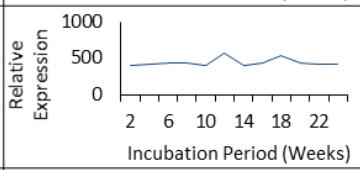	568	• 3.5% Ubiquitin-dependent - protein catabolism • 5.5% Neuron projection • 14.2% Nitrogen metabolism	7.4×10^{-7} 1.4×10^{-5} 1.4×10^{-5}
57	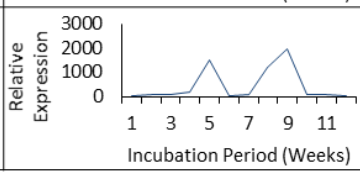	26	• 26.9% Hormone activity • 30.7% Receptor binding	1.1×10^{-11} 7.1×10^{-6}

Figure 2-5: Gene expression profiles and enrichment analysis for the top 5 clusters that were not associated with prion disease. The presence of enrichment is directly associated with the generation of a cluster based on levels of co-expression and explains the formation of these clusters. Cluster 57 contained genes associated with the pituitary gland and was included to demonstrate the effects of variable hybridisation.

2.3.4 Ontology

This was performed within BioLayout *Express*^{3D} with reference to the GNFv3 (Su *et al.*, 2002, Wu *et al.*, 2009), RNA TRAP (Doyle *et al.*, 2008, Heiman *et al.*, 2008) and finally serial cultured macrophages with lipopolysaccharide LPS endotoxin (Lattin *et al.*, 2008) to external datasets. A total of 377 genes out of 492 showed peaks in association with macrophages, microglia and osteoclasts confirming myeloid origin (Figure **2-6**). The remaining 115 were distributed among other the main CNS cell types either individually or as groups (Appendix 8-4).

Out of the 377 myeloid associated genes, 275 were associated with LPS activation of macrophages confirming the majority are also associated with innate immune system activation (Figure 2-7). An absence of a peak over LPS activated macrophages but a peak over microglia and pure macrophages was indicative of a constitutively expressed myeloid gene that is expressed independently of activation. The remaining 102 genes were classed as constitutively expressed myeloid genes. Many of the genes showed overlap in CNS cell origin and some transcripts were assigned to more than one cell type (Figure 2-8). BioLayout Express3D was also unable to further separate clusters (Appendix 8-3) providing additional support that many genes were expressed by more than one cell type.

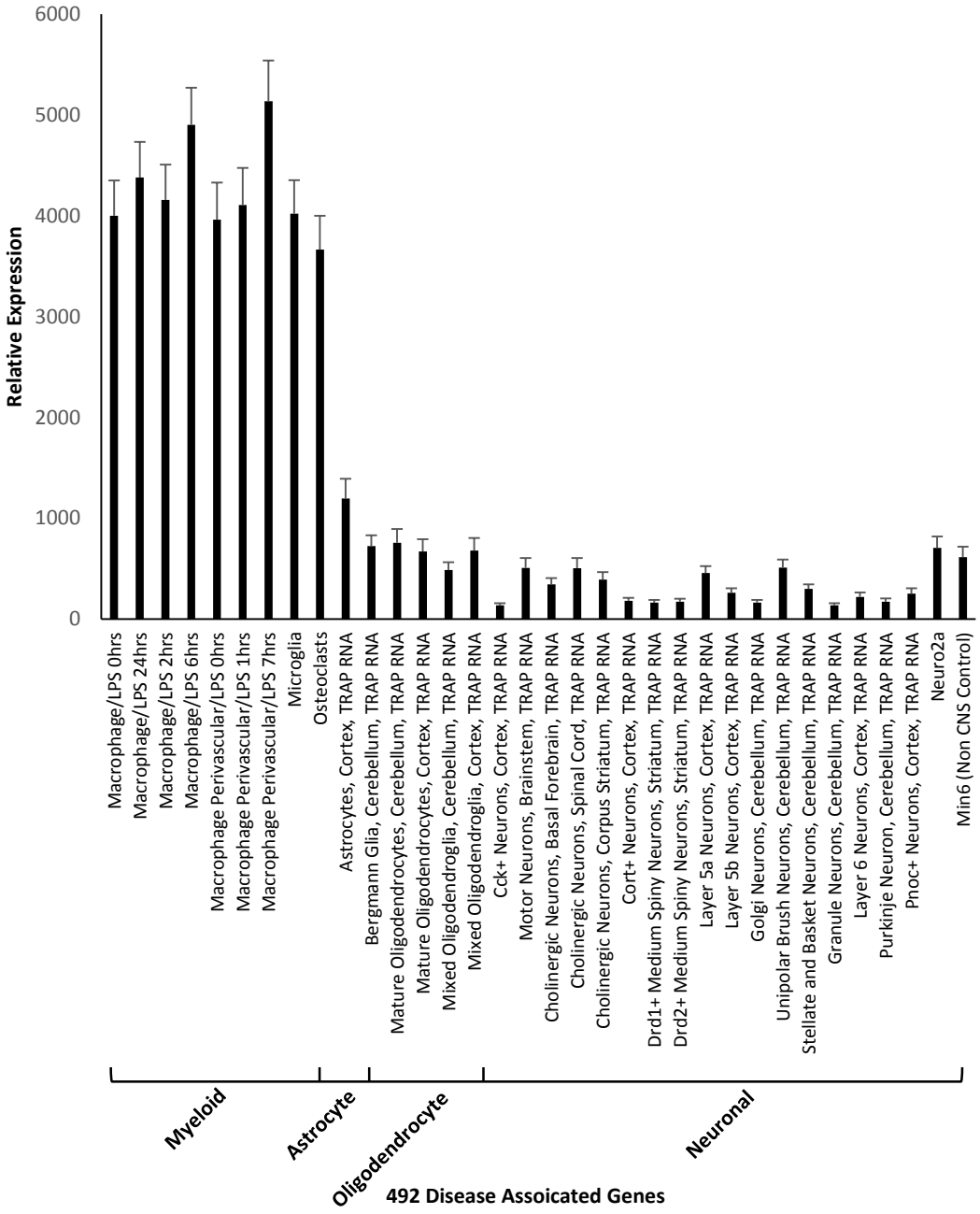

Figure 2-6: Cross reference of the expression data for 492 disease associated genes with co-normalised GNFv3, Trap and M0/LPS data within the expression viewer of BioLayout *Express*^{3D}. Shown as a mean expression profile, peaks are largest over myeloid associated purified cell datasets confirming the majority of the disease associated genes are microglial in origin. A considerable number are expressed by serially cultured macrophages activated with LPS confirming the genes are strongly associated with immune activation. Error bars equate to standard error.

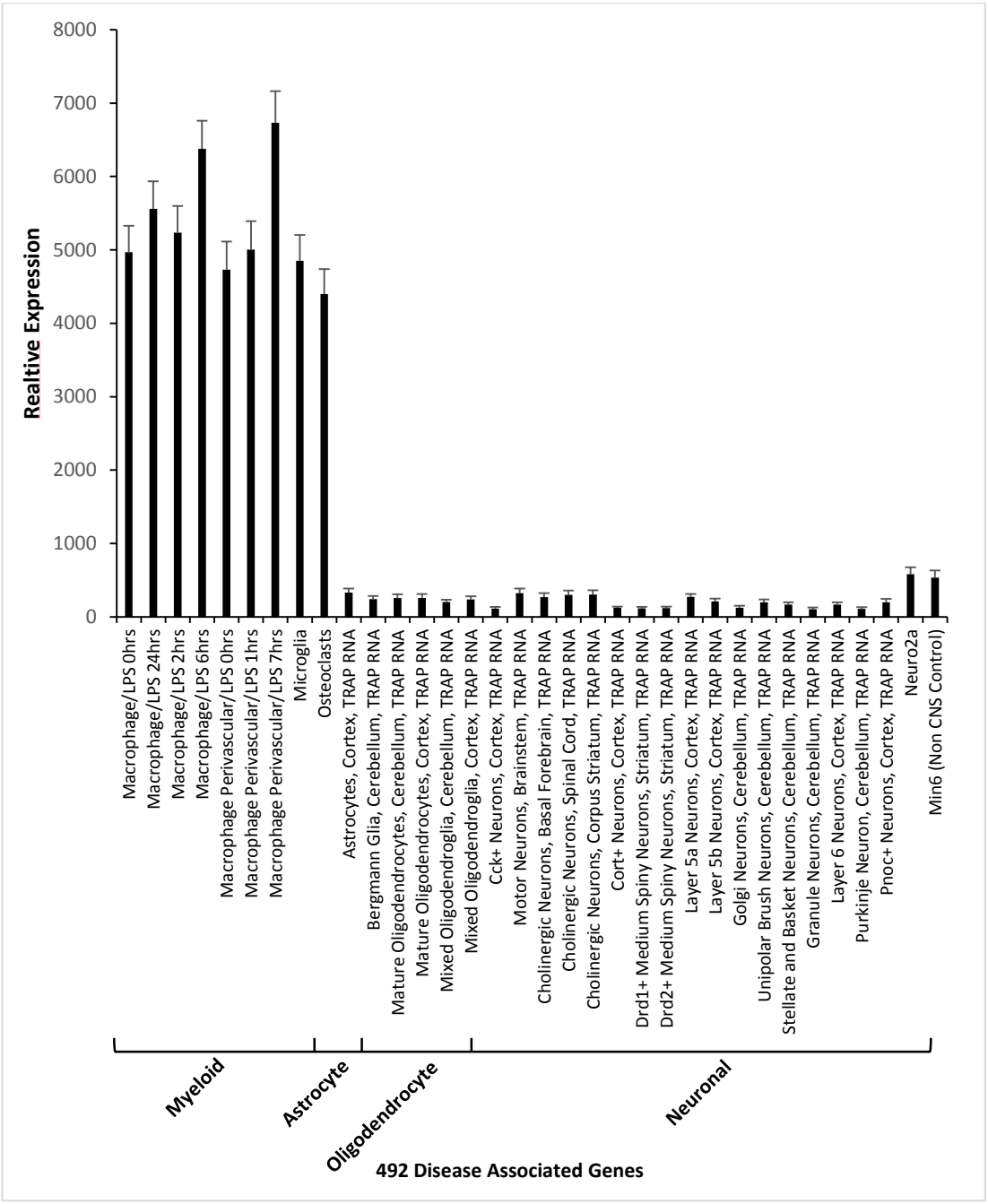

Figure 2-7: Cross reference of the expression data for the 377 myeloid specific genes with co-normalised GNFv3, Trap and M0/LPS data within the expression viewer of BioLayout *Express*^{3D}. Individually compared with the external datasets and view here as mean expression for all, the myeloid genes demonstrate nominal expression within other cell brain types. Error bars equate to standard error.

Myeloid & Astrocyte

CD9, Cd151, Clec5a, Cybrd1, Dhrs1, Efemp2, Eya4, Galnt4, Gfap, Gstm1, Klk8, Lpcat3, Ly86, Mtmr11, Npl, Nupr1, Pbxip1, Pdpn, Pnpla7, Prdx6, Retsat, S100a1, Sat1, Sh3pxd2b, Tlr3, Trf, Upp1, Vcam1, Zfp91

Myeloid & Neuron

A2m, Cyb5r3, Glipr2, Gpx1, Lgals1, Lgals3, Olfml3

Myeloid, Neuron and Astrocyte

Cd81, Cotl1, Cyp4v3, Dbi, Ifi27l1, Igfbp2, Itgb5, Ltc4s, Mt1, Mt2, Necap2, Npc2, Oat, Pdlim4, Rab31, Rab7l1, Rhbdf1, Rhoc, S100a13, Sh3glb1, Tmbim1, Tmem176a, Tmem176b, Tspan4, Ucp2, Vamp8, Vim

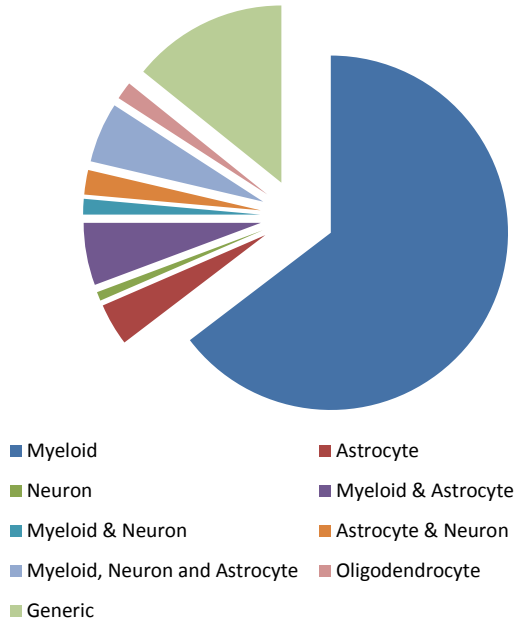

Astrocyte

Abhd4, Aldh1l1, Aqp4, Casp12, Chi3l1, Cyp4f14, Decr1, Fgfrl1, Gal3st4, Gm967, Id3, Naprt1, Plcd4, Plscr2, Prelp, Prrx2, Rbp1, Slc25a18, Sox9

Astrocyte & Neuron

Ccdc122, Fxyd1, Kcne1l, Lgi4, Lmcd1, Mlc1, S100a16, Slc14a1, Thbs3, Tsc22d4, Vwa1

Oligodendrocyte

Tppp3, Tmem98, Pdlim2, Klk6, Galntl2, Dbndd2, Apod, Adamtsl4

Neuron

Aldh1l2, Hspb8, Sema3d, Serping1

Myeloid

4632428N05Rik, A830007P12Rik, AA467197, Abi3, Adcy7, Adfp, AF251705, Aif1, Alox5ap, Anxa2, Anxa3, Anxa4, Arhgdib, Arpc1b, Aspg, Axl, B2m, Bcl2a1a, Bcl3, Brd4, C1qa, C1qb, C1qc, C3, C3ar1, C4b, Capg, Casp1, Casp8, Ccl12, Ccl2, Ccl3, Ccl5, Ccl6, Ccl8, Ccl9, Ccr5, Ccl6, Ccl8, Cd14, Cd37, Cd44, Cd48, Cd52, Cd53, Cd68, Cd72, Cd74, Cd84, Cd86, Cebpa, Cebpb, Ch25h, Clec4a3, Clec7a, Clic1, Cln3, Cmtm3, Cmtm6, Cmtm7, Cp, Crispld2, Csf1, Csf1r, Csf2rb, Csf3r, Cst7, Cstb, Ctsa, Ctsb, Ctsc, Ctsd, Ctsh, Ctsl, Ctss, Ctsz, Cxcl10, Cxcl13, Cxcl16, Cyba, Cybb, Ddx58, Ddx60, Dock2, Dtx3l, Ebi3, Edem1, EG667823 (Trim5), Emr1, Epsti1, Fas, Fcer1g, Fcgr1, Fcgr2b, Fcgr3, Fcgr4, Fcrls, Fermt3, Fgd2, Ftl1, Ftl2, Fuca1, Fxyd5, Fyb, Galnt6, Gbp2, Gbp3, Gbp3, Gbp6, Ggta1, Glipr1, Gmfg, Gngt2, Gns, Gpnmb, Gpr183, Gpr34, Gpr65, Gpr84, Gpsm3, Grn, Gusb, H2-Aa, H2-Ab1, H2-DMb2, H2-K1, H2-M3, H2-Q7, Havcr2, Hck, Hcls1, Hexa, Hexb, Hfe, Hmox1, Hpgd, Hsd3b7, Hvcn1, Icam1, Ifi204, Ifi205, Ifi27l2a, Ifi30, Ifi35, Ifi44, Ifi47, Ifih1, Ifit1, Ifit2, Ifit3, Ifitm3, Igtp, Iigp1, Ikzf1, Il10rb, Il13ra1, Inpp5d, Irf5, Irf7, Irf8, Irf9, Irgm1, Irgm2, Itgam, Itgax, Itgb2, Itpripl2, Kcnk6, Lag3, Lair1, Lamp2, Laptm5, Lat2, Lcp1, Lcp2, Lgals3bp, Lgals9, Lgmn, Lilrb4, Lpcat2, Lpxn, Lrrc33, Lst1, Ltbr, Ly9, Lyn, Lyz1, Lyz2, Mafb, Man2b1, Man2b2, Mdfic, Mmp12, Mpa2l, Ms4a6b, Ms4a6d, Ms4a7, Msn, Myd88, Myo1f, Naglu, Naip2, Naip5, Ncf1, Ncf2, Ncf4, Nckap1l, Nek6, Nfe2l2, Nlrc5, Oas1g, Oasl2, OTTMUSG00000000971, P2ry13, P2ry6, Parp12, Parp14, Parp3, Parp9, Phf20l1, Pld4, Plec1, Plek, Plp2, Plxnb2, Pon3, Pros1, Psmb8, Psmb9, Psme1, Psme2, Ptgds2, Ptplad2, Ptpn18, Ptpn6, Ptprc, Pycard, Pyhin1, Rab32, Rab3il1, Renbp, Rnase4, Rnaset2a, Rnf213, Rrad, Rsad2, Rtp4, S100a11, S100a4, S100a6, S1pr3, Samd9l, Samsn1, Sash3, Scpep1, Selplg, Sema4d, Sepx1, Sfpi1, Sgpl1, Sh3bp2, Shisa5, Siglec5, Siglech, Skap2, Slamf9, Slc11a1, Slc15a3, Slc29a3, Slc39a14, Slc43a3, Slc5a3, Slc7a7, Slfn2, Slfn8, Socs3, Spp1, Sqrdl, Srgn, Stat1, Stat3, Sulf2, Syngr2, Tagln2, Tap2, Tapbp, Tbxas1, Tcn2, Tgfb1, Tgfbr1, Tgfbr2, Tgif1, Tgm2, Thbs2, Tifa, Timp1, Timp2, Tln1, Tlr1, Tlr13, Tlr2, Tm4sf1, Tmem119, Tmem173, Tmem86a, Tnfaip2, Tnfaip8l2, Tnfrsf1a, Tor3a, Trem2, Trim25, Trim30, Trim34, Trim47, Trpt1, Tspo, Tyrobp, Ube1l, Unc93b1, Usp18, Vwa5a, Xaf1

Generic

1700112E06Rik, 5430427O19Rik, Afp, Aga, Ampd3, Angpt1, Atp6v0e, Avp, BC026585, Bdh2, Bmp2k, Capn3, Ccdc80, Cd9, Cebpd, Cklf, Clu, Cnn3, Col16a1, Cst3, Cyp7b1, Cyth4, D4Ertd22e, Dap, Ddr1, Dok1, E230029C05Rik, Ecm1, Emp1, Emp3, Entpd1, Ephx1, F13a1, Fam102a, Fam129b, Farp1, Fes, Fkbp7, Fzd9, Gba, Gbp6, Golm1, Gpr37l1, Hspb6, Idh2, Ifitm2, Igf1, Igsf6, Il33, Itpkb, Klhl6, Litaf, Lrrfip1, Mrps6, Nat2, Osmr, P2rx7, Palld, Phyhd1, Pik3ap1, Rgs10, Scamp2, Scrg1, Slco2b1, Spata13, Spsb1, Srebf1, Tax1bp3, Znrf2

Figure 2-8: The vast majority of the 492 genes are attributed to myeloid origin either as a single ontological association or mixed between cell types. There is a strong signal for innate immunity with a considerable number (coloured red) associated with innate activation of macrophages.

Determination of intracellular location and function of the myeloid component was investigated using ontology data from Ensembl Biomart. This facilitated construction of a cellular map of the myeloid genes found in the primary cluster which comprised the majority of the 492 genes (Figure 2-9) using yED graph editor software (http://www.yworks.com). In keeping with the results of cellular origin, data mining on Ensembl Biomart found genes associated with phagocytosis, endosomes/lysosomes and late innate immune response. Network edges formed from known protein-protein interactions gained from the STRING database revealed a compact self-contained system regulated by the cytokine ligating transcriptional regulator Stat1 (Figure 2-10). It is important to highlight that this map comprising only those genes demonstrating differential expression. The system spanned the entire cell ranging from extracellular lysozyme proteins to intercellular mediators of NADPH oxidase. Stat 1 is a key component of the JAK-STAT signalling pathway heavily involved in innate immune activation (Mowen *et al.*, 2001).

A strong interferon response was detected with almost a third of the total gene set found to be associated with the interferon system following data mining on Ensembl Biomart. The vast majority of these genes were found localised in the semi-separate secondary cluster (coloured purple in Figure 2-4). The majority of the genes in this cluster were BLl6 mouse in origin. The stronger interferon response characteristic of the C57BL/6 mice strains is well known (Schilling *et al.*, 2009) and resulted in the reduction in correlation of this cluster with the majority in the graph within BioLayout *Express*^{3D}. The interferon genes found in the primary cluster are almost exclusively myeloid associated.

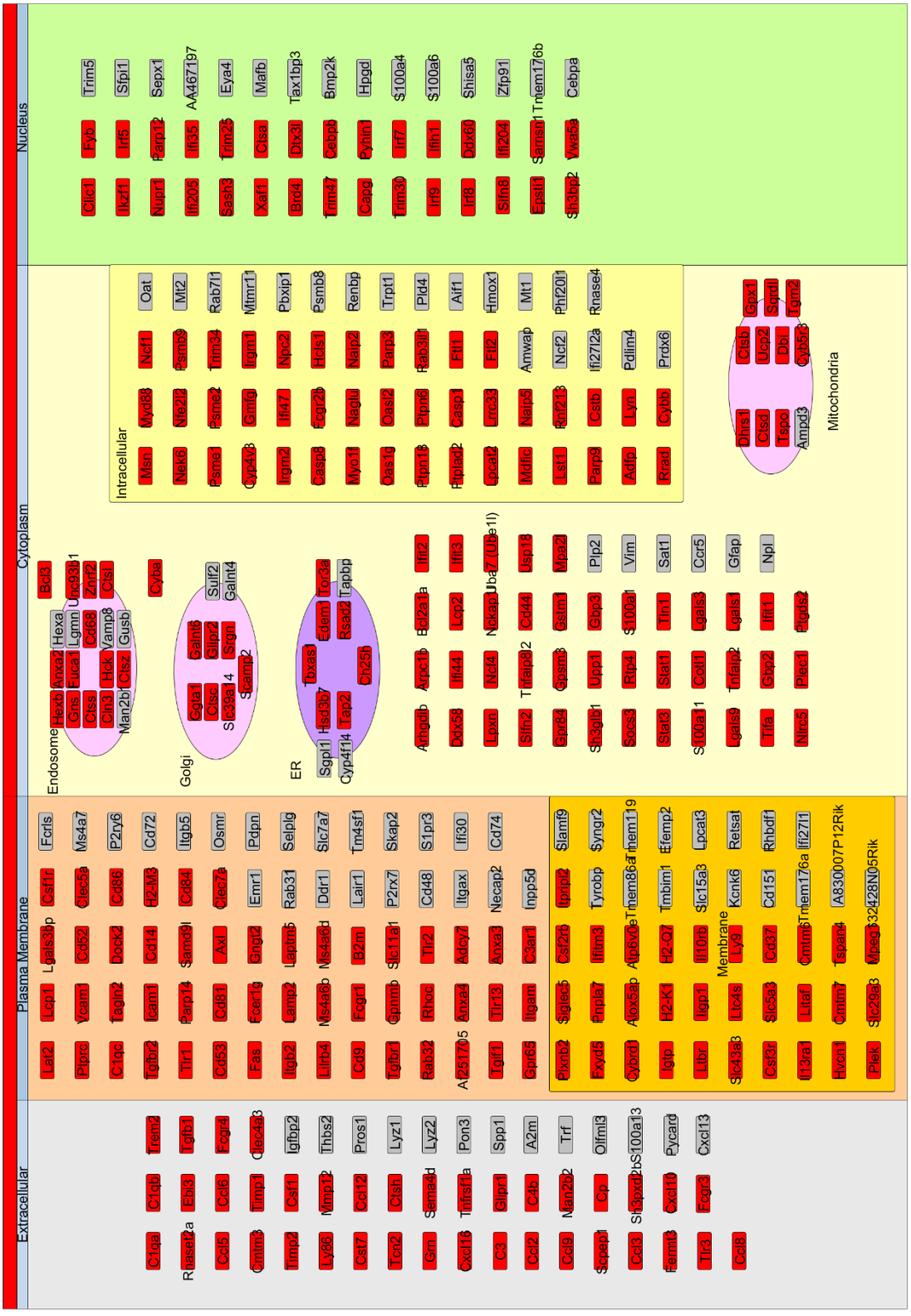

Figure 2-9: Cellular ontology map of myeloid genes found in primary cluster. The majority of genes found within the primary cluster were determined as myeloid in origin and are associated with innate immune activation of macrophages (red). The remaining genes (grey) are considered constitutively expressed macrophage genes. Collectively the signal is one of robust activation involving pro-inflammatory mediators, transcriptional regulation, cellular stress and the interferon response system.

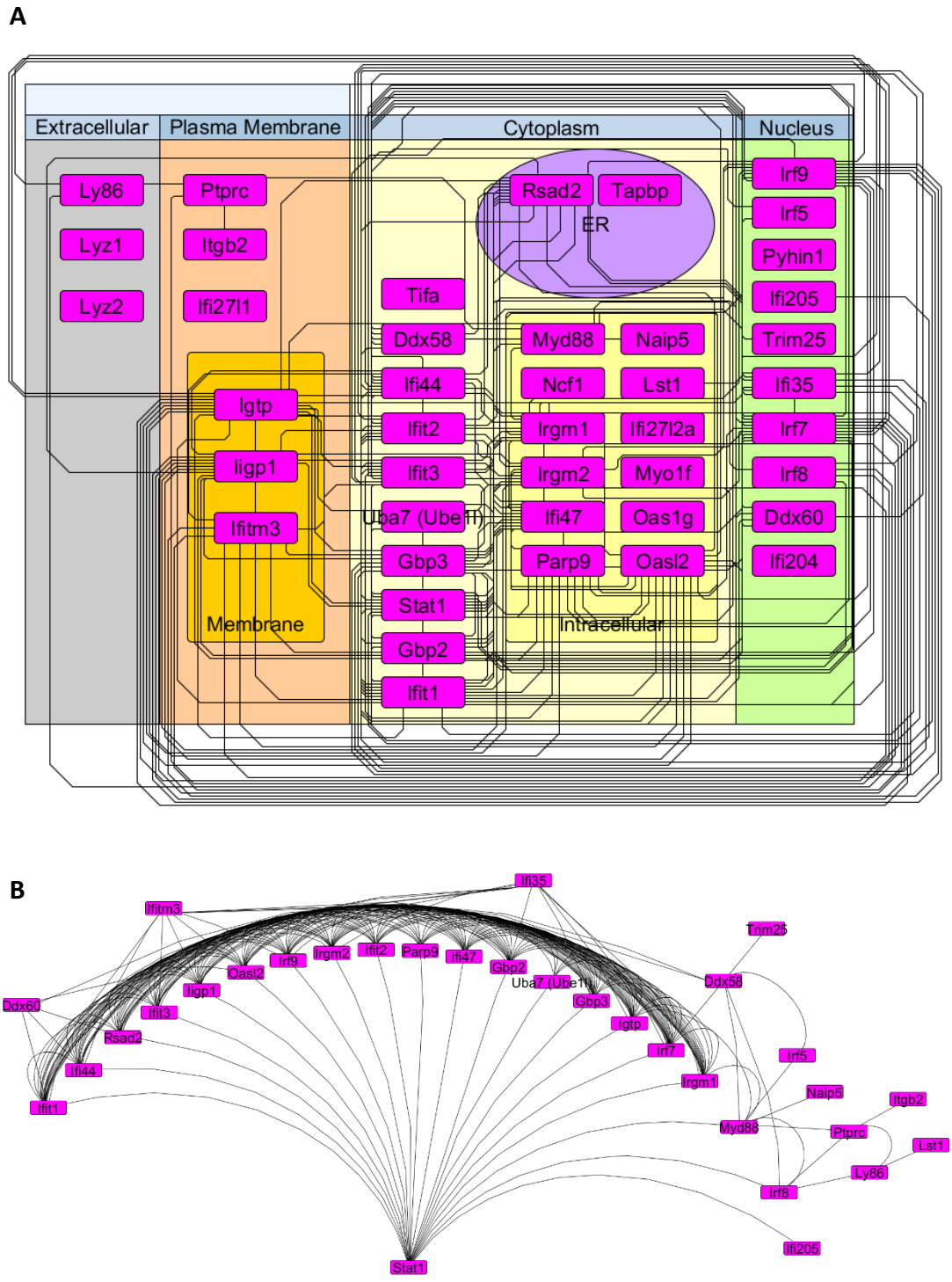

Figure 2-10: Myeloid associated interferon response genes. **A:** Ontological map of the myeloid associated interferon response genes reveals a tightly regulated transmembrane signalling system with extracellular lysozyme proteins and mediators of NADPH oxidase. **B:** The self-contained system is centred on the cytokine ligating transcriptional regulator Stat1.

2.3.5 Cytoskeletal Restructuring

Genes involved in actin and cytoskeletal restructuring were found associated with those genes identified as myeloid in origin. These include *Rhoc* (Ras homolog gene family, member C) which belongs to the Rho family and it is involved in signal transduction for amoeboid cell motility/actin cytoskeletal restructuring (Ridley, 2006) and are essential for adhesion (Hakem *et al.*, 2005). Adhesion within myeloid cells is supported by in an increase in expression of genes related to integrin pathways including *Icam1* ligation to alpha-M beta-2 ($\alpha_M\beta_2$) integrin formed from *Itgb2* (*Cd11b*) and *Itgb2* (*Cd18*) subunits (Hynes, 1992, Schenkel *et al.*, 2004). Integrin molecules including vcam1 are known to be used by myeloid cells to facilitate the entry across the endothelium to sites of nerve damage (Brown *et al.*, 1997). Also seen in support of myeloid adhesion was *Emr1* (F4/80) (Baud *et al.*, 1995). These same genes are required for diapedesis and the recruitment of myeloid cells is further supported by the presence of *Csf1* and *Csf1r*.

Formalins act as specific effectors for GTPase proteins involved in actin restructuring (Kitzing *et al.*, 2010) and in this dataset differential expression of *Cyb5r3* (cytochrome b5 reductase 3) was noted; a formalin closely associated with the Rho family (Fernandez-Borja *et al.*, 2005) and associated both with myeloid membrane restructuring for migration and phagocytic activity (Brandt *et al.*, 2007) and neural axon extension (Arakawa *et al.*, 2003). An increase in expression of *Dbi*, a neuromodulatory steroid released by neurons and glia was observed. It is expressed to induce a functional or structural alteration of the GABAergic system present in axon terminals, and is observed in both Parkinson's and Alzheimer's disease (Papadopoulos *et al.*, 2006). Interestingly, despite the increased stress and the need for energy neurons encounter during disease, the up regulation of both *Rhoc* and *Lgals1* seen in this dataset reflect the down-regulation of neurogenesis and prevention of hyper-proliferation.

2.3.6 Oxidative Stress

Also observed was an increase in *Ucp2* which is linked with an increase in synaptic plasticity, mitochondrial number and dendritic spine synapses, indicative of an increase in both energy consumption and remodelling in response to stress (Paradis *et al.*, 2003, Dietrich *et al.*, 2008, Islam *et al.*, 2012). Disturbances in mitochondrial functions reduce ATP synthesis and this has varying effects on the cells depending on their metabolic requirements. For neurons which have high metabolic requirements due to high overturn of activity at synapses this creates a more drastic effect than for other cell types. Evidence of a response during disease to oxidative stress is seen in the form of *Gpx1* (glutathione peroxidase 1) which plays an important regulatory role in the protection of neural cells in response to extreme oxidative stress during ischemia/reperfusion injury (Wong *et al.*, 2011).

Interestingly Cyb5r3 has also been implemented in mitochondrial distribution whereby overexpression *in-vitro* leads to a loss in mitochondrial motility and adhesion to actin (Minin *et al.*, 2006). Indeed genes expressed under conditions of stress were observed including S100a13 (S100 calcium binding protein A13). These are induced in conditions of stress bought about by Cu2+ oxidation (Mouta Carreira *et al.*, 1998, Landriscina *et al.*, 2001). Also noted was an increase in metabolism via amino acid consumption. This was primarily noted by an increase in *Oat* expression. OAT is associated with amino acid processing (Ventura *et al.*, 2010) and is required for conversion of the amino acid proline to L-ornithine and suggests an overall increase in metabolism akin to that seen under conditions of oxidative stress. Oxidative stress due to mitochondrial dysfunction is commonly described within neurodegenerative disease. This dataset strongly supports a microglia origin for this signature following overwhelming association with myeloid cells.

It was noted that there was a degree of contamination present in the purified cultures within the external data sets. Astrocyte cytoskeletal gene *Gfap*, considered solely expressed by astrocytes (Sofroniew and Vinters, 2010) was found, to a small extent,

within the purified microglia sample of the GNFv3 dataset. Consequently, 95 genes were accredited as full and partial astrocyte in origin for which the degree of overlap with other cell types, in particular myeloid, resulted in 20 of these as associated with strong (LPS) immune activation. Finally 57 genes as full or partial neuronal in origin were identified with 17 demonstrating immune activation.

2.3.7 Protein-to-Protein interaction

Evidence of protein to protein interaction was performed within STRING (http://string-db.org). Out of the 492 disease associated genes, 488 genes were taken through by STRING and joined with 2999 edges comprised solely from co-expression, experimental and database determined interactions. Adoption of the inbuilt MCL function located in STRING produced clusters with striking similarity (Figure 2-11) to that produced by BioLayout *Express*^{3D} in Figure 2-4 with the green cluster containing mainly interferon response markers and the main central cluster indicative of myeloid activation. Representation of the gene co-expression network by BioLayout *Express*^{3D} is therefore confirmed as concurrent with the current knowledge of protein behaviour in the literature.

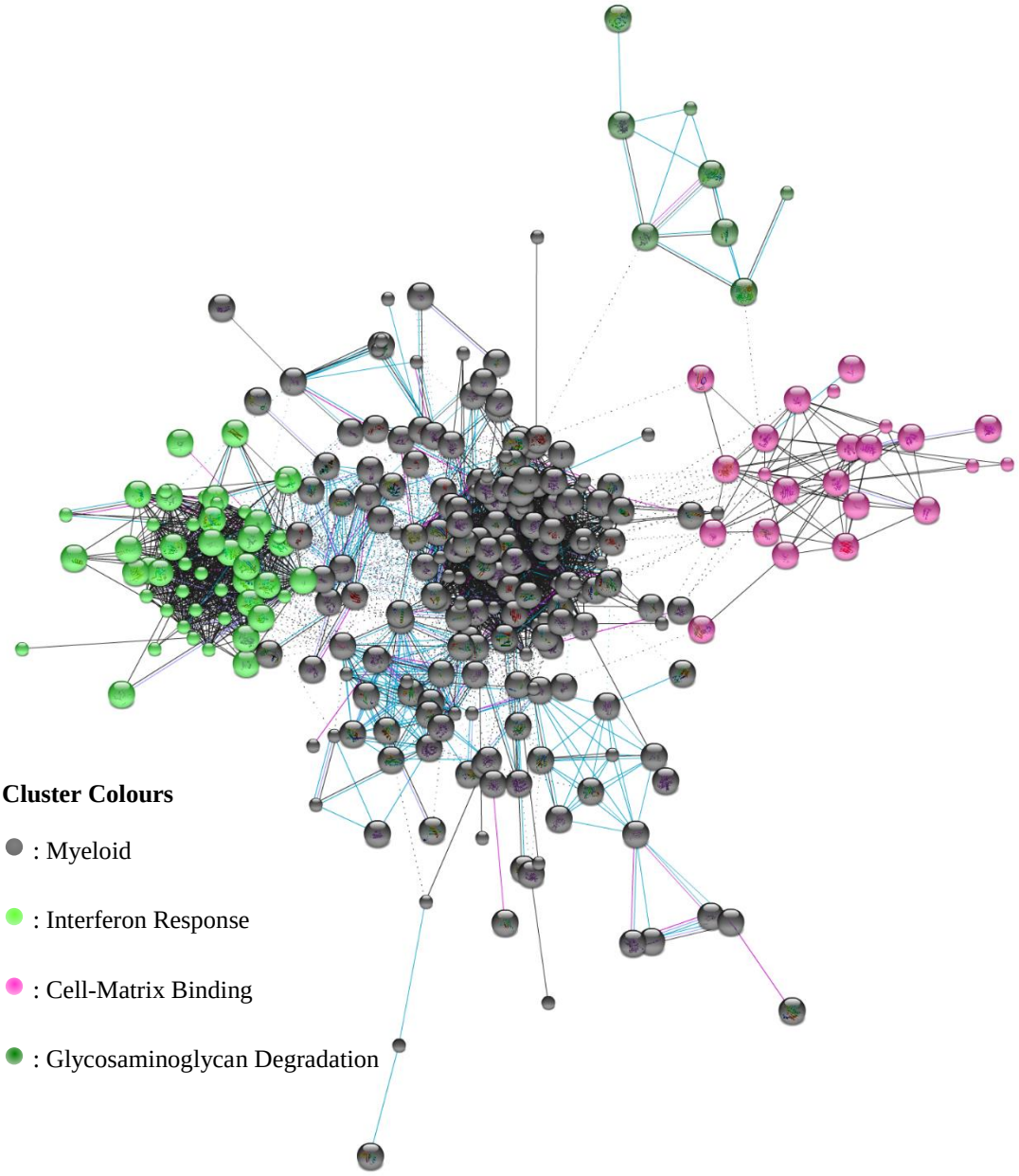

Figure 2-11: STRING generated evidence based protein-protein interaction map base on the input of the 492 disease associated transcripts. Connections between nodes are based on experimental evidence and clustering has been performed using MCL. The overall arrangement of three main clusters matched that generated by BioLayout *Express*^{3D} and included a dominant central myeloid cluster surrounded by interferon and matrix/adhesion associated clusters.

2.4 Discussion

The disadvantage of observing the disease progression based on analysis of tissue samples or small scale gene analysis mean results are viewed as part of a subjective hypothesis and conclusions drawn only from the limited number of tested variables. A global analysis of gene expression from time points taken during the course of developing prion disease pathology, has the potential to provide, in the unprocessed form, unbiased data that encompasses all the potential causative and consequential factors relating to disease development. The difficulty lies in trying to analyse the large amount of information generated in an impartial manner. BioLayout *Express*^{3D} was chosen for analysis of this dataset. The software has the ability to accommodate very large gene datasets which are viewed in a three dimensional neighbourhood with other genes based on a user defined threshold of co-expression. The capacity to handle very large datasets is integral to the software design in which the optimized graph layout and clustering algorithm are rendered within a hardware-accelerated OpenGL framework using the computer graphics processing unit and its inherent capability to handle very large numbers of calculations in a short period of time (Freeman *et al.*, 2007). This allowed rotational interaction with the graph; conferring a greater understanding of how cluster of genes are positioned in relation to one another and importantly in an environment in which there are no prior assumptions as to the data layout. The biological explanation is then led from the clusters with an explanation attributed to groups of genes now known to be linked with a shared expression. BioLayout *Express*^{3D} therefore provides a visual and unbiased instrument for identification of a gene both in terms of shared expression with other genes and expression differentiation when serial data is entered. By adopting parallel comparison with additional external datasets it was possible to convincingly attribute microglia as significant contributors in prion disease.

There are however limitations to a correlation of expression approach that must be taken into account. Correlation network software, including BioLayout *Express*^{3D} rely upon a normalised background level of expression to allow pairwise comparison to

be conducted. Therefore the inclusion of outliers can have a pronounced effect on measured distances throughout the sample (Westfall, 1993). Where outliers exist and are not readily detectable; typically through a small sample population size, there exists the potential to form false conclusions. It was for this reason that quality control checks were outsourced to Fios Genomics Ltd (Edinburgh, Scotland)/

At the global sample-to-sample level in BioLayout *Express*^{3D}, with the threshold matrix cut-off to 0.75, the robust quality control and normalisation techniques adopted by this study revealed an extremely tight correlation between all the mouse prion combinations. It was not until the threshold matrix cut-off was set to >0.98 were any differences detected between the mouse/prion strain combinations. The similarity of disease progression within the different strains in the study, despite demonstrating strikingly different disease pathologies, resulted in the generation of one highly organised graph of disease associated genes. Had the mouse/prion strain combinations displayed differing disease signatures, the resulting graph would have been divided into multiple separate components with no correlation between them. This confirmed the suitability of the dataset for finding markers shared by the mouse/prion strain combinations. In the B4053 strain a clear difference could be determined between nodes from infected and those from an uninfected source, yet it should be noted that this difference was still only detectable at a threshold matrix cut-off set to >0.98. The fact the difference was greater indicated a strong diverge of the infected from the uninfected B4053 mice but the overall grouping of the group-to-group dataset into one large graph does not make it possible to determine if cause of this difference is due to a more rapid and severe pathology.

No genes were found in which expression decreased with disease progression. The lack of down-regulation can be explained by the cluster based nature of analysis using BioLayout *Express*^{3D}. Due to the nature of microarray hybridisation there can be variation in gene hybridisation across different chips as part of a serial analysis. A study performing a fold difference analysis might mistakenly declare such variations,

both up and down, as a biological perturbation. BioLayout *Express*^{3D} compares the entire dataset for patterns of shared co-expression and clusters of genes sharing a high degree of correlation. It is however important to consider the limitations of whole brain RNA analysis. It is feasible for a smaller population, possibly demonstrating a down-regulated signal, to be diluted by the rest of the dataset.

Comparison with the external GNFv3, Brain TRAP and Macrophage/LPS datasets and in-depth search of the literature was used to assign cellular origin to each gene. Microglia dominated the signal with almost two thirds of the genes associated with myeloid origin. The vast majority of these were associated with an activated innate immune response. Mapping myeloid genes into ontological groups disclosed multiple pathways to be associated with each cluster. Pathways for each ontological functional group were compiled using STRING (http://string-db.org/) and as such reflect the current literature. Using the Pearson correlation function inbuilt into STRING generated a graph strikingly similar to that generated using the microarray data with BioLayout *Express*^{3D} and confirming the clustering to be correctly orientated with current literature.

The Microglial response in prion disease is usually associated with low levels of immune gene expression and has previously been reported within studies of the hippocampus of mice infected with ME7 (Brown *et al.*, 2003, Brown *et al.*, 2005). In those studies, microglia were activated and present in large numbers in this area of the brain at or near clinical even if relative gene expression was not found to be in proportion to the visible change in morphology brought about by activation. In this re-analysis dataset the activation signal was considerable stronger and the signal origin was at approximately 50% of total the incubation period. Of particular note was that the signal remained consistent throughout the entire course of disease. Switching on of specific pathways at distinct intervals was not observed. Activation was a gradual process with expression of just one set of disease associated genes steadily increasing in signal strength until death. This was concurrent across all the

prion/mouse strain combinations with little variation in the expression pattern between the different mouse/prion strains implying that all the models in this dataset shared a striking similarity in the disease associated expression. Furthermore, the expression profile is near identical between clusters implying simultaneously expression by multiple cell types in the brain.

Perhaps as a result of myeloid derived communication, the TGF-B pathway is evident. Presence of the TGF-β1 protein in prion disease and influence on microglial activation are well documented (Lodge and Sriram, 1996, Cunningham *et al.*, 2002). The TGF-β protein mediated inducement of differentiation/proliferation genes is seen throughout the analysis including *Egf*, which through Bmp2, interacts with the IL-10/STAT pathway and drives cellular proliferation (Fukuda *et al.*, 2007) with signal transduction mediated by secondary messenger's cAMP, cGMP, diacylglycerol, arachidonic acid, InsP3, and Ca^{2+}, and tertiary messengers through the phosphorylation of CREB and expression of C-FOS4. Many of the pathways detected have downstream associations with different cellular lineage to the origin. This provides a strong argument for a tightly controlled signal of intracellular, intra-lineage communication.

Also seen, and suggesting a strong glial interaction with neurons, were genes involved with neuronal cellular oxidative and metabolic stress as evidenced by *Mt1*, *Mt2* and *Nfe2l2*. The source of the differentiation/proliferation signals also appears to be both neuronal and glia in origin with differential expression of *Rhbdf1* and *Rab31*, involved with trafficking of TGF-a/b and EGFR (Nakagawa *et al.*, 2005, Liu *et al.*, 2006, Ng *et al.*, 2009). In the brain, TGF-a triggers neuronal and glial proliferation (Burgess, 1989, Fallon *et al.*, 2000).

Particular evidence of oxidative stress is seen via the increase in expression of the G protein-coupled Melatonin receptors1 and 2 (*Mt1* and *Mt2*). Melatonin is a strong anti-oxidant, linked with TGF-β, calcium influx regulation and osteoclast

differentiation (Pandi-Perumal *et al.*, 2006, Pandi-Perumal *et al.*, 2008). The overall effect of an increase in melatonin is considered to be neuroprotective (Ohtsuji *et al.*, 2008, Radogna *et al.*, 2009). Production is typically associated with myeloid cells in the CNS where it is involved in up-regulation of the immune response including IL-2 production (Carrillo-Vico *et al.*, 2004). Another gene for which expression increased in an effort to control oxidative levels in our dataset was Nuclear factor [erythroid-derived 2]-like 2 (*Nfe2l2*). The protein form of NFE2l2 is closely associated with MT1 and MT2 and forms part of the antioxidant response element (Ohtsuji *et al.*, 2008).

Astrocytes demonstrate a significant increase in metabolic genes involved in amino acid synthesis including Aldehyde dehydrogenase 1 family, member L1 (*Aldh1l1*). Actively involved in purine synthesis (Kutzbach and Stokstad, 1971) *Aldh1l1* is implemented with cellular proliferation (Krupenko and Oleinik, 2002). An increase in both astrocyte and microglia cell proliferation and differentiation is marked by numerous genes involved in the TGF-B1 pathway. The expression of *Tgf-B1* is already known to be strongly associated with prion disease where it is implicated in an effort to reduce microglial activation (Cunningham *et al.*, 2002). Seen here are genes involved primarily in differentiation and apoptosis including Rhomboid 5 Homolog 1 (*Rhbdf1)*, (Ras homolog family member C) *Rhoc*, Clusterin (*Clu*), stress-induced secreted protein 1 (*Dies1*), olfactomedin-like 3 (*Olfml3*), and BMP-2-inducible protein kinase (*Bmp2k*). Downstream effectors of these genes are directly implemented with the TGF-B pathway (Pappano *et al.*, 1998, Kearns *et al.*, 2001, Nakagawa *et al.*, 2005, Aloia *et al.*, 2010) suggesting a signal in direct competition with that for proliferation.

A strong interferon response was detected and comprised one third of the total gene set. The vast majority are found localised in a semi-separate cluster, swayed no doubt by the stronger interferon response characteristic of the C57Bl/6 mice strains (Schilling *et al.*, 2009). Only a few previous studies have documented the activation of the interferon response system (Riemer *et al.*, 2004) but none with such an early activation and as part of a tightly regulated system. The Interleukin 10 receptor 2 (*Il-*

10r2) is up-regulated; a receptor sharing considerable homology to members of class 1 and class 2 cytokine receptors and intrinsically involved in the interferon system (Moore *et al.*, 2001, Liu *et al.*, 2012). Activation of the IL-10 pathway results in a significant reduction of cytokine synthesis and inhibition of cytokine activity (Lodge and Sriram, 1996, Pestka *et al.*, 2004). In turn this would explain the increase in Suppressor of cytokine signalling 3 (*Socs3*) observed in our analysis: a potent inhibitor of *Ifn-γ*, *Il-10 Il-2* and *Il-4*-induced signal transduction (Gil *et al.*, 2001, Ding *et al.*, 2003). Activation of the IL-10R2 complex results in phosphorylation of both STAT1 and STAT3 and transcriptional initiation of *Socs1* and *Socs3* (Wehinger *et al.*, 1996) explaining the strong presence of STAT mediated pathways in this dataset. The role of STAT1 has been linked with PrP^C biology (Spudich *et al.*, 2005) and both STAT1 and STAT3 confer a neuroprotective function (Frigg *et al.*, 2006). This re-analysis suggested a dominant role of the STAT pathways within activated microglia and perhaps as a continuation of intracellular support by ramified microglia mediated by this pathway in the healthy brain (Zhu *et al.*, 2008).

2.4.1 Comparison with the Previously Published Conclusions in Hwang *et al.* (2009)

By using a variety of mice and strain combinations, the aim of the study by (Hwang *et al.*, 2009) was to identify a core set of regulatory genes involved in prion disease that are independent of variations in both mouse and prion strains and shared as a core by all mouse disease models. The group used a subtractive process to eliminate genes considered artefacts of a given mouse and prion strain combination. A particular prion strain can result in a short incubation period in one mouse strain but a significantly longer period in another mouse strain. At the same time a particular mouse strain can have differing incubation periods when exposed to differing prion strains. Therefore the study felt it important to understand that incubation time is not a property of any given prion strain or *Prnp* genotype, but was associated with interactions between host and infectious agent.

Consequently Tg4053 and *Prp*$^{0/+}$ mice were inoculated with RML and used as a filter to eliminate differentially expressed genes associated with differing (short and long) incubation times in a high PrP concentration environment. This ensures only differentially expressed genes associated with strain phenotype were entered. To eliminate differentially expressed genes associated with prion inoculation but not associated with prion infection, Prnp Null mice were inoculated with the RML prion strain (Appendix 8-2). Aged and genotype matched mice were inoculated with normal brain as controls.

Gene Ontology was applied to assign the identified differentially expressed genes into four main groups; PrP^{Sc} replication and accumulation, microglial and astrocyte activation, synaptic degeneration and neuronal cell death. Although a strong activation signature was both identified and examined in detail the majority were considered more important only at the later stages of the disease process. The lack of glial activation shown by a lack of up-regulation of *Cd14, Cd68*, *Gfap* and *C1qb* in long incubation period $PrP^{0/+}$ mice until the first histoblot detection of PrP deposition at 16 weeks was reported to suggest glial activation is in response to prion accumulation and not neuronal damage. Glial contribution was further played down by the suggestion that activation of endothelial cells through cytokine release would recruit cells from the periphery, shown by an increase in *Csf1*, and result in an increase in leukocyte numbers and hence leukocyte gene expression. The over activation of microglia secondary to exposure of PrP was suggested as a possibility for increased neuronal death. However the study concluded that severe neuronal stress resulting from perturbations within lipid raft mediated prion replication was the main and dominant signature within the disease.

2.4.2 Conclusions

Shown in this dataset and for the first time is a consistent and immune system dominated disease associated signal that remains consistent from around halfway through the incubation period. Contained within the expression profile are genes

involved in metabolic and oxidative stress, ER/Golgi associated quality control mechanisms, proliferation/differentiation, immune activation and at the same time suppression of both proliferation and activation phenotypes. The signals are strikingly intra-cellular in origin, which ties in with the formation of a one large inseparable cluster in BioLayout *Express*^{3D}, and indicative of a tightly regulated mechanism between differing cell populations in the diseased brain. Although microglia appear to dominate the overall signature, it indicates that increasingly stressful conditions are for some time successfully endured by all cell types long before the onset of the clinical phase of disease.

The nature of the inseparable multi-cellular signal would require teasing apart one cell type at a time to overcome the limitations of both whole brain RNA and post origin allocations, that although addressed in a novel way in this study, were still subject to signal contamination and incomplete/incorrect expression by external immature primary cultures that fail to represent the mature *in-vivo* expression. Single cell type analysis would provide an insight into what a cell is not contributing, an aspect often overlooked but vital in determining the correct direction of cell-cell communication pathways. The overall immune response described in this present study is both pro-inflammatory and anti-inflammatory and does not present with the hallmarks of either a classical or alternatively activated myeloid phenotype. Due to the potential incorporation of other cell types within the signal it is not possible to state for certain that this mixed phenotype is unique to prion disease. A single cell type analysis would therefore also facilitate in determining if the microglial response is specific to prion disease or a stereotypic LPS-type response by myeloid cells independent of any given perturbation.

3 Characterisation of the Response of BALB/cJ$^{Fms\text{-}EGFP/-}$ Mice to Prion Infection

3.1 Introduction

The aim of this chapter is to characterise prion infection in BALB/cJ$^{Fms\text{-}EGFP/-}$ mice and their suitability for studying the role of microglia during the course of infection. BALB/cJ$^{Fms\text{-}EGFP/-}$ mice are a novel genetically modified mouse line which express Enhanced Green Fluorescent Protein (EGFP) under control of the *C-fms* operon. *C-fms* encodes for macrophage colony-stimulating factor-1 (CSF-1), a myeloid linage specific growth factor that binds to colony-stimulating factor receptors (CSF-1R) on cells of myeloid origin. CSF-1 is directly involved in the survival, proliferation, and differentiation of mononuclear phagocytes (Stanley *et al.*, 1997). The *Fms-EGFP* reporter gene was first used in C57BL/6 mice to generate the Macrophage-Green (MacGreen) mouse model (Sasmono *et al.*, 2003). The *Fms-EGFP* reporter gene has now also been inserted into the BALB/cJ background generating the BALB/cJ$^{Fms\text{-}EGFP/-}$ strain of transgenic mice.

Mouse availability at the start of this project dictated the use of the BALB/cJ$^{Fms\text{-}EGFP/-}$ mice. BALB/cJ are well characterised with prion models and are heavily utilised in other neurodegenerative disease models and immunological studies (Appendix 8-6). All cells of myeloid origin that express the lineage specific growth factor *Csf-1* in the BALB/cJ$^{Fms\text{-}EGFP/-}$ mouse will yield EGFP. This also includes cells of neutrophilic granulocyte lineage sharing the same progenitor as monocytes (Sasmono *et al.*, 2007). For the purpose of studying microglia during neurodegenerative disease, the expression of EGFP by this group of cells allows for detailed analysis and easy isolation. The *Fms-EGFP* reporter insertion into BALB/cJ was by random integration and the precise location of the reporter in the genome was therefore unknown. Homozygosity for the *Fms-EGFP* reporter is fatal *in utero* suggesting knock-out of a vital sequence required for correct development *in utero*. Animals demonstrating heterozygosity appear to be unaffected and behave and interact normally with the wildtype animals suggesting the functional complimentary copy of the gene is

sufficient. In addition BALB/cJ$^{Fms\text{-}EGFP/-}$ share a comparable lifespan to the wild type animals (~800 days). The lack of apparent detrimental effects and the high availability of mice heterozygous for the *Fms-EGFP* reporter made the strain suitable for this project.

This chapter will cover two aims using infection with two very different prion strains. The first aim was to confirm that the BALB/cJ$^{Fms\text{-}EGFP/-}$ mice are susceptible to prion disease infection by direct comparison with the BALB/cJ wild type. The second aim was a serial investigation to document the sequence of events following infection. BALB/cJ$^{Fms\text{-}EGFP/-}$ and the wild-type background BALB/cJ mice were infected with either 79A or ME7 prion strains. These two well characterised strains were chosen due to the differences in original origin (Appendix 8-7) and the recognisable and reproducible pathology in mice both sharing the *Prnp-a* allele (Fraser and Dickinson, 1985). Successful infection by two very different strains demonstrating very different pathologies would confirm BALB/cJ$^{Fms\text{-}EGFP/-}$ are fully susceptible to, and suitable for use in studying, murine prion disease. Furthermore, previous unpublished work within the Neurobiology Division, The Roslin Institute & R(D)SVS, demonstrated prion strain dependant variability in persistence of infection of cultured microglia-like cells (Appendix 8-8).

3.1.1 Choice of Prion Infection Route and Serial Investigation Time Points

This experiment made use of an intraperitoneal route of infection. This route was adopted to ensure microglial activation was the result of a response to initial infection entering into the CNS environment, at the start of the neural phase of replication, in what amounts to a more natural route. By contrast the rapid dissemination of infectious material throughout both the CNS and periphery following an intracerebral injection does not allow for exact confirmation of the initial microglial response (Millson *et al.*, 1979).

The regional targeting of disease pathology in the brain of intraperitoneal and intracerebral infection is identical once uptake into the CNS has been achieved as the spread of prion disease pathogenesis in the brain is restricted to neuroanatomical pathways (Kimberlin and Walker, 1980, Kimberlin *et al.*, 1983, Scott *et al.*, 1992). Following disease entry into the CNS, the reduced complexity of entry into the brain with a peripheral route via rapid replication along neuroanatomical pathways results in a surprisingly shorter neural phase of replication, classed as the time from first detection of protein deposition to clinical onset, following a peripheral route than an intracerebral injection (Kimberlin and Walker, 1986, Langevin *et al.*, 2011). This can be observed in detail when the requirements for extra-neuronal replication are bypassed and the neural phase of replication is initiated from the outset following an intraspinal route of infection (Kimberlin *et al.*, 1987).

Although the replication phase in the brain is reduced using a peripheral route of infection, the disease incubation period is considerably longer than an intracerebral route. The speed of infectious uptake into the CNS is determined in the main by the concentration of available infectious material. Following injection, dissemination to tissues rapidly occurs with a higher rate of loss in titre following an i.p. route than an i.c. route (Kimberlin and Walker, 1978, Millson *et al.*, 1979). Accordingly the infectivity titre of an inoculum is lower when using a peripheral route and the period required prior to successful initial entry into and replication within the CNS is increased. This is further compounded by the complexity of the peripheral mechanisms of replication (Kimberlin and Walker, 1979, Brown *et al.*, 1999b) all of which are considered important for this project as microglia are extremely sensitive to signals both pertaining and outwith of the parenchyma (Nimmerjahn *et al.*, 2005).

It was therefore important to capture these initial events of peripheral and CNS replication phases, time points were carefully chosen based on expected incubation periods of ME7 and 79A within *Prnp-a* allele containing BALB/cJ$^{Fms\text{-}EGFP/-}$ and BALB/cJ mice using an i.p route (Appendix 8-9) To offset for potential delays in entry into the

CNS from using a peripheral route, time points in this study were included at 45% and 65% of the incubation period (Figure 3-1) to document pre-clinical disease uptake in the CNS.

Studies focusing on the hippocampus, made due to the regular architecture and well characterised location of the pyramidal neuronal population found in this region, revealed the first immunostained PrP was detectable in the hippocampal CA1 pyramidal cell layer 70 dpi and proceeded vacuolation, synaptic loss and axon degeneration; all observed to steadily increase from 100 dpi (Johnston *et al.*, 1998, Jeffrey *et al.*, 2000, Brown *et al.*, 2001, Jeffrey *et al.*, 2001) with significant loss by terminal (Belichenko *et al.*, 2000). These hippocampal studies utilised the ME7 Scrapie strain inoculated into the F1 cross produced from pairing of the *Prnp-a* allele containing C57BL mouse strain with the *Prnp-b* containing VM strain. The resulting CVF1 mouse strain (CV) harbours both *Prnp* alleles (*Prnp-a/b*). The ME7/CV model following intracerebral inoculation, demonstrates an incubation period of 32 weeks (226 days) with extensive and widespread diffuse deposition of PrP throughout the brain by terminal (Jeffrey *et al.*, 2001). The activation of astrocytes and microglia was also observed from 100 dpi with the former observed to actively internalise degenerating axons (Jeffrey *et al.*, 2000, Jeffrey *et al.*, 2001). Crucially the ME7/CV model demonstrates the activation of microglia to be 30 days after the initial detection of PrP deposition and is therefore in disagreement with the aforementioned ME7 inoculations into *Prnp-a* allele C57BL6/J mice. Whether microglia are the cause of developing pathology or merely responding to damage has still not been resolved highlighting the need, as per this analysis, to focus on early stages of the disease.

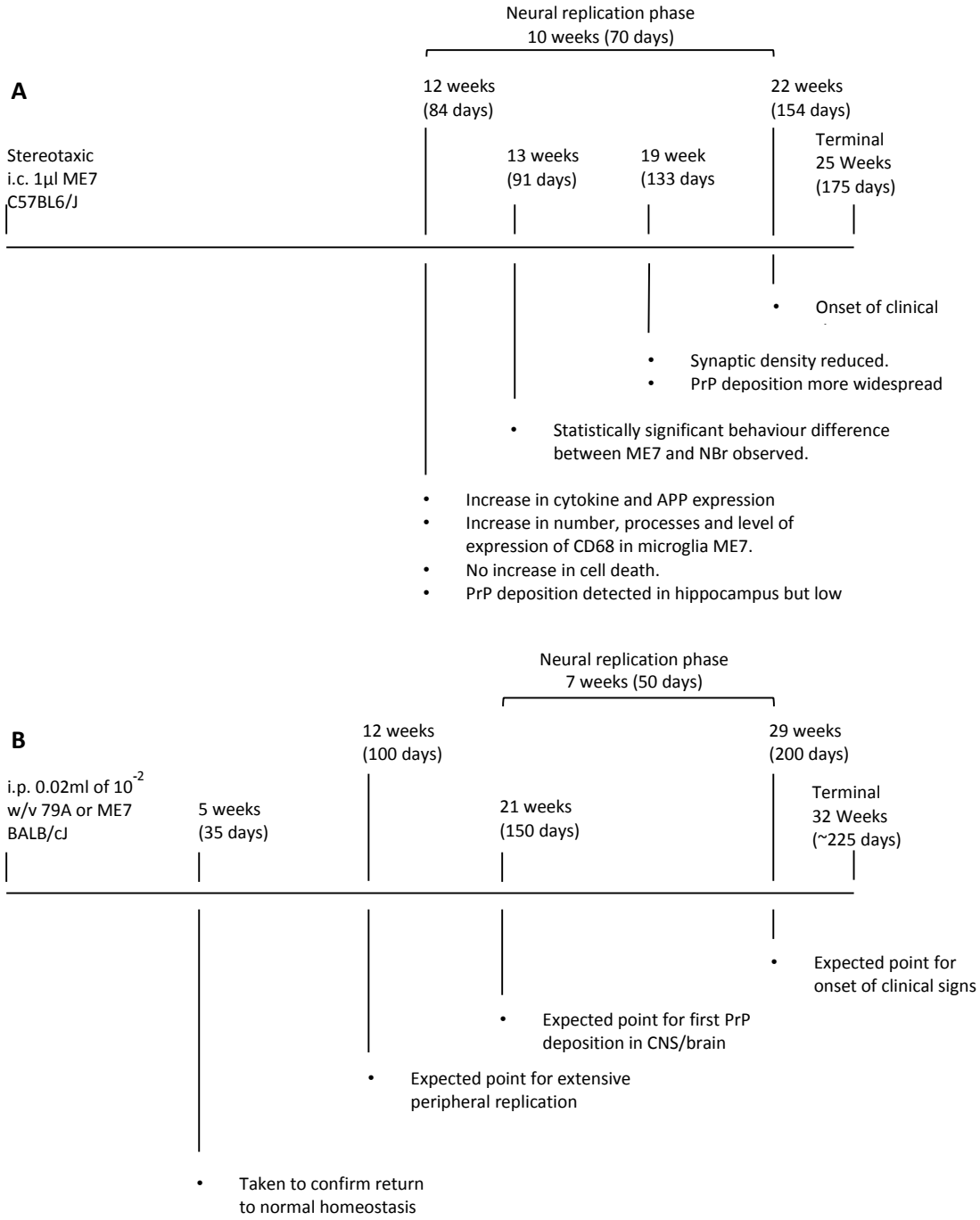

Figure 3-1: Early events documented for ME7 infection in C57BL6/J mice (*Prnp-a*) following stereotaxic i.c. inoculation based on work performed by (Cunningham *et al.*, 2003) and (Cunningham *et al.*, 2005a). **A:** Early signs of microglia activation and PrP deposition were first observed at approximately 50% of the incubation period. **B:** Expected points of pathological events following i.p. infection in BALB/cJ$^{Fms\text{-}EGFP/-}$ and BALB/cJ mice, also *Prnp-a*, adjusted to reflect differences in incubation periods and available titre of infections material.

3.2 Methodology

3.2.1 Experimental Set up

The breeding of BALB/cJ$^{Fms\text{-}EGFP/-}$ mice was performed with the pairing of a BALB/$^{cJFms\text{-}EGFP/-}$ with a BALB/cJ bought from Charles River Laboratories (Elpinstone). Pairs contained either a male or a female BALB/$^{cJFms\text{-}EGFP/-}$. The breeding pairs were mixed with regards to the gender of the BALB/$^{cJFms\text{-}EGFP/-}$ parent and no difference was noted in offspring number or quality between the two pairing alternatives for the gender of the BALB/$^{cJFms\text{-}EGFP/-}$ mouse. Offspring were genotyped for presence of the *Fms-EGFP* reporter. Animals negative for the reporter gene were considered to be wild type BALB/cJ and selection for these animals was considered the same as choosing a BALB/cJ bought from Charles River Laboratories (Elpinstone). All groups were gender matched. Mice with an average age of 116 days ± 1.2 SE were given an intraperitoneal injection with 0.02 ml of 10^{-2} w/v of either 79A or ME7 infected brain homogenate suspended in PBS and with a 1 ml syringe (Table 3-1) sourced from C57BL/6J mice (Appendix 8-10). Additional mice, run in parallel, were inoculated with 0.02 ml of 10^{-2} w/v normal brain homogenate suspended in PBS to serve as controls for the act of inoculation.

Table 3-1: Mice used for BALB/cJ$^{Fms\text{-}EGFP/-}$ characterisation study infected with either 79A or ME7 mouse-adapted Scrapie prion strains. Control mice were inoculated with normal brain (NBr) homogenate. Mice were split into two experiments with the NBr inoculated mice serving as controls for both.

Experimental Setup: BALB/cJ$^{Fms\text{-}EGFP/-}$ Characterisation					
Serial Cull Point (Days)	**Number of Animals**	**Genotype**	**Age at Injection (Days ± SE)**	**Inoculum**	**Route of Infection**
Terminal Disease	12	BALB/cJ$^{Fms\text{-}EGFP/-}$	126 ± 1.9	79A	i.p.
	12	BALB/cJ	129 ± 1.3	79A	i.p.
	12	BALB/cJ$^{Fms\text{-}EGFP/-}$	101 ± 1.5	ME7	i.p.
	12	BALB/cJ	101 ± 0.8	ME7	i.p.
	6	BALB/cJ$^{Fms\text{-}EGFP/-}$	131 ± 0.7	NBr	i.p.
150	9	BALB/cJ$^{Fms\text{-}EGFP/-}$	127 ± 0.1	79A	i.p.
	9	BALB/cJ$^{Fms\text{-}EGFP/-}$	103 ± 3.6	ME7	i.p.
	6	BALB/cJ$^{Fms\text{-}EGFP/-}$	127 ± 0.8	NBr	i.p.
100	9	BALB/cJ$^{Fms\text{-}EGFP/-}$	124 ± 1.3	79A	i.p.
	9	BALB/cJ$^{Fms\text{-}EGFP/-}$	104 ± 2.4	ME7	i.p.
	6	BALB/cJ$^{Fms\text{-}EGFP/-}$	126 ± 0.7	NBr	i.p.
35	9	BALB/cJ$^{Fms\text{-}EGFP/-}$	121 ± 2.6	79A	i.p.
	9	BALB/cJ$^{Fms\text{-}EGFP/-}$	102 ± 3.1	ME7	i.p.
	6	BALB/cJ$^{Fms\text{-}EGFP/-}$	122 ± 2.2	NBr	i.p.

3.2.2 Scoring of TSE Clinical Signs and Lesions

All mice were monitored daily for general health. Mice belonging to the groups to be taken to terminal disease were scored every 7 days for clinical signs from 65% of the incubation period (150 dpi) when first PrP protein accumulation was predicted to be present indicating the onset of the neural replication phase. This was performed using a modified version of the coding system first introduced by Dickinson *et al.* (1968) and now universally adopted:

1: The animal is healthy with no signs of abnormal behaviour.

2: Possibly prion disease affected: Abnormalities observed but necessarily due to prion disease, including lethargy, unkempt appearance and weight loss.

+: Prion disease affected: Animal has clinical signs of prion disease including hunching, unkempt appearance, weight loss, wet genitalia, semiperminant inactivation (freezing) and poor balance.

g: The animal portrays abnormalities in gait but not necessarily due to prion disease.

G: The animal has a clinical score of 2 with gait abnormality.

Mice were culled following two consecutive recordings of a '+' score. If disease signs were considered very severe the animal was culled following just one instance of a '+' to reduce suffering. To allow for standardization both within this project and with prion disease experiments in the literature, brains were cut to a template following a standard operating procedure, almost universally adopted, to produce 6 µm haematoxylin and eosin stained tissue sections (Fraser and Dickinson, 1967). Lesion scoring was performed on 9 grey matter (of which mice have a correspondingly higher proportion than human brain) and three white matter regions (Figure 3-2). Lesions were scored on a scale of 1-5 within the grey matter and 1-3 within the white matter. A score of 1 is indicative of the presence of minor vacuolation of which origin cannot be confirmed. A score of 2 or greater is indicative of lesions associated with prion disease.

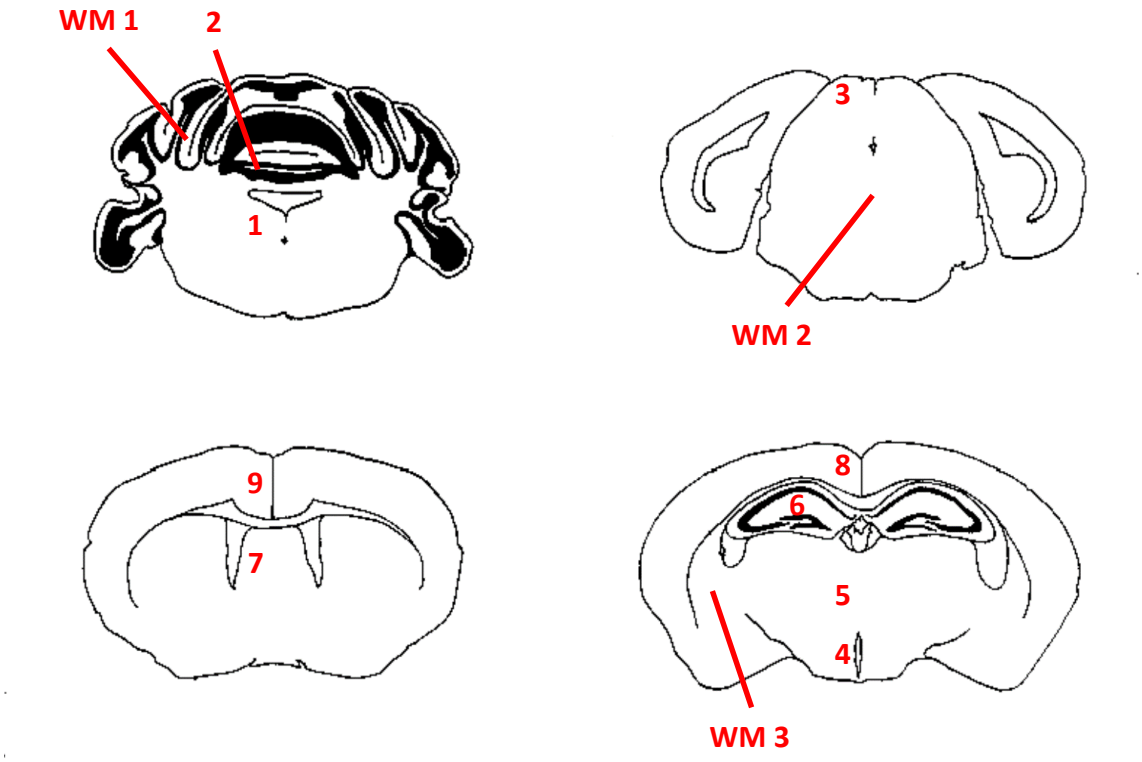

Figure 3-2: Standardised lesion scoring regions. Lesion scoring was performed on 9 grey matter and 3 white regions: **1:** medulla, **2:** cerebellum, **3:** superior colliculus, **4:** hypothalamus, **5:** thalamus, **6:** hippocampus, **7:** septum, **8:** retrosplenial cortex**, 9:** cingulate & motor cortex, **WM 1:** cerebellum, **WM 2:** decussation of cerebral peduncle and **WM 3:** basal cerebral peduncle.

3.2.3 Genotyping of BALB/c and BALB/cJ$^{Fms\text{-}EGFP/-}$ Mice

Genotyping for presence of the *Fms-EGFP* reporter gene was performed both as part of animal selection and following experimental cull to confirm original genotype designation. Primers for the *Fms-EGFP* reporter gene and the fatty acid binding protein 500 (*Fabpi500*) positive control gene were obtained from Eurofins MWG Operon. The *Fabpi500* gene (Green *et al.*, 1992, Chmurzyńska, 2006), multiplexed into the reactions, was utilised for quality control by ensuring the lack of an EGFP band is due to the absence of the transgene and not due to failure of the PCR.

3.2.3.1 Preparation of Primers

Primers for *Fms-EGFP* reporter gene and *Fabpi500* positive control gene were obtained from Eurofins MWG Operon (Ebersberg, Germany) as a lyophilised powder in 2 ml screw top tubes synthesised in the following sequences:

EGFP Forward:	5'-GCA CGA CTT CTT CAA GTC CGC CAT GCC-3'
EGFP Reverse:	5'-GCG GAT CTT GAA GTT CAC CTT GAT GCC-3'
Fabpi500 Forward:	5'-CCT CCG GAG AGC AGC GAT TAA AAG TGT CAG-3'
Fabpi500 Reverse:	5'-TAG AGC TTT GCC ACA TCA CAG GTC ATT CAG-3'

Each primer pair was rehydrated in the required volume of distilled H_2O (Gibco, 15230) specified by the manufacturer for each individual tube to make 100 µM primer stock solution. Aliquots of 60 µl were made and stored at -20°C in 0.5 ml tubes.

3.2.3.2 DNA Extraction from Ear Punch Biopsy of Mice Obtained from Breeding Colony

An ear biopsy, performed as part of routine ear mark, was taken using an ear punch and placed in a labelled 2 ml screw top microcentrifuge tube. To each tube, 180 µl Buffer ATL (QIAGEN DNeasy™ 69506) was added followed by 20 µl Proteinase K

(QIAGEN DNeasy™ Kit, 69506). These tubes were then incubated overnight at 55°C with oscillation at 150 rpm.

Following incubation a premix of 200 µl Buffer AL (QIAGEN DNeasy™ 69506) and 200 µl ethanol was added to each tissue lysate and vortexed for 15 sec to mix. Each lysate was transferred to a new DNeasy™ spin column contained within a new 2 ml collection tube and centrifuged at 6000 *x g* (8000 rpm on Eppendorf Centrifuge 5415D) for 1 min. Flow through and collection tube were subsequently discarded and the spin column placed in a new collection tube.

To each spin column 500 µl Buffer AW1 (QIAGEN DNeasy™ 69506) was applied prior to centrifuge at 6000 *x g*. Flow through and collection tube were subsequently discarded and the spin column placed in a new collection tube. To each spin column 500µl buffer AW2 (QIAGEN DNeasy™ 69506, UK) was applied prior to centrifuge at 6000 *x g* (8000 rpm on Eppendorf Centrifuge 5415D) for 3 min to fully dry the column membrane. Flow through and collection tubes were discarded and spin columns carefully transferred to clean labelled 1.5 ml microcentrifuge tubes.

To each column, 200 µl Buffer AE (QIAGEN DNeasy™ 69506, UK) was applied directly to the membrane and incubated under cover at room temperature (25°C) for 1 min. To elute DNA, all spin columns were subjected to a final centrifuge at 6000 *x g*. All 1.5 ml tubes contained DNA were transferred to 4°C storage.

3.2.3.3 DNA Extraction from Prion Infected Tail Biopsy following Experimental Cull

A 1 cm tail tip was cut from each mouse when culled and stored at -20°C. From each frozen tail tip, a 2 mm section was removed using a clean disposable scalpel and placed into a labelled 2 ml screw top tube. A fresh disposable scalpel was utilised for each tail to avoid contamination. To each tube 800 µl Tissue Lysis Buffer was added and then incubated overnight at 55°C with oscillation at 150 rpm.

Following incubation, 600 µl Phenol/Chloroform 1:1 was added to each tube and mixed thoroughly by vortex. All tubes were then centrifuged at 10000 *x g* (13000 rpm on Eppendorf Centrifuge 5415R) for 5 min. The top 600 µl aqueous phase was transferred to a new 1.5 ml microcentrifuge tube and 20 µl of 3 M sodium acetate followed by 600 µl isopropanol added and inverted 15 times to mix. Sealed tubes were then left to stand for 10 min at room temperature (25°C).

The DNA was precipitated at 10000 *x g* for 2 min then washed in 200 µl 70% ethanol at 10000 *x g* for 1 min and left to air dry at room temperature (25°C) for 10 min. The DNA pellet was resuspended in 200 µl Buffer AE (QIAGEN, 19077) and transferred to 4°C storage until required.

3.2.3.4 Polymerase Chain Reaction using QIAGEN Type-it™ Mutation Detection Kit or Microzone MegaMix-Blue.

Primer stock solution aliquots were removed from -20°C storage and thawed at room temperature. An *Fms-EGFP* primer pair 10 µM working solution prepared by mixing 60 µl of *Fms-EGFP* F stock solution and 60 µl of *Fms-EGFP* R stock solution with 480 µl distilled H_2O. The *Fabpi500* primer pair 10 µM working solution was prepared by mixing 60 µl of *Fabpi500* F stock solution and 60 µl of *Fabpi500* R stock solution with 480 µl distilled H_2O. The primer pair mix was then prepared by combining 20 µl *Fms-EGFP* Primer pair 10 µM working solution with 20 µl *Fabpi500* Primer pair 10 µM working solution made up to 500 µl with Tris EDTA buffer.

Stock PCR solution was prepared on ice by mixing 6.5 µl double distilled H_2O (ddH_2O), 12.5 µl 2x MasterMix (QIAGEN Type-it™ Kit, 206343), 2.5 µl Primer Pair Mix and 2.5 µl CoralLoad Dye (QIAGEN Type-it™ Kit, 206343). Alternatively a stock PCR solution was prepared on ice by mixing 48 µl MegaMix-Blue (Microzone 2MMB-100), 0.5 µl *Fms-EGFP* 10 µM primer pair working solution and 0.5 µl *Fabpi500* 10 µM Primer pair working solution.

The Stock PCR solution was then mixed by vortex and 24 µl aliquots transferred by pipette into labelled 0.10 ml tubes with one for each PCR genotype reaction. Also included were three extra tubes for negative, positive and ddH_2O controls. To each tube; 1 µl target DNA from a mouse to be genotyped was added and vortexed to mix. DNA from a mouse known to be *Fms-EGFP* positive was added as a positive control, and DNA from a mouse known to be *Fms-EGFP* negative was used as a negative control. To the tube marked ddH_2O, a 1 µl aliquot of the same volume of ddH_2O used in preparing the master mix was included. The PCR cycle run was performed in in a thermocycler (Geneamp PCR System 9700) with 35 cycles of denaturation at 94 °C for 30 sec, annealing at 65 °C for 30 sec and elongation at 72 °C for 3 min.

3.2.3.5 Gel Electrophoresis Visualisation of PCR Amplified DNA

PCR products were removed from 4°C storage and, if required, supplemented with loading dye. For each tube, 5 µl was loaded into a 2% agarose gel prepared using TAE buffer and ethidium bromide. Visualisation and image capture was performed under ultra violet light.

3.2.4 Tissue Processing

3.2.4.1 Paraffin Wax Embedded Tissues

Mice were culled by cervical dislocation at 35, 100, 150 days post inoculation (dpi) and at terminal stage. Tissues were fixed in formal saline then placed in > 99% formic acid for 1 hour to reduce titre infectivity by ≥ 1.0 and ≥ 5.0 log titres when mice were challenged with 0.02ml of 10^{-2} w/v infected brain material (Taylor *et al.*, 1997). Brain tissue was sectioned as per the standard method first developed by Fraser and Dickinson (1967), and outlined in SOP-PSG-008 used by the Pathology Department at The Roslin Institute (Figure 3-1), prior to embedding in paraffin wax. Sections were cut on a microtome at a thickness of 6 µm.

3.2.4.2 Frozen Tissue Fixation and Cryostat Sectioning

Brain tissue was taken directly from BALB/cJ$^{Fms\text{-}EGFP/-}$ mice and placed into 5 ml pre chilled 4% paraformaldehyde solution for 2 hours at 4°C. Following fixation tissues were transferred to pre chilled 18% sucrose solution overnight at 4°C.

Following incubation brain tissue was dissected and arranged on a thin layer of optimum cutting temperature (OCT) freezing compound (Cellpath, KMA-0100-00A) in a tissue mould (Surgipath, 03065) following the procedure outlined in SOP-PSG-008 used by the Pathology Department at The Roslin Institute (Figure 3-1). Once aligned correctly the brain sections were covered completely in additional freezing compound.

The moulds were then lowered into a beaker of isopentane (BDH, 103641T) clamped over a Dewar of liquid nitrogen in which 1 cm of the beaker was submerged below the nitrogen surface. Moulds were removed by forceps after 1 min and left to dry for 10 sec before the frozen OCT embedded tissue blocks were prised out of the moulds. All blocks were stored at -40°C on dry ice until completion of procedure and then transferred to permanent storage at -70°C.

Frozen OCT embedded tissue blocks to be sectioned were removed from -70°C storage and placed within the -20°C working area of the cryostat (LEICA CM 1900) for 10 min to reduce the block temperature to within working limits. Tissue blocks were mounted onto the cryostat chucks using several drops of OCT freezing compound and correctly aligned with aid of the cryostat mounting tool. The chuck and tissue block combination were then mounted onto the microtome and the temperature of both the environment and microtome adjusted to -20°C. Sections were cut at 6 µm using a new microtome blade and immediately placed onto microscope slides. Slides were then air dried overnight in the dark before storage at -20°C until required.

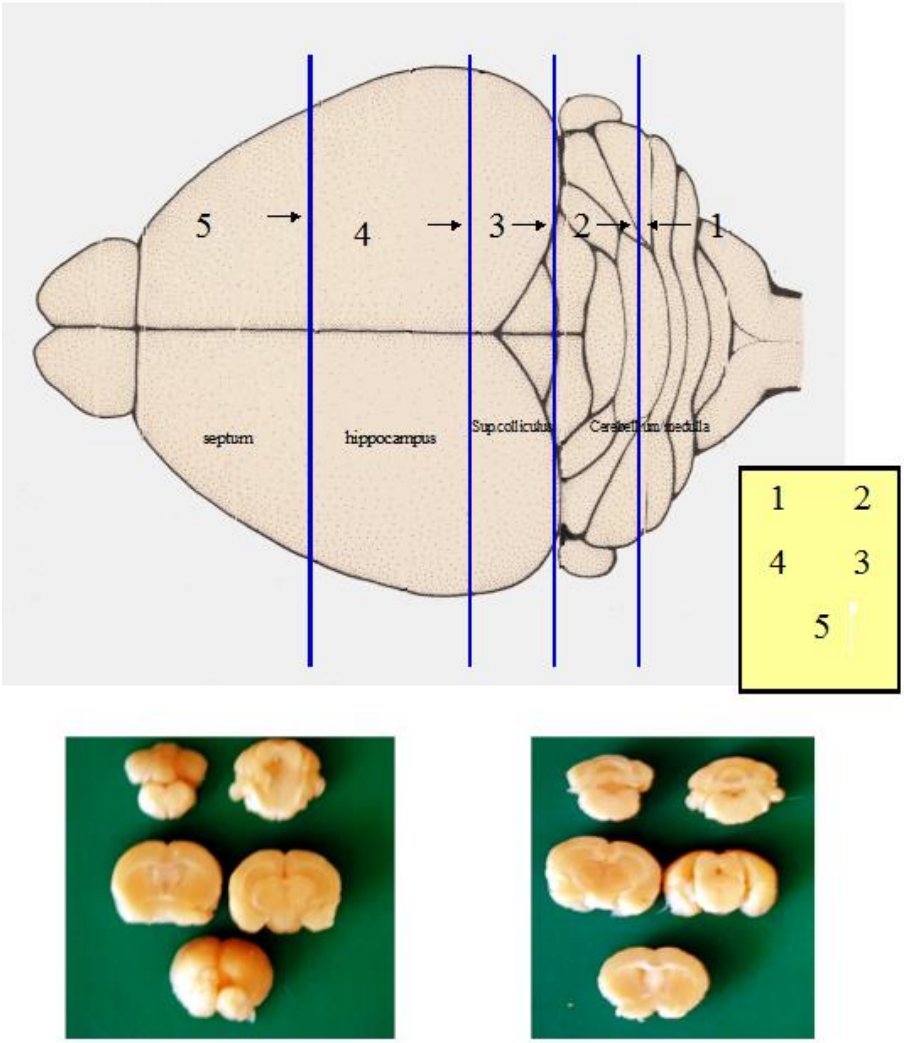

Figure 3-3: Trimming and embedding levels for mouse brain sectioning detailed in SOP-PSG-008 and used by the Pathology Department at The Roslin Institute

3.2.5 Immunohistochemistry

3.2.5.1 Labelling of PrP Deposition with 6H4 anti-mouse PrP Primary Antibody

Prionics (Switzerland) 6H4 is a mono-clonal mouse antibody that detects amino acids 144 – 152 in the human protein. It also has a high affinity for the mouse protein, indicating the replacement of tyrosine with a tryptophan at position 145 in murine PrP has no impact on binding affinity.

All paraffin wax embedded 6 µm thick brain tissue sections were taken through xylene to remove paraffin wax and finally successively diminishing concentrations of ethanol ending in dH_2O to both remove the xylene and rehydrate the tissue. Following rehydration, antigen retrieval was performed in an autoclave at 121°C for 15 min in dH_2O and then incubated in formic acid for 10 min at room temperature to aid antigen retrieval. The slides were washed thoroughly in running tap water prior to blocking of endogenous peroxidase with 1% H_2O_2 (Sigma-Aldrich, H1009) in 100% methanol for 10 min. The slides were again rinsed in running tap water then placed into phosphate buffered saline supplemented with 0.2% bovine serum albumin in PBS (PBS/BSA) wash buffer for 5 min at room temperature.

All sections were blocked with serum-free mouse protein block (Dako, X0909) or normal goat serum diluted to 1 µg ml^{-1} with antibody diluent (phosphate buffered saline supplemented with 1% bovine serum albumin) for 20 min at room temperature. Following blocking, the serum was tapped off each slide and monoclonal mouse 6H4 (Prionics, 01-011, Switzerland) primary antibody applied at 0.5 µg ml^{-1} to the experimental slides and left to incubate overnight at room temperature. Negative control slides were treated overnight with mouse mixed immunoglobulin control (Invitrogen, 14175-053) at room temperature.

3.2.5.2 Labelling of Microglia Cells with Allograft inflammatory factor 1 (AIF1)

Antigen retrieval was performed in the microwave (600 Watt) in 0.1 M citrate buffer at pH 6.0. Endogenous peroxidase was blocked with 1% H_2O_2 (Sigma-Aldrich, H1009) in 100% methanol for 10 min, then rinsed in running tap water and placed into phosphate buffered saline supplemented with 0.2% bovine serum albumin (PBS/BSA) wash buffer for 5 min at room temperature.

All sections were blocked with 20% normal goat serum diluted with antibody diluent for 20 min at room temperature. Following blocking the serum was tapped off each slide and polyclonal rabbit anti-allograft inflammatory factor 1 (Abcam, ab108539) primary antibody diluted to 0.5 µg ml^{-1} was applied to the experimental slides and left to incubate overnight at room temperature. Control slides were treated with serum.

3.2.5.3 Application of Secondary Antibody & Enzymatic Location of Antibody/Enzyme Complexes

Following overnight incubation the primary antibody and serum was tapped off and slides were washed three times for 5 min in PBS/BSA wash buffer keeping controls separate. Addition of an intermediate enzymatic reacting incorporating the deposition of biotinylated phenolic compound increases the available biotin molecules onto which streptavidin-biotin-peroxidase is catalysed. These regents are commercially incorporated into the Catalysed Signal Amplification (CSA) System (Dako, K1500). The CSA amplification kit (Dako, K1500, Cambridgeshire UK), if used, was applied following the manufactures instructions, otherwise secondary biotinylated antibody at a concentration of 1 µg ml^{-1} was applied to all slides for 1 hour at room temperature followed by three 5 min washes in PBS/BSA wash buffer. All slides were then incubated in Vectastain avidin/biotinylated enzyme complex (Vector, PK-6100) for 30 min at room temperature followed by three 5 min washes in PBS/BSA wash buffer. Slides were then incubated for 5 minutes in 3,3'-

Diaminobenzidine tetrahydrochloride solution acting as a substrate for added H_2O_2 to enzymatically locate the avidin/biotinylated enzyme complex by generating a dark brown oxide.

Slides were then placed into PBS/BSA wash buffer for 5 min at room temperature and rinsed in running tap water before immersion for 1 min in haematoxylin followed by a 1min immersion in Scott's tap water to blue nuclei. Finally the slides were rinsed in running tap water and taken to xylene through successively increasing concentrations of ethanol to dehydrate the tissues. Hydrophobic mounting of coverslips was performed using Pertex mounting medium (Cellpath, SEA-0104-004) and all sections were then left to dry overnight. Sections were viewed on a Nikon E800 bright field microscope and images captured using Image Pro software.

3.2.6 Statistics

Comparison between two populations was performed using a two-tailed *t*-Test assuming a variance depending upon the outcome of an *f*-Test for variance. Such a system is optimised for a smaller number of populations in utilising a wider distribution curve to ensure a higher value is required for the *t*-critical to become significant. The *f*-test ensured that variance was correctly identified as equal or un-equal and provided additional insurance against making a Type I/II error. Comparison of Kaplan-Meier plots was performed using the survdiff Log Rank Test function (Harrington and Fleming, 1982) located within the survival package of R (Version x64 3.1.2):

Log Rank Test: $$\chi^2 = \sum \frac{(\Sigma O_{jt} - \Sigma E_{jt})^2}{\Sigma E_{jt}}$$

O_t = Total Number of Events (Sum of *O1* and *O2*)

E_t = Expected Number of Events (*Et* = *Nt**(*Ot*/*Nt)*

3.3 Results: Suitability of BALB/cJ$^{Fms\text{-}EGFP/-}$ for use in Prion Disease Infection

3.3.1 Clinical Signs and Incubation Period

Mice infected with 79A or ME7 prion strains and belonging to the groups taken out to terminal disease were scored every 7 days for clinical signs from 150 dpi. Signs recorded were lethargy, hair unkempt/loss, and hunching with no discernible indication of a difference in clinical signs between either genotype. Only one mouse was observed to have gait problems and none were discerned to suffer from wetness around the genitalia. Results were initially noted as a '2' on the scoring sheet and a '+' if noted at the next consecutive evaluation. The onset of clinical signs was determined as a mean average of the dpi for each mouse from the BALB/cJ$^{Fms\text{-}EGFP/-}$ and BALB/cJ groups infected with either prion strain. The BALB/cJ$^{Fms\text{-}EGFP/-}$ and BALB/cJ groups infected with 79A first demonstrated clinical signs at 201 ± 6.0 days standard error (SE) and 209 ± 4.2 days SE respectively. For the BALB/cJ$^{Fms\text{-}EGFP/-}$ and BALB/cJ groups infected with ME7 the onset of clinical signs was 295 ± 8.9 days SE and 306 ± 9.1 days SE. No statistical difference ($p > 0.05$) was noted between the onset of clinical signs for either mouse genotype inoculated with either prion strain (Figure 3-4A). Control BALB/cJ$^{Fms\text{-}EGFP/-}$ inoculated with normal brain homogenate were culled at 250 days after showing no signs of clinical disease. The total disease incubation periods were also determined as a mean average with BALB/cJ$^{Fms\text{-}EGFP/-}$ and BALB/cJ mice infected with either 79A culled at 225 ± 6.3 days SE and 227 ± 6.5 days SE respectively and BALB/cJ$^{Fms\text{-}EGFP/-}$ and BALB/cJ mice infected with either ME7 culled at 310 ± 8.6 days SE and 317 ± 9.5 days SE respectively. Statistical significance ($P > 0.05$) between disease incubation periods was not noted between BALB/cJ$^{Fms\text{-}EGFP/-}$ and BALB/cJ mice infected with either 79A or ME7 (Figure 3-4B). Individual values were used to construct Kaplan-Meier survival curves for each group (Figure 3-5). Both BALB/cJ$^{Fms\text{-}EGFP/-}$ and BALB/cJ showed very similar patterns in the overall spread of cull dates indicating no marked differences in either disease pathogenesis or population dynamics of size, gender and inoculum titre.

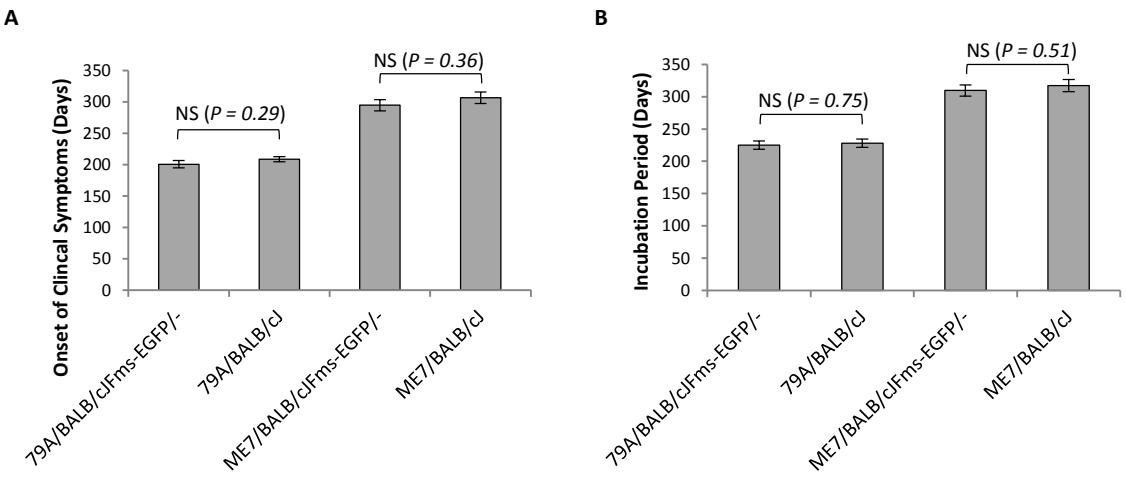

Figure 3-5: Incubation period and onset of clinical signs for BALB/cJ$^{Fms\text{-}EGFP/-}$ or BALB/cJ following intraperitoneal challenge with either 79A or ME7 prion strains. **A:** Onset of clinical signs for BALB/cJ$^{Fms\text{-}EGFP/-}$ and BALB/cJ mice. A slight increase in sample distribution determined by *f*-Test assumed unequal variance, however no statistically significant difference was found for onset of clinical signs (*t*-Test two-sample assuming unequal variances) between BALB/cJ$^{Fms\text{-}EGFP/-}$ and BALB/cJ mice infected with either prion stain. **B:** Mean incubation periods for BALB/cJ$^{Fms\text{-}EGFP/-}$ and BALB/cJ. No statistically significant difference found (*f*-Test for variance then *t*-Test two-sample assuming equal variances) between BALB/cJ$^{Fms\text{-}EGFP/-}$ and BALB/cJ mice infected with either prion stain. Error bars equate to standard error.

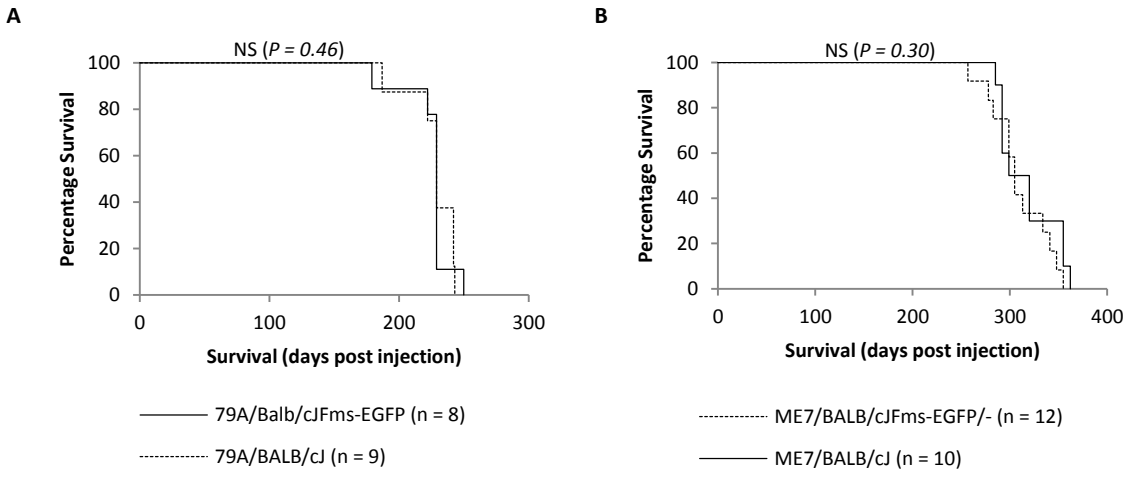

Figure 3-4: Kaplan-Meier survival curves for BALB/cJ$^{Fms\text{-}EGFP/-}$ or BALB/cJ following intraperitoneal challenge with either 79A or ME7 prion strains. **A:** BALB/cJ$^{Fms\text{-}EGFP/-}$ and BALB/cJ infected with 79A or **B:** ME7 prion stains both have curves with a high degree of overlap indicating no notable difference between BALB/cJ$^{Fms\text{-}EGFP/-}$ and BALB/cJ infected with either prion strain (statistical analysis performed using performed using the survdiff function (Log Rank test) located within the survival package of R).

3.3.2 Grey Matter Lesion Scoring

All brain tissues embedded in paraffin wax were investigated for the presence of prion disease associated lesions. In addition to confirming infection, a vacuolation score profile provides a semi-quantitative and highly reproducible pattern allowing for correct strain identification (Bruce *et al.*, 1991). Strain typing in this manner also serves as a powerful tool for comparing the disease pathogenesis of two different mouse genotypes infected with the same prion strain. Any impact upon infection of prion disease by the *Fms-EGFP* transgene in BALB/cJ$^{Fms\text{-}EGFP/-}$ mice would be revealed upon comparison with wild type BALB/cJ mice.

All mice culled at 35, 100 and 150 dpi were clinically negative at the time of death and all scored pathologically negative with scores of 0 in all regions. All mice that scored as pathologically positive for prion disease demonstrated brain regions with lesions associated with prion infection (Figure 3-6). The severity of lesions was more severe with ME7 infection with the majority of tested regions containing a higher proportion of scores at 2 or above. Lesion profiles for both BALB/cJ$^{Fms\text{-}EGFP/-}$ and BALB/cJ groups infected with ME7 show a comparable trend in grey matter regional targeting indicating no significant difference between infection in BALB/cJ regardless of the presence of the *Fms-EGFP* reporter.

By contrast 79A infection demonstrated far fewer regions containing vacuolation indicating a more targeted pathology. It should be noted that scoring of several regions, particularly the superior colliculus area and septum area were scored with slight differences for BALB/cJ$^{Fms\text{-}EGFP/-}$ and BALB/cJ infected with 79A. A minimum of 6 animals is required for correct lesion profiling and although 8 BALB/cJ and 9 BALB/cJ$^{Fms\text{-}EGFP/-}$ animals incorporated, not all regions were captured successfully in paraffin wax resulting in a minimum of 6 sections for some scored regions.

Although the 79A scoring met the minimum requirements, the difference in curves between the BALB/cJ and BALB/cJ$^{Fms\text{-}EGFP/-}$ mice may be the product of a reduced

scoring population and/or poor quality paraffin wax sections. By contrast, a minimum of 9 BALB/cJ and 10 BALB/cJ$^{Fms\text{-}EGFP/-}$ sections from 10 and 12 animals respectfully was obtained from ME7 infected mice. It is also important to consider when strain typing, the final incubation period and the pattern of PrP deposition. The latter do not show any significant differences (Section 3.3.3) and as such the use of 79A in BALB/cJ$^{Fms\text{-}EGFP/-}$ and BALB/cJ mice was considered acceptable for future experimental use.

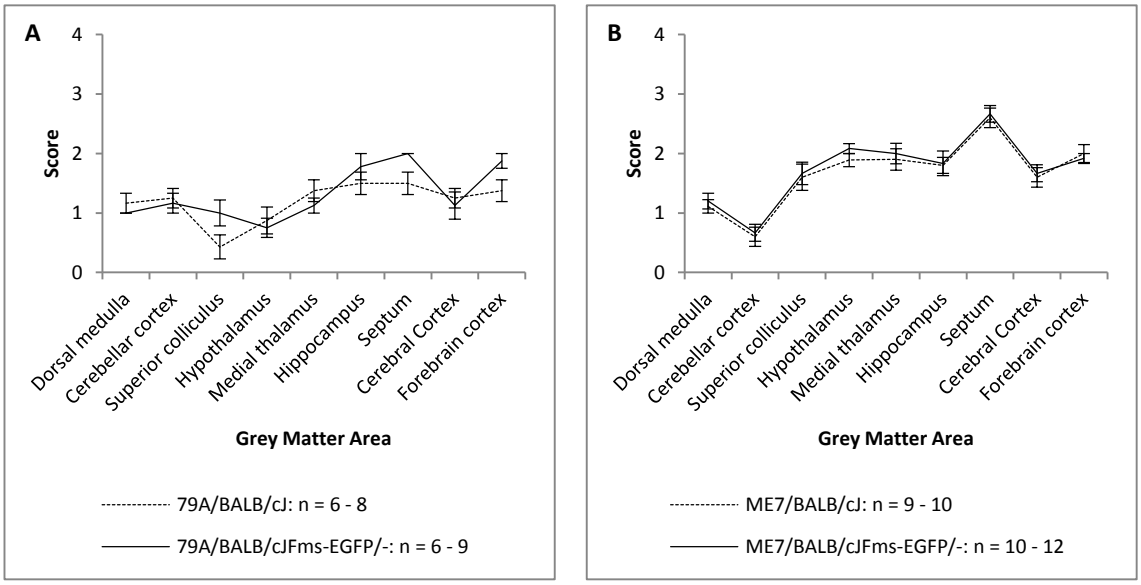

Figure 3-6: Scrapie lesion density profiles in BALB/cJ and BALB/cJ$^{Fms\text{-}EGFP/-}$ mice following intraperitoneal challenge of **A:** 79A or **B:** ME7 Scrapie prion strains. Both prion strains show a similar pattern of targeting in BALB/cJ mice regardless of *Fms-EGFP* reporter presence although there are some differences in the superior colliculus and septum between the two mouse genotypes infected with 79A. NB: lesion curves should not be visualised as a continuous data line chart.

3.3.3 Terminal Stage PrP Staining using 6H4 Anti-PrP Antibody

The conversion of the host prion protein (PrP^{C}) into the misfolded insoluble PrP^{Sc} is one of the defining principles of prion infection. The accumulation of PrP can be visualised as deposits in the brain using immunohistochemistry. The pattern of deposition in the brain of mice is strain specific and highly reproducible.

Immunohistochemical analysis of PrP deposition forms an important component in the identification of host infection and strain identification.

Tissues obtained from BALB/cJ$^{Fms\text{-}EGFP/-}$ mice were subjected to 1 hour immersion in formic acid. Immersion in formic acid reduces the infectivity of mouse-adapted Scrapie by ≥ 1.0 and ≥ 5.0 log titres respectfully when mice are challenged with 0.02ml of 10^{-2} w/v infected brain material (Taylor *et al.*, 1997). To ascertain if the 6H4 antibody was suitable for use with formic acid treated tissues immunohistochemistry was carried out on formic acid treated control sections taken from the institute archives and incorporated a titration of 6H4 to determine the optimum concentration. PrP deposition was detectable at all tested concentrations of 1.25 µg ml^{-1}, 0.80 µg ml^{-1}, 0.60 µg ml^{-1}, 0.50 µg ml^{-1}, 0.25 µg ml^{-1}, 0.10 µg ml^{-1} and 0.05 µg ml^{-1} confirming the suitability of 6H4 on formic acid treated sections. Experimental 79A infected BALB/cJ$^{Fms\text{-}EGFP/-}$ and BALB/cJ sections were then incubated with 6H4 at 0.50 µg ml^{-1}; the concentration found to be optimum for 6H4. However only weak PrP staining was detected in the thalamus of all experimental sections (Figure 3-7 A-C).

To improve 6H4 staining intensity the procedure was incorporated with the Dako CSA signal amplification kit. Use of 6H4 with the Dako CSA kit on a small sample of 79A terminal BALB/cJ$^{Fms\text{-}EGFP/-}$ and BALB/cJ sections resulted in stronger staining than the use of 6H4 alone (Figure 3-7 D-F).

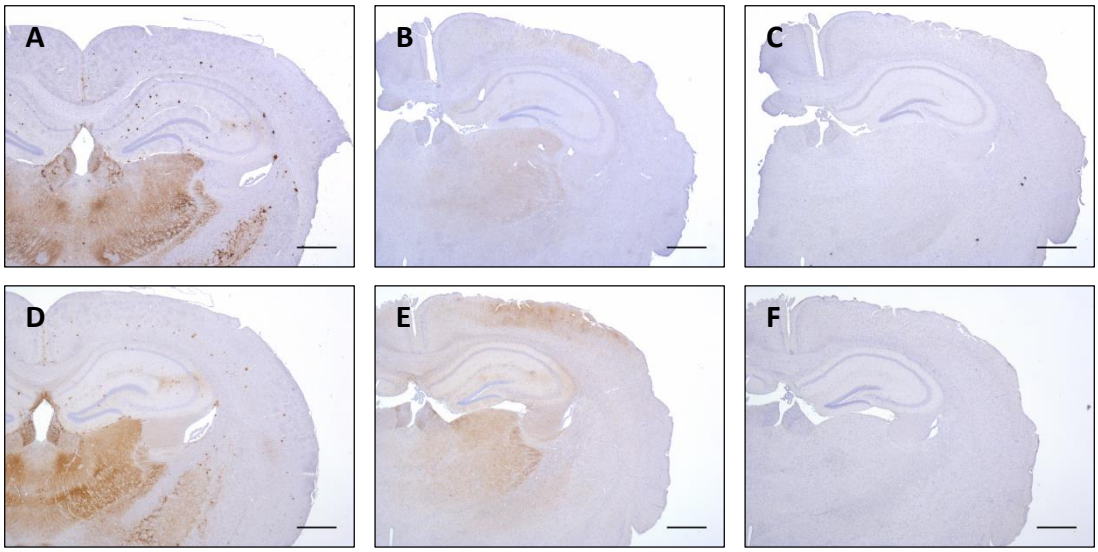

Figure 3-7: Optimising 6H4 anti-PrP antibody for use with experimental sections. **A:** 6H4 alone at 0.5 µg ml^{-1} on 87V/VM positive control **B:** 6H4 alone at 0.5 µg ml^{-1} on terminal 79A/ BALB/cJ$^{Fms\text{-}EGFP/-}$. **C:** Negative control using 0.5 µg ml^{-1} mouse isotype control. **D:** 6H4 at 0.5 µg ml^{-1} in combination with Dako CSA amplification on 87V/VM positive control. **E:** 6H4 at 0.5 µg ml^{-1} in combination with Dako CSA amplification on terminal 79A/ BALB/cJ$^{Fms\text{-}EGFP/-}$. **F:** Negative control using 0.5 µg ml^{-1} mouse isotype control in combination with Dako CSA amplification. In all instances sections from the same animal were utilised for comparison. Deposition visualisation of PrP using 6H4 on experimental BALB/cJ$^{Fms\text{-}EGFP/-}$ sections is considerably stronger when used in combination with signal amplification. Scale bars equate to 500 µm.

BALB/cJ$^{Fms\text{-}EGFP/-}$ and BALB/cJ brain sections from mice challenged i.p. with 79A or ME7 were stained for PrP deposition using 6H4 at 0.5 µg ml^{-1} in combination with the Dako CSA amplification kit (Figure 3-8). Included in the same immunohistochemical assays were brain sections from BALB/cJ$^{Fms\text{-}EGFP/-}$ mice inoculated with normal brain homogenate. These mice served as controls to confirm that the act of i.p. injection had no impact on mouse health or disease pathogenesis. Background staining was minimal on all sections. No PrP deposition was present on brain sections inoculated with normal brain homogenate although some non-specific staining, residing only on the surface of the section, was observed in the corpus callosum and the fimbria hippocampus; both white matter regions surrounding the hippocampus. BALB/cJ$^{Fms\text{-}EGFP/-}$ and BALB/cJ mice infected with 79A at terminal stage of disease demonstrated diffuse deposition of PrP as fine punctate particles throughout most of the brain. Accumulation of the misfolded protein was strongest in the thalamus extending back to the medulla and was indicative of successful 79A infection (Bruce, 1993, Cancellotti *et al.*, 2010). To a lesser extent, deposition in the hippocampus was found in all animals, while deposition in the cortex was found in some but not all animals. Despite cross reference with records of litter mates and gender no explanation for the latter observation was found.

In the ME7 infection deposition of PrP at terminal stage of disease was found in the thalamus as a heavy accumulation of fine punctate plaques (Figure 3-9). Larger plaque aggregates were found in the oriens and CA3 regions of the hippocampus. Similar to 79A, fine diffuse deposition was found extending back from the hippocampus and thalamus to the medulla.

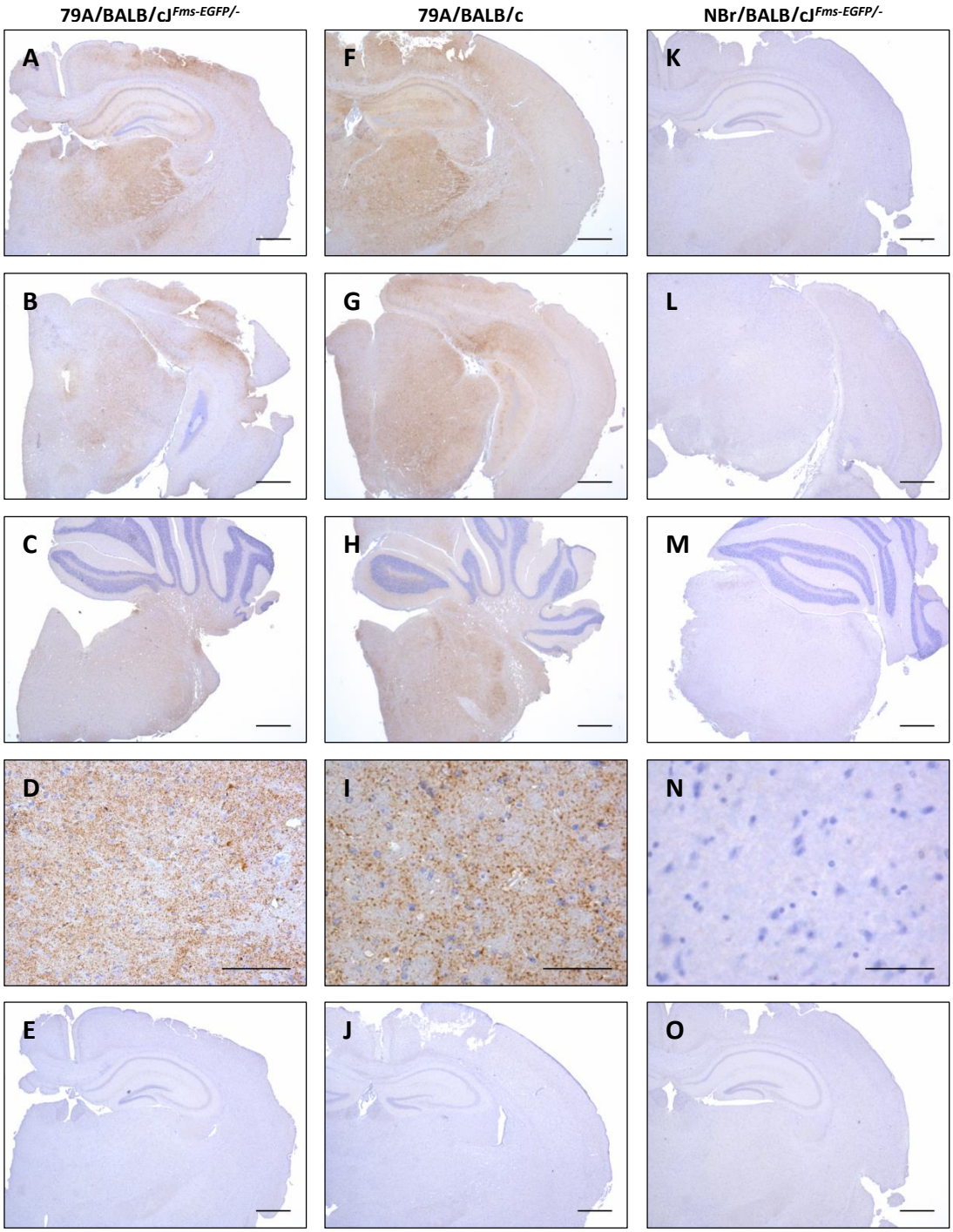

Figure 3-8: Staining for PrP deposition using 6H4 with Dako CSA signal amplification on terminal BALB/cJ$^{Fms\text{-}EGFP/-}$ mice challenged i.p. with 79A. **A:** Deposition of PrP in BALB/cJ$^{Fms\text{-}EGFP/-}$ mice is heaviest in the thalamus, cortex and to a lesser extent in the hippocampus. Deposition can be traced from the thalamus back through **B:** the midbrain, neo-cortex and finally **C:** the medulla. **D:** 400 x magnification reveals thalamic deposition to comprise of diffuse punctate aggregates. **E:** 79A/BALB/cJ$^{Fms\text{-}EGFP/-}$ IgG control. The deposition pattern of 79A PrP in BALB/cJ mice **F-I:** is as per BALB/cJ$^{Fms\text{-}EGFP/-}$ mice with the same regional targeting. **J:** 79A/BALB/cJ IgG control. **K-N:** Included in the same assay were BALB/cJ$^{Fms\text{-}EGFP/-}$ inoculated with normal brain homogenate. **O:** NBr/BALB/cJ$^{Fms\text{-}EGFP/-}$ IgG control No pathology or deposition was observed in these mice. All images representative. Scale bars equate to 500 µm except **D, I** and **N** where scale bars equate to 50 µm.

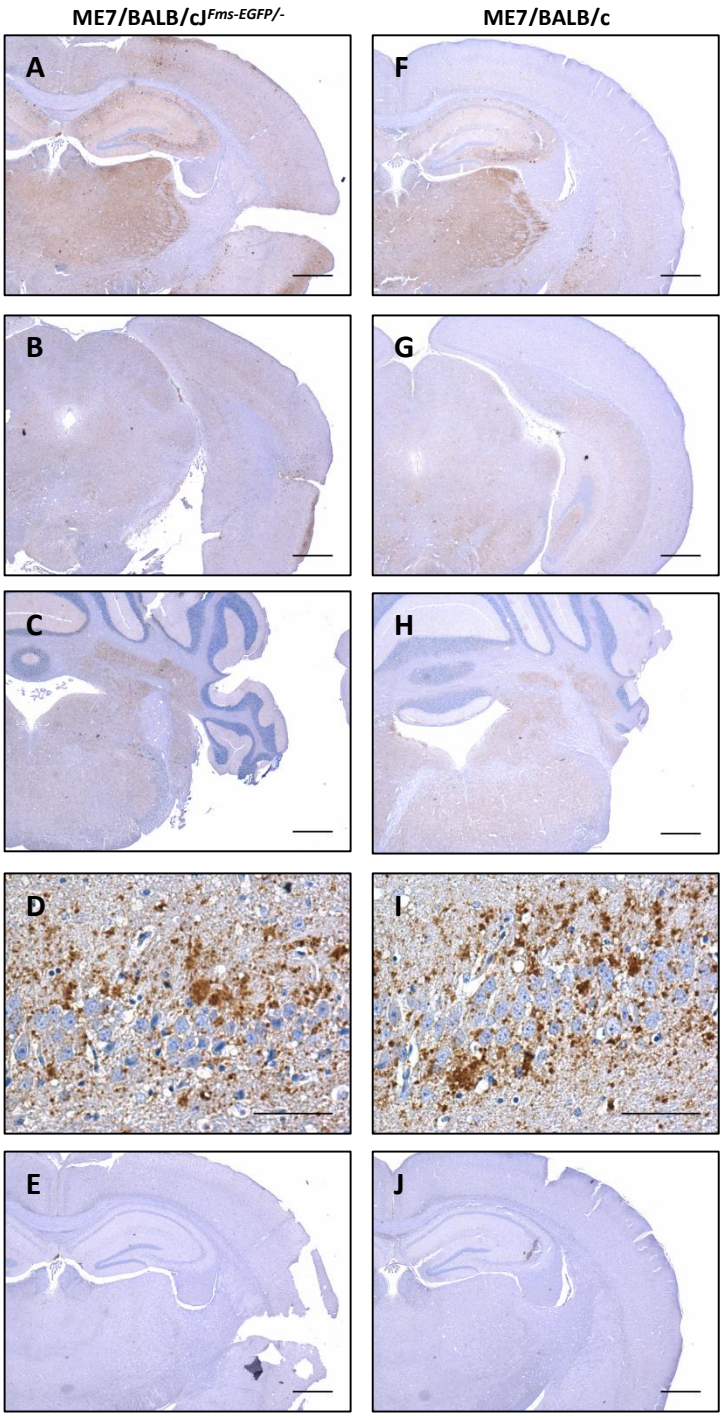

Figure 3-9: Staining for PrP deposition using 6H4 with Dako CSA signal amplification on terminal BALB/cJ$^{Fms\text{-}EGFP/-}$ mice challenged i.p. with ME7. **A:** Deposition of PrP in BALB/cJ$^{Fms\text{-}EGFP/-}$ mice is heaviest in thalamus and hippocampus. Similar to 79A, deposition can be traced back through **B:** the midbrain, neo-cortex and finally **C:** the medulla. **D:** 400x magnification of the C3 region of the hippocampus revealed formations of plaques amongst punctate aggregates. **E:** ME7/BALB/cJ$^{Fms\text{-}EGFP/-}$ IgG control. The deposition pattern of ME7 PrP in BALB/cJ mice **F-I:** is as per BALB/cJ$^{Fms\text{-}EGFP/-}$ mice with the same regional targeting. **J:** ME7/BALB/cJ IgG control. No pathology or deposition was observed in these mice. All images representative. Scale bars equate to 500 µm except **D & I** where scale bars equate to 50 µm.

3.3.4 Terminal Stage Microglia Staining using AIF1 Antibody

Microglia were stained with microglia specific anti-allograft inflammatory factor 1 (AIF1) (Abcam, ab108539). Resting microglia stained with AIF1 display a ramified morphology with a small central body and long delicate processes. Conversely activated microglia exhibit a large central body and shorter thicker processes (Streit, 2002). Microglia in BALB/cJ$^{Fms\text{-}EGFP/-}$ and BALB/cJ mice challenged i.p. with 79A and examined at the terminal stage of disease displayed activated morphology in areas containing PrP deposition including the thalamus, medulla and hippocampus (Figure 3-10 A-B). In addition to morphological activation microglia were typically spaced closer together at ~25 µm. In areas without deposition microglia did not show morphological activation and were typically distributed at the normal resting spread in these mice of 50 – 100 µm apart. No difference was observed in microglia activation or regional accumulation between BALB/cJ$^{Fms\text{-}EGFP/-}$ and BALB/cJ mice.

BALB/cJ$^{Fms\text{-}EGFP/-}$ and BALB/cJ mice challenged with ME7 and taken to terminal stage of disease also displayed activated microglia in regions of PrP deposition. In areas of larger plaque deposits dispersed amidst diffuse aggregates (Figure 3-10 C-D), microglia are activated and closely spaced.

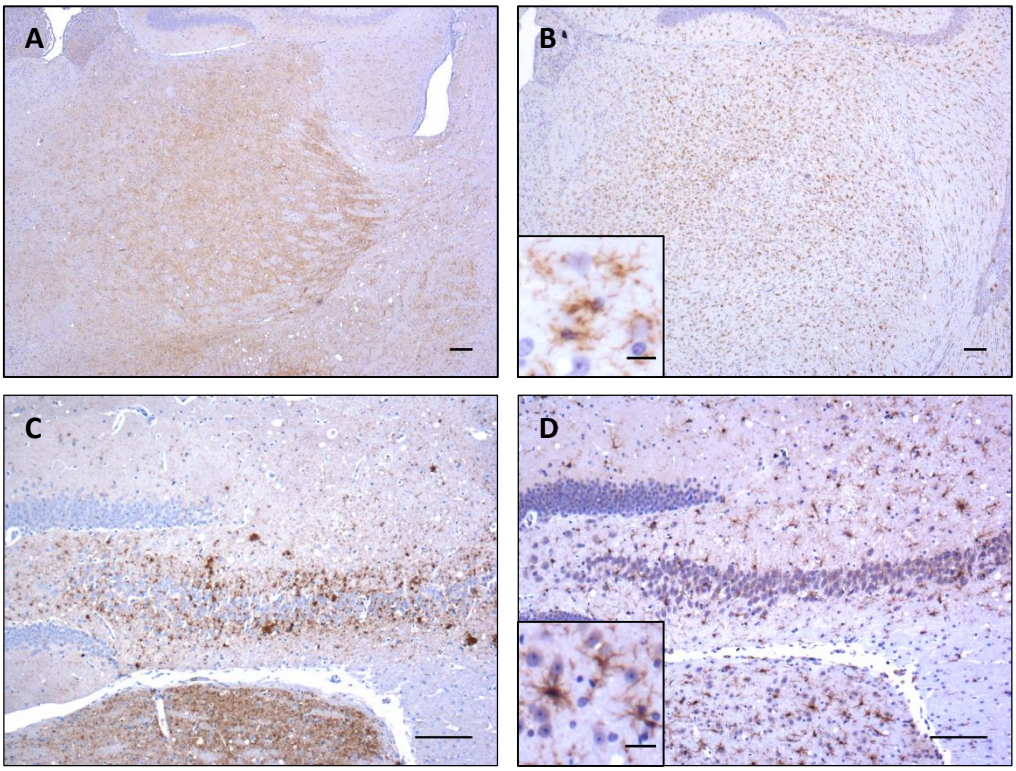

Figure 3-10: Terminal stage microglia activation is associated with PrP deposition in terminal BALB/cJ$^{Fms\text{-}EGFP/-}$ and BALB/cJ mice. **A:** Terminal Stage 79A PrP deposition is found as diffuse aggregates in the thalamus within which **B:** activated microglia demonstrating enlarged central body and shortened processes accumulate. **C:** Terminal stage ME7 PrP (6H4 staining) deposition is found as diffuse aggregates in the thalamus with larger plaques dispersed at ~ 100 µm in the hippocampus (dentate gyrus shown). **D:** Microglia (AIF1 staining) can be found tightly spaced at ~25 µm in areas of diffuse PrP deposition but do not appear to be cluster around the location of plaques. All images representative. Scale bars equate to 50 µm. Inset scale bars equate to 10 µm.

3.3.5 Influence of Gender on Disease Pathogenesis

It was noted that there was no gender dependant difference on incubation period in animals infected by 79A, but a small but statistically significant difference was noted in mice infected with ME7. This was also reflected in a difference in survival spread with female mice succumbing later than males (Figure 3-11).

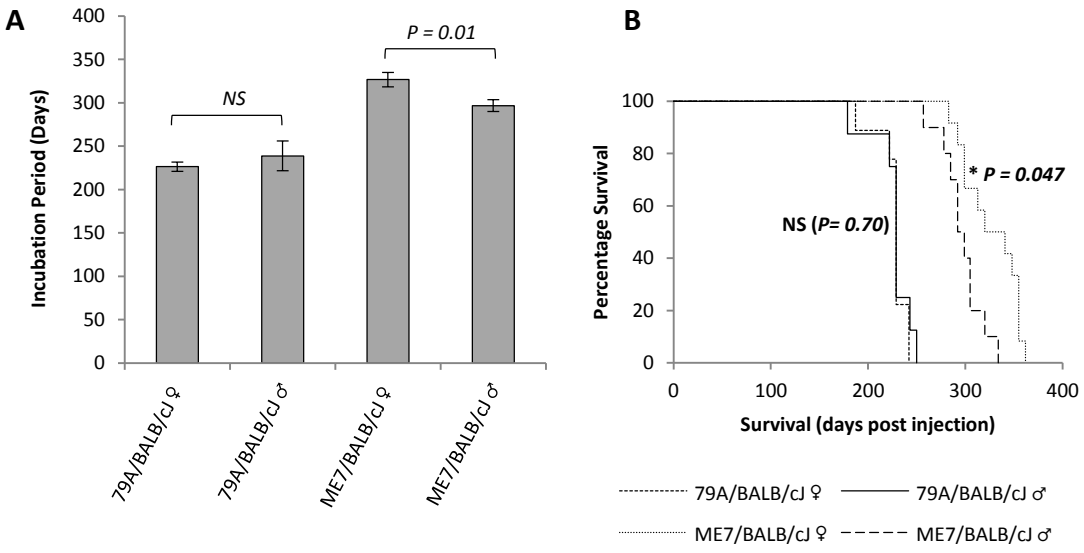

Figure 3-11: Gender differences in mean incubation period and survival of grouped BALB/cJ$^{Fms\text{-}EGFP/-}$ and BALB/cJ challenged i.p. with either 79A or ME7. **A:** Mice infected with 79A showed no significant difference in incubation period but mice infected with ME7 did demonstrate a small but significant difference between the genders (*f*-Test for variance then *t*-Test: Two-Sample Assuming Unequal Variances). **B:** This is reflected in the tight survival curves for both genders infected with 79A. A small but significant difference was also noted between the survival curves between male and female mice infected with ME7 (statistical analysis performed using performed using the survdiff function (Log Rank test) located within the survival package of R).

3.3.6 EGFP Preservation in BALB/cJ$^{Fms\text{-}EGFP/-}$ mice

To utilise the EGFP expression required that tissues taken were into 4% paraformaldehyde, thereby fixing the tissues prior to sucrose immersion, freezing in freezing media (OCT) and sectioning on a Cryostat. Tissues from three culled BALB/cJ$^{Fms\text{-}EGFP/-}$ 79A terminal stage animals were taken though to cryostat sectioning at 6 µm. Despite confirmation of the correct BALB/cJ$^{Fms\text{-}EGFP/-}$ genotype, EGFP fluorescence was extremely faint due to significant levels of overpowering background auto-fluorescence from blood related artefacts that could not be removed (Appendix 8-11).

Further experiments were undertaken utilising uninfected healthy BALB/cJ$^{Fms\text{-}EGFP/-}$ in an effort to preserve EGFP to investigate two options available in fixing fresh tissues using paraformaldehyde; Perfusion with saline and post-fixation by soaking in paraformaldehyde or perfusion directly with paraformaldehyde following saline. Perfusion with saline in both cases removed all blood related artefacts. The contrast between the vibrancy of EGFP expression between perfused-fixed and post-fixed was considerable (Figure 3-12) with finely branched microglial processes visualised following perfusion fixation.

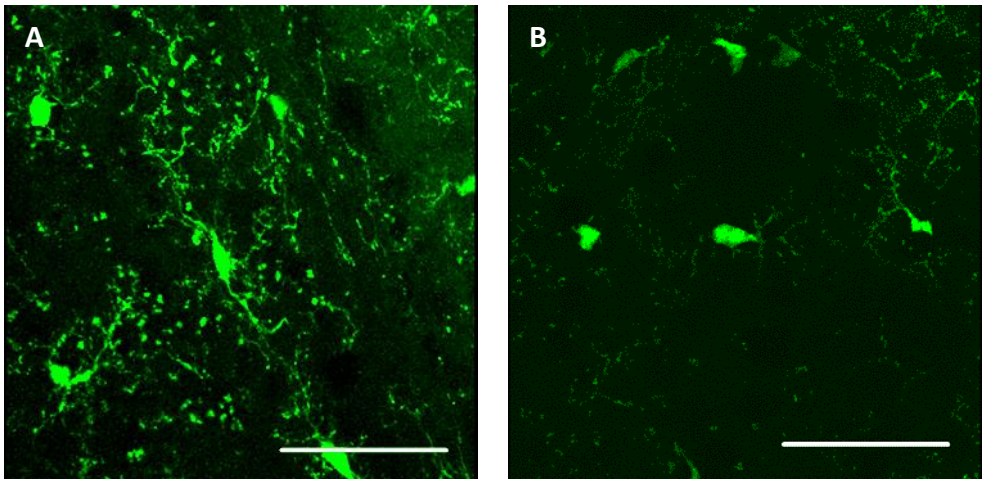

Figure 3-12: Compiled Z-stack Confocal images (Zeiss LSM 5 Pascal) of 25 µm BALB/cJ$^{Fms\text{-}EGFG/-}$ brain sections from healthy mice (thalamus shown). **A:** Perfusion-fixed microglia express vibrant EGFP with finely detailed ramified processes. Cells are typically spaced 50 µm apart in an even distribution**. B:** By contrast EGFP expression is much reduced in post-fixed samples and ramified processes are not as well defined. All images representative. Scale bars equate to 50 µm.

3.4 Results: Serial Investigation of BALB/cJ$^{Fms\text{-}EGFP/-}$ and BALB/cJ Mice Challenged with 79A or ME7 Prion Strains

3.4.1 Time Course Microglia and PrP Deposition Staining

The earliest accumulation of PrP deposition following 79A i.p. challenge was found in the medulla at 150 dpi or 65% of the total incubation period (Figure 3-13). Microglia were seen accumulating in the medulla in the same region as protein deposition yet did not show a strong morphological appearance of activation. In areas lacking PrP deposition, microglia demonstrated a normal ramified appearance and distribution. No evidence of microglia accumulation, activation or PrP deposition could be found within any of the ME7 injected brain sections taken from pre-clinical serial investigation time points of 35, 100 or 150 dpi.

It was important to ensure injection of foreign material did not elicit a lasting cycle of inflammation that could lead to misinterpretation of microglial response (Betmouni and Perry, 1999). This is particularly important as microglia are sufficiently sensitive to respond to peripheral stimuli (Nimmerjahn *et al.*, 2005). Animals culled at 35 dpi presented with no signs of pathology and scored clinically negative. There was also no evidence of microglia activation at this time confirming that any perturbation, if present, following inoculation of infected and uninfected material was quickly resolved.

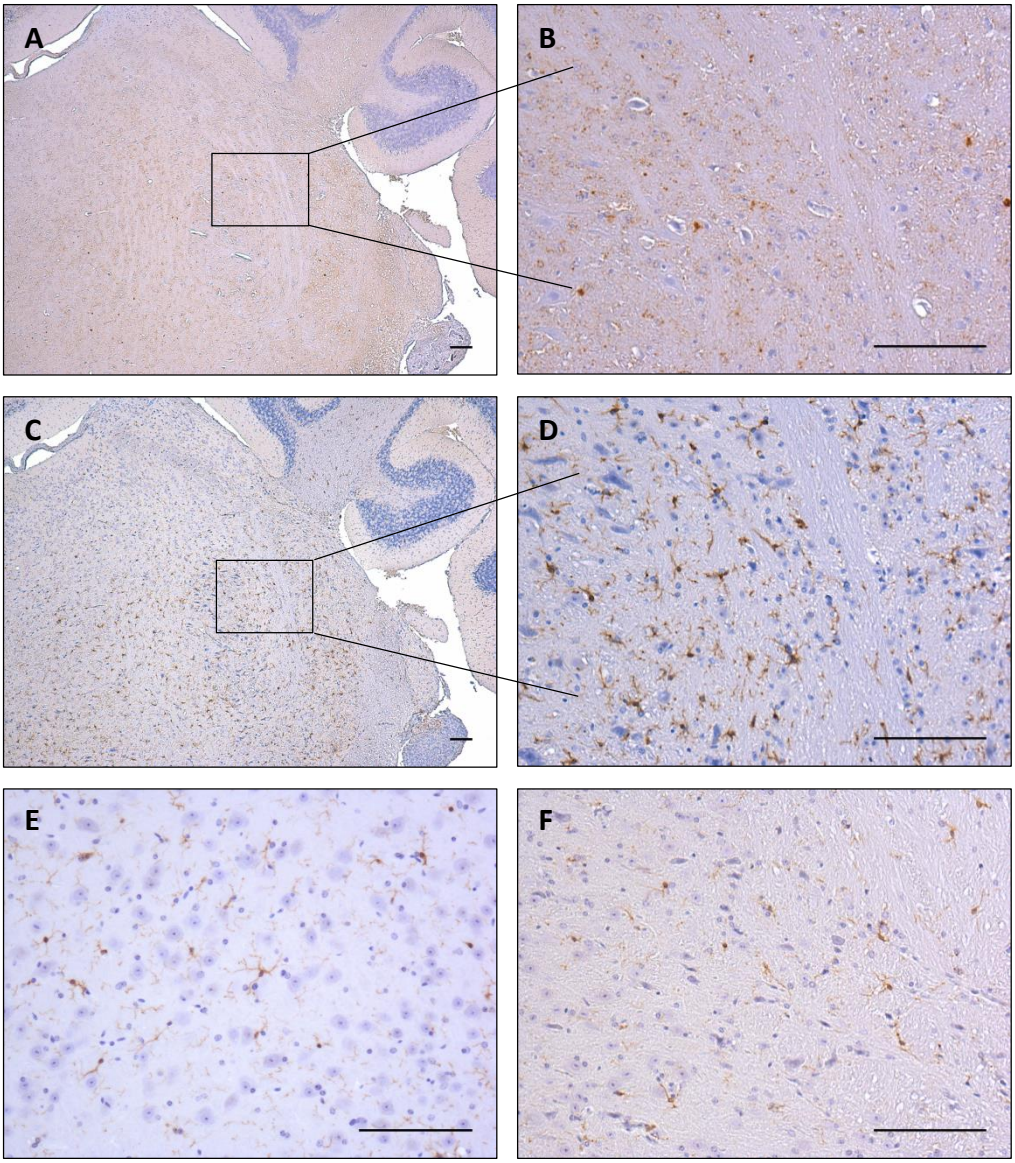

Figure 3-13: Time Course of microglia activation in BALB/cJ$^{Fms\text{-}EGFP/-}$ and BALB/cJ mice challenged i.p. with 79A. **A/B:** Earliest accumulation of PrP (6H4) is at 150 dpi in the Medulla. Microglia can be seen **C/D:** as accumulating in the same areas of deposition**. E/F:** Normal Microglia in the thalamus and medulla respectively of mice challenged with normal brain demonstrate a ramified appearance and greater separation at ~ 50 µm. All images representative. Scale bars equate to 100 µm.

3.5 Discussion

3.5.1 Suitability of BALB/cJ$^{Fms\text{-}EGFP/-}$ mice for use in Prion Disease Infection

The use of EGFP expression by microglia allows for novel and detailed investigations into the role of these cells in protein mis-folding diseases. BALB/cJ$^{Fms\text{-}EGFP/-}$ mice containing the *fms-EGFP* reporter gene and wild type BALB/cJ mice were challenged i.p. with 79A or ME7 mouse adapted Scrapie. The aim of this experiment was twofold; the first objective was to confirm that BALB/cJ$^{Fms\text{-}EGFP/-}$ are suitable for use as an *in-vivo* model for prion disease and behave as per BALB/cJ mice. The second aim was to address when and where microglia activations occurs in response to initial infection entering into the CNS environment. A peripheral route of infection was therefore adopted as it is the only route in which this is accurately encapsulated and it lacks the direct perturbation of the central nervous system that occurs with an intracerebral inoculation.

Both BALB/cJ$^{Fms\text{-}EGFP/-}$ and BALB/cJ genotypes presented with specific regional targeting hallmarked by the accumulation of PrP deposition and vacuolation. At terminal disease stage, and common to both prion 79A and ME7, the thalamus was the main target with extensive diffuse aggregates of PrP matching that seen in the literature for infection for these strains (Bruce *et al.*, 1991, Cancellotti *et al.*, 2010). Animals challenged with ME7 also presented with larger plaque deposits dispersed amongst diffuse deposits in the thalamus along with the dentate gyrus, CA3 and oriens layers of the hippocampus. Deposition was also detected in the brain through to the medulla.

The initial batch of mice chosen for the terminal group of 79A injections were aged 116 days ± 1.2 SE at the point of inoculation. All subsequent animals were therefore aged to match at inoculation to maintain consistency. The impact of age beyond 600 days on prion disease infection in mice is well documented with the requirement for clinical disease of a fully functioning lymphoid system (Brown *et al.*, 1999b, Brown *et*

al., 2009). Loss associated with normal aging of splenic margin zone, and associated Follicular Dendritic Cell mediated uptake and replication of infectious material also has a marked effect on whether the disease reaches clinical or remains sub-clinical without entering the CNS (Brown *et al.*, 2011). Disruption of the lymphoid system does not produce noticeable affects until > 400 days old at the point of injection. Consequently, and as all mice inoculated presented with clinical signs indicative of an advanced disease stage, it does not seem likely that the starting age of 116 day old BALB/cJ$^{Fms\text{-}EGFP/-}$ and BALB/cJ mice would have any impact on disease pathogenesis. Indeed past experiments documented in the divisional archives for BALB/cJ mice challenged i.p. with 0.02ml of 10^{-2} w/v 79A infected brain material (Appendix 8-12) revealed a starting age of ~ 100 days would not have a discernible impact on disease progression. Limited information on starting age for i.p. infection of BALB/cJ with ME7 could be found however the data was considered sufficient based upon 79A alone. It would therefore seem unlikely that this starting age would have an influence on the longer than expected incubation periods associated this batch of ME7. The incubation period should have been approximately 250 days and not the yielded time of approximately 300 days.

The only tentative explanation for the longer incubation period for i.p. ME7 infection of both BALB/cJ$^{Fms\text{-}EGFP/-}$ and BALB/cJ genotypes was attributed to the source material used to generate the infected inoculum. This comprised C57Bl/6J mice infected, by an intracerebral route, with ME7 infected mouse brain which almost invariably yields an incubation period of 160 days. The animals chosen to generate the source ME7 material () succumbed at a slightly longer incubation period of 166 and 171 days. Factoring in the 5.3% difference in expected outcome once averaged may explain the 20% difference in expected outcome for the longer than expected incubation period following i.p. infection of BALB/cJ$^{Fms\text{-}EGFP/-}$ and BALB/cJ mice; the difference between the two percentages a result of a lower starting titre and higher titre loss from the aforementioned increase in material dissemination following a peripheral route inoculation (Section 3.1.1).

The similarities between lesion profiling, incubation period and deposition pattern of BALB/cJ$^{Fms\text{-}EGFP/-}$ and BALB/cJ mice following both 79A and ME7 infection suggests no discernible impact on disease susceptibility or pathogenesis in the presence of the *Fms-EGFP* transgene. Knowledge of the targeted regions in the brain as part of a time course, combined with the lack of any noticeable difference between genders, strongly supported the continued use of the 79A prion strain for future experimentation with BALB/cJ$^{Fms\text{-}EGFP/-}$ mice. The difference between the origins of 79A and ME7 prevented any future predictions on the pathogenesis of ME7 to be drawn from the results of 79A infection. Combined with the slight but statistically significant difference between genders, and a lack of successful characterisation of the earlier events surrounding ME7 disease pathogenesis, the continued use of ME7 for further study in this project was severely limited. The ME7 time course was not an informative experiment although the terminal stage results did contribute towards confirming the suitability of the BALB/cJ$^{Fms\text{-}EGFP/-}$ strain for use in further prion infection research.

3.5.2 Use of EGFP Fluorescence

Following the culling of three BALB/cJ$^{Fms\text{-}EGFP/-}$ mice terminally challenged with 79A it was realised that the procedural methods for visualising EGFP by cryostat sectioning were not compatible with analysis of prion disease related lesions. Lesion scoring is an integral part of prion strain verification and necessary for confirmation of infection by a specific prion strain. Sectioning on a cryostat introduced distortion of the tissue causing uncertainty in the origin of lesions. The protocols were modified for all subsequent tissues to be taken into formal saline for embedment in paraffin wax after which no EGFP was detectable. Later efforts with uninfected BALB/cJ$^{Fms\text{-}EGFP/-}$ mice overcame difficulties with preserving EGFP and would allow future experiments to be carefully designed to exploit this novel feature allowing for imaging software

quantification of microglia number and morphology to be performed on fluorescent images.

3.5.3 79A Infection Time Course Analysis of Microglia Activation and PrP deposition

The role of microglial interaction with mis-folded protein in prion disease has not been fully explored with only limited evidence for focal distribution of activated microglia with PrP deposition (Williams *et al.*, 1994, Williams *et al.*, 1997, Rezaie and Lantos, 2001). Coinciding with initial observation of mis-folded protein in the medulla at 150 dpi in BALB/cJ$^{Fms\text{-}EGFP/-}$ and BALV/cJ mice challenged i.p. with 79A, this *in-vivo* model presents an accumulation of microglia in the same vicinity as PrP deposition. In areas lacking PrP deposition no accumulation or morphological change of microglia was observed. By the terminal stage of disease microglia are densely accumulated in areas of PrP deposition and present with an amoeboid morphology comprising enlarged central bodies with considerably shortened processes.

The use of AIF1, a constitutively expressed microglia marker widely used to determine activation based on morphology alone, is limited by not reflecting the more subtle stages of initial microglia activation. These data reveal a difference between the initial microglia recruitment response to prion invasion of the CNS and a more visible morphological activation once the disease has become widespread. This suggests a disparity between morphological activation and the changes, presumably protein translational in nature (Streit *et al.*, 1989a), required to instigate recruitment of surrounding microglia. To address this shortfall attempts were made to stain microglia with CD68 (Cambridge Bioscience, 137002) and I-A/I-E (Cambridge Bioscience 107602) markers of migration and phagocytic function respectfully. A lack of time prevented optimisation of these assays and staining with CD68 and I-A/I-E was unsuccessful. Also unsuccessful were assays to co-localise microglia and PrP deposition to investigate interaction using immunofluorescence. With additional

time alternative antibody clones and antigen retrieval methods could have been explored.

The previous chapter revealed a strong microglia and astrocyte response to infection regardless of prion strain. This signal was impossible to separate between the two types of cells. The observation of microglia accumulation at deposits of PrP without showing significant visible morphological activation would suggest that analysis of the microglia transcriptome alone following an i.p. 79A challenge would provide insight into the initial microglia response to prion disease. To date this has not been performed on isolated microglia as part of a serial investigation and certainly not as part of a peripheral route capturing the early events of microglia response as infection enters their domain.

3.5.4 ME7 Infection Time Course Analysis of Microglia Activation and PrP deposition

The lack of accumulation of PrP deposition or microglial response in the pre-clinical time points of brains of ME7 infected mice is attributed to the longer than expected incubation period. It is likely that the selected time points were too early to document infection of the CNS. Limited information could be found in the archives for peripheral inoculation of BALB/cJ mice with ME7 however data published by Outram (1976) revealed an expected incubation period of 261 days when using a peripheral route of infection (). The same serial investigation time points mice infected with 79A were therefore decided upon to encompass the same expected pathological events. Unforeseeable was the considerably longer incubation time of 310 and 317 days in BALB/cJ$^{Fms\text{-}EGFP/-}$ and BALB/cJ respectfully despite utilising the same inoculum concentration and the experiment was not informative.

3.5.5 Conclusion

These data demonstrate the suitability of the BALB/cJ$^{Fms\text{-}EGFP/-}$ mouse prion disease model with no significant differences between animals heterozygous for the *Fms-EGFP* transgene and the wild type BALB/cJ background. Of the two prion strains tested, the 79A prion strain was shown to have a more targeted pathology commending this strain for further use with BALB/cJ$^{Fms\text{-}EGFP/-}$ mice. The ME7 experiments would need repeating with later time points or alternatively an entirely new inoculum batch to document the early events of microglia activation.

The peripheral route model described in this present study portrays the initial microglial response to coincide with first PrP detection, matching that of intracerebral inoculated 79A (Giese *et al.*, 1998), but not other prion strains shown in the literature to significantly proceed or follow PrP accumulation (Williams *et al.*, 1994, Manuelidis *et al.*, 1997, Williams *et al.*, 1997, Baker *et al.*, 1999). The data presented here therefore suggests a disparity between initial recruitment and later morphological activation. By utilising the novel BALB/cJ$^{Fms\text{-}EGFP/-}$ mouse line, and information gained on the targeted regions in which microglia respond, further experiments would utilise EGFP expressing microglia by fluorescence microscopy or *ex-vivo* analysis and image quantification to fully document the specific timing the microglia response.

4 Serial Investigation of Microglia Response to Developing Prion Disease

4.1 Introduction

The aim of this chapter is to assess the response of microglia to developing prion infection by utilising the EGFP expression in BALB/cJ$^{Fms\text{-}EGFP/-}$ mice. Microglia expressing EGFP facilitated the quantification of the multi-stage transition made by microglia from a resting state to a state of full morphological activation. The time course in chapter 3 used infection of BALB/cJ$^{Fms\text{-}EGFP/-}$ mice with the 79A prion stain and showed how PrP deposition first occurred within the medulla. Chapter 2, describing a re-analysis of microarray first published by Hwang *et al.* (2009), revealed a strong signal of myeloid activation and cellular stress that steadily increased in strength as prion disease progressed. It is hypothesised that microglia first accumulate at sites of replication before demonstrating a significant and recognisable activation morphology.

The BALB/cJ$^{Fms\text{-}EGFP/-}$ mice strain was shown to behave as per the BALB/cJ wild type previously in Chapter 3. The strain is eminently suitable for further study using the 79A prion disease strain. Briefly, paraffin wax embedded brain sections from BALB/cJ$^{Fms\text{-}EGFP/-}$ and BALB/cJ mice challenged i.p. with 79A and stained with AIF-1 (Abcam) revealed microglia respond in sites of PrP deposition. The initial reaction was shown as an accumulation of microglia in the medulla at 150 dpi followed by a marked morphological activation in the thalamus at terminal disease. The necessity in those experiments of using paraffin wax sections to ascertain the clinical and pathological features of BALB/cJ$^{Fms\text{-}EGFP/-}$ mice in response to prion infection inhibited the full exploitation of the novel *Fms-EGFP* transgene marker. By taking mice at serial points post 79A infection from BALB/cJ$^{Fms\text{-}EGFP/-}$ and harvesting brain tissue with a method fully compatible with visualisation of EGFP, this chapter describes the use of microglia EGFP expression to quantify changes in morphology in the medulla and thalamus.

In BALB/cJ$^{Fms\text{-}EGFP/-}$ mice, microglia activation appeared to coincide with initial deposition of PrP, raising the importance, if a correct interpretation of the initial cause of activation is to be determined, of ensuring activation coincides with initial entry of infection into the brain. A peripheral route of infection is the only route in which this is accurately encapsulated (Millson *et al.*, 1979) and was again adopted to ensure microglia can be determined as responding to infection travelling from the periphery into the brain.

Previous experiments in this study had the last time point taken at 65% of the incubation period (150 dpi). The experiments did not therefore document the spread of pre-clinical infection from the medulla to other areas of the brain between this time point and terminal disease. Onset of clinical signs was found to be at ~ 200 days thereby including an additional cull point at this time should document this critical stage of disease. The onset of clinical disease has been shown to coincide with a significant reduction in synaptic density and behavour changes (Cunningham *et al.*, 2003). Focus was made on specific regions; the medulla as the predicted ingress point, the thalamus as a region specifically targeted by replication of PrP once infection spread forwards into the brain. Finally the hippocampus and cerebellum were chosen as regions demonstrating less concentrated PrP depostion.

binding of an antibody specific to microglia or the mutagenic incorporation of a fluorescent marker continue to be the standard methods employed in immunohistochemistry or immunofluorescence assays to visualise microglial morphology. The transgenic incorporation of markers are favourable as the method effectively removes any concern over incomplete ligation of antibody conjugated markers (Sasmono *et al.*, 2007). Microglial activation is described as a marked increase in diameter of the central body and a distinct reduction in the length and number of processes with engorgement of those remaining (McGeer *et al.*, 1993). Full activation reveals a cell countenance almost circular in appearance and, prevalently in the literature, termed as amoeboid.

Determination of visual microglia activation is typically accomplished by incarnating morphological activation as a scoring system based on appearance (Lemstra *et al.*, 2007), percentage of activated cells per defined area (Kauppinen *et al.*, 2008) or quantifying intensity of bound antibody (Gallaher *et al.*, 2012). Analysis of digital images using imaging software to quantify specific cellular features has been shown, by direct comparison with methods requiring user interpretation, to give results with less variability between sample populations (Donnelly *et al.*, 2009, Yamada and Jinno, 2013). This study utilised software mediated quantification of microglia number and morphological change in an effort to reduce human induced error or misinterpretation.

4.2 Methodology

4.2.1 Experimental Design

Groups of BALB/cJ$^{Fms\text{-}EGFP/-}$ mice were challenged by an intraperitoneal (i.p.) injection with 0.02 ml of 10^{-2} w/v 79A or Normal brain homogenate (NBr) and culled with serial investigative time points of 35, 100, 150, 200 dpi and terminal stage disease (Table 4-1). The infected material used to produce the new 79A inoculum was sourced from the same batch of animals as previous experiments. The initial age of animals at challenge was 113 days ± 1.4 SE to ensure that disease progression would be comparable to previous chapters.

Table 4-1: Mice used for BALB/cJ$^{Fms\text{-}EGFP/-}$ microglia quantification study challenged i.p. with 79A mouse-adapted Scrapie prion strain. Control mice were inoculated with normal brain (NBr) homogenate. All mice were culled by saline perfusion followed immediately by 4% paraformaldehyde perfusion. * Used for pathological analysis of strain verification only. † Used to confirm resolution of inflammation following inoculation only.

Serial Cull Point (Days)	Animal Number	Genotype	Age at Infection (Days ± SE)	Inoculum	Route
Terminal	8 *	BALB/cJ$^{Fms\text{-}EGFP/-}$	124 ± 6.0	79A	i.p.
200	4	BALB/cJ$^{Fms\text{-}EGFP/-}$	115 ± 1.1	79A	i.p.
	4	BALB/cJ$^{Fms\text{-}EGFP/-}$	116 ± 4.4	NBr	i.p.
150	4	BALB/cJ$^{Fms\text{-}EGFP/-}$	98 ± 5.0	79A	i.p.
	4	BALB/cJ$^{Fms\text{-}EGFP/-}$	123 ± 6.9	NBr	i.p.
100	4	BALB/cJ$^{Fms\text{-}EGFP/-}$	106 ± 4.6	79A	i.p.
	4	BALB/cJ$^{Fms\text{-}EGFP/-}$	100 ± 2.0	NBr	i.p.
35	4 †	BALB/cJ$^{Fms\text{-}EGFP/-}$	138 ± 2.7	79A	i.p.
	4 †	BALB/cJ$^{Fms\text{-}EGFP/-}$	134 ± 2.6	NBr	i.p.

4.2.2 Tissue collection

Mice were anaesthetised using isoflurane (Merial Animal Health Ltd, Vm08327/4131) with additional oxygen to maintain a steady condition of anaesthesia. Mice were culled by cardiac puncture perfusion using a Watson Marlow 205U multichannel cartridge pump supplying 20 ml ice cold diethylpyrocarbonate (DEPC) treated Hank's Balanced Salts Solution (HBSS) through a 26G x 0.45 mm microlance (BD 300300). The flow rate was held constant at 5.0 ml min^{-1} before switching to 20 ml 4% paraformaldehyde at pH 7.4 on ice. Brains were removed and placed in 4% paraformaldehyde at 4°C for 24 hours. Those removed from animals culled at 35, 100, 150 and 200 dpi were then rinsed in HBSS and incubated for a further 24 hours in 20% Sucrose solution at 4°C. Sucrose penetration was confirmed by a lack of buoyancy whereupon tissues were rinsed in HBSS, snap frozen in isopentane precooled at –40°C, wrapped in foil and then stored at –20°C in an absence of light.

4.2.3 Tissue Sectioning

Thicker sections were required for Z-section confocal microscopy. Frozen brain tissue was therefore sectioned at 25 µm on a freezing block microtome and taken into ethylene glycol/glycerol based cryoprotectant solution in 12 well plates in sequence. Each well then contained sequential sections, distanced apart by 300 µm. The plates were stored at –20°C in an absence of light. When required, sections were floated onto glycerol treated microscope slides using HBSS. Sections were air dried at room temperature in an absence of light for 24 hours before overlaid with coverslips adhered with hard-set mounting medium (Vector Laboratories, H1400). Brain tissue taken from animals culled at terminal stage were processed directly from 4% paraformaldehyde and sectioned as per the standard method first developed by Fraser and Dickinson (1967), and outlined in SOP-PSG-008 used by the Pathology Department at The Roslin Institute, prior to embedding in paraffin wax. Sections were cut on a microtome at a thickness of 6 µm.

4.2.4 Imaging

BALB/cJ$^{Fms\text{-}EGFP/-}$ sections were imaged using a Zeiss LSM-5 Confocal module attached to a Zeiss Axioskop 2 FS-MOT upright microscope operating LSM Pascal image capture software (AIM). EGFP excitation was initiated with an argon 488 nm laser with emission capture though a secondary dichroic beam splitter NFT 545 diverting all light below 545 nm to a single channel operating a BP505-600 nm band pass filter plate.

Images for cell number quantification were captured as a 50 optical slice (each 1 airy unit) Z-stack at x10 magnification (Zeiss Plan-Neofluar x10 / 0.30 objective) and compiled into a single composite image using ImageJ software 1.48a (Schneider *et al.*, 2012). Images were converted to a threshold-adjusted binary 8 bit image and quantification of EGFP expressing microglia cell number was performed using particle analysis within ImageJ.

From a series of 9 coronal sections, spaced 300 µm apart and encompassing the thalamus and medulla, 3 sections were chosen at random. Within each chosen section, 3 images for morphological quantification were captured as a 20 optical slice (each 1 airy unit) Z-stack taken at x40 magnification (Zeiss Plan-Neofluar x40 / 1.30 objective) in combination with immersion oil (Immersol, Zeiss 518F). Additional images were recorded on adjacent sections if the total number of EGFP expressing microglia was below 50 cells.

Microglia total radius, measured from the longest visible projection, was measured directly within ImageJ on AIM software scaled Z-stack compilations. Euclidean distance mapping was performed on an 8-bit processed binary image to generate a 32-bit distance map. Using the region of interest function within ImageJ a histogram was compiled for each individual cell showing the shortest measured distances, recorded as a grey value, between a foreground pixel and the nearest background (zero value) pixel (Leymarie and Levine, 1992). The lower the mean grey bin value, the lower the number of longer recorded distances. This was interpreted as a finer

structured cell indicative of a more ramified morphology. By virtue of the methodology adopted, cell number was also attained.

4.2.5 Statistics

Comparison between two populations was performed using a two- tailed *t*-Test assuming a variance depending upon the outcome of an *f*-Test for variance. Such a system is optimised for a smaller number of populations in utilising a wider distribution curve to ensure a higher value is required for the *t*-critical to become significant. The *f*-test ensured that variance was correctly identified as equal or un-equal and provided additional insurance against making a type I or type II error.

4.3 Results

4.3.1 Clinical Signs and Incubation Period

Infected mice were scored every 7 days for clinical signs from 150 dpi. Prion disease signs recorded included lethargy, hair unkempt, hair loss and hunching. Problems with gait or wet genitalia were very rarely seen and only 1 mouse was culled with these. The onset of clinical signs was determined, as an average, to be 198.5 ± 1.0 days SE (Figure 4-1A). Mice were culled at terminal disease stage following an incubation period of 229.4 ± 3.6 days SE with a tight survival spread (Figure 4-1B). All BALB/cJ$^{Fms\text{-}EGFP/-}$ mice challenged with 79A and culled at 35, 100, and 150 dpi did not present with clinical signs. Mice culled at 200 dpi were starting to show clinical signs. BALB/cJ$^{Fms\text{-}EGFP/-}$ inoculated with normal brain homogenate showed no signs of clinical disease or ill health in general.

Lesion scoring was performed using the method first described by Bruce *et al.* (1991) on paraffin wax embedded brain sections taken from mice showing confirmed clinical disease . These produced lesion profiles very similar to 79A peripheral challenges of BALB/cJ$^{Fms\text{-}EGFP/-}$ and BALB/cJ previously covered in chapter 3 (Figure 4-1C). Deposition of PrP, stained for with the 6H4 antibody (Prionics, Switzerland), revealed widespread and strong punctate aggregation in the thalamus with less, but still detectable levels throughout the rest of the brain including the hippocampus.

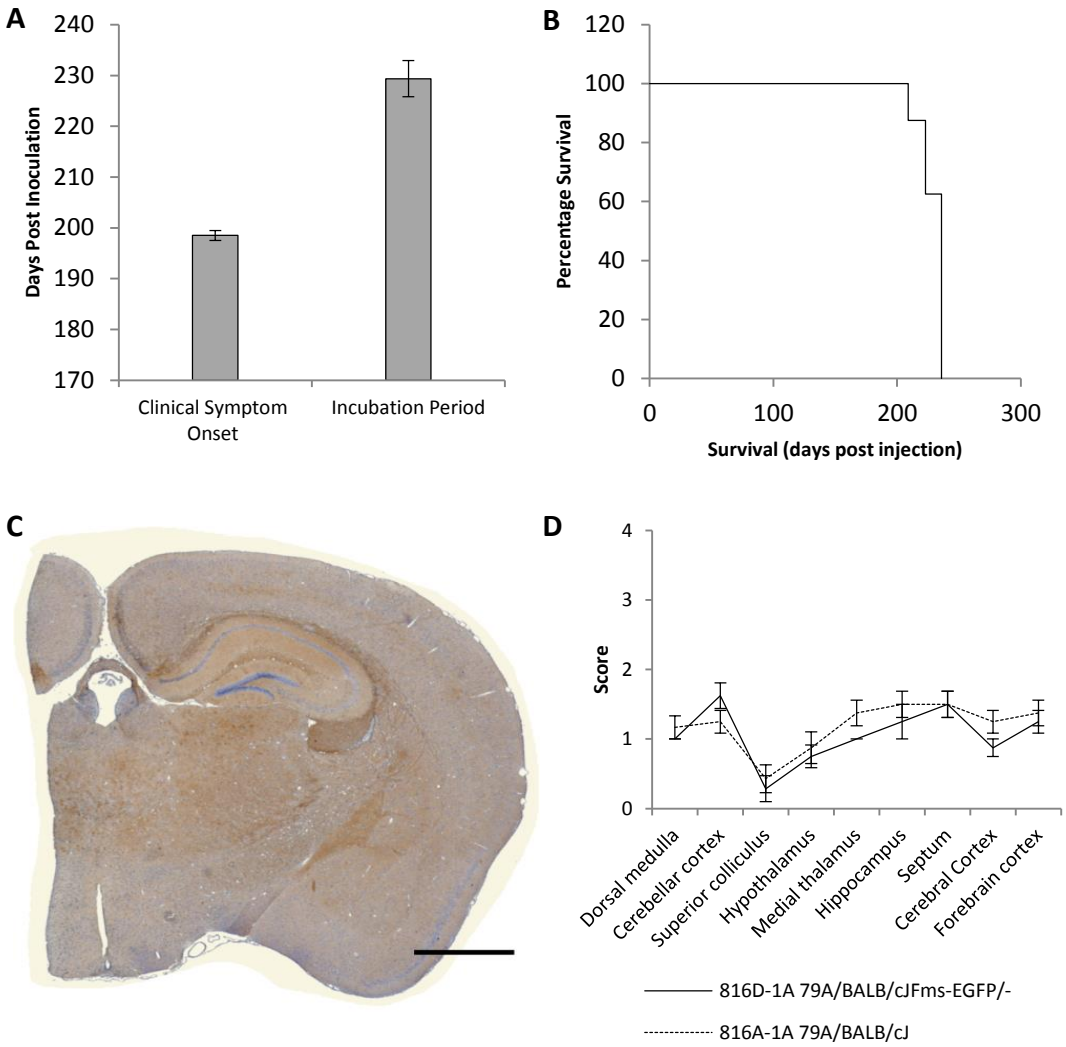

Figure 4-1: Strain typing confirmed the BALB/cJ$^{Fms\text{-}EGFP/-}$ mice were successfully infected i.p. with 79A. **A-B:** The onset of clinical signs, the interval at which terminal stage is achieved and the spread of terminal acquisition are very similar to previous experiments. **C:** Deposition of PrP at terminal (stained with 6H4) presents with previously documented targeting by fine punctate aggregates. **D:** Lesion profile scoring is very similar to that found in BALB/cJ mice challenged i.p. with 79A documented in previous chapters. The scoring for all regions is below 2 indicative of mild valuation pathology. Scale bar equates to 1mm.

Successful infection was confirmed with attainment of near identical disease incubation period, onset of clinical signs, terminal lesion profile and PrP deposition to that seen in chapter 3 and previously published data (Bruce, 1993, Cancellotti *et al.*, 2010). The final pattern of PrP deposition was identical to that observed with an intracerebral route (Giese *et al.*, 1998, Cancellotti *et al.*, 2010) indicative of achievement of the same final pathology, regardless of route, once infection has infiltrated the CNS (Kimberlin and Walker, 1978). A lack of time prevented optimising the immunohistochemical staining of pre-clinical PrP on the paraformaldehyde perfusion-fixed sections.

4.3.2 Time Course Investigation

Sections were analysed on a confocal miroscope. Microglia, observable by EGFP expression on paraformaldehyde perfuse-fixed sections, were vibrant and clearly observable in all infected and uninfected BALB/cJ$^{Fms\text{-}EGFP/-}$ mice. Microglial processes expressed EGFP and permitted highly detailed and accurate analysis. Paraformaldehyde is known to excite at 488 nm on a long-pass filter if present in sufficient quantity to allow for an unacceptable quantity of formaldehyde to form. Formaldehyde is able to bind to amines within the sample including amine-containing endogenous flavins inciting auto fluorescence across a wide spectrum (Andersson *et al.*, 1998, Billinton and Knight, 2001). Some sections obtained from this experiment contained fine punctate deposits of autofluorescence indicative of flavins when exited at 488 nm. Compilations from multiple Z stack images neutralised this affect and prevented incorporation into the data.

4.3.2.1 EGFP Visualisation by Confocal Microscopy

At 35 and 100 dpi microglia in the medulla presented with a resting ramified phenotype with long thin processes extending into the brain parenchyma. The cells were evenly distribution with a typical separation of 50 – 100 µm and with processes of up to 75 µm in length. At these early time points there was no difference between

infected and uninfected animals. By 150 dpi, 65% of the total incubation period, microglia in the medulla of prion infected mice were spaced closer at ~ 25 µm apart; the result of a higher concentration of microglia than that of the resting state seen in the parallel normal brain inoculated control mice (Figure 4-2). The number of microglia was maintained at 200 dpi in the medulla. It was at this later time point that microglia in all infected mice demonstrated both shortened processes and a considerably enlarged central body indicative of reactive microglia. By contrast the microglia in uninfected animals at the same time point remained ramified in appearance with no change in cell number.

Microglia in the thalamus at 100 and 150 dpi had a ramified appearance in both infected and uninfected animals with no apparent difference between the two groups. As per the medulla the cells were evenly distributed at these pre-clinical time points. At 200 dpi a considerable increase in cell number was observed in all infected animals (Figure 4-3). Such a concentration meant a degree of contact or overlap was evident between the processes of neighbouring cells. A grossly enlarged central body with short and thickened processes were evident on the vast majority of cells within this region. The microglia in uninfected control animals at 200 dpi continued to present with a ramified appearance as per pre-clinical and uninfected animals.

Within the dentate gyrus (Figure 4-4) and cerebellum EGFP expressing microglia were typically observed as spaced 50 to 100 µm apart up to and including 200 dpi. The appearance of microglia in these regions remained ramified at all tested time points and there was no notable difference between infected and uninfected mice.

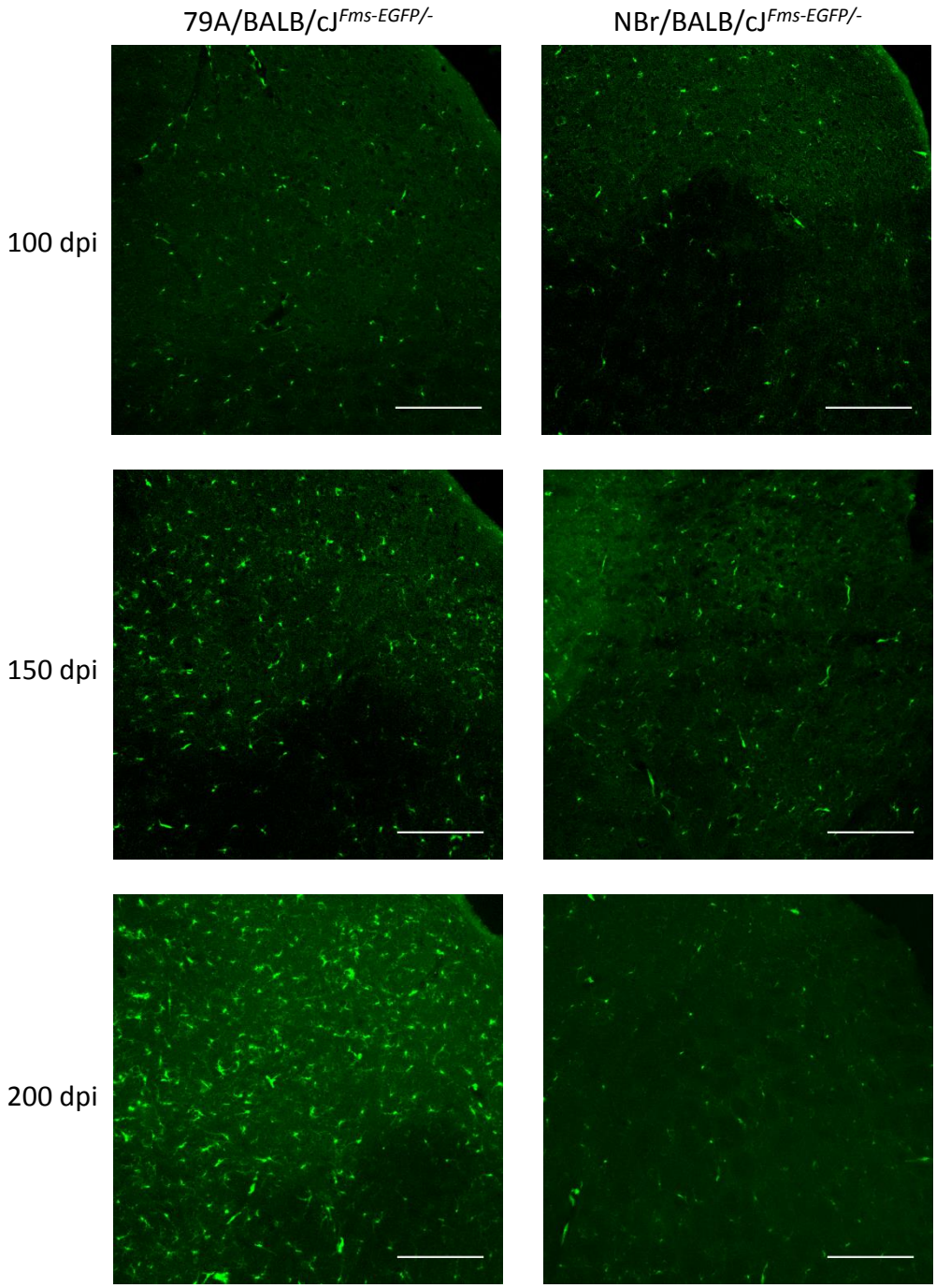

Figure 4-2: EGFP expressing microglia in the medulla of BALB/cJ$^{Fms\text{-}EGFP/-}$ mice following i.p. challenge with 79A at 100, 150 and 200 dpi. EGFP expressing microglia were seen to first increase in number in the medulla at 150 dpi. The accumulation of microglia separated at 25 µm was maintained through to 200 dpi. Before 150 dpi, and in NBr inoculated mice, microglia were seen to adopt a normal resting separation of 50 - 100 µm. Scale bars equate to 200 µm.

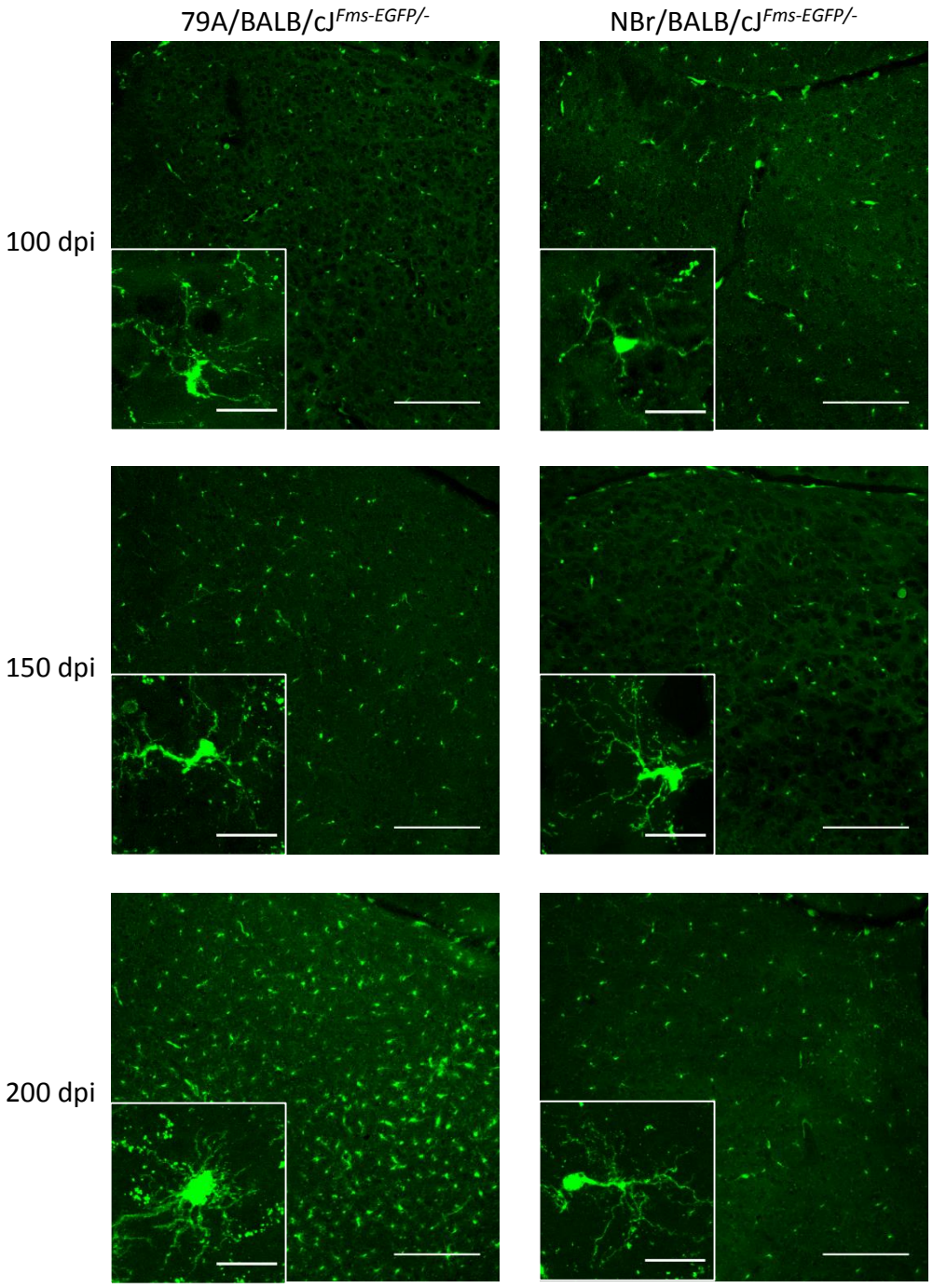

Figure 4-3: EGFP expressing microglia in the thalamus of BALB/cJ$^{Fms\text{-}EGFP/-}$ mice following i.p. challenge with 79A at 100, 150 and 200 dpi. No difference in the number of EGFP expressing cells was observed in the thalamus until 200 dpi when a concentration of reactive microglia spaced less than 25 µm was observed. Before 200 dpi, and in the NBr inoculated mice, microglia were observed as spaced at 50 - 100 µm and adopt a normal ramified morphology. Scale bars equate to 200 µm. Inset scale bars equate to 20 µm.

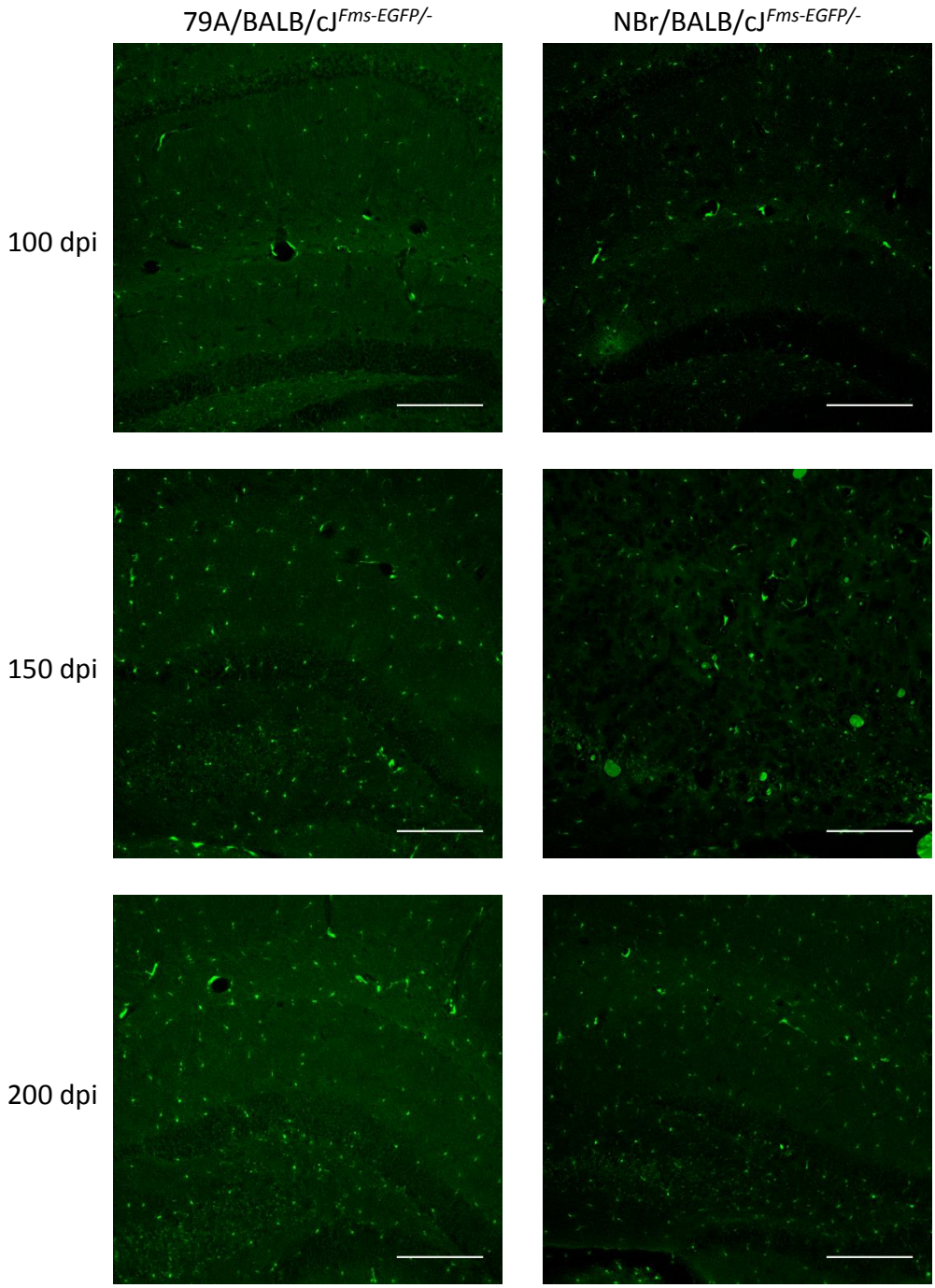

Figure 4-4: EGFP expressing microglia in the dentate gyrus region of the hippocampus of BALB/cJ$^{Fms\text{-}EGFP/-}$ mice following i.p. challenge with 79A at 100, 150 and 200 dpi. During normal resting state, observable in the NBr inoculated animals, microglia in the hippocampus are regularly spaced at 50 µm. This same resting state distribution was observed in the 79A challenged animals at all intervals indicating no significant change in response to infection in this brain region. Scale bars equate to 200 µm.

4.3.2.2 Quantification of EGFP expressing Microglia

Particle analysis, on threshold adjusted binary images of low magnification images encapsulating an entire brain region, was performed to capture all EGFP expressing cells. A statistically significant increase of ~ 50% in microglia cell number in the medulla was confirmed at 150 dpi (Figure 4-5) matching the onset of first observed PrP deposition (Chapter 3). This accumulation of microglia was retained as disease developed. At 200 dpi a statistically significant increase in microglia number in the thalamus of ~ 100% was observed.

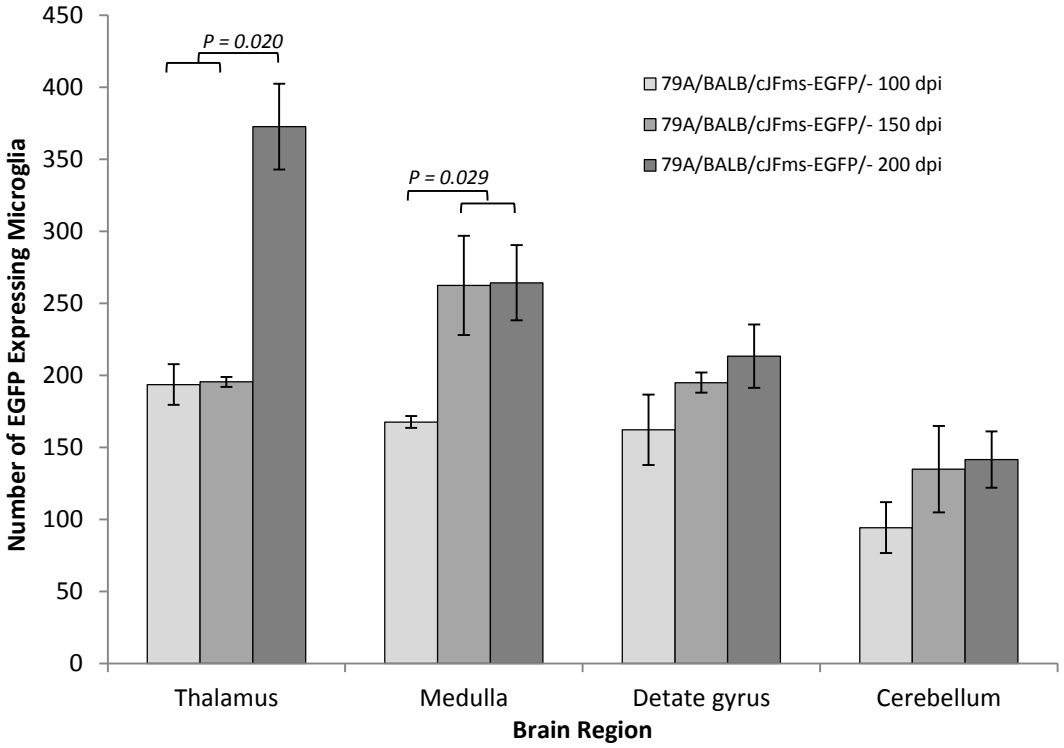

Figure 4-5: Broad area quantification of regional microglia cell number in BALB/cJ$^{Fms\text{-}EGFP/-}$ mice. Following i.p. challenge with 79A at 100, 150 and 200 dpi. EGFP expressing cells were counting using ImageJ particle analysis function on x10 magnification 25µm Z-stack compiled images each comprising 50 optical slices. The thalamus and medulla are shown previously to be areas heavily targeted by PrP deposition. The dentate gyrus and the cerebellum are areas with less concentrated PrP deposition. Microglial density increases in the medulla by ~ 50% at 150 dpi whereupon numbers remain constant in this region as PrP deposition spreads anteriorly. By 200 dpi microglia density in the thalamus had increased by ~ 100%. ‡ Mean statistical value determined using *t*-Test assuming variances determined by *f*-Test.

Quantification of EGFP expressing microglia radius and process complexity was performed on Z-stack compiled images. Microglia in the thalamus at 200 dpi presented with a reduction in process length and an engorged central body consistent with morphological activation (Figure 4-6A). Complexity of protrusion branching and central body area was encapsulated by 32-bit Euclidean distance mapping on threshold adjusted 8-bit binary images. Microglia increased by a mean Euclidean distance of ~ 1 µm (Figure 4-6B). Such a change indicated a considerable mean increase in Euclidean distance required to travel from any given pixel in the cell to the next nearest white, or non-data pixel and reflects the larger and less complex area the cell occupies. The number of cells per 0.05 mm² doubled to ~ 14 cells (Figure 4-6C). By contrast microglia in the thalamus prior to 200 dpi in both infected and infected mice were fewer in number and shared a mean Euclidean of 2 µm reflecting a more complex ramified morphology comprising long fine processes and a small central body area.

The radius and mean Euclidean distance of microglia in the medulla of infected mice remain unchanged at 100 dpi (Figure 4-7) with no difference observable when compared to control mice. By contrast, at 200 dpi, microglia in the medulla presented with all the hallmarks of morphological activation as evidenced by the reduction in radius from an average of 30 µm down to 20 µm. The reduction in radius was matched by an increase in Euclidean distance by 1 µm similar to that seen in the microglia in the thalamus, and indicative of shorter thicker processes and a larger central body.

A difference was noticed in the mean Euclidean distance of microglia in the thalamus between normal brain inoculated animals and that of 79A infected mice at 100 and 150 dpi and prior to any detectable pathology (Figure 4-6C). No statistical difference was detected between any possible combinations of normal brain groups (Appendix 8-13).

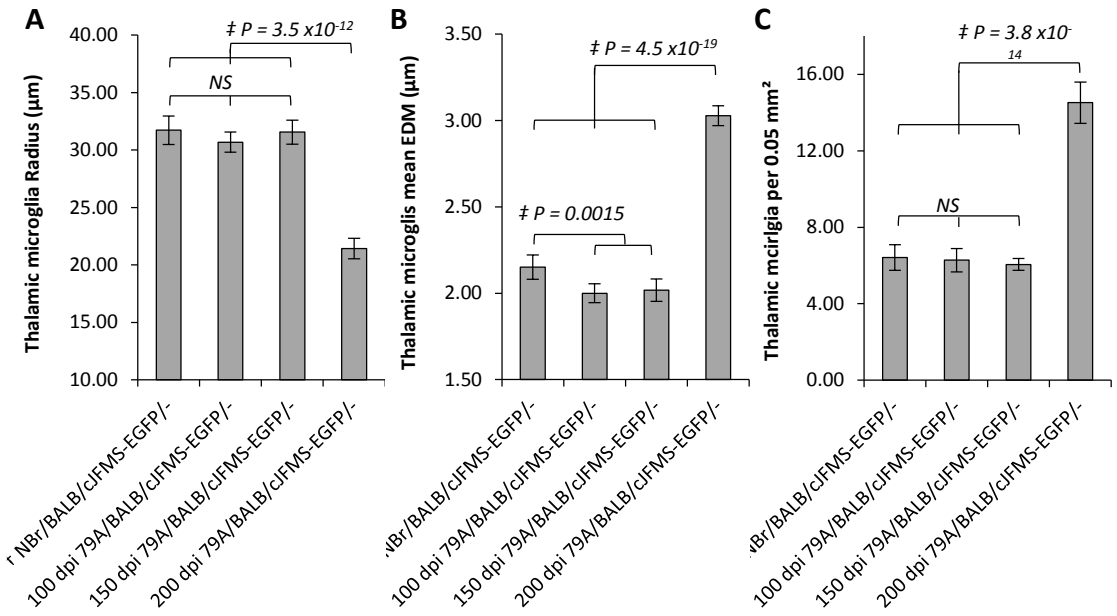

Figure 4-6: Software determined quantification of EGFP expressing microglia in the thalamus and medulla of BALB/cJ$^{Fms\text{-}EGFP/-}$ mice challenged i.p. with 79A or NBr at 100, 150 and 200 dpi. **A-B:** At 200 dpi, microglia present with an engorged central body and shortened processes conferring a significant reduction in radius. Euclidean distance mapping affords a highly sensitive quantification of cell complexity encompassing both cell body size and process branching. The reduction in cell radius at 200 dpi is reflected in a mean Euclidean distance increase of 1 µm. Distance mapping also detailed a slightly less complex cell type in the NBr animals. **C:** Microglia density in the thalamus at 200 dpi has increased by ~ 100%. † Comprises mean for all NBr inoculated BALB/cJ$^{Fms\text{-}EGFP/-}$ mice at all serial investigation time points. ‡ Mean statistical value. *NS* = Not Significant

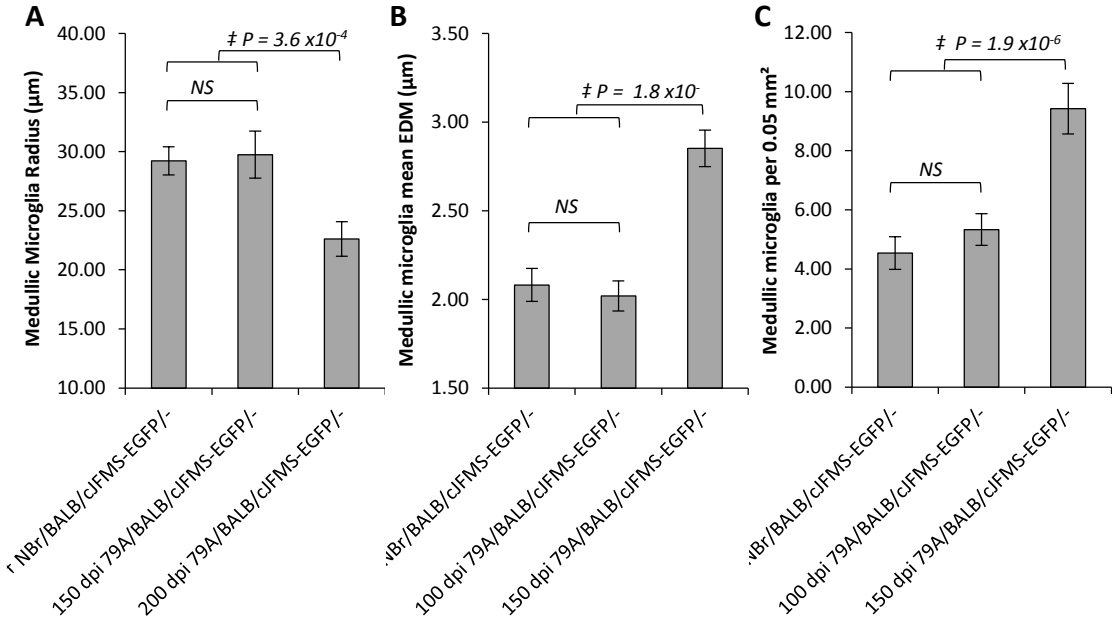

Figure 4-7: Medullic microglia react in much the same way as the Thalamus at 200 dpi. Statistical significance determined using T-test assuming variances determined by F-test. † Comprises mean for all NBr inoculated BALB/cJ$^{Fms\text{-}EGFP/-}$ mice at all serial investigation time intervals. ‡ Mean statistical value. *NS* = Not Significant

4.4 Discussion

The injection by an intraperitoneal route of 0.02 ml of 10^{-2} w/v 79A infected mouse brain in the BALB/cJ$^{Fms\text{-}EGFP/-}$ mouse model was shown in chapter 3, and now in this chapter, to induce a robust prion disease with a predictable incubation period and clearly defined stages of progression. Described in chapter 3 was the use of anti-PrP antibody staining to reveal strong deposition of diffuse punctate PrP aggregates. These were first observable as small patches in the medulla at 65% of the incubation period. Deposition could then be traced forwards through the midbrain before heavily targeting the thalamus with the onset of clinical signs at 90% of the total incubation period measured from the point of injection until cull.

The spread of diffuse PrP deposition within a 79A infection is a gradual increase in the intensity of deposition throughout the brain as the disease progresses (Giese *et al.*, 1998). The experiments in this study also portray a gradual spread from the site of entry at the rear of the brain, presumably induced by the choice of route and transmission along the spinal cord and CNS nerve fibres (Kimberlin *et al.*, 1983). This is matched by the widespread but nominal presence of vacuolation when mice were scored at terminal disease. Vacuolation supports the targeting of pathology to the areas of strongest deposition at terminal with the highest scores present in the thalamus then targeting traced back through to the midbrain following scoring of the septum nuclei.

Using the microglia-specific marker anti-AIF1 it was noticed that the first reaction by microglia in the medulla was an accumulation of cells in same areas of punctate PrP deposition at 65% of the incubation period. No further serial time points were taken between this point and 200 dpi by which time microglia had adopted an activated morphological appearance with short stubby processes and a grossly enlarged central body. These data suggested that microglia appeared to first react with an increase in numbers at the targeted sites of PrP deposition and changed morphology as a secondary response. Although microglial morphological response to induced parenchyma injury can be sudden in the healthy brain (Nimmerjahn *et al.*, 2005),

studies suggest that the translational response is more a more gradual affair (Streit *et al.*, 1989a). Furthermore misinterpretation of microglial contribution can ensue as the initial response, morphological changes, voltage potentials and production of immune related receptors are not necessarily linked (Yamada and Jinno, 2013) raising the importance of a detailed and full quantitative analysis of the microglia morphological response to infection when investigating the role these cells play in the disease. Described in Chapter 3 was the appearance of PrP deposition in the dentate gyrus and cerebellum. The results in this chapter would suggest that microglia are not responding to the deposition of misfolded protein. It could be conluded therefore that either a threshold level of deposition is required before microglia react, or alternatively microglia are responding to a different purtubation in their enviroment. To experimentally test this would require additional time points to record the gradual increase of deposition in an area that demonstrates a high load of misfold protein. Using the 79A and BALB/cJ model the thalamus would be the ideal region to futher invesigate the relationship between the accumulation of misfolded protein and the early stages of microglial activation between the 150 and 200 dpi time points taken in this present analysis.

Quantification of images to determine microglia morphology inherently requires the assumption that the entire cell including all fine protrusions has been captured at the point of exposure. The use of antibody conjugated markers in immune-assays are reliant on antibody penetration of the tissue and successful binding throughout the cell. An alternative is the use of a constitutively expressed fluorescence markers in which the signal is known to be uniform throughout the cell. Providing the tissues are harvested and processed correctly the use of a transgenic marker effectively removes all concerns regarding incomplete capture of cell features. The BALB/cJ$^{Fms\text{-}EGFP/-}$ mouse model has strong constitutive EGFP expression within all cells of myeloid origin (Sasmono *et al.*, 2003) and made the strain eminently suitable for quantifying the morphology of microglia in the prion diseased brain.

Euclidean distance mapping affords a highly sensitive determination of distance change (Schneider *et al.*, 2012) and was applied to images of EGFP expressing cells to quantify cell complexity. By the onset of clinical disease, microglia demonstrated a clear change towards a less complex Euclidean distance; the result of a more amoeboid morphology. The main areas of microglia activation and accumulation were restricted to the medulla and thalamus indicating the microglia response was strongest in regions known to be targeted by PrP deposition.

Interestingly the sensitivity of Euclidean distance mapping was sufficiently high to detect a small but statistically significant difference, within the thalamus, between the mean Euclidian distance of the control microglia and infected animals in the absence of any detectable pathology. The data acquired in this experiment was not sufficient to explain the difference but does serve to highlight the importance of always ensuring differences between controls and tested populations are made on a two-tailed assumption.

A lack of time prevented full morphological quantification of medullic microglia at the initial site of response. The x40 quantification of the thalamus supported the increase in cell number determined from the x10 magnification regional cell count. Consequently it was reasonable to assume that x10 quantification of the medulla was sufficient alone as confirmation that, from 150 dpi, microglia accumulated in this region without the need to count cells at a higher magnification. In addition the self-explanatory images for EGFP expression in the medulla provide clear visual evidence.

All cells of myeloid origin express EGFP in BALB/cJ$^{Fms\text{-}EGFP/-}$ mice. Consequently it is not possible to distinguish between the resident microglia population and the possible influx of monocytes. There is strong evidence by multiple groups that reveal the negligible degree of monocyte influx into the brain during neural inflammation (Ajami *et al.*, 2007, Mildner *et al.*, 2007) with evidence for the requirement of non-physiological disruption to the blood brain barrier for any influx to occur (Mildner *et*

al., 2007). The resident microglia pool is reported to be highly self-sufficient and microglia are rapidly produced when additional or replacement cells are required (Ajami *et al.*, 2007, Ajami *et al.*, 2011, Varvel *et al.*, 2012). There is also some recent evidence to suggest a resident AIF1^{-ve} and nestin^{+ve} microglia progenitor resides in the CNS and can differentiate rapidly into new microglia within a matter of days (Kim *et al.*, 2014).

Microglia have been observed as activated prior to any detectable PrP deposition yet in a transmissibly infectious environment (Betmouni *et al.*, 1996, Manuelidis *et al.*, 1997) implementing microglia as either responding to PrP below the threshold of detection, an additional trigger or actively involved as a causative agent. Other studies report the accumulation of PrP deposition as the initiation of microglia response (Williams *et al.*, 1994, Williams *et al.*, 1997). There are no detectable clinical signs associated with this early immune response with initial detection of abnormalities in behaviour coinciding with neuronal synaptic stripping (Cunningham *et al.*, 2003, Siskova *et al.*, 2013). Microglia appear not to be implemented in stripping during prion disease (Siskova *et al.*, 2009), despite conflicting observations of active stripping by microglia as an important component of normal homeostasis (Schafer *et al.*, 2012, Ji *et al.*, 2013), in response to injury (Wake *et al.*, 2009) and in other neurodegenerative diseases (Trapp *et al.*, 2007, Kettenmann *et al.*, 2013). Although readily apparent when these sections were viewed using a confocal microscope, the lack of cell radius and Euclidean distance quantification mean that these data are not sufficient to state categorically if the morphological response is indeed secondary to the apparent increase in cell number. The data in this experiment therefore suggests, but cannot state for certain, that there is a separation of microglia activation into two components; accumulation at the site of perturbation as the first and initial response, and the morphological activation as the second.

The next chapter will further investigate the microglial response to developing pathology by analysing the transcriptome of microglia isolated from BALB/cJ$^{Fms\text{-}EGFP/-}$

mice infected with 79A at the same time points as the preceding chapters. The aim was to determine the function of the morphologically activated cells at stages of disease when misfolded protein was both still minimal and, later on in the process, much more evident. Crucially, by isolating microglia their specific contribution could be determined in the absence of immunomodulators released by the other cell types found in the brain; in particular astrocytes, which were shown in Chapter 2 to respond with a signal that was tightly correlated with microglia.

5 The Microglia Transcriptome during Prion Disease Progression

5.1 Introduction

In chapter 3 and 4 it was shown than microglia responded to prion disease infection in the medulla by accumulating in areas of initial PrP deposition and did so with minimal change in overall morphology. Towards the latter stages of the disease, EGFP expressing microglia presented with a phenotype consistent with an activated inflammatory phenotype. Processes were shortened, the central soma was engorged and activated cells were widespread throughout the brain. This data suggested a disparity between initial response and morphological activation. In the healthy brain microglia comprise only 10% of the cells in the adult mouse brain, yet chapter 2 revealed the dominate source of differential gene expression in mouse-adapted prion disease to be microglial in origin. This is supported in the literature where an immunological signal has been observed as part of prion disease expression anyslsis (Brown *et al.*, 2003, Booth *et al.*, 2004, Riemer *et al.*, 2004, Xiang *et al.*, 2004, Brown *et al.*, 2005, Skinner *et al.*, 2006, Xiang *et al.*, 2007, Moody *et al.*, 2009), implicating microglia as an important cell in the neurodegenerative process.

The inflammatory phenotype typically associated with prion disease has been shown to be remarkably anti-inflammatory (Walsh *et al.*, 2001, Baker and Manuelidis, 2003). Transforming growth factor, TGF-β1, a down regulator of cytokine release has been shown to be the dominant, differentially expressed anti-inflammatory cytokine present in murine prion disease models (Cunningham *et al.*, 2002). Via the TGF-β1 signalling pathway, the cytokine plays a key role in limiting microglia activation (Lodge and Sriram, 1996) and is evident throughout the disease process (Boche *et al.*, 2006, Abutbul *et al.*, 2012). The growth factor also provides microglia with a phenotype akin to the resolution of apoptotic cells and wound healing (Fadok *et al.*, 1998). Little is known on the impact of such a phenotype in neurodegenerative diseases with considerable debate on the neurotoxic or neuroprotective function of microglia.

The evidence for the negative impact of inflammatory cytokines on neurodegenerative diseases is aimed at testing what has been termed the inflammatory (or cytokine) hypothesis (Cerejeira *et al.*, 2010). Central to the hypothesis is the enzyme indoleamine 2, 3 dioxygenase, the rate-limiting enzyme in the kynurenine pathway that converts the essential amino acid tryptophan to kynurenine (Rafice *et al.*, 2009). The downstream production by the kynurenine pathway of neurotoxin quinolinic acid (QUIN), a potent neurotoxic N-methyl-D-aspartate receptor agonist, is most relevant to neurodegenerative diseases (Stone and Perkins, 1981, Stone, 2001, Fernandes *et al.*, 2008). The pathway is initiated by inflammatory cytokines including TNF-α, INF-γ (O'Connor *et al.*, 2009), which in turn mediate NF-κB translocated activation of the kynurenine pathway (Robinson *et al.*, 2006). Microglia contain the complete pathway and express neurotoxic QUIN (Heyes *et al.*, 1996, Espey *et al.*, 1997, Guillemin *et al.*, 2005) and as such have been implemented as the main effector for the inflammatory hypothesis in neurodegenerative diseases (Henry *et al.*, 2009, Yamada *et al.*, 2009).

The activation signature of macrophages, and indeed microglia, has traditionally be classed into M1 (Classical) or M2 (alternative). A resting (M0) macrophage in the presence of certain epitopes able to bind to membrane bound pattern recognition receptors is activated as part of a stereotypic signalling cascade mediated by transcription factor nuclear factor kappa B (NFkB) (Pahl, 1999, Boldrick *et al.*, 2002). This leads to increased expression and extracellular release of pro-inflammatory cytokines TNF-a, IL-1 and IL-6 in addition to proteases, superoxide anions, nitric oxide and reactive oxygen-nitrogen species including N_2O_3, NO_2 and an overall transmembrane epitope profile considered as an M1 phenotype. (reviewed in Martinez *et al.*, 2008). Other resident macrophages within the vicinity, and $LY6C^{Hi}$ monocytes chemotactically attracted into the site of insult, are in turn also activated leading to the macrophage population at the site of inflammation to be dominated by the M1 phenotype (Geissmann *et al.*, 2003).

A balance has to be struck in the triggering of inflammation; too little a response and the risk is further injury, too much and the ensuing damage caused by inflammation can result in consequences worse than the original infection; extracellular proteases and free radicals are highly damaging to surrounding tissue (Wells *et al*., 2005). It is important therefore for resolution of inflammation to take place to prevent further damage and begin the healing process. The macrophage is a principle component in maintaining this balance. This is particularly the case in the periphery where the dominant cell found at a site of innate inflammation is the polymorphonuclear neutrophil. Neutrophils express generous quantities of superoxide creating a highly oxidizing environment, which combined with a short half-life and mass apoptosis leads to the rapid buildup of potentially toxic cellular matter that must be recognised and removed by macrophages (Savill *et al.*, 1989, Babior *et al.*, 2002). These macrophages are in turn are stimulated to express TGF-b1 inducing a change from a pro-inflammatory toward an alternatively activated or anti-inflammatory wound-healing phenotype (Fadok *et al.*, 1998, Huynh *et al.*, 2002, Kim *et al.*, 2004).

The alternatively activated or M2 macrophage is a blanket term collectively used to class macrophages that are involved in the resolution of inflammation. There are several subtypes of M2 and includes those derived for the aforementioned accumulation of TGF-b1 (M2c) or by a reduction in the available epitope able to bind to pattern recognition receptors in combination with a gradual excess of IL-4 (M2a). The source of IL-4 is from both the now dominate M1 type macrophage and recruited CD4+ T-helper cells (Stein *et al.*, 1992, Shimoda *et al.*, 1996). The presence of IL-4 stimulates newly recruited $LY6C^{Hi}$ monocytes, and residing M1 macrophages, to adopt an M2 activation profile. Both M2a and M2c macrophage phenotypes do not release high levels of pro-inflammatory cytokines, reactive oxygen species or MHC class II and are potent inhibitors of macrophage and $CD4^{+}$ t helper cell proliferation (Schebesch *et al.*, 1997). Despite a limited role in MHC mediated antigen presentation, M2a and M2c macrophages are highly efficient phagocytes b are able to clear dead and dying cells without triggering further inflammation (Fadok *et al.*,

1998). The final subtype, M2b, is induced in the presence of gradually increasing levels of IL-10 released from both nearly all immune cell types. M2b macrophages release high levels of IL-10 that exert a powerful anti-inflammatory influence within their environment (Gerber and Mosser, 2001) but are otherwise very similar to classically activated M1 macrophages and are therefore considered as immunoregulatory (Anderson and Mosser, 2002b, Sironi *et al.*, 2006). The M2b macrophage phenotype is also actively involved in CD4+ T-helper cell differentiation (Anderson and Mosser, 2002a).

Within the central nervous system, the general premise of a shift from a prevailing neurotoxic M1 signature towards a neurotrophic M2 dominance has been well characterised within rodent models of both acute injury of the spinal cord and traumatic brain injury using cortical impact (Kigerl *et al.*, 2009, Hsieh *et al.*, 2013, Turtzo *et al.*, 2014). Within chronic neurodegenerative the activation profile is not so easy to distinguish as there are many variables to consider. These include the type of disease, the point in time that microglia are investigated during the disease development, the age (Flanary *et al.*, 2007, Sierra *et al.*, 2007, Hart *et al.*, 2012, Lai *et al.*, 2013), gender (Loeuillet *et al.*, 2010, Akhtar *et al.*, 2011), microglial population dynamics (see Chapter 1) and finally the impact of secondary insults, particularly those pertaining from the periphery, shown to impart a functional shift in microglia activation profile (see Chapter 1). There is also recent research indicating a marked regional heterogeneity of microglial demonstrated both by resident microglia residing in different areas of the brain (de Haas *et al.*, 2008, Lai *et al.*, 2011, Hart *et al.*, 2012) and a difference in function between resident and potential recruited blood-derived monocytes; the latter thought to be considerably more neuroprotective (Shechter *et al.*, 2009, London *et al.*, 2011, Butovsky *et al.*, 2012). Therefore the activation profile of microglia during chronic neurodegeneration should be considered much more diverse with analysis focusing more on determining microglial function within a specific environment.

An immune response however is not cell-centric and is maintained and regulated by the actions of numerous communicating cell groups and not just those cells considered to be a part of the immune system. A complete serial analysis of the whole microglia transcriptome in response to developing prion disease has not been performed. Furthermore, isolation of microglia from a diseased brain will provide a unique microglia orientated angle of this multi-cellular response to developing pathology. Furthermore ramified microglia are known to dynamically interact with surrounding cells including neurons and continually express neurotrophic factors (Wake *et al.*, 2009, Tremblay *et al.*, 2010). It is not therefore possible for microglia to first respond in a support capacity without resulting to an inflammatory response; a situation seen both in aging and acute insult to the brain (van Dam *et al.*, 1992, Van Dam *et al.*, 1995, Konsman *et al.*, 1999).

The aim of this chapter was to successfully isolate adult microglia from adult BALB/cJ$^{Fms\text{-}EGFP/-}$ mice infected, as a time course, with the 79A mouse-adapted Scrapie strain. In light of the potential regional heterogeneity demonstrated by microglial populations the ideal experiment would have incorporated microdissection of different brain regions. It was found that obtaining a working protocol of regional isolation of microglia, and sufficient RNA downstream, was not practical within the confines of this project. This analysis therefore focused on the whole brain microglial population. The time points chosen were the same as the previous chapter thereby allowing for determination of the specific contribution made by microglia at these interesting stages of the disease. BioLayout *Express*^{3D} software was used to select groups of genes considered to show a disease assoicated expression profile and determine the specific functional contribution to the host immune response made by microglia, and the potential impact this may have within the brain parenchyma. In addition, microglia are not the only source of immunomodulators and equally importantant, and indicative of the greater power of single cell type isolations, will be what microglia are not expressing.

5.2 Methodology

5.2.1 Experimental Design

Groups of gender matched BALB/cJ$^{Fms\text{-}EGFP/-}$ mice were challenged i.p. with either 0.02 ml of 10^{-2} w/v 79A infected or normal brain material sourced from C57BL/6J mice. The average initial age of animals at challenge was 116 days ± 2.1 SE to ensure that disease progression would be comparable to previous chapters. For each inoculum; groups of four mice at 35, 100, 150 and 200 dpi were anaesthetised using isoflurane (Merial Animal Health Ltd, VM08327/4131) with additional oxygen to maintain a steady condition of anaesthesia. Mice were culled by cardiac puncture perfusion using a Watson Marlow 205U multichannel cartridge pump supplying 20 ml ice cold 0.1% diethylpyrocarbonate (DEPC) treated Hank's Balanced Salts Solution (HBSS) through a 26G x 0.45 mm microlance (BD 300300) at a flow rate of 5.0 ml min^{-1}. Brains were carefully isolated and taken into ice cold 0.1% DEPC treated HBSS.

5.2.2 Isolation of Microglia from Experimental BALB/cJ$^{Fms\text{-}EGFP/-}$ Mice

Brains were dissociated on a GentleMACS™ Dissociator (Miltenyi Biotec, 130-095-235) using the Neural Tissue Dissociation Kit P (Miltenyi Biotec #130-092-628); adjusting the reagent volumes to match brain weight following measurement in 1 ml ice cold Hanks balanced Salt Solution without Ca^{2+} & Mg^{2+} (Invitrogen, 14175-053). Brain tissue was sectioned into six roughly equal sized pieces to aid disassociation prior to adding the tissue to the first enzyme solution. Following dissociation, the tissue was passed through a 40 µm filter then rinsed twice with 10 ml HBSS with Ca^{2+} & Mg^{2+} at 300 *x g* for 10 min at 4°C. The final cell pellet was re-suspended in 16 ml 35% Isotonic Percoll® (GE Healthcare, 17-0891-02), split between two 15 ml centrifuge tubes and overlaid at 150 µl sec^{-1} with 5 ml ice cold 0.1% DEPC treated HBSS. The resulting Percoll® gradient was centrifuged at 400 *x g* for 45 min at 4°c using no brake. The resulting pellets were then suspended and recombined into a final volume of 5 ml ice cold 0.1% DEPC treated HBSS. Cells were then again pelleted at 400 *x g* for 5 min at 4°c using no brake, re-suspended in 90 µl ice cold MACs buffer

(Miltenyi Biotec), 10 µl CD11b (microglia) microbeads (Miltenyi Biotec, 130-093-634) and incubated at 4°C for 15 min with gentle shaking.

Following incubation with CD11b microbeads, the cell suspension was washed in 1 ml ice cold MACs buffer at 300 *x g* for 5 min at 4°C, then re-suspended in 500 µl ice cold MACs buffer. Cells were passed through magnetised LS columns (Miltenyi Biotec, 130-042-401) using three x 3 ml washes of ice cold MACs buffer. A depleted sample was kept for FACS confirmation of CD11b depletion. Cells positive for CD11b were removed from demagnetised LS columns using the supplied plunger into 5ml ice cold MACS buffer, then pelleted at 400 x g for 5 min at 4 °C. The pellet was then re-suspended in 1 ml ice cold MACs buffer before four x 50 µl samples were removed and three of the samples blocked with 1 µg ml^{-1} purified anti-mouse CD16/32 Fc receptor antibody (Cambridge Bioscience, 101302). The remaining solution (approximately 0.25 ml) containing on average $3x10^5$ $CD11b^{+ve}$ cells and was pelleted at 400 x g for 5 min at 4°C and stored at -70°C until required.

Microglia identification markers were stained (Table 5-1) with phycoerythrin (PE) anti-mouse CD11b (Cambridge Bioscience, 101208) and allophycocyanin (APC) anti-mouse CD45 (Cambridge Bioscience, 109814). A further 50 µl was stained with PE Rat IgG2b (Cambridge Bioscience, 400608) and APC Rat IgG2a (Cambridge Bioscience, 400512) isotope controls and a final 50 µl was left unstained to serve both as negative control and verification of correct BALB/$cJ^{Fms\text{-}EGFP/-}$ genotype. All samples were then incubated for 20 min at 4°C with gentle shaking prior to rinsing in 1ml MACs buffer at 400 *x g* for 5 min at 4°c. Determination of cell viability was achieved using 1 µl of 1 mM SYTOX® Blue dead cell stain (Invitrogen, S34857) added to each tube 5 min prior to FACS analysis. All cell samples were analysed on a BD FACS Aria IIIu 4-laser/11 detector Cell Sorter running BD FACSDiva™ Software (BD Biosciences). Subsequent analysis of FACS data was also performed using Summit v4.3 software (Dako/Beckham Coulter).

Table 5-1: Fluorochromes utilised to identify viable $Cd11b^{+ve}$ and $Cd45^{+ve}$ microglia.

Fluorochrome	Excitation Laser (nm)	Emission (nm)
CD11b-PE & IgG2b-PE	565	578
CD45-APC & IgG2a-APC	633	660
EGFP (For BALB/cJ$^{Fms\text{-}EGFP/-}$)	488	507
SYTOX® Blue	405	480

5.2.3 Total RNA Extraction

The protocol for isolating total RNA from microglia was first perfected using the BV2 microglia like cell line. This was in accordance with the three R's (Replace, Reduce, and Refine) ensuring whenever possible live animals were not used when an alternative was available (Russell, 1959).

At all stages, RNA isolation was performed in RNase-free Microcentrifuge Tubes (Applied Biosystems, AM12400). Homogenisation of isolated microglia cells was performed by adding 0.75 ml of TRIzol® Reagent (Life Technologies, 15596026), pre-warmed to room temperature, to the 0.25 ml cell suspension (see section 5.2.2). Gentle mixing by pipette was used to facilitate cell lysis prior to incubation at room temperature for 5 min to ensure complete dissociation. Separation of nucleic acids from organic molecules was performed with the addition of 0.2 ml 1-Bromo-3-chloropropane per 1 ml TRIzol® reagent. Each tube was capped securely and rigorously shaken by hand for 15 seconds prior to further incubation for 3 min at room temperature.

Phase separation was performed using centrifugation at 12,000 x *g* for 15 min at 4°C. Each tube was then angled at 45 degrees and the upper clear acidic aqueous phase containing dissolved ribonucleic acids removed carefully by pipette. To mitigate any chance of DNA crossover, 15% of the aqueous phase, above the interphase, was left

behind. Precipitation of the RNA was initiated with the addition of 0.5 ml 100% absolute molecular grade isopropanol (Fisher Scientific, BP2618) per 1 ml of TRIzol® reagent used in initial homogenisation. Also added was 1 µg ml^{-1} neat linear acrylamide (Ambion, AM9520) to act as an inert co-precipitant carrier. RNA was induced to pellet by centrifugation at 12,000 x *g* for 10 min at 4°C. The pellet was invariably minuscule; to prevent loss the supernatant was carefully removed into a new sterile tube to capture the pellet if accidently removed.

The resulting total RNA pellet was then washed in 100% absolute molecular grade ethanol (Fisher Scientific, BP2818) using a vortex. Brief centrifugation at 7,500 x *g* for 5 min at 4°C allowed the pellet to resettle, thereby facilitating removal of all the remaining ethanol. The pellet was left in an extraction hood for 5 min to air dry while ensuring the pellet was not allowed to completely dry out. The total RNA pellet was finally suspended in 20 µl of RNase-free water (Invitrogen, 10977035) and incubated at 55°C for 15 min. Nanodrop analysis for 260:280 nm and 260:230 nm absorbance ratios was performed immediately on a NanoDrop® ND-1000 spectrophotometer (NanoDrop Technologies, Delaware USA). The remaining sample was then stored at -70 °C until required.

5.2.4 Analysing RNA Purity

Total RNA quality was checked on an Agilent 2100 Bioanalyser. For each sample, 1 µl of total RNA at a concentration of 1 ng μl^{-1} in RNase-free water (Invitrogen, 10977035) was loaded onto a Eukaryote Total RNA Pico Series II chip (Agilent Technologies, 5067-1513) along with appropriate gel-dye matrixes and ladder following the manufacturer's instructions. The chip was then placed on an IKA vortex with appropriate chip adapter (Agilent Technologies, 5065-9966) for 5 min at 2400 rpm then loaded into the Agilent 2100 Bioanalyser. The 28S:18S rRNA ratio and quantity were analysed within Agilent 2100 expert software as an indication of the mRNA quality within the total RNA sample. In addition, and by using the entire electrophoretic trace, the software also calculated RNA integrity values (RIN) to serve

as a further indicator of mRNA quality. A RIN value of >7.0 was immediately passed as suitable for analysis. Samples with a RIN value of lower than 7.0 where individually assessed for inclusion in the analysis.

5.2.5 Microarray Hybridisation

Microglial RNA processing was handled by ARK Genomics (The Roslin Institute & R(D)SVS). The mRNA converted to double-stranded cDNA containing biotin, using a single round of amplification, from both the poly-A 3′ tail and randomly using the NuGen Ovation® picoSL WTA system (NuGen, 3310) followed by the NuGen Encore® Biotin module biotin labelling process (NuGen, 4200). The cDNA samples were hybridised to Affymetrix Mouse Gene 1.1 arrays on an Affymetrix GeneTitan® Multi-Channel instrument (Affymetrix, High Wycombe, UK) incorporating the hybridisation, washing, staining and scanning stages. Annotation and quality control was performed with the Affymetrix Expression Console. Normalisation was undertaken using the robust multi-array average expression measure (Irizarry *et al.*, 2003).

5.2.6 Group-to-Group Data Analysis: Selection of Genes of Interest

With a Pearson correlation matrix cut-off threshold set to r = 0.7, annotated .expression files were loaded into BioLayout *Express*^{3D} as a .Expression file and pairwise correlations were calculated for each probeset on the array against all other probesets ($P^2/2$ pairwise calculations, where P is the number of probesets). Values of $r \geq 0.7$ were saved as a binary '.pearson' file for future analysis.

The user-defined correlation threshold within BioLayout *Express*^{3D} was set at 0.90 for visualisation of biological relationships of interest in a highly structured graph consisting of nodes (probesets) connected by edges of expression correlation. To identify groups of co-expressed genes, clustering of the graph was performed using the graph based Markov clustering (MCL) algorithm (Dongen, 2000) which has been designed to function with simple or weighted graphs. The inflation value was set at

2.3. The algorithm operates on the principle of generating artificial paths through the data from which Markov stochastic matrices apply the mathematical results of the random walks directly to the graph. Using the expression viewer it was possible to observe the expression of probe sets in each cluster and identify those demonstrating a convincing disease-associated signature. Clusters with a high level of noise or an unconvincing expression profile were dropped from the analysis. The chosen genes were entered into a new .Expression file.

5.2.7 Sample-to-Sample Data Analysis

The genes of interest were loaded into BioLayout *Express*^{3D} and transposed to show sample-to-sample level. The matrix threshold cut-off was maintained at 0.90. Edges were set to colour by weight and nodes were searched for and coloured for clarity.

5.2.8 Gene Ontology

Gene ontology was determined by uploading the Affymetrix chip ID of the disease-associated genes into the Ensembl Biomart data mining tool (ensembl.org/biomart) using the *Mus musculus* (GRCm38.p2) genes dataset (Ensembl Genes 74). Filters were applied to restrict results to the Affymetric Microarray MoGene 1 0 stv1 probe sets. To increase accuracy for correct selection of function, filters for external GO evidence code, domain and name were applied with a preference where possible for experimental evidence codes.

5.2.9 Known and Predicted Protein-Protein Interactions

Disease-associated genes were inputted into STRING (http://string-db.org) (Jensen *et al.*, 2009) as a multiple sequence with predicted associations attributed to *Mus musculus*. Within the network viewer, edges were restricted to evidence based prediction for co-expression, experimental and database determined interactions. The graph was organised dynamically by initiating the relaxation feature to force nodes to adopt a distance proportional to the STRING global score.

5.2.10 Biological Pathway Analysis

Determination of the involvement of the identified disease-associated genes in biological pathways was performed using the Reactome peer reviewed pathways database (http://www.reactome.org) (Vastrik *et al.*, 2007). Genes were entered as a list into the data analysis section. Comparison with *Mus musculus* pathways was performed using the species comparison section built into Reactome to ensure suggested pathways were fully applicable to mice.

5.2.11 Statistics

Fold-change difference was calculated on mean averages for the arrays at 150 and 200 dpi. The difference chosen was that generated between the equivalent normal brain control time point, plus or minus standard error. BioLayout utilised Pearson correlation distance to determine the measure of similarity between a group of n-dimensional probesets. Probesets were therefore included in the graph based purely on whether they correlate with other probesets above a user defined threshold reducing the number of edges down from an impractical $-1.0 \geq P \leq 1.0$. Within this analysis all probeset pairs with a Pearson correlation coefficient ≥ 0.7 were plotted.

5.2.12 BV2 Microglia-like Cell Line Culture

BV2 cells were kindly supplied by Dr Barry McColl (The Roslin Institute &R(D)SVS) as cells at a concentration of $x10^6$ cells ml^{-1} cryopreserved in freezing media (10% dimethyl sulfoxide and 90% foetal calf serum). The cells were gently thawed to room temperature (21°C) then added to 9 ml of pre-warmed (37°C) tissue culture media comprising L-glutamine Dulbecco's modified eagle medium (Gibco, 11965) containing 10% foetal calve serum (Sigma, 12133C) , 100 U ml^{-1} penicillin, and 100 µg ml^{-1} streptomycin (Gibco, 15140-148) in a sterile pre-treated T80 flask (Thermo-Scientific, 178905). The flask was then incubated in 5% CO_2 and saturated with H_2O at 37°C.

Passage of BV2 cell culture was performed every 3 days. The cells were washed twice in 6 ml phosphate buffered saline pH 7.4 without Ca^{2+} & Mg^{2+} (Gibco 10010-015). Following washing the cells were lifted from the flask surface with 2 ml 0.25% trypsin (Gibco, 25200) and incubated for 1 min at 37°C. The flask was tapped sharply by hand to ensure all cells were dislodged prior to the addition of 8 ml fresh pre-warmed (37 °C) tissue culture media. The cell solution was removed into a sterile 15 ml centrifuge tube and gently pelleted at 200 x *g* for 5 min with no brake. The pellet was suspended in 10 ml pre-warmed (37 °C) tissue culture media and transferred to a new a sterile pre-treated T80 flask and transferred to the incubator.

5.3 Results

5.3.1 Cell Isolation

Initial attempts to isolate microglia from a total mouse brain single cell suspension utilised FACS cell sorting of EGFP expressing cells. A variety of enzyme solutions were tested including the neural tissue dissociation kit P (Miltenyi Biotec) both with and without the automated Tissue Dissociator (Miltenyi Biotec), or various collagenase/dispase mixtures (adapted from Njie *et al.* (2012) and Cardona *et al.* (2006a)) with gentle shaking at 37°C followed by passing the tissue through a sieve. Regardless of the method attempted the yield of EGFP expressing cells was approximately $2x10^4$ and insufficient for RNA extraction. It was noted that there was an extremely high level of debris and myelin within the sample and attempts at myelin removal using magnetic beads was only partially successful. Unfortunately the cells did not survive the sorting process despite attempts to optimise both the collection buffer solution and FACS nozzle pressure. It was therefore decided that removal of the myelin was critical to the process and the protocol was adapted to incorporate a 35% / 75% interphase using a discontinuous Percoll™ gradient as described by Cardona *et al.* (2006a). Samples were stained with CD11b-PE and CD45-APC. The collected interphase was found to be considerably cleaner with less debris (FIGURE). EGFP cells isolated from BALB/cJ$^{Fms\text{-}EGFP/-}$ mice were directly correlated with the $Cd11b^{hi}$ and $cd45^{mid}$ population. Perfusion was confirmed as successful with negligible $cd11b^{hi}$ and $cd45^{hi}$ monocyte contamination. There was also negligible presence of $CD45^{hi}$ and $CD11b^{lo}$ T and B cells. Analysis revealed the pre-sort purity of microglia to be >95% yet it was not possible to FACS sort more than $2x10^4$ microglia from the collected interphase and cells still did not survive the FACS sorting process.

Allowing microglia to pellet by removing the 35% / 75% interphase had an immediate improvement with 3 x 10^5 $cd11b^{hi}$ cells sorted with a purity of > 95 % (Figure 5-1). Parallel trials of a variety of enzyme mixtures confirmed the mixture adapted from Cardona *et al.* (2006a) generated the highest yields of cd11bhi microglia. Incubating

brain fragments in digestive enzymes both prior and following homogenisation was also compared with FACS analysis confirmed the cell suspension contained considerably less debris when tissue was incubated in enzyme prior to homogenisation. Perfusion was also adopted to remove bone marrow derived monocyte contamination. Viable microglia were successfully isolated following a switch from FACS sorting to CD11b magnetic microbeads.

The population size of cells isolated by CD11b microbeads was determined by FACs analysis of a sample. Yields isolated from whole brain were consistent at $3x10^5$ cells. During protocol workup, additional confirmation by haemocytometer on a bright phase microscope confirmed both the population count and a rounded refractive appearance indicative of healthy viable cells. The isolation procedure was highly reproducible and each brain yielded $3x10^5$ viable microglia independent of time point.

5.3.2 Microglia Purity

Samples of isolated microglia were analysed by FACS to confirm population purity. To ensure consistency the same gated regions were maintained throughout when analysing the results within Dako Summit 4.3 software. Purity of EGFP expressing cells stained with CD11b microglial and CD45 pan-macrophage fluorochrome conjugated antibodies was confirmed at 93% ± 0.52 SE (Figure 5-2). The remaining 7% were not tested but further gene expression analysis was performed on the isolated microglia confirming purity of isolated microglia was high (See section 5.3.3). Adult Microglia are typically $CD11b^{High}$ and $CD45^{Mid}$ (Ginhoux *et al.*, 2010) and the slightly lower than expected CD11b forward and side scatter is attributed to competition for available antigen between the CD11b microbeads and CD11b-PE marker. The number of $CD45^{high}$ cells, indicative of monocyte contamination, was negligible. No non-specific binding or auto-fluorescence was seen with appropriate isotope controls or unstained samples. Cell viability was confirmed at 97% ± 0.43 SE using SYTOX® Blue live-dead stain.

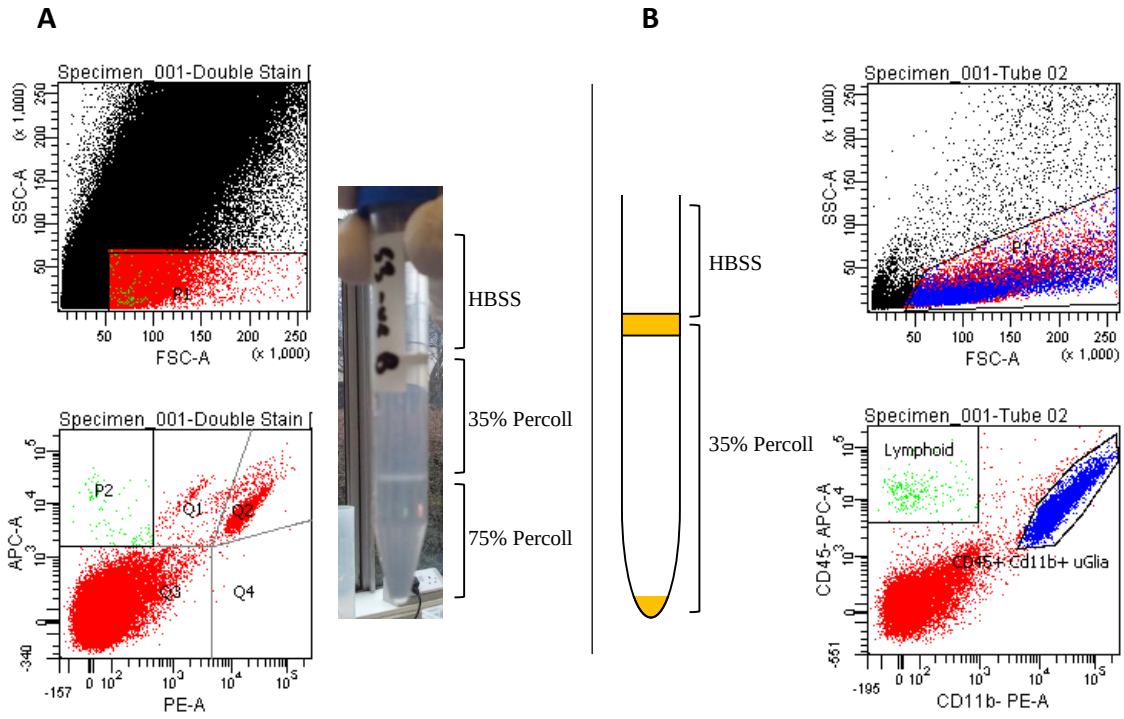

Figure 5-1: Microglia Isolation using a discontinuous Percoll™ gradient. A: Following centrifugation microglia collect at the 35%/75% Percoll™ interphase as a faint white band and the majority of the myelin collects at the 75%/HBSS interphase. Side and forward scatter FACS analysis revealed a considerable volume of debris and myelin that ranged in size and complexity throughout the scale. Low granularity regions confirmed the presence of a population of CD11b and CD45 positive cells (Region Q2). B: A significant reduction in debris and an increase by an order of magnitude in the number of CD11b and CD45 positive cells and was achieved following removal of the 35%/75% Percoll™ interphase and collection of a cell pellet.

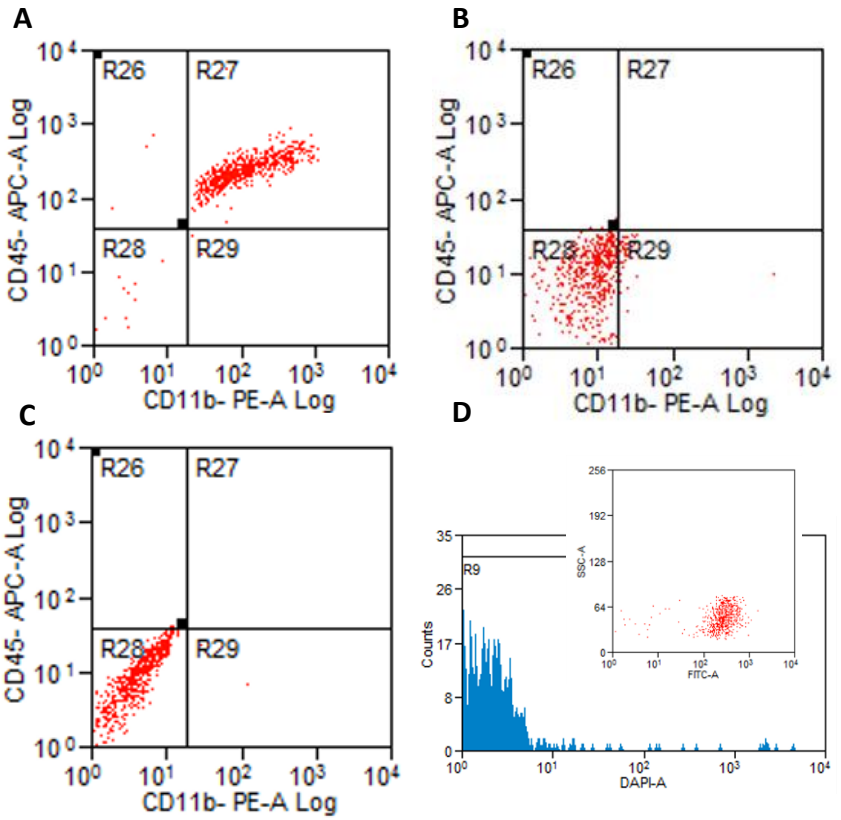

Figure 5-2: FACS sample analysis of CD11b microbead purified microglia. **A:** Cells stained with and positive for CD11b-PE & CD45-APC demonstrate a high purity. **B:** Isotope control and **C**: negative control show no non-specific binding or auto-fluorescence respectively. **D:** Cell viability was confirmed using SYTOX® live-dead stain. Inset: Isolated cells are EGFP positive.

5.3.3 Quality Control

Isolation of total RNA from microglia samples proved difficult to accomplish. The 260:280 nm and 260:230 nm absorbance ratios, determined on a NanoDrop® ND-1000 spectrophotometer, yielded an average of 1.77 ± 0.07 SE and 0.37 ± 0.03 SE respectfully. The average quantity of total RNA was found on the Nanodrop® to be low at 36.54 ng μl^{-1} ± 2.94 SE. Total RNA integrity quality control, based on an Agilent 2100 Bioanalyser electropherogram, revealed the majority of the samples to have weak peaks at 40 and 47 seconds indicative of digested 18S and 28S ribosomal subunit RNA (Figure 5-3). There was also noise between 35 and 50 seconds indicative of partial sample digestion. In all curves the peak for 28S ribosomal RNA was lower than the 16S peak indicative of borderline-acceptable levels of digestion within even the better samples. The samples with the highest evidence for digestion also had high peaks between 20 and 25 seconds, overlapping the marker peak, and associated with fragments of < 100 base pairs. In these poorer quality samples the 18S and 28S ribosomal peaks demonstrated a shift to the left. No evidence of DNA contamination was noticed either interfering with the 28S peak or baseline of the electropherogram beyond 50 seconds. Arbitrary RIN values were also correspondingly low.

The two best samples from each group, independent of gender, were selected for microarray array hybridisation (Table 5-1) giving 16 samples with an average RNA quantity of 38.97 ng μl^{-1} ± 5.80 SE and an average RIN value of 6.01 ± 0.26 SE. The remaining samples were considered unsuitable for further analysis.

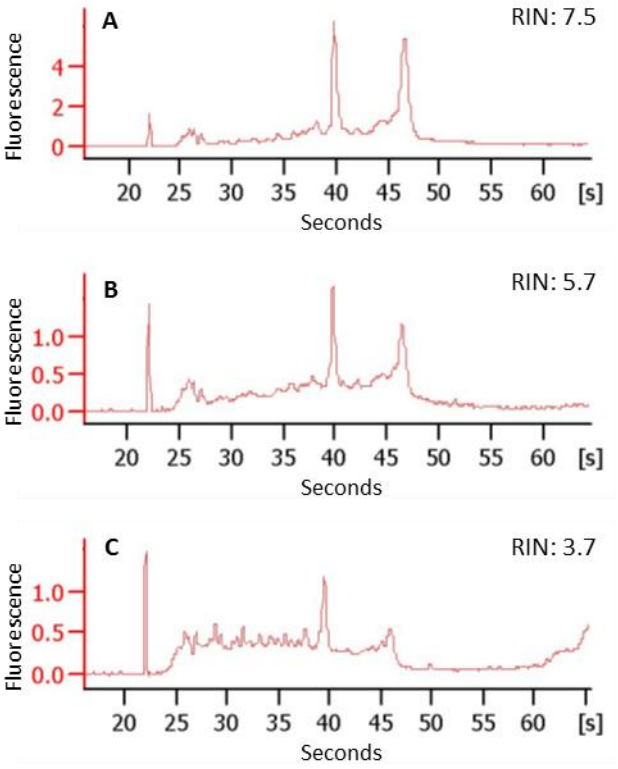

Figure 5-3: Agilent Bioanalyser 2100 procured electropherograms of total RNA integrity. **A:** The better samples had more intense peaks at 40 and 47 seconds indicative of intact 18S and 28S ribosomal subunit RNA. **B:** The majority of the samples demonstrated weaker 18S and 28S ribosomal RNA peaks and noise indicative of partial sample digestion. **C:** The poorest quality samples demonstrated significant digestion with strong peaks associated with small fragments < 100 base pairs and left shift.

Table 5-2: Microglia Total RNA samples chosen to take forward in the analysis following quality control checks for RNA integrity.

dpi (Days)	Inoculum	Gender	RNA Conc. (ng/µl)	Agilent RIN Value
200	79A	♀	31.12	7.5
200	79A	♂	26.7	6.2
150	79A	♀	20.91	7
150	79A	♂	87.95	4
100	79A	♀	99.19	6.5
100	79A	♂	17.15	6
35	79A	♀	66.77	7.6
35	79A	♀	36.35	4.6
200	NBr	♀	24.43	6.8
200	NBr	♂	20.92	4.9
150	NBr	♀	32.62	7
150	NBr	♀	25.55	4.5
100	NBr	♀	27.37	6.7
100	NBr	♀	50.04	6.4
35	NBr	♀	24.18	5.8
35	NBr	♀	32.26	5.6

Microarray quality control was performed on sample-independent probe intensity to highlight defects that typically arise from high background noise, low signal intensity and array sectional bias. Mapping the log2 probe intensity for the raw data to a grey scale allowed for relative comparison of the medium values (Figure 5-2). Some variation was to be expected using un-normalised data but the plot revealed all array intensity levels to be comparable both across the entire sample population and within individual groups.

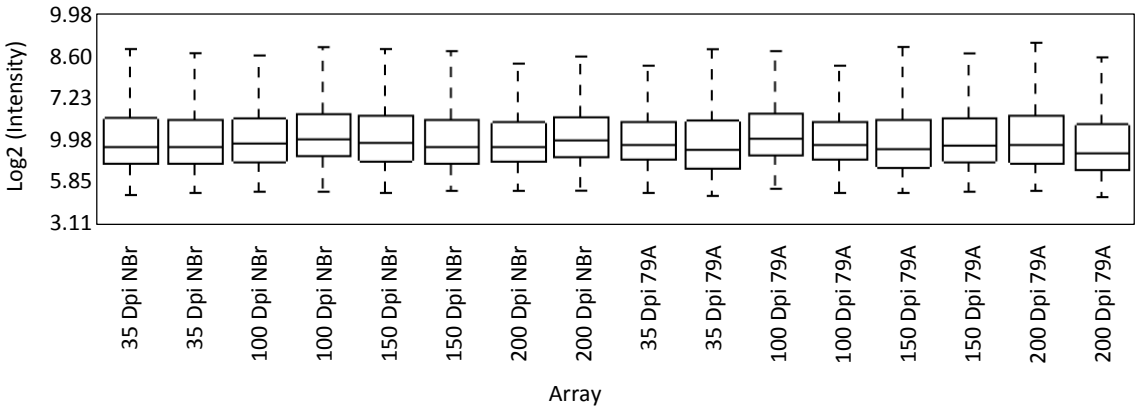

Figure 5-4: Box plots of log2 probe intensity for raw un-normalised arrays. Array intensity is comparable both within groups and across the entire array population.

Post-normalisation quality control analysis was performed within the reading plate on the Affymetrix GeneTitan® Multi-Channel instrument and included the generation of an array-array correlation matrix plot based upon log2-scaled Pearson correlation distance for RMA normalised sample signal intensity (Figure 5-5). The plot revealed the 100 dpi array from the 79A infected group had less correlation to the rest of the array population. The concentration of RNA for this sample was also appreciably lower than the other samples in the population (Table 5-2). This array was subsequently dropped from the analysis. The remaining arrays all demonstrated high levels of correlation indicating acceptable signal intensity homogeneity across the normalised sample population.

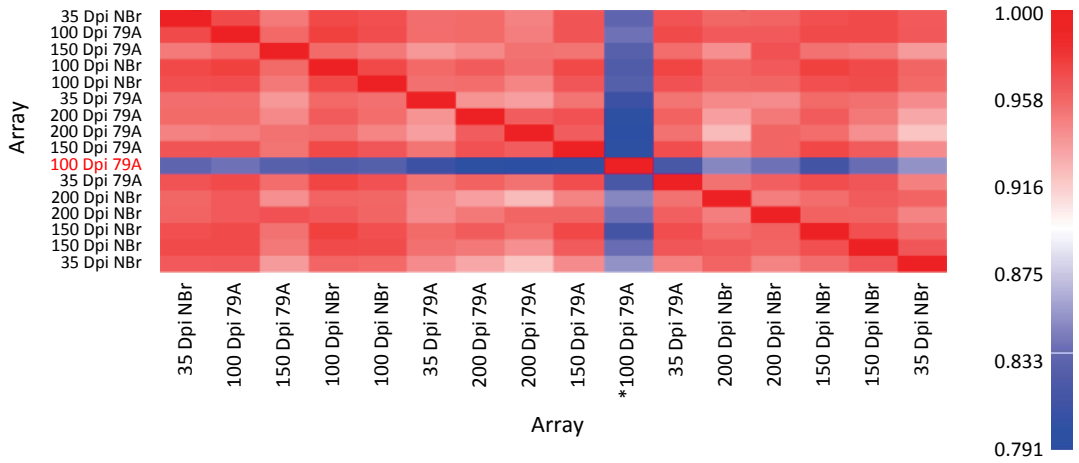

Figure 5-5: Array-array correlation matrix plot of RMA normalised array signal intensity. * One array, for the infected 100 dpi time point demonstrated less correlation of intensity with the rest of the arrays in the analysis.

Following acquisition and normalisation of isolated microglia microarray data, a selection of genes, either well known in the literature or previously identified in chapter 2 as cell specific for microglia, astrocytes, neurons or oligodendrocytes were searched for within both the uninfected and infected datasets. The relative expression for each was determined as an average and plotted in comparison. This confirmed the purity of isolated microglia was high with minimal expression of genes associated with the other main brain cell types (Figure 5-6). Importantly, astrocyte-

specific glial fibrillary acidic protein (*Gfap*) (Pekny *et al.*, 1995) was expressed at negligible levels confirming the presence of *Gfap* found in the isolated microglia external datasets used in Chapter 2 were contaminated with astrocytes.

Table 5-3: The microarrays analysed in this study arranged by time point. One array was dropped in the 100 dpi 79A infected group following quality control checks

Time Point (dpi)	Number of 79A/BALB/cJ$^{Fms\text{-}EGFP/}$ Microarrays	Number of NBr/BALB/cJ$^{Fms\text{-}EGFP/}$ Microarrays
35	2	2
100	1	2
150	2	2
200	2	2

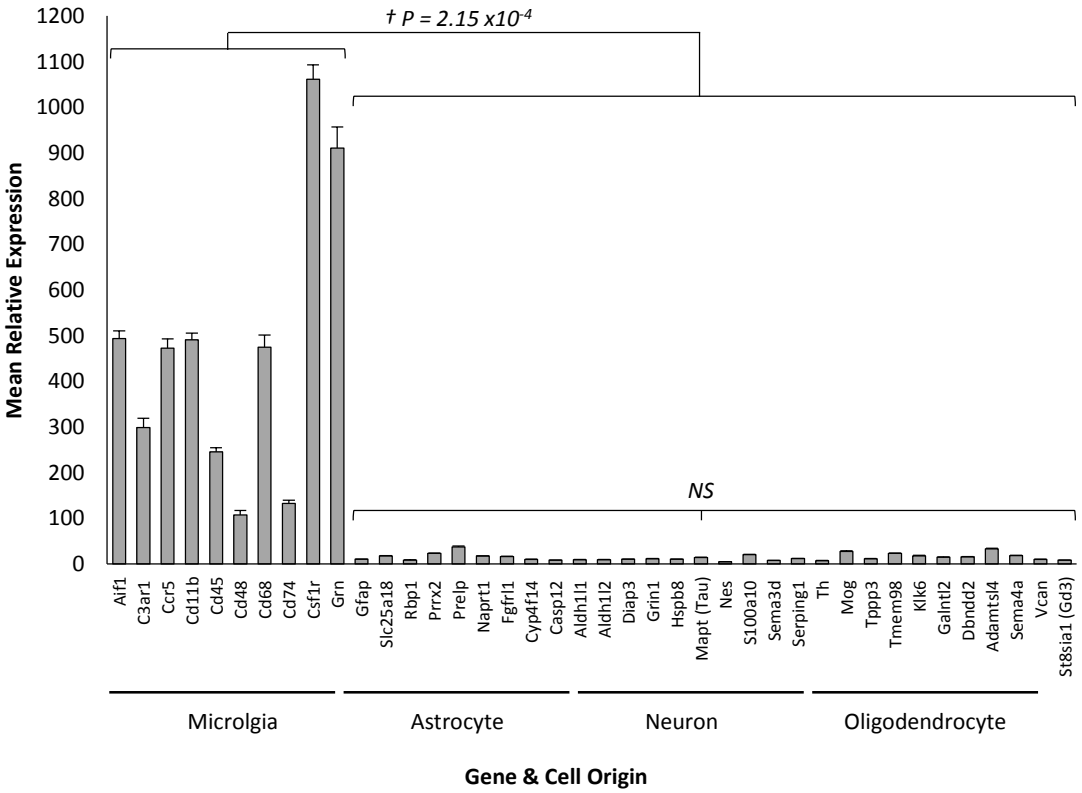

Figure 5-6: Isolated microglia are relatively pure. For each cell type the relative expression of ten genes, which are well-known and/or previously identified in chapter 2 of this study as being cell-specific markers of the four main brain cell types, were plotted using the uninfected microarray data generated from purified microglia. † Mean statistical values determined using t-Test assuming variances determined by f-Test. NS = Not Significant. Error bars equate to ± SE.

Group-to-Group Selection of Genes of Interest using BioLayout *Express*^{3D}

The data set was perceived as extremely linear requiring a high correlation threshold of 0.90 to allow for visualisation of nodes of biological interest, and ensure only nodes that portrayed a differential expression were incorporated in the graph. This resulting in the dropping of a considerable proportion of transcripts that were not highly correlated with each other and not therefore considered biological interesting. The bulk of the biologically interesting nodes were displayed in a graph comprising 2592 nodes, joined by 125,004 edges, grouped into two separate components and organised into 60 clusters by MCL (Figure 5-7). The two components shared no edges and consequently the two components shared no correlation. The top most component contained the clusters with a convincing disease signature. It was from this component that the clusters considered relevant to the disease were chosen using the expression profile viewer built into BioLayout *Express*^{3D}. Clusters with a weak and/or noisy signal were considered unconvincing and dropped from the analysis. In total 28 clusters were considered to demonstrate a convincing disease signature and analysed further. The remaining 32 were dropped.

The bottom most component comprised genes which, when shown as an average for the arrays for each group, appeared to demonstrate a decrease in expression. Predominantly the genes within this component were associated with olfactory pheromone receptors and odorant induced signal transduction. None of the clusters containing these genes were found within, or joined by edges, to those with an increase in expression in the adjacent component. Furthermore the average relative expression change for the genes with a decrease in expression was small with a fold difference between infected and controls at 200 dpi of 0.63 ± 0.01 SE. It was therefore decided that the genes associated with a decrease in expression offered an unconvincing disease-associated signature and were dropped from the analysis.

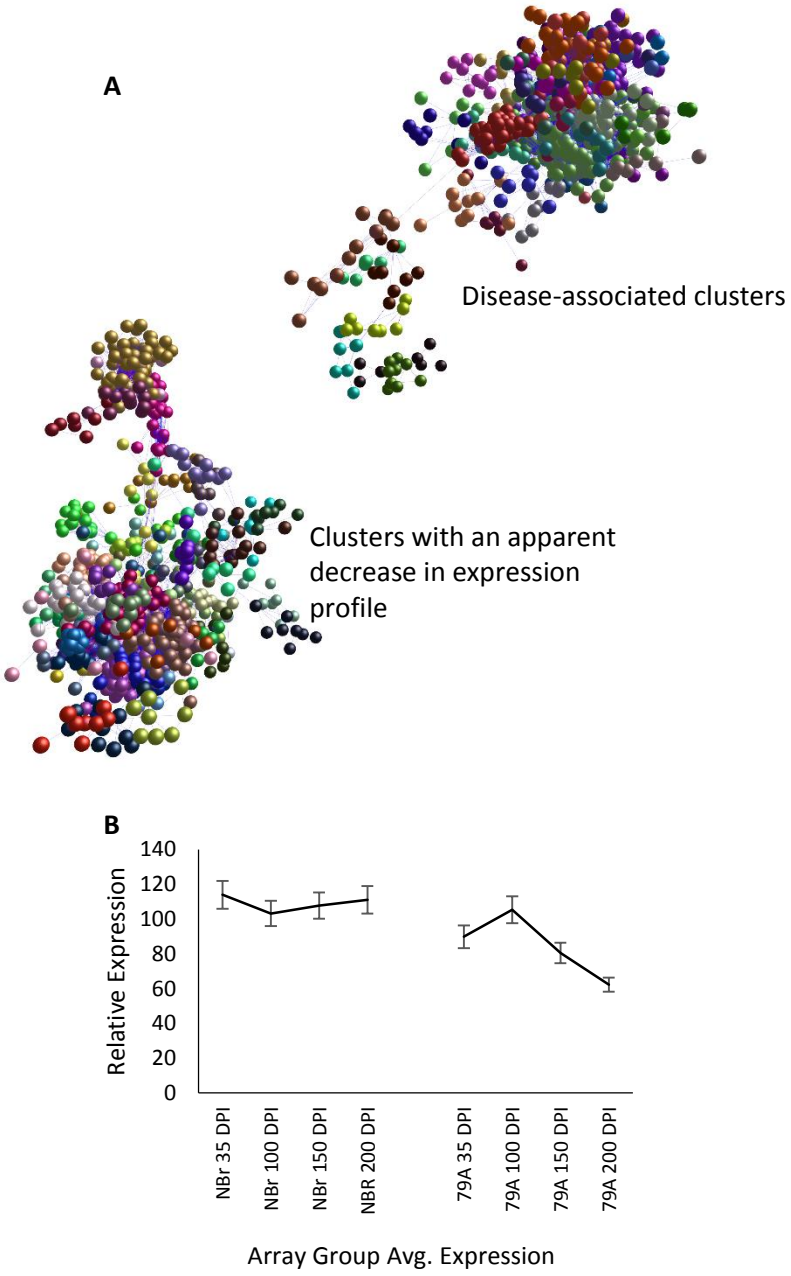

Figure 5-7: BioLayout Express3D generated group-to-group clustered graph of total array data obtained from all time points. **A:** With a Pearson correlation matrix threshold set at 0.90 a graph was produced comprising 2592 probesets joined by 125,004, organised into 123 clusters by MCL (inflation 2.3) and comprised two separate components that demonstrated no correlation with each other. The upper component expression profile was for an increase in expression at the later stages of disease. **B:** The lower component mean expression profile for all nodes portrayed a decrease in expression from 100 dpi. The expression changes are weak and unconvincing when compared to expression by control animals. Error bars equate to standard error.

5.3.4 Parallel Pathology of 79A infected BALB/cJ$^{Fms\text{-}EGFP/-}$ Mice

The determination of the pathogy of infection by the 79A prion strain, using an intraperitetonal route, in the BALB/cJ$^{Fms\text{-}EGFP/-}$ strain of mice has been the subject of other chapters within this study. Briefly BALB/cJ$^{Fms\text{-}EGFP/-}$ mice infected intraperitetonally with 79A first displayed accumulation of fine punctate PrP deposition in the medulla at 150 dpi (65% of the incubation period). This coincided with an increase in microglia numbers in the same region of the medulla. The onset of clinical signs associated with prion disease was at 200 dpi and coincided with widespread accumulation of punctate PrP deposits and microglia activation throughout the brain. The concentration of both PrP protein and activated microglia was particularly heavy in the thalamus. Within this analysis, infected mice used to confirm correct strain type, were culled with terminal disease at 225 days. The experimental source of the inoculum and the origin of the mice used in this experiment was the same as that used throughout this project allowing for direct comparison between chapters.

5.3.5 Disease-Associated Differentially Expressed Genes

The vast majority of the identified disease-associated microglia genes demonstrated an increase in expression at 200 dpi. This coincided with the widespread and significant deposition of punctate PrP and microglia activation (Chapters 3 and 4). At 150 dpi the average (mean) expression for these genes did not rise more than 1.5 fold above the basal levels of expression established by the normal brain inoculated control mice. Any observable morphological response by microglia at this time is restricted to the medulla and the detection of any, and presumably weaker, signal produced by this small group of cells would be diluted by the use of total brain microglia.

The chosen clusters of interest were loaded into BioLayout *Express*^{3D} with a correlation threshold set at 0.90 to allow for visualisation of transcripts with

biological interest within the resulting structure. A single graph was produced that comprised 741 nodes, joined by 29297 edges, and organised using the MCL algorithm into 2 large clusters and 13 smaller clusters. All clusters shared a similar gene expression profile with a clear increase in expression at the 200 day time point. The organisation into a single graph, with a similar expression profile for all nodes, demonstrated the homogeneity of the signal produced by whole brain microglia. Animals inoculated with normal brain material presented with normal background levels of variation expected of microarrays and showed no significant change in expression throughout the disease period. There was no difference in expression between male and female mice. Consequently gender had no impact on the disease process within this analysis.

Transposing the 741 genes of interest to display a sample-to-sample (array) level graph within BioLayout *Express*^{3D} revealed the two arrays from the 79A infected 200 dpi time point had less correlation with the rest of the nodes and a high degree of correlation with each other. This was performed at the same correlation threshold of 0.90 as the group-to-group analysis. Therefore the overall change in expression produced by microglia at 200 dpi was of sufficient magnitude to induce a clear separation from arrays produced from the uninfected control and pre-200 dpi infected groups.

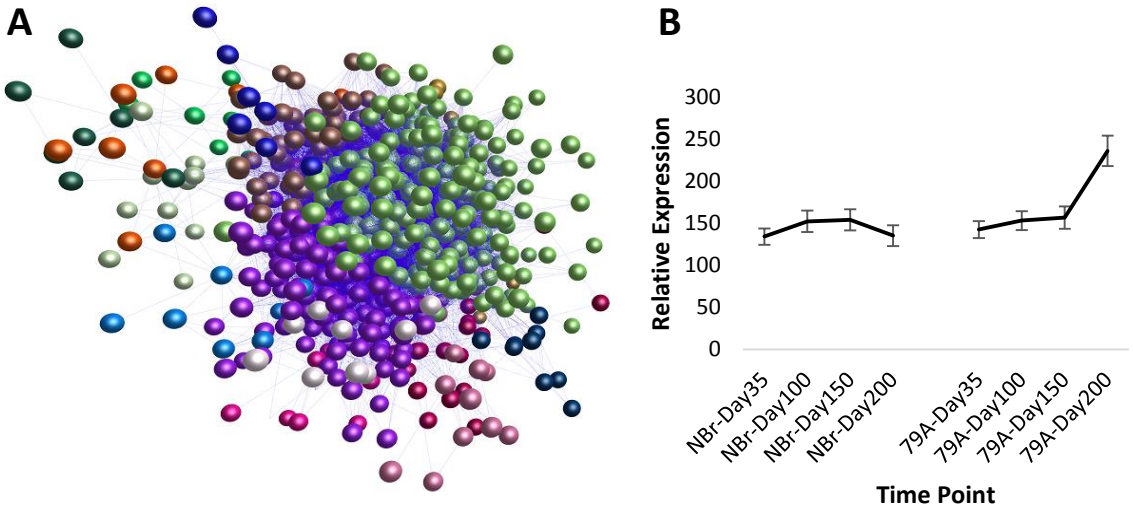

Figure 5-8: BioLayout *Express*^{3D} group-to-group graph at a correlation threshold of 0.90 created from the transcripts demonstrating a disease-associated signal. A: The graph was highly organised and comprised two main clusters. B: The expression profile for the array averages within each group revealed a strong increase in expression at 200 dpi.

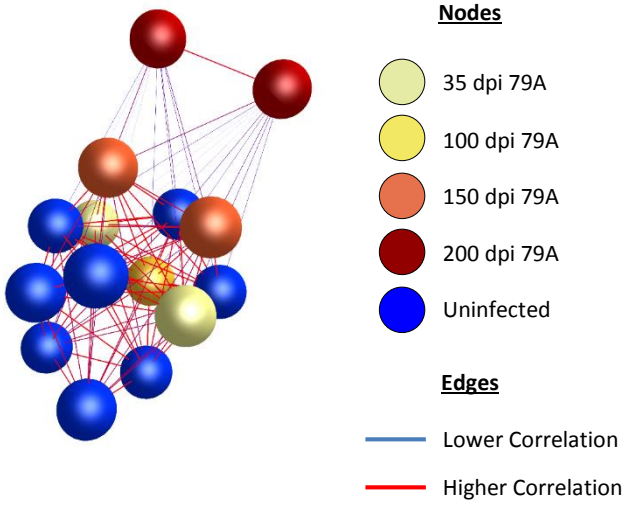

Figure 5-9: Global microarray sample-to-sample transposed BioLayout *Express*^{3D} graph. Prion infected and uninfected pre-200 dpi arrays are highly correlated and organised into one component. Displaying high inter-correlation but lower correlation with the rest of the population are the arrays for the 200 dpi infected group. Note: nodes have been coloured only for clarity and are not indicative of MCL clustering

Gene ontology was performed for each gene using the data made available on the Ensembl Biomart database to allow for functional associations to be determined (Figure 5-10). Just under two thirds of the 741 identified differentially expressed disease-associated genes were attributed to metabolism and the maintenance of homeostasis. The correct determination of differentially expressed metabolic genes to a specific cell type is only possible through the type of single cell type analysis presented here. Metabolic genes are typically expressed by all tissue cells types making identification of the cellular origin from a multicellular population impossible.

Genes that were related to the immune response comprised just under a quarter of the total (Figure 5-10). The 6% of genes associated with cytoskeletal changes and migration were classed into their own groups respectively. Due to the multirole function of genes associated with cytoskeletal changes and migration these groups could have been incorporated as part of the immune response. Indeed many of the pathways associated with membrane reshuffling were also found associated with migration and phagocytosis by myeloid cells on the Ensembl database. However as microglia are known to be highly motile in the healthy brain environment (Nimmerjahn *et al.*, 2005) a degree of caution was felt appropriate. Genes associated with differentiation were directly incorporated into the immune system as it was felt that genes associated with differentiation that were isolated from a microglia only population could only be attributed to pathways associated with activation and the subsequent differentiation of recruited inflammatory monocytes. The genes associated with mitosis were kept as a separate group for clarity as the increase in microglia numbers observed in prion disease could be considered as self-sufficient turnover by the resident microglia population (Parkhurst *et al.*, 2013).

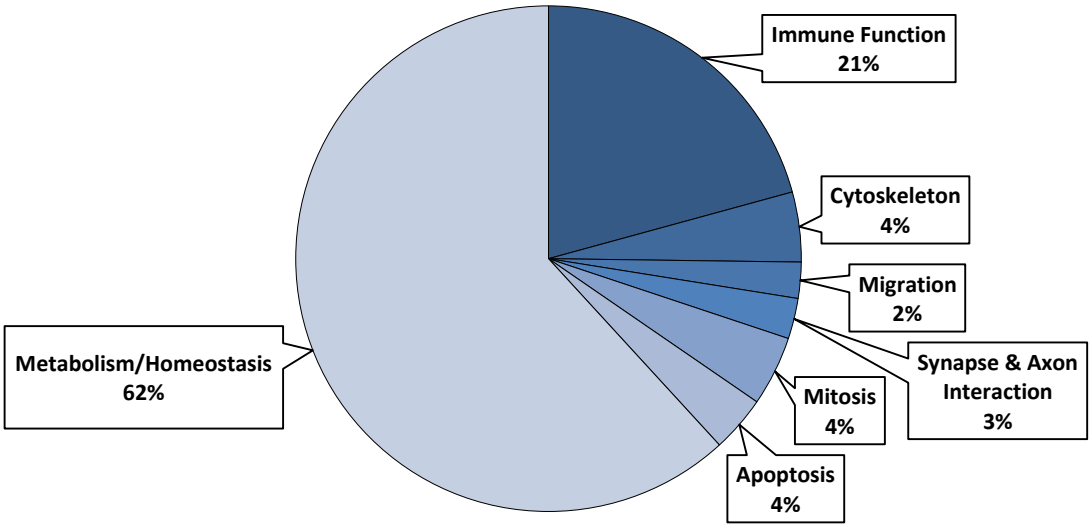

Figure 5-10: Regulated disease-associated genes allocated by function. Using the Ensembl Biomart database the majority of the regulated genes were ascribed to metabolism and homeostasis. Genes associated with immune system, for which differentiation has been included, comprise only a fifth. This highlights the power of a signal cell isolation in correctly determining the association of metabolic genes

To investigate the protein-protein interactions the 741 genes of interest were loaded into STRING (http://string-db.org). STRING produced a graph in which the vast majority of the nodes were separated into two loosely connected but highly correlated components (Figure 5-11). The larger of the two components comprised the proteins associated with metabolism, ribosomal function and translation. The second component was comprised of those proteins involved in immune system signalling and innate immune activation. The immune system component displayed the potential for further separation into separate clusters if MCL could be applied. However each potential cluster did not appear to relate to a specific immune function.

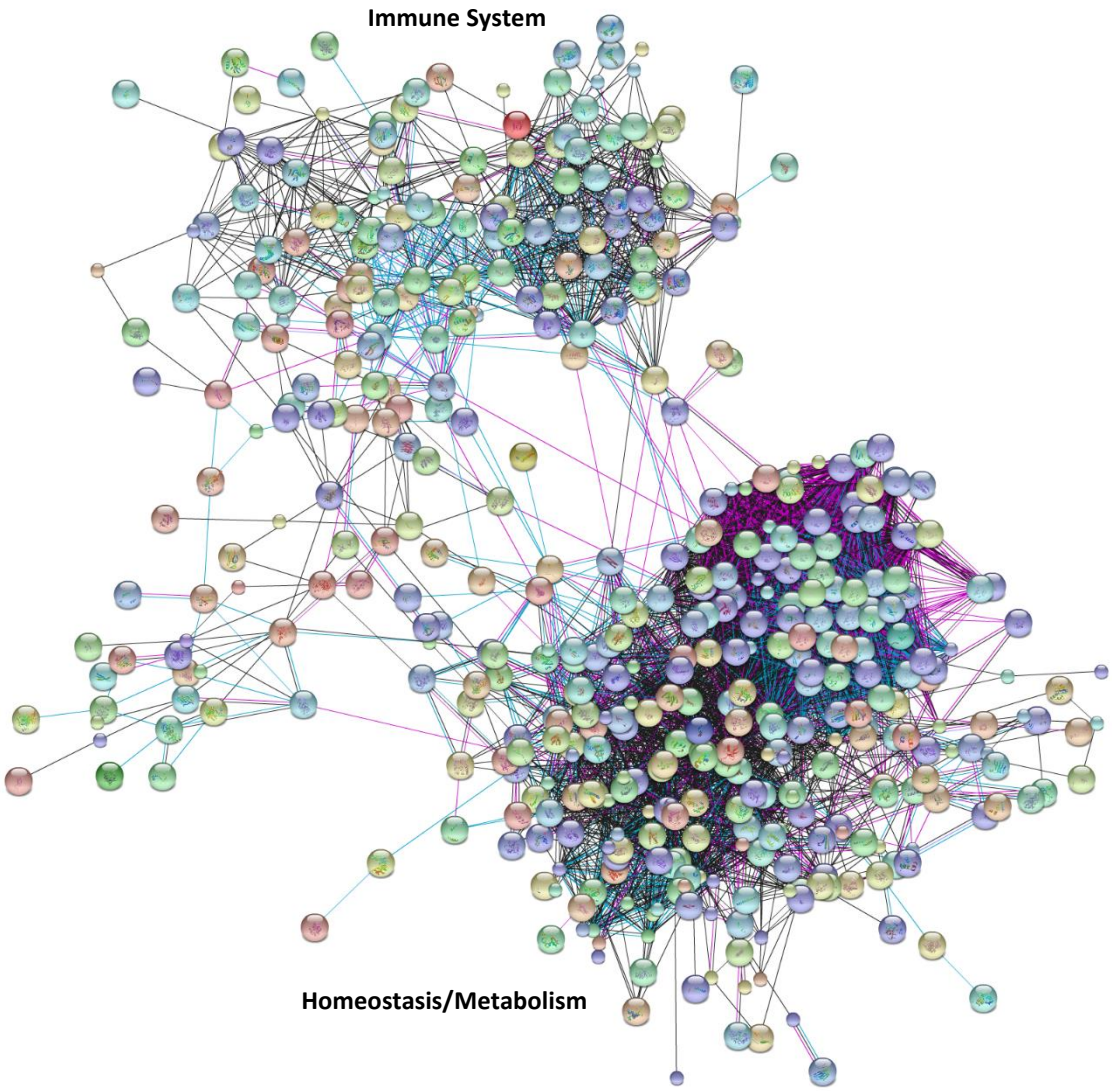

Figure 5-11: STRING generated map of known protein-protein interactions. The vast majority of the nodes are located into two loosely connected yet highly correlated components comprising nodes associated with homeostasis and metabolism in one and the immune system in the other.

5.3.6 Gene Enrichment Analysis

Enrichment analysis of the 741 identified genes using the FuncAssociate database, confirmed the breakdown of the transcripts into groups by specific function; translation, energy production, immune response, interferon response and cell stress (Table 5-1). All functional terms had a *P*-value of considerably greater than $1x10^{-3}$ with an average of $2.90x10^{-06}$. Immunological response comprised the single largest category in respect to total gene number. The signature was one of proteolysis, with NF-KB mediated cytokine cascades and innate immunity. The GO enrichment functional groups of mitochondria, ribosome, cell stress, apoptotic process and proliferation had the largest individual grouping of genes, thereby confirming the dominant metabolic processes present within the signature.

Fold change analysis based on the difference between infected and control mean average for the arrays at 150 and 200 dpi revealed a spread of differential changes to the increase in expression that were subsequently organised into bins (Table 5-5). A cut-off of >1.2 was chosen for the fold change difference at 150 dpi as the bulk of the genes at this time point did not portray a convincing increase in expression. For the genes that did demonstrate a noted increase in expression at 150 dpi, an increase in fold change from 150 to 200 dpi was noted for all but 9 genes; *Baiap2*, *Fbxw4*, *Fus*, *Gosr2*, *Impad1*, *Rab1b*, *Slc6a6*, *Usp15* and *Vac14*. Intriguingly *Usp15* encodes for a receptor stabiliser for the TGFβ1 receptor (Inui *et al.*, 2011). Also of note, the genes *Vac14, Slc6a6, Fus*, *Fbxw4* and *Baiap2* have all been implemented as neuronal synaptic stabilisers, neurotransmitter transporters and regulators of neuronal differentiation (Heller-Stilb *et al.*, 2002, Kim *et al.*, 2009, Hoeck *et al.*, 2010, Huang *et al.*, 2010, Zhang *et al.*, 2012). The majority of the genes with a fold change of between 1.0 and 2.0 are enriched for protein translation. The fold change increases of greater than 2.0 were dominated by genes highly enriched for the innate immune response including, chemotaxis, antigen presentation and NFκB mediated cytokine signalling cascades.

Table 5-4: GO enrichment terms determined from the identified 741 differentially expressed genes using FuncAssociate 2.0 revealed protein translation, respiration, cellular stress and components of the myeloid immune system to be significantly represented. All terms have a *P*-value of considerably less than 0.001.

GO Ontological Annotation	GO ID	*P*-value	Gene Number	% Within Differentiated Dataset
Protein Translation				
ribosome	GO:0005840	6.37E-54	72	9.72
translation	GO:0006412	3.52E-26	67	9.04
ribosome biogenesis	GO:0042254	2.70E-12	27	3.64
endoplasmic reticulum	GO:0005783	1.11E-05	68	9.18
Energy Production				
mitochondrion	GO:0005739	1.10E-13	111	14.98
generation of precursor metabolites and energy	GO:0006091	1.94E-05	21	2.83
respiratory chain	GO:0070469	1.92E-13	19	2.56
Immune Response				
lysosome	GO:0005764	1.55E-12	42	5.67
regulation of cytokine production	GO:0001817	1.47E-09	38	5.13
chemokine receptor binding	GO:0042379	2.20E-09	13	1.75
regulation of locomotion	GO:0040012	1.03E-07	41	5.53
endosome	GO:0005768	6.35E-07	41	5.53
cell proliferation	GO:0008283	3.00E-06	78	10.53
I-kappaB kinase/NF-kappaB cascade	GO:0007249	8.03E-06	19	2.56
innate immune response-activating signal transduction	GO:0002758	1.38E-05	12	1.62
Interferon Response				
response to interferon-gamma	GO:0034341	1.32E-07	12	1.62
response to interferon-beta	GO:0035456	1.60E-07	9	1.21
response to type I interferon	GO:0034340	8.99E-07	7	0.94
Cell Stress				
response to stress	GO:0006950	2.53E-13	138	18.62
apoptotic process	GO:0006915	5.05E-07	82	11.07
response to wounding	GO:0009611	3.06E-06	45	6.07

Table 5-5: Differentially expressed genes of interest at arranged by time point and fold change. GO ontology data shown for genes lists that were enriched for function.

Fold Change	Gene	GO Enrichment
150 dpi		
≥ 1.2 - ≤ 1.49	1700021F05Rik, 1810037I17Rik, 2700094K13Rik, Acot10, Anxa3, Atox1, Axl, Baiap2, Bst2, Capg, Ccdc23, Ccl4, Cd52, Cd83, Cd86, Cdc37, Ch25h, Chchd3, Chmp1b, Chst1, Churc1, Cmc1, Coro1c, Csnk2b, Cstb, Cxcl9, Dnajb14, E330009J07Rik, Etf1, Ezr, Fam92a, Fbxw4, Fdx1, Fgl2, Fgr, Fus, Gba, Gosr2, Grpel1, H2-D1, H2-gs10, H2-Q7, Hebp1, Impad1, Impdh2, Itgax, Kif3a, Klf10, Lox, Lrpap1, Naf1, Ndufa6, Nfkbia, Nfkbib, Nfkbie, Ngfrap1, Nmi, Pfkfb3, Ppap2a, Prdx4, Psmb2, Psmb3, Rab1b, Rasgef1b, rp9, Rpl14, S1pr1, Sass6, Scand1, Slc6a6, Snhg8, Sqstm1, Tceb2, Tmem160, Tnf, Tnfaip2, Tnfaip3, Tpd52, Tpi1, Uqcr10, Usp15, Utp11l, Vac14, Xdh, Yaf2, Zcchc17, Znrd1	Negative regulation of cytokine production: $P = 5.7 \times 10^{-6}$ Positive regulation of immune system process: $P = 1.52 \times 10^{-5}$ Defence response: $P = 2.37 \times 10^{-5}$
150 dpi		
≥ 1.5 – ≤ 1.99	Gem, Il1b, Niacr1	Regulation of adiponectin secretion: $P = 3.51 \times 10^{-8}$
200 dpi		
≥ 1.0 - ≤ 1.49	1110007C09Rik, 1200014J11Rik, 2010011I20Rik, 2700007P21Rik, 2810405K02Rik, Adh5, Aif1, Alcam, Apob, Arl2, Arrdc4, Asah1, Asph, Atl2, Atp2b1, Azin1, Baiap2, C4b, Caprin1, Casd1, Ccny, Cd300lf, Cenpc1, Cep135, Cfl1, Chmp7, Cic, Cln8, Creb3, Csf2rb2, Ctns, Ctsd, Cuedc2, Cyp4v3, Diap2, Dnlz, Dnmt3a, Drap1, Dtnbp1, Ebna1bp2, Ecd, Eif1a, Eif2s2, Erbb2ip, Erlec1, Evi2a, Exoc2, Extl3, Fam32a, Fbxw4, Fcf1, Flna, Fth1, Ftl1, Ftl2, Furin, Fus, Gabarapl1, Galnt6, Gcnt2, Gfpt1, Glrx5, Gm10653, Gm15772, Gm5805, Gns, Golim4, Gosr2, H2-T10, Iigp1, Ikbke, Il10rb, Il12b, Impad1, Irf9, Itgb1, Kctd2, Klhdc4, Lamp2, Ldhb, Mcm6, Mfap1a, Mina, Mirn692-2b, Mtmr2, Mxd4, Naca, Ncf1, Nd1, Ndufb2, Ndufv1, Nkap, Nono, Npat, Npm1, Nup98, Nus1, Pdcd5, Pde4dip, Pfkfb3, Pgam1, Pgap1, Pigl, Pigu, Plekhh2, Plin2, Plxnb2, Ppm1m, Ppp1cc, Ppp1r15b, Prdx5, Prpf6, Ptgfrn, Ptplad2, Rab1b, Rap2a, Rbm42, Rbx1, Rcc2, Rnaseh2b, Rnf13, Rpl21, Rpl3, Rps2, Rps27a, Rps29, Rps4x, Rps6, S100a1, Sart3, Scnm1, Sdcbp, Sec63, Slc6a6, Snf8, Sph21_3049, Srp72, Sssca1, St14, St5, Surf4, Syncrip, Synj2, Tacc3, Taf5l, Tatdn2, Tbc1d22a, Tlr1, Tmx3, Top2a, Tpt1, Trip12, Ubxn1, Uhrf1bp1l, Usp15, Vac14, Xrn2, Zfp868, Znhit1	Protein targeting to ER: $P = 6.07 \times 10^{-7}$ Ribosome small subunit: $P = 1.75 \times 10^{-5}$

Table continues overleaf:

Fold Change	Gene	GO Enrichment
200 dpi		
≥ 1.5 – ≤ 1.99	1110059G10Rik, 1500032L24Rik, 1700021F05Rik, 1700112E06Rik, 2010107E04Rik, 2310003F16Rik, 2310039H08Rik, 4931406C07Rik, A430005L14Rik, Abca1, Acadl, Acbd6, Acot10, Adap1, Adar, Aggf1, Akr1a4, Alas1, Aldoa, Anapc13, Ankra2, Ap3s1, Apbb2, Apitd1, Aplp2, Apobec1, Apoe, App, Arhgap24, Arl6ip5, Arpc1b, Arpc5l, Atp1a3, Atp5h, Atp5l, Atp6ap2, Atp6v0e, Atp6v1g1, Atxn10, Bag1, BC003266, Bcas2, Bhlhb9, Bloc1s2, Bst2, C3ar1, Cadm1, Calu, Ccdc23, Ccdc90a, Ccl8, Ccl9, Cct2, Cd14, Cd180, Cd200r4, Cd83, Cd86, Cdc37, Cenpo, Cetn3, Cfdp1, Chchd3, Chst1, Chst2, Clec5a, Cndp2, Colec12, Commd1, Cops5, Cops6, Coq7, Cox4i1, Cox5b, Cox6a1, Cox6b1, Cox7a1, Cox8a, Csnk2b, Ctbs, Ctla2a, Ctnnb1, Ctsa, Ctsb, Ctse, Ctsh, Cul4b, Cux1, Cxcl14, Cxcl9, Cycs, D10Wsu52e, Dctn6, Ddx1, Dek, Derl1, Dna2, Dnajb14, Dpp7, Dpy19l4, Dram2, Dscc1, Dusp2, Eef1b2, Efcab2, Eid1, Eif2ak2, Eif3e, Eif3h, Eif3l, Eif4b, Ell2, Enpp1, Eprs, Etf1, Exosc9, Fam165b, Fam167b, Fam174a, Fam50a, Fau, Fdx1, Fnip2, Fuca1, Fundc2, Fxyd5, Gaa, Gadd45a, Galc, Galnt7, Gba, Gca, Gde1, Ghitm, Glb1, Glrx5, Gm10063, Gm10136, Gm12191, Gm2695, Gm6251, Gm6548, Gm9975, Gmds, Gnb2l1, Gng5, Gnl3, Gnpda2, Gnptab, Golph3, Got1, Gpr84, Gpx4, Grasp, Grinl1a, Grpel1, Gsto1, Gusb, Gyg, Hat1, Hcst, Hgf, Higd2a, Hint1, Hmgn3, Hprt, Hsd17b11, Hspe1, Idh1, Ifi30, Ifih1, Ifit1, Il2rg, Ipo5, Irf1, Irgm1, Isg15, Katna1, Kif3a, Klf10, Lamp1, Ldha, Lgals3, Lilrb4, Lrp12, Lrpap1, Lsm2, Ly6e, Lyst, Lyz2, Map3k7, Map3k8, Mapkapk2, Mbd2, Mcee, Mcm3, Mfsd1, Mmgt2, Mospd2, Mrpl22, Mrpl34, Mrpl39, Mrpl52, Mrps33, Mrps9, Mrrf, Ms4a4c, Ms4a6c, Mtap4, Myl6, Naa50, Naf1, Naip2, Ndufa3, Ndufa8, Ndufb11, Ndufc2, Ndufv3, Nedd8, Neu1, Nfkbib, Nfkbie, Nipsnap3b, Nme1, Nol7, Npc2, Npnt, Nptn, Nrp1, Nuak2, Nucb1, Nucb2, Oasl2, Ogfr, Ola1, Olfr110, Osbpl8, Oxct1, Parp14, Parp9, Pdcd6, Peci, Pfdn1, Pfkl, Pgk1, Plau, Plekha1, Plekha3, Postn, Ppap2a, Prkar1a, Psat1, Psma7, Psmb1, Psmb2, Psmb4, Psmd8, Psme1, Ptbp1, Ptgs2, Ptpra, Pus3, Rab12, Ranbp1, Rassf4, Rer1, Rlf, Rnf128, rp9, Rpl10a, Rpl11, Rpl12, Rpl13, Rpl13a, Rpl14, Rpl18a, Rpl19, Rpl22, Rpl26, Rpl27, Rpl27a, Rpl28, Rpl31, Rpl35, Rpl35a, Rpl36, Rpl36a, Rpl36al, Rpl37, Rpl37a, Rpl38, Rpl39, Rpl39l, Rpl4, Rpl41, Rpl5, Rpl6, Rpl7, Rpl8, Rplp0, Rps10, Rps14, Rps15a, Rps15a-ps6, Rps16, Rps17, Rps18, Rps19, Rps20, Rps23, Rps25, Rps27, Rps3, Rps3a, Rps5, Rps7, Rps8, Rragc, Sap30, Sass6, Scand1, Sdc3, Sdc4, Sdf4, Sec61b, Serp1, Setd3, Sgpl1, Shfm1, Slamf9, Slc11a2, Slc23a2, Slc25a4, Slc38a6, Slc7a11, Slfn5, Snap29, Snord38a, Snrpd3, Snrpf, Snx17, Snx24, Snx3, Spcs1, Spopl, Sqstm1, Srd5a3, St8sia6, Stk3, Sulf2, Surf1, Syngr1, Taf10, Tank, Tapbp, Tceb1, Tcp1, Tmem154, Tmem160, Tmem222, Tmem49, Tmsb10, Tnfaip2, Tomm7, Tpi1, Tpm4, Trim30a, Ttc1, Ttc30b, Tubb2a, Txndc5, Uba52, Uqcrb, Utp11l, Utp14a, Utp3, Vat1, Vim, Vps28, Vps29, Xdh, Zbp1, Zc3h12a, Zfp704, Znrd1	Ribosome: $P = 4.02 \times 10^{-48}$ Protein targeting to ER: $P = 1.23 \times 10^{-52}$ SRP-dependent cotranslational protein targeting to membrane $P = 2.08 \times 10^{-53}$ Protein localisation to membrane: $P = 2.11 \times 10^{-32}$ Lysosome: $P = 7.11 \times 10^{-7}$ Antigen processing via MHC class 1: $P = 8.68 \times 10^{-5}$

Table continues overleaf:

Fold Change	Gene	GO Enrichment
200 dpi		
≥ 2.0 – ≤ 2.49	0610031J06Rik, 1500011K16Rik, 1500012F01Rik, 1810027O10Rik, 1810037I17Rik, 2310028O11Rik, 2700094K13Rik, 2900010M23Rik, 3830403N18Rik, 5430435G22Rik, Anxa3, Anxa5, Atox1, Atp5k, Atp6v1a, Bcl2a1c, Bcl2a1d, Casp4, Ccdc122, Cd274, Cd48, Cd72, Chmp1b, Churc1, Cks1b, Cmc1, Coro1c, Cox17, Creg1, Ctsz, Cxcl11, Cxcr4, Cybb, D14Ertd668e, Eif3k, Eya4, Ezr, F2r, Fam92a, Fgl2, Fgr, Fmn1, Glipr1, Gltp, Gm2a, Gm5921, Gpr65, H28, H2-t9, Hebp1, Hif1a, Higd1a, Ifi204, Ifitm3, Igbp1, Irf7, Itga5, Krtcap2, Lsmd1, Ly9, Mif, Milr1, Mrpl36, Msr1, Myo5a, Naa20, Ndufa4, Ndufb5, Nfkbia, Ngfrap1, Ninj1, Nmi, Oas1g, Pcyt1a, Pfdn5, Pld3, Prdx1, Prdx4, Prim1, Psmb6, Ptger4, Rap2b, Rasgef1b, Rhoc, Romo1, Rpl22l1, Rpl32, Rpl37a, Rpp38, Rps12, Rps21, Rps26, Rsad2, S1pr1, Selm, Smpdl3a, Snhg8, Snrpe, Srp14, Stat1, Tbca, Timp2, Tlr2, Tmed3, Tmem9b, Tnfaip3, Tor3a, Tpd52, Txndc17, Ubl5, Uqcr10, Uqcrh, Usmg5, Vcam1, Vkorc1, Vti1b, Yaf2, Zcchc17	Positive regulation of cytokine secretion: $P = 1.50 \times 10^{-6}$ I/NFκB cascade: $P = 2.09 \times 10^{-5}$ LPS-mediated signalling pathway: $P = 8.89 \times 10^{-6}$
200 dpi		
≥ 2.5 – ≤ 2.99	Anxa4, Atp5e, Bcl2a1a, Bcl2a1b, Bola2, Capg, Ccrl2, Cd84, Cd9, Chst11, Cox6a2, Ctsl, Fabp5, Gla, H2-gs10, H2-Q7, Hscb, Hspb11, Id2, Ifit2, Il1b, Lag3, Lgals1, Ly6a, Mir29a, Mmp12, Myeov2, Myo1e, Ndufa2, Ndufa6, Plaur, Psmb3, Robld3, Rps11, Serpine2, Sp100, Ssr4, Tceb2, Wbp5	Regulation of glia cell differentiation: $P = 1.06 \times 10^{-6}$
200 dpi		
≥ 3.0 – ≤ 3.99	Axl, Ccl4, Ccl5, Ch25h, Cpd, Cstb, Cxcl16, E330009J07Rik, Gas2l3, Gem, H2-D1, H2-K1, I830012O16Rik, Ifi44, Impdh2, Ndufa1, Nexn, Niacr1, Rilpl2, Rps27l, Slfn2, Tnf	Lymphocyte chemotaxis: $P = 8.86 \times 10^{-7}$ Antigen processing and presentation of endogenous antigen: $P = 2.70 \times 10^{-7}$ Chemokine receptor binding: $P = 1.268 \times 10^{-5}$
200 dpi		
≥ 4.0 – ≤ 4.99	Cd52, Csf1, Cst7, Fam20c, Fcgr4, Ifi202b, Lox, Rtp4	N/A
200 dpi		
≥ 5.0	Apoc1, Clec7a, Cxcl10, Cxcl13, Gadd45b, Ifi27l2a, Ifit3, Itgax, Lgals3bp, Lpl, Spp1	Response to virus: $P = 1.09 \times 10^{-6}$ Leukocyte chemotaxis: $P = 2.26 \times 10^{-5}$ Protein-Lipid complex remodelling: $P = 3.65 \times 10^{-5}$

5.3.7 Gene Ontology Analysis

Determination of the sub-cellular component for each gene considered to be associated with metabolism/homeostasis was performed from data obtained from the Ensembl Biomart database. This enabled the location of each gene to be plotted onto a cellular map and further organised by function (Figure 5-12). The identified cellular components included a significant increase in expression of genes associated with ribosomes within the rough endoplasmic reticulum and cytoplasm. Indeed the bulk of the metabolic genes were associated with the structurally distinct proteins that comprised the subunits of ribosomes and thereby implying an increase in ribosome numbers and/or ribosome turnover. No doubt associated with the increase in translation are allocation of genes to protein processing including vesicular transport and prefoldin complexes. Also present was a significant concentration of genes associated with proteolysis, including proteasome based ubiquitination.

Consistent with the increase in metabolic load were a considerable number of genes associated with oxidative phosphorylation and energy production in mitochondria including subunits for cytochrome-c oxidase, NADH dehydrogenase and lactate dehydrogenases; the latter associated with breakdown of increased levels of lactate in situations of respiratory stress (Brooks *et al.*, 1999). Indications of oxidative stress are evidenced by the presence of DNA repair processes including expression of transcriptional regulator and DNA damage-dependant nuclear protein poly(ADP-ribosyl)ation-14 (*Parp14*) (Ame *et al.*, 2004, Mehrotra *et al.*, 2011). Furthermore, pathway analysis using the Reactome database revealed the increase in expression of *Fam50a* (family with sequence similarity 50, member A), and sources of ubiquitin through *Uba52* (ubiquitin A-52 residue ribosomal protein fusion product) and *Rps27* (ribosomal protein S27), offer tentative evidence of involvement of the DNA damage-activated Fanconi anemia complex (Gurtan and D'Andrea, 2006).

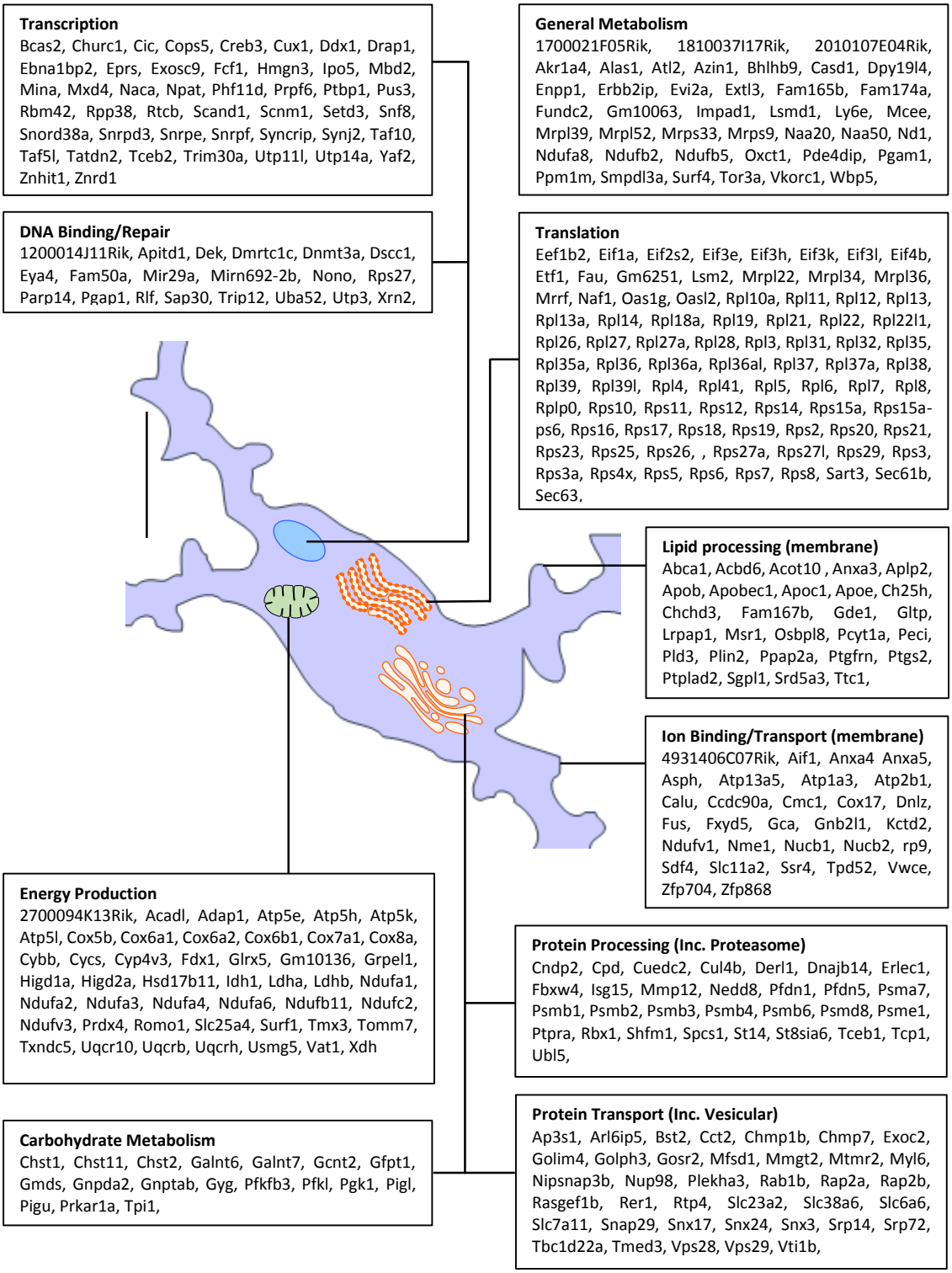

Figure 5-12: Genes of interest associated with metabolism and homeostasis. A considerable number of genes with an increase in expression are associated with protein translation and processing. The increased metabolic load is reflected in the increase in expression of genes associated with energy production.

The identified genes of interest association with a specific function out with metabolism/homeostasis were plotted onto a cellular map using ontology data obtained from the Ensembl Biomart database. This enabled the location of each gene to be determined and further organised by function (Figure 5-13). The overall expression profile from this set of genes is one of robust pro-inflammatory myeloid cell activation. The increased expression of lysosomal-associated membrane protein, ATPase proton pumps and numerous lysosomal enzymes including cathepsins, histocompatibility subunits and genes involved in membrane restructuring strongly support antigen presentation and a classic hallmark of classically activated innate immune cells. Surface markers CD48 CD86, CCL8, CXCL9, CXCL13, and TLR2 are all typically associated with a pro-inflammatory classical activation phenotype (Mantovani *et al.*, 2004, Martinez *et al.*, 2008, Elishmereni and Levi-Schaffer, 2011, Samuel and Kroner, 2011).

The expression of numerous pro-inflammatory cytokines and chemokines, including IL-1b and TNF-a, indicate active processing within the caspase-1 mediated inflammasome (Franchi *et al.*, 2009). Expression was also increased for caspase-4 (*Casp-4*); implicated as an 'inflammatory caspase' in regulating inflammasome function (Martinon and Tschopp, 2007, Sollberger *et al.*, 2012). Other pro-inflammatory genes found within this dataset, and reported to be neurotoxic, include matrix metalloproteinase 12 (*Mmp12)* (Bai *et al.*, 2014) and prostaglandin-endoperoxide synthase 2 (*Ptgs2*) (Minghetti, 2004). The latter is known to be expressed in prion disease (Walsh *et al.*, 2000, Kim *et al.*, 2007, Minghetti and Pocchiari, 2007) and a target of non-steroidal anti-inflammatory drugs (NSAIDs) used in clinical trials to treat neurodegenerative diseases by inhibiting prostaglandin synthesis (Vane, 1971).

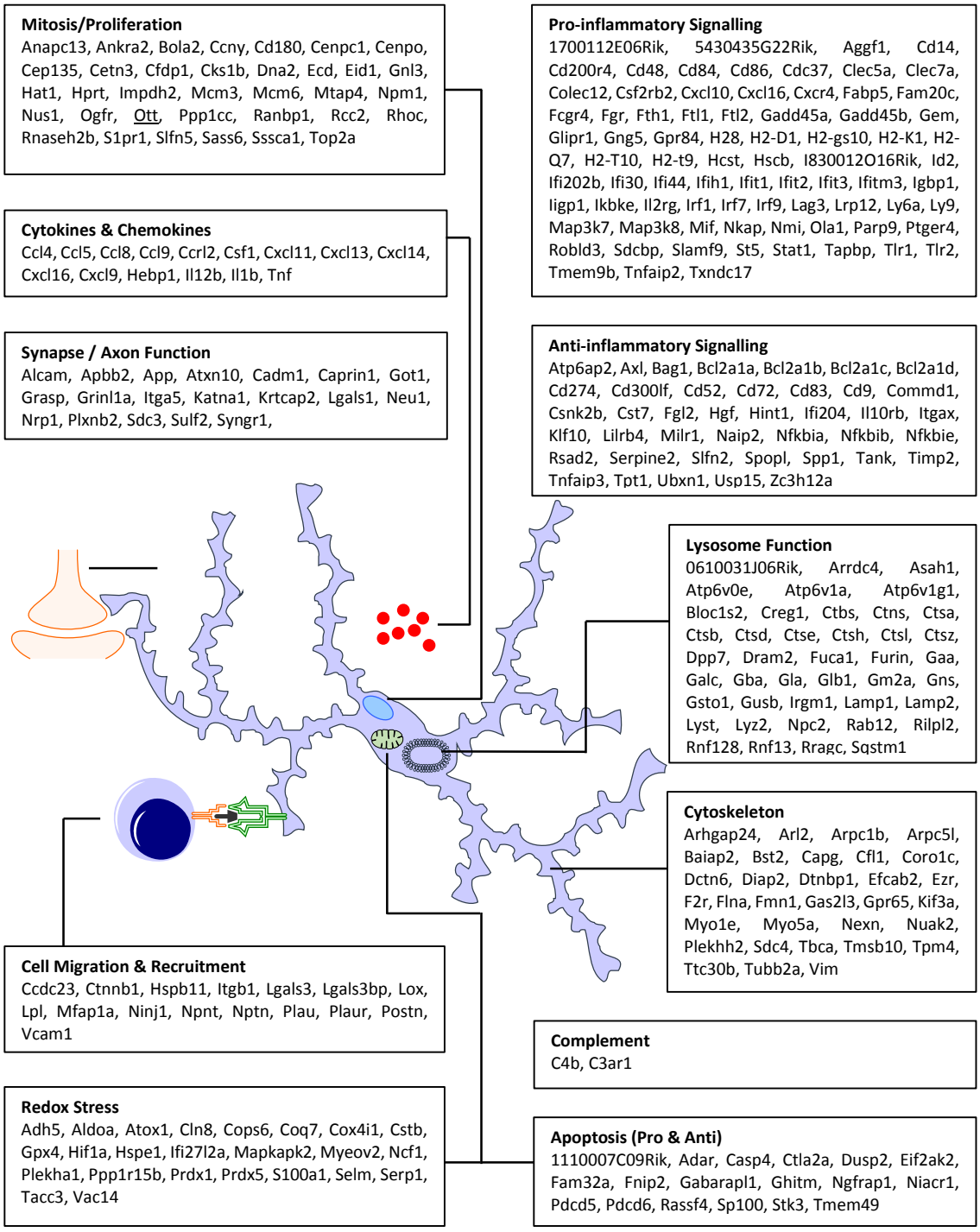

Figure 5-13: Genes of interest associated with immune activation and cell-to-cell signalling. Genes have been grouped by both function and cellular location. The signature is one of robust pro-inflammatory innate immune activation.

The increase in levels of *IL-1*, *Tnf-α* and *Csf1* strongly portray the microglia activation profile as pro-inflammatory and not one of atypical down-regulation or resolution of inflammation (Figure 5-14A). The presence of a significant increase in transcripts involved with proteasome activity and major-histocompatibility mediated antigen presentation combined with expression of CXCR3 ligand genes required for both direct interaction with and recruitment of INF-γ producing CD4+ T cells (Whiting *et al.*, 2004) offers a microglia activation state more akin to classically activated macrophages. Also of note, and crucial to the maintenance of a chronic response to inflammatory cytokines, was that expression of *Nfκb* remained stable despite an increase in expression of NFκB inhibitors *Nfκbia*, *Nfκbib*, *Nfκbie* that have been shown to inhibit formation of NFκB at the transcription stages (Sun *et al.*, 1993, Arenzana-Seisdedos *et al.*, 1995).

The marked presence of cytokines IL-1, TNF-a, but not IL-6, would suggest the response by microglia is lacking in the full spectrum of cytokines expected from a classical form of activation via the myeloid differentiation primary response 88 (MYD88)-dependant pathway (Akira and Takeda, 2004). Pathway analysis of this dataset within the Reactome database revealed many of the elements of the MYD88-independent pathway were represented by the differentially expressed genes within this study. This is supported by the lack of differential expression of Myd88 (Appendix 8-14).

Interestingly *Tgfb1* was not differentially expressed by microglia during the disease process (Figure 5-14B). The level of expression of *Tgfb1* was nominal throughout the disease process and to be expected from a constitutively expressed protein intricately involved in microglia homeostasis (Abutbul *et al.*, 2012). However expression of Smad anchor for receptor activation (*Sara*) is negligible indicating no translocation of SMAD proteins; core intracellular complexes of the TGFb1 signalling pathway (Heldin *et al.*, 1997, Tsukazaki *et al.*, 1998). Further indications to the lack of active TGFb1 signalling is demonstrated by negligible expression of suppressor-of-

cytokine-signalling 3, 4 and 5 (*Socs3-5*); implying no inhibition to the JAK/STAT signalling pathway mediated suppression of cytokine signalling (Shuai and Liu, 2003). Also of note was the lack of any discernible increase in expression of the TGF-b1 receptor with only the presence of *Usp15* known to act as the TGF-b1 receptor stabiliser (Inui *et al.*, 2011). As mentioned previously the lack of significant fold-change increase in expression of *Usp15* also indicates the lack of active TGF-B1 mediated signalling as a significant contributor to the disease response by microglia. Furthermore there were no transcripts associated with either MAPK and SMAD2/3 further downstream and directly associated with the TGF-B1 mediated signalling pathway (Abutbul *et al.*, 2012).

Microglia are known to interact with neurons (Tremblay *et al.*, 2010, Siskova and Tremblay, 2013) and numerous genes associated with axon elongation, synapse regulation and neurotransmitter release were observed to increase in expression. Interestingly this analysis partners the expression of these genes with microglia and adds them to the growing body of evidence for microglia involvement in neuron regulation (Vukovic *et al.*, 2012, Ji *et al.*, 2013, Miyamoto *et al.*, 2013, Schafer *et al.*, 2013, Sogn *et al.*, 2013).

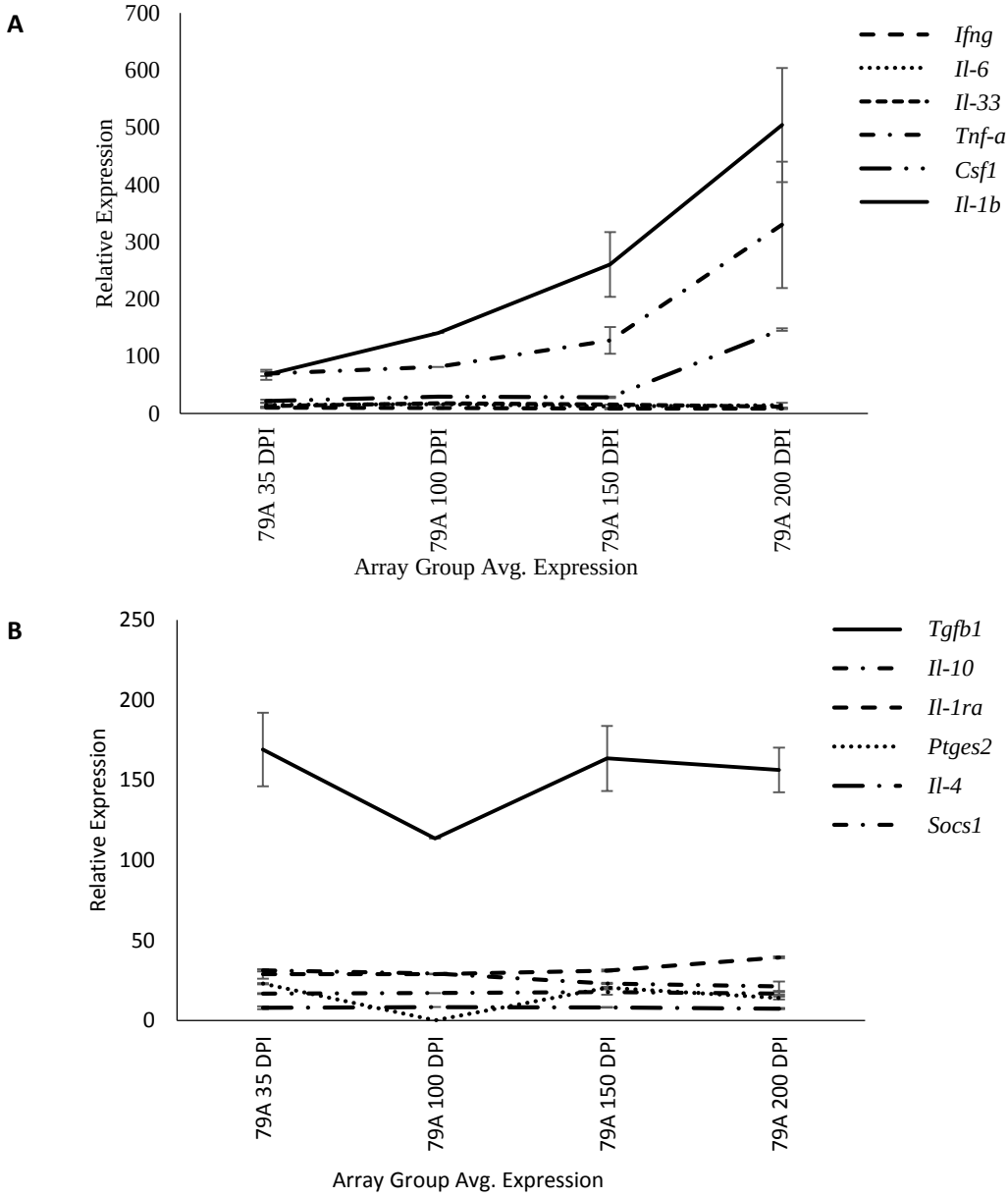

Figure 5-14: Expression of inflammatory cytokines and transcription factors associated with the regulation of activation phenotype of microglia. **A:** Strong increase in expression of *Tnf-a*, *Il-1b* and *Csf1*, but not cytokines associated with recruitment and escalation toward acquired immunity imply a robust but self-sufficient pro-inflammatory response by microglia in mouse-adapted prion disease. **B:** Nominal and unchanged expression of *Tgf-b1* is matched by a lack of expression of downstream transcripts mediated by *Tgf-b1* activity.

5.4 Discussion

5.4.1 Acquisition of the Microglia Transcriptome

The increase in expression of Il-1β is interesting as this goes against previous literature using murine prion disease in which expression of the mRNA is seen at levels no higher than uninfected control animals (Walsh *et al.*, 2001).

Isolating microglia from adult mice required extensive modification to the procedures published in the literature (Fleige *et al.*, 2001, Cardona *et al.*, 2006a, de Haas *et al.*, 2007, Nikodemova and Watters, 2012, Njie *et al.*, 2012). The accumulation of myelin within the brain suspension was not successfully removed by any of the unmodified protocols. The viscid nature of myelin resulted in contamination to the pure microglia suspended in the isolation solution and difficulty in processing the sample by FACS analysis. This was most likely due to the age of the mice at the time of recovery. The level of myelin lipid composition increases in rodent brain with age (Norton and Poduslo, 1973). The published methods utilised a discontinuous Percoll® gradient to allow microglia to collect within an interphase, and typically described microglia isolation from postnatal, weaned and young adult mice; not mice hundreds of days old. The volume of myelin encountered in in this analysis, from adult mice aged over 1 year, resulted in invariable myelin contamination to the target interphase. The yield of microglia within the interphase was also very low at $x10^4$ cells. The quantity and quality of total RNA isolated from this number of cells was insufficient; presumably a result of myelin-induced failure for microglia to separate during centrifugation. To address this the Percoll® discontinuous gradient was altered to allow all cells to pellet rather than collect in an interphase and combining the procedure with microglia-specific magnetic microbeads. This substituted the Percoll® gradient from a means to isolate microglia to one solely of myelin removal. Once perfected, the adopted procedure for isolation of microglial cells was highly consistent at $3x10^5$ cells per brain.

The quantity of total RNA yielded from isolated microglia extracted from experimental animals was minimal. Quality control checks revealed numerous samples to be degraded. This necessitated rejection of half of the samples with the consequence that the tested population was much reduced in size with only two arrays per group. Gender matching of experimental mice within the groups was also no longer possible, although gender difference did not appear to impact on disease-associated gene expression and did not present with further downstream complications. The RNA required amplification in order to generate sufficient cDNA. Amplification of RNA can induce a small level of bias following truncation of the 5' transcript end by successive application rounds (Brooks *et al.*, 1995, Baugh *et al.*, 2001, McClintick *et al.*, 2003). Bias was mitigated by utilising an amplification kit that incorporated random primers with the oligo-deoxythymine primers during initial strand synthesis. The chosen amplification kit was also specifically designed for small and degraded RNA samples. Random primers anneal throughout the sequence thereby mitigating premature termination at the 5' end of longer mRNA sequences (Feinberg and Vogelstein, 1983, Stangegaard *et al.*, 2006).

The loss of experimental RNA samples and the use of two arrays per time point limited the ability to perform statistical analysis beyond determining simple fold change in expression. The less the number of arrays within a tested population, the greater the requirement for homogeneity between arrays to overcome variance. Consequently it would not have been possible to determine, if conflicting results were yielded, which array was displaying the correct expression profile. Many experiments using limited numbers of arrays have yielded convincing and publishable results. These studies overcame the lack of sample repetition by either using a significance analysis of microarrays (SAM) approach in which a constant was applied to the dataset from which reference was then made for each gene in turn (Tusher *et al.*, 2001), or by using an empirical Bayesian approach to determine the distribution

variance from the data itself (Baldi and Long, 2001). The SAM approach has seen use with microarray studies of prion disease (Xiang *et al.*, 2004, Kim *et al.*, 2008).

The use of the cluster based approach described here does present with limitations as the method is fully reliant on high correlation between arrays. The overall signal correlation between arrays in this analysis was high as evidence by the overall low variance between the arrays and consequently the expression profile is one of a convincing disease signature. Some notable examples of transcripts that were not incorporated into the clustering processes including *Tnf-a*. Due to the variance in the increase of expression between the two 200 dpi arrays, the gene was not clustered within the set correlation threshold of BioLayout *Express*^{3D}. Indeed, the expression profile was entirety unique to *Tnf-a* and consequently the gene was not incorporated into any clusters by MCL. Despite this, the large increase in expression of *Tnf-a* in response to disease was confirmed by both arrays and therefore the gene was considered disease-associated. This also served to highlight the importance of familiarity with the entire dataset at the individual gene level.

5.4.2 Inflammatory profile

The inflammatory phenotype typically associated with *in-vivo* prion disease has been shown to be remarkably anti-inflammatory (Walsh *et al.*, 2001, Baker and Manuelidis, 2003). The growth factor TFG-B1 has been shown to be the dominant anti-inflammatory cytokine present in murine prion disease models (Cunningham *et al.*, 2002). Via the TGF-B1 signalling pathway, the cytokine plays a key role in limiting microglia activation (Lodge and Sriram, 1996) and is evident throughout the disease process (Boche *et al.*, 2006, Abutbul *et al.*, 2012) providing microglia with a phenotype concurrent with the resolution of inflammation and wound healing (Fadok *et al.*, 1998). The lack of differential expression of *Tgf-b1* within this dataset was therefore marked in its absence. The cytokine is also required for the correct function of, and is itself unable to pass, the blood brain barrier (Kastin *et al.*, 2003, Dohgu *et al.*, 2004, Garcia *et al.*, 2004). This study therefore suggests that the increased

expression of TGF-B1 noted in other studies is not microglial in origin but is expressed by another group of cells from within the CNS. Alternatively it is possible that the peripheral route adopted in this analysis resulted in a markedly different, and more pro-inflammatory phenotype to that seen when using an intracerebral route.

Microglia are sensitive to inflammatory signals passed across the blood brain barrier into the central nervous system (Dantzer, 2004, Lemstra *et al.*, 2007, Quan and Banks, 2007). A peripheral inflammatory signal has been observed in prion disease following a peripheral route of infection (Newsom *et al.*, 2011), but not following an intracerebral route (Cunningham *et al.*, 2005a). It would also appear that following infection, pre-activated T-cells are found to populate the CNS (Lewicki *et al.*, 2003, Iken *et al.*, 2011) suggesting activation of these cells takes place in the periphery before cross over into the CNS. Furthermore the timing and type of activation in the multicellular environment of the central nervous system has a marked influence on the overall neurotrophic or neurotoxic phenotype of the microglia response (Gomez-Nicola *et al.*, 2013). Consequently the choice of a peripheral route, complete with the obligatory peripheral pathogenesis stages, different timing and type of response by microglia could result in a markedly different inflammatory phenotype.

The presence of CXCR3 ligands, in addition to acting as chemo-attractants for activated $CD4^+$ and $CD8^+$ T-cells (Campanella *et al.*, 2008) are implicated with the interferon response as part of a multi-cellular response within the brain parenchyma (Klein *et al.*, 2005). The presence of T-cells in the brains of mice infected with murine prion disease is well known, although it is not clear how full functionality is maintained without the presence of INF-γ (Lewicki *et al.*, 2003). The presence of increased expression for *Cd274*, which encodes for a membrane bound H7-protein receptor, is intriguing as has been implemented in co-stimulation of acquired immune cells. The receptor is required for successfully myeloid cell interaction with activated T cells during antigen presentation (Linsley and Ledbetter, 1993). Within macrophages, CD274 is inducible, enhances expression of IL-10 in the host cell and

plays a key role in inhibiting $CD4^+$ T-cell activation (Loke and Allison, 2003). CD274 is also a required IL-2 dependant cofactor for IL10 production (Tamura *et al.*, 2001). Despite this, and as per *Tgfb1*, expression of the *Il1r* receptor was increased but not *Il10*. The lack of evidence for T-cell co-stimulation, combined with no presence of anti-inflammatory cytokine transcripts, including *Il-4* and *Il-10*, implies the chronic maintenance of a classical activation phenotype (Varin and Gordon, 2009).

The lack of differential expression of myeloid differentiation primary response 88 (*Myd88)*, *I-6* and the presence of many IFN-inducible genes within this dataset supports transcriptional regulation of cytokine cascades within microglia to be via the Myd88-independent pathway (Akira and Takeda, 2004). As a key adaptor protein in the Toll-like and IL-1 family of receptors, the protein MYD-88 is rapidly expressed in myeloid cells in response to antigen and leads to NFκB mediated changes to transcription (Kawai *et al.*, 1999). Where the expression of the protein form of MYD88 is lacking, the response to antigen is delayed and activation of NFκB is via IFN-inducible genes (Hoebe *et al.*, 2003, Yamamoto *et al.*, 2003). The resultant cytokine profile of Myd88-independent activation is also marked by the absence of IL-6 (Adachi *et al.*, 1998). The targeted removal of Myd88 does not interfere with prion disease pathogenesis (Prinz *et al.*, 2003) indicating the innate immune response is not dependent upon the MYD88-dependant pathway. Experimental evidence using mouse-adapted prion diseases has also uncovered the protective effects of innate interferon regulatory factors via toll like receptors and the Myd88-independent pathway (Spinner *et al.*, 2008, Ishibashi *et al.*, 2012). The results in this analysis further confirm the importance of interferon response genes in prion disease and builds upon the results of the multi-cellular analysis of chapter 2 in which an entire cluster of interferon response genes was observed. Therefore the possibility of transcriptional regulation via the MYD8-independent pathway is a core component of the microglia response to prion disease and offers a convincing explanation for the unique and self-sufficient pro-inflammatory response by microglia.

The strong translational signal, as evidenced by increased expression of genes encoding ribosomal subunits, supported an increased level of activity within microglia. As neither mRNA nor ribosomes have a particular long half-life within the eukaryotic cytosol, the cell must continually produce ribosomes to function correctly (Retz and Steele, 1980, Warner, 1999, Tourrière *et al.*, 2002). There is also a close association between mRNA stability and ribosomal density implying an increase in ribosome density is beneficial to the cell when increased burdens on translation are imposed (Dana and Tuller, 2012, Edri and Tuller, 2014). Consequently the increased level of expression of genes associated with translation was to be expected within activated microglia.

5.4.3 Cytoskeletal Modification: Migration or Sampling?

There is considerable debate on whether the observable regional increase in microglia in chronic disease is due to mitosis, migration or influx of differentiated peripheral monocytes. The use of parabiosis has demonstrated a limited role for monocyte influx during acute injury (Mildner *et al.*, 2007, Ajami *et al.*, 2011), yet the impact of a peripheral inflammatory response as part of the overall pathology has not been fully explored. Just as the peripheral priming of T-cells has been demonstrated as a requirement for their entry into the CNS (Lewicki *et al.*, 2003), peripheral activation of monocytes would equally facilitate the contribution of monocytes to the resident microglia population. By incorporating a peripheral route of infection in this study, the mechanisms for cell migration including adhesion adherence, chemokine release and matrix restructuring are intriguing as all would support both resident migration and peripheral influx.

The increase in expression of genes involved with actin binding and restructuring imply microglia are undertaking changes in morphology. Resting microglia are known to use protrusions to continuously sample the immediate surroundings (Nimmerjahn *et al.*, 2005) and actively make and break physical contact with neighbouring cells (Tremblay *et al.*, 2010). The protrusions are guided by extracellular adenosine

triphosphate and adenosine diphosphate acting as chemokinetic ligands to purinergic receptors (Sasaki *et al.*, 2003, Franke *et al.*, 2007). In the perturbed environment of a neurodegenerative disease it is conceivable that an increasing extracellular gradient of chemoattractants would explain the heightened mRNA expression for process motility. Furthermore microglia recruitment in prion disease is aided by C-C chemokine receptor ligation and the increase in expression of the rectors was noted in this analysis (Marella and Chabry, 2004, Marella *et al.*, 2005).

Table 5-6: Comparison between the identified disease-associated differential expressed gene lists of this analysis and that of Chapter 2. A total of 93 genes were found to be shared. These were highly enriched for functions relating to response by the innate immune system.

Shared Genes Between the Two Analyses	GO Enrichment
Aif1, Anxa3, Anxa4, Arpc1b, Axl, Bcl2a1a, C3ar1, C4b, Capg, Ccl5, Ccl8, Ccl9, Cd14, Cd48, Cd52, Cd72, Cd84, Cd86, Ch25h, Clec7a, Csf1, Cst7, Cstb, Ctsa, Ctsb, Ctsd, Ctsh, Ctsl, Ctsz, Cxcl10, Cxcl13, Cxcl16, Cybb, Fcgr4, Ftl1, Ftl2, Fuca1, Fxyd5, Galnt6, Glipr1, Gns, Gpr65, Gpr84, Gusb, H2-K1, H2-Q7, Ifi204, Ifi27l2a, Ifi30, Ifi44, Ifih1, Ifit1, Ifit2, Ifit3, Ifitm3, Iigp1, Il10rb, Irf7, Irf9, Irgm1, Itgax, Lag3, Lamp2, Lgals3bp, Lilrb4, Ly9, Mmp12, Naip2, Ncf1, Oas1g, Oasl2, Parp14, Parp9, Plxnb2, Psme1, Ptplad2, Rpl37a, Rsad2, Rtp4, Sgpl1, Slamf9, Slfn2, Spp1, Stat1, Sulf2, Tapbp, Timp2, Tlr1, Tlr2, Tnfaip2, Tor3a, Trim30	Innate Immune Response: $P = 4.54 \times 10^{-24}$ Response to stress: $P = 7..5 \times 10^{-13}$ Chemokine receptor binding: $P = 7.96 \times 10^{-10}$ Lysosome: $P = 2.83 \times 10^{-9}$ Response to type I interferon: $P = 7.46 \times 10^{-7}$

5.4.4 Comparison with the Re-analysis described in Chapter 2

In chapter 2, microglia dominated the expression profile acquired from a multi-cellular source. In this analysis isolated microglia present with a highly pro-inflammatory activation phenotype. Comparison of the gene list from this analysis with the genes considered myeloid in origin from the analysis in chapter 2 revealed 29.2% of the genes were shared. These genes were highly enriched for the innate immune response (Table 5-6). It is important to point out here that the two analyses were not directly comparable. The analysis in Chapter 2 was performed on data obtained from mouse experiments using an intracerebral route and whole brain total RNA and therefore differs from the peripheral route and single cell source of total

RNA used here. The use of a single cell RNA source, combined with a consistent yield of isolated microglia from each time point, resulted in the known concentration of cDNA per cell that was hybridised to the microarray. This is not possible using a whole brain isolate where the number of cells is not known and neither is the proportion of microglia contributing to the overall signal. Consequently the relatively low level of gene overlap is not surprising. Where the two studies complement each other is in the overall conclusion. Both analysis's reveal a robust chronic inflammatory response confirming the importance of microglia to the disease process.

5.4.5 Conclusion

The relatively low number of microarrays utilised in this study identified a considerable number of differentially expressed genes associated with the microglia response to prion disease. Additional microarrays would no doubt have increased accuracy of both the number of identified genes and the difference in expression. Yet the results offer a convincing signature of myeloid activation that matches the morphological timing of microglia activation seen in previous chapters. Microglia in this analysis were shown to express a disease signature markedly more pro-inflammatory than that currently portrayed in the literature for prion disease. Within other protein-misfolding diseases, notably Alzheimer's; microglia are observed as expressing a repertoire of pro-inflammatory cytokines including TNF-α (Bhaskar *et al.*, 2014), IL-1β and IL-6 (Griffin *et al.*, 1995, Tarkowski *et al.*, 1999). The potential of generating a neurotoxic microenvironment from expression of the genes within this inflammatory signature is high. Despite this, the presence of genes normally shown to be associated with neuronal synapses, but shown here to be expressed by microglia, suggests ongoing intercellular interaction with other cell types residing within the brain.

The isolation of microglia from prion infected mice has been limited to one laboratory and was not performed to demonstrate the in-vivo expression profile per se but to confirm the high level of infectivity maintained by an isolated cell population that

harbour negligible amounts of misfolded protein (Baker and Manuelidis, 2003). As such, the microglia were rested in cell culture media for16- to 18-h post isolation to facilitate downstream transmission infection studies. Consequently the transcriptome of incubated microglia would not be comparable to the transcriptome acquired immediately after isolation and the study focused on the gene expression differences between uninfected and infected microglia with respect to harbouring the disease. This has not stopped the study being referred to repeatedly as confirmation of a unique down-regulated activation phenotype of microglia in prion disease, despite no evidence confirming the source of anti-inflammatory immunomodulators in whole brain studies, including TGF-B1 (Cunningham *et al.*, 2002, Boche *et al.*, 2006), are indeed attributed to microglia. Isolated microglia and astrocytes from murine models of Alzheimer's Disease as part of an extensive study by (Orre *et al.*, 2014) also yielded a marked increase in pro-inflammatory markers, yet this was also concurrent with a reduction in neuronal synapse endocytosis support. The disadvantages of expensive genetic modification required to initiate murine Alzheimer's Disease models were highlighted in a lack of microglia expression overlap between the murine dataset and a post death acquired human Alzheimer's Disease dataset. The same was not true of the differentially expressed immune genes found within the astrocyte dataset. Astrocytes are able to express and act as immune cells in their own right and are known to phagocytise dead and dying neurons (Tashiro *et al.*, 1998, Schultz *et al.*, 2004, Chung *et al.*, 2013) and are also implicated in neuronal toxicity via expressed nitric oxide and inducible nitric oxide synthase (Bal-Price and Brown, 2001). It was for this reason that a microglia isolation approach was adopted in this present study and a degree of caution should be applied where attribution of innate immune gene expression to microglia has been assumed in studies adopting a whole brain transcriptome analysis.

A study by (Godbout *et al.*, 2005) using microarray analysis of adult and aged BALB/cJ mouse brain noted the activation of the peripheral immune system by administration of LPS resulted in activation of an innate immunological response within the central

nervous system. This was characterised by compliment and classical pro-inflammatory markers including IL-1, IL-6 and antigen presentation MHC complexes and was greatly inflated in aged mice. This heightened classical innate immune activation was also noted in numerous other sickness behaviour studies utilising LPS to initiate a response (van Dam *et al.*, 1992, Combrinck *et al.*, 2002, Dantzer, 2004). The lack of expression of *Inf-γ*, *Il-6* and *Il-33* by microglia, all well-defined classical pro-inflammatory cytokines in this present study suggests that the pro-inflammatory response is unique to this model of prion disease and is not a classical stereotypic LPS type response and is furthermore self-sufficient and maintained by resident microglia alone (Romano *et al.*, 1997, Schmitz *et al.*, 2005, Kakkar *et al.*, 2012).

6 Discussion

Interest in the other cells that accompany neurons within the central nervous system has rapidly increased, indicating a shift from the neuro-centric focus which once dominated research into neurodegenerative diseases. Indeed, at the 2011 Society of Neuroscience annual conference, held in Washington, USA, the term 'microglia' was searched on the society's conference website with such frequency that it made number 6 in the list of top 10 searches made Hughes (2012). The aim of the present study was set up to investigate the role of activation of microglia in chronic neurodegenerative disease. Models of mouse-adapted prion disease were chosen as the basis for studying microglia as they demonstrate robust neuronal loss invariably leading to fatality, accumulation of misfolded protein and crucially, activation of glial cells.

6.1 Determining Microglia Contribution in the Multicellular Environment of Prion Disease

Endogenous PrP^C is associated with cellular membrane bound lipid rafts (Naslavsky *et al.*, 1997, Agostini *et al.*, 2013) and is recycled every few minutes from the cell surface via pinocytic clathrin-coated pits, and then back to the surface within recycling endosomes (Mironov *et al.*, 2003, Sunyach *et al.*, 2003). The accumulation of misfolded PrP protein in neuronal membranes has been blamed for dysfunction of neurotransmitter receptors (Kristensson *et al.*, 1993, Diez *et al.*, 1997) and the protease resistance of the misfolded form has been implicated in mitigating the accumulation of misfolded PrP in lysosomes following membrane recycling (Caughey *et al.*, 1991, Bouzamondo-Bernstein *et al.*, 2004). Furthermore the N-terminal truncation of PrP is strongly associated with lysosomal proteases (Caughey *et al.*, 1991, Dron *et al.*, 2010) with the consequence that the presence of cholesterol biosynthesis genes, glycosylation pathways, endosomal/lysosomal pathways and lysosomal catharsis have all been associated with neurons in many transcriptome studies of prion disease (Brown *et al.*, 2004, Xiang *et al.*, 2004, Brown *et al.*, 2005,

Skinner *et al.*, 2006, Xiang *et al.*, 2007, Guillerme-Bosselut *et al.*, 2009). However, the presence of genes linked with endosome/lysosome trafficking and proteases are also associated with protein degradation by phagocytic immune cells. This study initially made use of a comprehensive microarray dataset of prion disease in mice, made available in the public domain, with which to determine the contribution of microglia and confirm the origin of many of these pathways.

The dataset was analysed using BioLayout *Express*^{3D}; a novel software tool that supports the visualisation and clustering of correlation networks. The dominant signal of differentially expressed genes was found to be associated with innate immunity. By utilising an original approach of co-normalising cell-specific datasets from a variety of different brain cell types and macrophage activation profiles it was determined that the immune signal was overwhelmingly myeloid in origin and not just a component of the overall response suggested by other microarray studies of the disease (Brown *et al.*, 2003, Booth *et al.*, 2004, Riemer *et al.*, 2004, Xiang *et al.*, 2004, Brown *et al.*, 2005, Skinner *et al.*, 2006, Xiang *et al.*, 2007, Moody *et al.*, 2009). Indeed only 8.5% of the identified genes were found to be exclusively expressed by other brain cell types including a mere 4 genes specifically identified as neuronal in origin. The very high correlation seen between nodes within BioLayout *Express*^{3D} generated clusters further suggested the genes of interest were highly related to one another. A predominantly single cell type origin would offer an explanation for this. This study therefore implies a degree of caution should be applied to the interpretation of published multicellular studies in which an assumption of cellular origin, particularly toward neurons, has been made for a given gene without evidence to validate that claim.

6.2 Characterising the Morphological Response of Microglia Activation

To further investigate the strong microglia response an *in-vivo* model of prion disease was instigated. The microglia in this mouse model expressed EGFP under control of the *Cfms* operon. Consequently all cells of myeloid origin expressed EGFP and the

confirmation that these mice were suitable for infection by mouse-adapted prion disease was described in chapter 3. The quantification of the EGFP expressing microglia in chapter 4 confirmed activation was strong in areas of misfolded protein during the later stages of the disease. Still-ramified microglia were shown to accumulate in areas of initial misfolded protein deposition within the medulla. This suggested an independence of the initial motile response of microglia from the full morphological activation observed at later stages of the disease. Although further evidence would be required to fully quantify this motile response, the confocal generated fluorescent images were very clear in qualitatively visualizing ramified microglia in these regions. It has been noted in prion disease that the timing and type of activation in the multicellular environment of the central nervous system has a marked influence on the overall neurotrophic or neurotoxic phenotype of the microglia response (Gomez-Nicola *et al.*, 2013). Therefore if the initial and later response of microglia to misfolded protein are independent then it opens up many opportunities to alter the early and late behaviour of microglia and influence their activation at different stages of disease, with the aim of achieving a neurotrophic phenotype.

6.3 The Transcriptomic Analysis of Microglia Activation in Prion Disease

The overall consensus for the profile of activated microglial phenotype in protein misfolding diseases including Alzheimer's, Parkinson's and prion disease is one of a down-regulated anti-inflammatory phenotype dominated by the differential expression of TGF-β (Fadok *et al.*, 1998, Baker *et al.*, 1999, Walsh *et al.*, 2001, Cunningham *et al.*, 2002, Perry *et al.*, 2002, Baker and Manuelidis, 2003). The data presented in Chapter 5, in which the transcriptome of isolated microglia was investigated during prion disease suggest a considerably more pro-inflammatory phenotype. The recent study performed by Gomez-Nicola *et al.* (2013), in which an artificial switch to a pro-inflammatory microglia phenotype delayed disease progression, would imply that such a phenotype confers a degree of neuroprotection. The reason behind the clear difference in the overall phenotype seen in previous

studies to the data presented here is unclear. The lack of inflammation within the control mice, run in parallel to the infected mice, rules out an artefact of isolation as a cause. The obvious difference is route of infection. The deliberate use of a peripheral route in this study was to ensure that microglia would respond to initial infection entering into the CNS environment. Certainly the longer incubation period witnessed in peripheral routes, and the longer incubation period observed by Gomez-Nicola *et al.* (2013) following a switch from an anti to a pro-inflammatory phenotype using an intracerebral route is intriguing.

Despite an overwhelming microglia-centric interpretation, the results of chapters 2 and 5 cannot completely rule out the contribution of neurons in the disease process. This is due to the limitations of determining cellular origin from a whole brain study. The use of overlaid single-cell type datasets was heavily reliant on homogeneity between what are effectively independent populations of arrays. The results in chapter 5 were microglia cell centric and as such do not supply data on the other cells found in the brain. The results do however strongly confirm the independence of microglia from misfolded prion protein processing. The expression levels of *Prnp* in the dataset analysed in Chapter 5 remained negligible and unchanged throughout the length of the experiment both in infected and control animals. Microglia are known to harbour negligible quantities of PrP protein in both endogenous and misfolded isoforms (Baker *et al.*, 2002, Ford *et al.*, 2002). Therefore it is unlikely that the observed differential expression of genes associated with membrane trafficking and protein degradation are associated with intracellular prion protein processing by microglia. Furthermore microglia are known to inefficiently phagocytise extracellular misfolded protein in numerous neurodegenerative diseases *in-vivo* (Stalder *et al.*, 1999, Tahara *et al.*, 2006, Bolmont *et al.*, 2008, Hughes *et al.*, 2010). This study therefore implies it is unlikely that the presence of transcripts for membrane trafficking and protein degradation are involved with the processing of extracellular misfolded protein, and shifts the focus considerably towards an immunological related function within microglia.

6.4 The Response of Microglia to Disruption in the Central Nervous System: Cause or Consequence?

The correlation of microglial morphology with the immunophenotype imparted by the cytokine and receptor repertoire imparts microglia with the ability to function in a highly specialised, yet plastic, manner unique to the localised microenvironment at that time plasticity (Streit *et al.*, 1988, Perry *et al.*, 2010). Consequently is not sufficient to draw a conclusion on microglial function by describing the morphology and testing for the presence of a few selected immune-related receptors or cytokines. This study adopted a transcriptomic approach in combination with quantifying morphology and was thereby able to identify numerous key genes and pathways key to determining the role of these cells within the prion diseased brain.

At 200 dpi microglia in the 79A/BALB$^{Fms\text{-}EGFP/-}$ show all the hallmarks of morphological activation with shortened processes and engorged soma. A microglial response was also seen at 150dpi in the medulla however this was restricted to accumulation and these cells did not present with significant morphological changes. The time points chosen in this study do not allow for determination of whether microglia are responding prior or after parenchymal perturbation or misfolded protein but these data do strongly suggest that morphological changes and initial motile response are separate. The accumulation of still ramified microglia into the medulla at 150 dpi should not therefore be dismissed as a lack of function as clearly the act of motility would imply the cells are responding to a chemotactic gradient. Previous studies have highlighted the dominance of an immune related signal in specific brain regions. A study by Riemer *et al.* (2004) adopted a peripheral route infecting C57bl6 mice with 139A and performed microarray analysis on isolated cortex, medulla and Pons as a time course study at 100, 125, 150 and terminal stage. A dominant innate immune signal was observed throughout the tested regions with greater expression fold change noted in the medulla and coinciding with the presence of disease-associated vacuolation in this region. Others have isolated the hippocampus to allow for

quantifying neuronal loss in the pyramidal layers evident with this region and noted the increase in immune related genes to coincide with substantial neuronal loss at (Brown *et al.*, 2004, Brown *et al.*, 2005).

Microglia are known to interact with neurons in both the healthy brain and migrate to areas of injury (Nimmerjahn *et al.*, 2005, Tremblay *et al.*, 2010, Chen *et al.*, 2014). The involvement of localised inflammation in triggering and facilitating axonal regeneration has been thoroughly documented (Lu and Richardson, 1991). More recent work has determined that microglial accumulation is not just an influx made as part of an innate immunologic response, but strongly supports the hypothesis that microglia are intrinsic to axonal processing. Elegant in-vivo models utilising a peripheral nerve graft within the thalamus documented the accumulation of ramified, or at most partially activated, microglia at the site of active axonal regeneration with close contact documented between grafted neurons and microglia (Shokouhi *et al.*, 2010).

A strong gene expression signal was seen at 200dpi and a less strong signal at 150. The expression of cytokines is very pro-inflammatory but there is no differential expression of IL-6 or components of the MYD88 pathway that are typically associated with a classically activated phenotype. These data therefore suggest an activation profile that is specific to prion disease. If it most likely this is unique to the *in-vivo* environment as co-cultures of microglia and neurons in the presence of $PrP^{106-126}$ induces a stereotypic response with CD14 mediated detection of damaged neurons and increased expression of IL-6 (Bate *et al.*, 2005), and matching the stereotypic neurotoxic response observed in co-cultures of neurons in the presence of LPS activated microglia (Chao *et al.*, 1992). These data presented in this study therefore conclude that microglia are responding in a prion specific manner but further analysis of the model would be required to determine if microglia response is a cause or consequence of the developing pathology and if the timing of activation coincides with neuronal loss.

6.5 Microglia Activation Phenotype

Overall this study demonstrates that microglia present with a transcriptomic phenotype considerably more pro-inflammatory than the 'down-regulated' phenotype prevalent in the literature, predominately described by one laboratory using a very specific stereotactic intracerebral inoculation; where the immune response has been described as comprising low levels of pro-inflammatory cytokines with elevated TGF-B1 (Fadok *et al.*, 1998, Baker *et al.*, 1999, Walsh *et al.*, 2001, Cunningham *et al.*, 2002, Perry *et al.*, 2002, Baker and Manuelidis, 2003, Siskova *et al.*, 2009, Stanton *et al.*, 2009, Hughes *et al.*, 2010). The lack of differential expression of TGF-B1 within the microglial isolation dataset is therefore marked in its absence. The lack of matrix metalloproteinase MMP3, required for TGF-B1 release, provides further evidence the cytokine is not produced in microglia. The cytokine is also required for the correct function of, and is itself unable to pass, the blood brain barrier (Kastin *et al.*, 2003, Dohgu *et al.*, 2004, Garcia *et al.*, 2004) ruling out any contribution from the periphery towards increased levels of the cytokine in the parenchyma. Elements of the TGF-B1 pathway were noted in the whole brain re-analysis. This study therefore concludes that the increase in level of TGF-β1 is not microglial in origin and if the level of the cytokine does increase it must be expressed by another group of cells from within the CNS. Also of note was the lack of any discernible increase in expression of the TGF-B1 receptor with only the presence of Usp15 known to act as the receptor stabiliser (Inui et al., 2011). Furthermore there were no transcripts associated with either MAPK and SMAD2/3 further downstream and directly associated with the TGF-β1 mediated signalling pathway (Abutbul et al., 2012).

6.6 Improvements to this Study

In chapters 3 and 4 it was suggested that microglia migrate to areas of misfolded protein by 150 dpi (65% of the incubation period) before undergoing morphological

changes indicative of activation. Although genes associated with cellular migration were found at 150 dpi the fold change was not considerable. This could be an artefact of signal dilution as comparatively fewer cells were observed to migrate than were fully activated by 200 dpi. To address this an increase in the sample population is suggested and could be met by either repeating the experiment with a larger number of arrays or by isolating microglia in specific regions. The latter would also serve to increase the sample population by virtue of increasing the number of target microglia per array. Regional analysis would also further the research into the role of microglia. Recent research has shown that microglia activation is highly plastic and the resultant phenotype is dependent upon the specific insult perceived by microglia in a given area (Perry *et al.*, 2010, Hanisch, 2013, Hanisch and Gertig, 2014). Microglia in different regions of the brain also demonstrate phenotypic differences (Sasaki and Nakazato, 1992, Ong *et al.*, 1995, Torres-Platas *et al.*, 2014), an effect exaggerated during healthy aging (Sheffield and Berman, 1998, Kullberg *et al.*, 2001). The data presented in this study offers a global view and the overriding similarity in co-expression shown using clustering in BioLayout *Express*^{3D} would suggest that activated microglia in the brain act in a homogenous population. It is possible however that the differential expression of activated cells masks that of cells that are not morphologically activated or responding with such vigour. Therefore a hypothesis can be generated that microglia in differing regions might generate a different activation phenotype in response to the same stimuli. This would offer an explanation for the apparent regional targeting of microglia activation observed in many neurodegenerative diseases (Williams *et al.*, 1994, McGeer *et al.*, 2003, Brink *et al.*, 2005).

The possibility of capturing the differences between the response of microglia could be further extended through the use of single cell capture techniques, a technique that has successfully been used on both glia and neurons (Majer *et al.*, 2012, Parakalan *et al.*, 2012). The power of these techniques has been advanced further with the possibility of obtaining transcriptomic data from extremely small RNA yields,

down to that isolated from a single cell (Tang *et al.*, 2010, Shalek *et al.*, 2013, Picelli *et al.*, 2014). Evidence would suggest that microglia interaction with neurons in the healthy brain is related to modulation of synaptic dendrites through phagocytosis (Tremblay *et al.*, 2010, Tremblay and Majewska, 2011, Siskova and Tremblay, 2013). The use of techniques to investigate cellular interaction at a microenvironment level could be implemented to capture the transcriptome of individual cells interacting as part of a multi-partite synapse, or clustered around a specific plaque of misfiled protein. This might elude to the specific mechanisms that result in the breakdown of homeostasis within the brain which are proposed to be key to the multicellular hypothesis governing neuronal loss observed in neurodegenerative diseases.

6.7 Future Work

To investigate into the cause or consequence events of microglial activation with the 79A/BALB$^{Fms\text{-}EGFP/-}$ model with regard to neuronal interaction would require ensuring the migration of microglia and their subsequent activity towards full activation are captured in a location where neuronal populations can either be counted or specific evidence for harm documented. These data presented here would support a focus on the medulla where microglia and expressed markers of activation phenotype can both be easily visualised using immunohistochemistry, in addition to viable isolated at a regional level to determine specific function. An additional time point taken between 150 dpi and 200 dpi should be sufficient to document the changes in activation phenotype following influx into the medulla and toward areas of perturbation as hallmarked by the presence of PrP deposition at 150 dpi. The focus should however be on neuronal interaction and not whether microglia were reacting prior or following PrP deposition.

Not documented in this study, were two further experiments run in parallel to those described in chapter 6. The first involved isolating total brain RNA from half brains taken from the same mice as used in the experiments of chapter 4. The second involved isolating total RNA and half brain fixed-tissue from mice as part of an aging

time course. Uniquely the starting age of the mice in these experiments was the same, thereby allowing the parallels between healthy aging and neurodegenerative disease to be determined. There was not sufficient time to analysis the total brain RNA or aging experiment. Tissue and samples were frozen and it would be hoped are exploited in the near future. A comparison of the transcriptomes of isolated microglia with that of whole brain would aid in determining the specific contribution made by microglia in the host immune response by eliminating the immunomodulators present in the diseased brain but expressed independently of microglia. It is important to note that microglia are not the only source of immunomodulators. Astrocytes, as the most numerous glial cell, are also able to express many 'classical' markers of activation (Tashiro *et al.*, 1998, Schultz *et al.*, 2004).

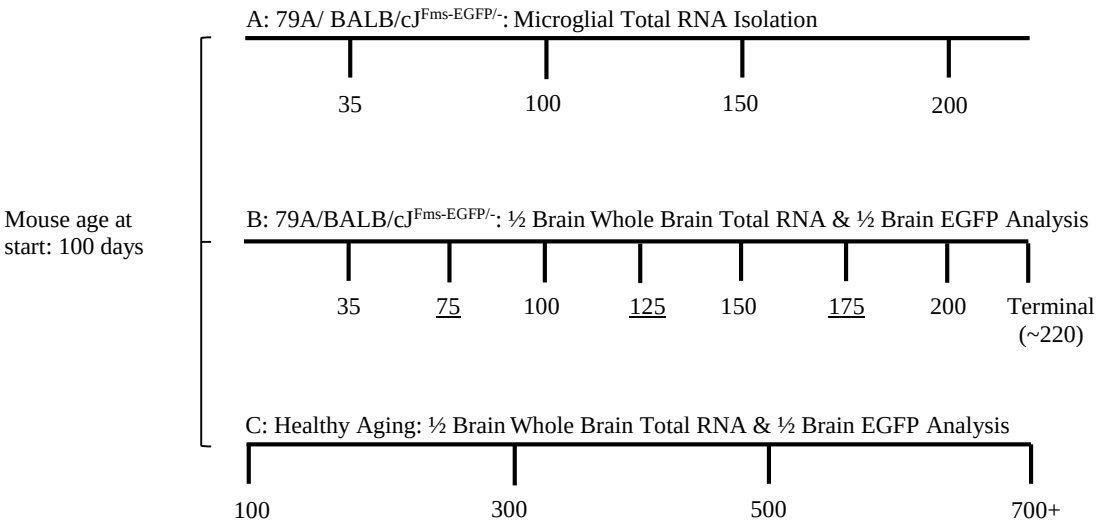

Figure 6-1: A series of BALB/cJFms-EGFP/- in-vivo experiments completed in parallel to document the role of microglia in neurodegenerative prion disease and healthy aging. Crucially all three experiments use mice aged at approximately 100 days old at the point of inoculation or experimental start to allow for comparison. **A:** Described in Chapter 4; a time course of total RNA transcriptome analysis from isolated microglia. **B:** Time course analysis of microglia morphology through EGFP quantification as described in chapter 4. The ½ brains for total RNA isolation were processed and RNA frozen. **C:** Healthy ageing experiment utilising where possible already aged BALB/cJ Fms-EGFP/- mice retired from use as breeding stock. The ½ brains for both total RNA isolation and EGFP quantification were processed and samples frozen.

The impact of pro-inflammatory products on the brain is often deleterious to neuronal function. Microglia are extremely sensitive to systemic inflammation and the increase in circulating inflammatory products seen in the elderly presents as an increase in delirium and depression when combined with an underlying neurodegenerative disease (Cerejeira *et al.*, 2010). Furthermore a secondary infection typically results in rapid worsening of the dementia. Activated microglia in both an aged and neurodegenerative environment can be considered 'pre-primed' and rapidly switch to a considerably more pro-inflammatory phenotype following further systemic insult (Cunningham *et al.*, 2005b, Godbout *et al.*, 2005, Palin *et al.*, 2008, Field *et al.*, 2010, Murray *et al.*, 2012). Crucially, upon resolution of the secondary infection, the severity of the dementia does not return to that seen pre-infection (MacLullich *et al.*, 2009, van Gool *et al.*, 2010). Efforts have been made to treat many neurodegenerative diseases through administration of nonsteroidal anti-inflammatory drugs (Rogers *et al.*, 1993, Lim *et al.*, 2000, Jantzen *et al.*, 2002). The aim was to block cyclooxygenases, and stimulate peroxisome proliferator-activated receptors-γ mediated inhibition of inflammatory cytokine synthesis (Lehmann *et al.*, 1997, Combs *et al.*, 2000). The clinical trials saw mixed results due to the importance of the maintaining long term dosage combined with early administration of the drugs at or near onset of diagnosis for any benefit to be incurred (Stewart *et al.*, 1997, Breitner *et al.*, 2011). There are also complications resulting from heterogeneity within the human population including alleles associated with increased risk of generating chronic neurodegenerative disease in later life (Szekely *et al.*, 2008).

The majority of the differentially expressed genes identified in this study from isolated microglia were associated with an increase in metabolic load and protein translation and included genes associated with respiratory stress and DNA repair. Although to be expected from an activated myeloid cell, the association of metabolic genes with microglia from the diseased brain could only be determined following successful isolation of this group of cells, and are therefore unique to this present study. The use of bone marrow derived myeloid cells as the delivery vector for gene

therapy as a means to treat neurodegenerative diseases is rapidly gaining in popularity following initial successes pioneered in lysosomal storage disorders (Wynn *et al.*, 2009, Langford-Smith *et al.*, 2012, Sergijenko *et al.*, 2013). The potential for exploiting this great of genes is extensive as rather than administering anti-inflammatory drugs to illicit a microglial response, the metabolic genes identified in this present study could be utilised via a gene therapy approach to limit the ability for microglia to response. As per the lysosomal storage disorders trials the altered microglia would be induced to repopulate central nervous system following adoption of irradiation induced selective to reduce the number of resident microglia.

6.8 Final Conclusion

The data presented in this study is at odds with the current consensus on *in-vivo* microglia activation in chronic protein misfolding diseases and portrays a considerably more pro-inflammatory and phagocytic microglia activation phenotype. The disease associated signature in the multicellular transcriptome is dominated by microglia, implying these cells are crucial to the disease process. Concurrent with the activation profile is a signature of heavy metabolic which contain a considerable number of new and potential targets to influence the response of microglia, including for the first time targets associated with the intracellular metabolic pathways the cells require in order to maintain a chronic level of activation. Protein misfolding diseases typically have a very long incubation period in which there is a steady and progressive increase in misfolded protein deposition, neuroinflammation and synaptopathy as the disease progresses. By contrast the clinical phase is relatively short and is the culmination of the steadily progressing pre-clinical pathological artefacts. Therapeutic intervention is therefore preferable in the pre-clinical stages when attempts can be made to limit the pathology. This study has revealed many new targets for reducing pre-clinical microglial activation that have not previously been associated with microglia in neurodegenerative diseases. The considerable number of identified transcripts associated with translation offers many intriguing possibilities of manipulating the activity of microglia.

7 References

Abutbul, S., Shapiro, J., Szaingurten-Solodkin, I., Levy, N., Carmy, Y., Baron, R., Jung, S. & Monsonego, A. 2012. Tgf-Beta Signaling through Smad2/3 Induces the Quiescent Microglial Phenotype within the Cns Environment. *Glia,* **60,** 1160-1171.

Adachi, O., Kawai, T., Takeda, K., Matsumoto, M., Tsutsui, H., Sakagami, M., Nakanishi, K. & Akira, S. 1998. Targeted Disruption of the Myd88 Gene Results in Loss of Il-1- and Il-18-Mediated Function. *Immunity,* **9,** 143-150.

Adams, D. H., Caspary, E. A. & Field, E. J. 1969. The Incorporation of [3h]Thymidine, [14c]Orotic Acid, [14c]Uridine-Diphosphoglucose and [14c]Glucosamine into a Post-Ribosomal Fraction of Normal and Scrapie-Affected Mouse Brain and Spleen. *Journal of General Virology,* **4,** 89-100.

Agostini, F., Dotti, C. G., Perez-Canamas, A., Ledesma, M. D., Benetti, F. & Legname, G. 2013. Prion Protein Accumulation in Lipid Rafts of Mouse Aging Brain. *PloS One,* **8,** e74244.

Ajami, B., Bennett, J. L., Krieger, C., McNagny, K. M. & Rossi, F. M. V. 2011. Infiltrating Monocytes Trigger Eae Progression, but Do Not Contribute to the Resident Microglia Pool. *Nature Neuroscience,* **14,** 1142-1149.

Ajami, B., Bennett, J. L., Krieger, C., Tetzlaff, W. & Rossi, F. M. V. 2007. Local Self-Renewal Can Sustain Cns Microglia Maintenance and Function Throughout Adult Life. *Nature Neuroscience,* **10,** 1538-1543.

Akhtar, S., Wenborn, A., Brandner, S., Collinge, J. & Lloyd, S. E. 2011. Sex Effects in Mouse Prion Disease Incubation Time. *PloS One,* **6,** 13-13.

Akira, S. & Takeda, K. 2004. Toll-Like Receptor Signalling. *Nature Reviews: Immunology,* **4,** 499-511.

Alliot, F., Godin, I. & Pessac, B. 1999. Microglia Derive from Progenitors, Originating from the Yolk Sac, and Which Proliferate in the Brain. *Brain Research. Developmental Brain Research,* **117,** 145-152.

Alliot, F., Lecain, E., Grima, B. & Pessac, B. 1991. Microglial Progenitors with a High Proliferative Potential in the Embryonic and Adult Mouse Brain. *Proceedings of the National Academy of Sciences of the United States of America,* **88,** 1541-1545.

Aloia, L., Parisi, S., Fusco, L., Pastore, L. & Russo, T. 2010. Differentiation of Embryonic Stem Cells 1 (Dies1) Is a Component of Bone Morphogenetic Protein 4 (Bmp4) Signaling Pathway Required for Proper Differentiation of Mouse Embryonic Stem Cells. *Journal of Biological Chemistry,* **285,** 7776-7783.

Alper, T., Cramp, W. A., Haig, D. A. & Clarke, M. C. 1967. Does the Agent of Scrapie Replicate without Nucleic Acid? *Nature,* **214,** 764-766.

Alper, T., Haig, D. A. & Clarke, M. C. 1966. The Exceptionally Small Size of the Scrapie Agent. *Biochemical and Biophysical Research Communications,* **22,** 278-284.

Ame, J. C., Spenlehauer, C. & de Murcia, G. 2004. The Parp Superfamily. *Bioessays,* **26,** 882-893.

Ancuta, P., Rao, R., Moses, A., Mehle, A., Shaw, S. K., Luscinskas, F. W. & Gabuzda, D. 2003. Fractalkine Preferentially Mediates Arrest and Migration of Cd16+ Monocytes. *The Journal of Experimental Medicine,* **197,** 1701-1707.

Anderson, C. F. & Mosser, D. M. 2002a. Cutting Edge: Biasing Immune Responses by Directing Antigen to Macrophage Fc Gamma Receptors. *Journal of Immunology,* **168,** 3697-3701.

Anderson, C. F. & Mosser, D. M. 2002b. A Novel Phenotype for an Activated Macrophage: The Type 2 Activated Macrophage. *Journal of Leukocyte Biology,* **72,** 101-106.

Andersson, H., Baechi, T., Hoechl, M. & Richter, C. 1998. Autofluorescence of Living Cells. *Journal of Microscopy,* **191,** 1-7.

Annunziato, F., Cosmi, L., Liotta, F., Maggi, E. & Romagnani, S. 2012. Defining the Human T Helper 17 Cell Phenotype. *Trends in Immunology,* **33,** 505-512.

Antony, J. M., Paquin, A., Nutt, S. L., Kaplan, D. R. & Miller, F. D. 2011. Endogenous Microglia Regulate Development of Embryonic Cortical Precursor Cells. *Journal of Neuroscience Research,* **89,** 286-298.

Arakawa, Y., Bito, H., Furuyashiki, T., Tsuji, T., Takemoto-Kimura, S., Kimura, K., Nozaki, K., Hashimoto, N. & Narumiya, S. 2003. Control of Axon Elongation Via an Sdf-1alpha/Rho/Mdia Pathway in Cultured Cerebellar Granule Neurons. *Journal of Cell Biology,* **161,** 381-391.

Araque, A., Parpura, V., Sanzgiri, R. P. & Haydon, P. G. 1998. Glutamate-Dependent Astrocyte Modulation of Synaptic Transmission between Cultured Hippocampal Neurons. *European Journal of Neuroscience,* **10,** 2129-2142.

Arenzana-Seisdedos, F., Thompson, J., Rodriguez, M. S., Bachelerie, F., Thomas, D. & Hay, R. T. 1995. Inducible Nuclear Expression of Newly Synthesized I Kappa B Alpha Negatively Regulates DNA-Binding and Transcriptional Activities of Nf-Kappa B. *Molecular and Cellular Biology,* **15,** 2689-2696.

Asuni, A. A., Cunningham, C., Vigneswaran, P., Perry, V. H. & O'Connor, V. 2008. Unaltered Snare Complex Formation in an in Vivo Model of Prion Disease. *Brain Research,* **1233,** 1-7.

Auffray, C., Fogg, D., Garfa, M., Elain, G., Join-Lambert, O., Kayal, S., Sarnacki, S., Cumano, A., Lauvau, G. & Geissmann, F. 2007. Monitoring of Blood Vessels and Tissues by a Population of Monocytes with Patrolling Behavior. *Science,* **317,** 666-670.

Babior, B. M., Lambeth, J. D. & Nauseef, W. 2002. The Neutrophil Nadph Oxidase. *Archives of Biochemistry and Biophysics,* **397,** 342-344.

Bachstetter, A. D., Morganti, J. M., Jernberg, J., Schlunk, A., Mitchell, S. H., Brewster, K. W., Hudson, C. E., Cole, M. J., Harrison, J. K., Bickford, P. C. & Gemma, C. 2011. Fractalkine and Cx3cr1 Regulate Hippocampal Neurogenesis in Adult and Aged Rats. *Neurobiology of Aging,* **32,** 2030-2044.

Bai, Y., Zhu, Z., Gao, Z. & Kong, Y. 2014. Tlr2 Signaling Directs No-Dependent Mmp-9 Induction in Mouse Microglia. *Neuroscience Letters,* **571,** 5-10.

Baker, C. A., Lu, Z. Y., Zaitsev, I. & Manuelidis, L. 1999. Microglial Activation Varies in Different Models of Creutzfeldt-Jakob Disease. *Journal of Virology,* **73,** 5089-5097.

Baker, C. A. & Manuelidis, L. 2003. Unique Inflammatory Rna Profiles of Microglia in Creutzfeldt–Jakob Disease. *Proceedings of the National Academy of Sciences of the United States of America,* **100,** 675-679.

Baker, C. A., Martin, D. & Manuelidis, L. 2002. Microglia from Creutzfeldt-Jakob Disease-Infected Brains Are Infectious and Show Specific Mrna Activation Profiles. *Journal of Virology,* **76,** 10905-10913.

Bal-Price, A. & Brown, G. C. 2001. Inflammatory Neurodegeneration Mediated by Nitric Oxide from Activated Glia-Inhibiting Neuronal Respiration, Causing Glutamate Release and Excitotoxicity. *Journal of Neuroscience,* **21,** 6480-6491.

Baldi, P. & Long, A. D. 2001. A Bayesian Framework for the Analysis of Microarray Expression Data: Regularized T -Test and Statistical Inferences of Gene Changes. *Bioinformatics,* **17,** 509-519.

Baldwin, M. A., Pan, K. M., Nguyen, J., Huang, Z., Groth, D., Serban, A., Gasset, M., Mehlhorn, I., Fletterick, R. J., Cohen, F. E. & et al. 1994. Spectroscopic Characterization of Conformational Differences between Prpc and Prpsc: An Alpha-Helix to Beta-Sheet Transition. *Philosophical Transactions of the Royal Society of London. Series B: Biological Sciences,* **343,** 435-441.

Ban, E., Haour, F. & Lenstra, R. 1992. Brain Interleukin 1 Gene Expression Induced by Peripheral Lipopolysaccharide Administration. *Cytokine,* **4,** 48-54.

Barrett, T. & Edgar, R. 2006. Gene Expression Omnibus: Microarray Data Storage, Submission, Retrieval, and Analysis. *Methods in Enzymology,* **411,** 352-369.

Barrett, T., Troup, D. B., Wilhite, S. E., Ledoux, P., Rudnev, D., Evangelista, C., Kim, I. F., Soboleva, A., Tomashevsky, M. & Edgar, R. 2007. Ncbi Geo: Mining Tens of Millions of Expression Profiles--Database and Tools Update. *Nucleic Acids Research,* **35,** 760-765.

Basler, K., Oesch, B., Scott, M., Westaway, D., Walchli, M., Groth, D. F., McKinley, M. P., Prusiner, S. B. & Weissmann, C. 1986. Scrapie and Cellular Prp Isoforms Are Encoded by the Same Chromosomal Gene. *Cell,* **46,** 417-428.

Basta, G., Lazzerini, G., Massaro, M., Simoncini, T., Tanganelli, P., Fu, C., Kislinger, T., Stern, D. M., Schmidt, A. M. & De Caterina, R. 2002. Advanced Glycation End Products Activate Endothelium through Signal-Transduction Receptor Rage: A Mechanism for Amplification of Inflammatory Responses. *Circulation,* **105,** 816-822.

Bate, C., Boshuizen, R. & Williams, A. 2005. Microglial Cells Kill Prion-Damaged Neurons in Vitro by a Cd14-Dependent Process. *Journal of Neuroimmunology,* **170,** 62-70.

Bate, C., Langeveld, J. & Williams, A. 2004. Manipulation of Prpres Production in Scrapie-Infected Neuroblastoma Cells. *Journal of Neuroscience Methods,* **138,** 217-223.

Bate, C., Reid, S. & Williams, A. 2001. Killing of Prion-Damaged Neurones by Microglia. *Neuroreport,* **12,** 2589-2594.

Baud, V., Chissoe, S. L., Viegas-Pequignot, E., Diriong, S., N'Guyen, V. C., Roe, B. A. & Lipinski, M. 1995. Emr1, an Unusual Member in the Family of Hormone Receptors with Seven Transmembrane Segments. *Genomics,* **26,** 334-344.

Baugh, L. R., Hill, A. A., Brown, E. L. & Hunter, C. P. 2001. Quantitative Analysis of Mrna Amplification by in Vitro Transcription. *Nucleic Acids Research,* **29,** E29.

Belichenko, P. V., Brown, D., Jeffrey, M. & Fraser, J. R. 2000. Dendritic and Synaptic Alterations of Hippocampal Pyramidal Neurones in Scrapie-Infected Mice. *Neuropathology and Applied Neurobiology,* **26,** 143-149.

Benzing, W. C., Wujek, J. R., Ward, E. K., Shaffer, D., Ashe, K. H., Younkin, S. G. & Brunden, K. R. 1999. Evidence for Glial-Mediated Inflammation in Aged App(Sw) Transgenic Mice. *Neurobiology of Aging,* **20,** 581-589.

Betmouni, S. & Perry, V. H. 1999. The Acute Inflammatory Response in Cns Following Injection of Prion Brain Homogenate or Normal Brain Homogenate. *Neuropathology and Applied Neurobiology,* **25,** 20-28.

Betmouni, S., Perry, V. H. & Gordon, J. L. 1996. Evidence for an Early Inflammatory Response in the Central Nervous System of Mice with Scrapie. *Neuroscience,* **74,** 1-5.

Bhaskar, K., Maphis, N., Xu, G., Varvel, N. H., Kokiko-Cochran, O. N., Weick, J. P., Staugaitis, S. M., Cardona, A., Ransohoff, R. M., Herrup, K. & Lamb, B. T. 2014. Microglial Derived Tumor Necrosis Factor-Alpha Drives Alzheimer's Disease-Related Neuronal Cell Cycle Events. *Neurobiology of Disease,* **62,** 273-285.

Bianchi, M. E. 2007. Damps, Pamps and Alarmins: All We Need to Know About Danger. *Journal of Leukocyte Biology,* **81,** 1-5.

Billinton, N. & Knight, A. W. 2001. Seeing the Wood through the Trees: A Review of Techniques for Distinguishing Green Fluorescent Protein from Endogenous Autofluorescence. *Analytical Biochemistry,* **291,** 175-197.

Birkett, C. R., Hennion, R. M., Bembridge, D. A., Clarke, M. C., Chree, A., Bruce, M. E. & Bostock, C. J. 2001. Scrapie Strains Maintain Biological Phenotypes on Propagation in a Cell Line in Culture. *EMBO Journal,* **20,** 3351-3358.

Blackmore, D. G., Golmohammadi, M. G., Large, B., Waters, M. J. & Rietze, R. L. 2009. Exercise Increases Neural Stem Cell Number in a Growth Hormone-Dependent Manner, Augmenting the Regenerative Response in Aged Mice. *Stem Cells,* **27,** 2044-2052.

Blackmore, D. G., Reynolds, B. A., Golmohammadi, M. G., Large, B., Aguilar, R. M., Haro, L., Waters, M. J. & Rietze, R. L. 2012. Growth Hormone Responsive Neural Precursor Cells Reside within the Adult Mammalian Brain. *Scientific Reports,* **2,** 250.

Boche, D., Cunningham, C., Docagne, F., Scott, H. & Perry, V. H. 2006. Tgf[Beta]1 Regulates the Inflammatory Response During Chronic Neurodegeneration. *Neurobiology of Disease,* **22,** 638-650.

Boehme, S. A., Lio, F. M., Maciejewski-Lenoir, D., Bacon, K. B. & Conlon, P. J. 2000. The Chemokine Fractalkine Inhibits Fas-Mediated Cell Death of Brain Microglia. *Journal of Immunology,* **165,** 397-403.

Boellaard, J. W., Kao, M., Schlote, W. & Diringer, H. 1991. Neuronal Autophagy in Experimental Scrapie. *Acta Neuropathologica,* **82,** 225-228.

Boje, K. M. & Arora, P. K. 1992. Microglial-Produced Nitric Oxide and Reactive Nitrogen Oxides Mediate Neuronal Cell Death. *Brain Research,* **587,** 250-256.

Boldrick, J. C., Alizadeh, A. A., Diehn, M., Dudoit, S., Liu, C. L., Belcher, C. E., Botstein, D., Staudt, L. M., Brown, P. O. & Relman, D. A. 2002. Stereotyped and Specific Gene Expression Programs in Human Innate Immune Responses to Bacteria. *Proceedings of the National Academy of Sciences of the United States of America,* **99,** 972-977.

Bolmont, T., Clavaguera, F., Meyer-Luehmann, M., Herzig, M. C., Radde, R., Staufenbiel, M., Lewis, J., Hutton, M., Tolnay, M. & Jucker, M. 2007. Induction of Tau Pathology by Intracerebral Infusion of Amyloid-Beta -Containing Brain Extract and by Amyloid-Beta Deposition in App X Tau Transgenic Mice. *American Journal of Pathology,* **171,** 2012-2020.

Bolmont, T., Haiss, F., Eicke, D., Radde, R., Mathis, C. A., Klunk, W. E., Kohsaka, S., Jucker, M. & Calhoun, M. E. 2008. Dynamics of the Microglial/Amyloid Interaction Indicate a Role in Plaque Maintenance. *Journal of Neuroscience,* **28,** 4283-4292.

Bolstad, B. M., Irizarry, R. A., Astrand, M. & Speed, T. P. 2003. A Comparison of Normalization Methods for High Density Oligonucleotide Array Data Based on Variance and Bias. *Bioinformatics,* **19,** 185-193.

Bolton, D. C., McKinley, M. P. & Prusiner, S. B. 1982. Identification of a Protein That Purifies with the Scrapie Prion. *Science,* **218,** 1309-1311.

Booth, S., Bowman, C., Baumgartner, R., Sorensen, G., Robertson, C., Coulthart, M., Phillipson, C. & Somorjai, R. L. 2004. Identification of Central Nervous System Genes

Involved in the Host Response to the Scrapie Agent During Preclinical and Clinical Infection. *Journal of General Virology,* **85,** 3459-3471.

Boscia, F., Esposito, C. L., Di Crisci, A., de Franciscis, V., Annunziato, L. & Cerchia, L. 2009. Gdnf Selectively Induces Microglial Activation and Neuronal Survival in Ca1/Ca3 Hippocampal Regions Exposed to Nmda Insult through Ret/Erk Signalling. *PloS One,* **4,** e6486.

Boucsein, C., Zacharias, R., Farber, K., Pavlovic, S., Hanisch, U. K. & Kettenmann, H. 2003. Purinergic Receptors on Microglial Cells: Functional Expression in Acute Brain Slices and Modulation of Microglial Activation in Vitro. *European Journal of Neuroscience,* **17,** 2267-2276.

Boutin, H., LeFeuvre, R. A., Horai, R., Asano, M., Iwakura, Y. & Rothwell, N. J. 2001. Role of Il-1alpha and Il-1beta in Ischemic Brain Damage. *Journal of Neuroscience,* **21,** 5528-5534.

Bouzamondo-Bernstein, E., Hopkins, S. D., Spilman, P., Uyehara-Lock, J., Deering, C., Safar, J., Prusiner, S. B., Ralston, H. J., 3rd & DeArmond, S. J. 2004. The Neurodegeneration Sequence in Prion Diseases: Evidence from Functional, Morphological and Ultrastructural Studies of the Gabaergic System. *Journal of Neuropathology and Experimental Neurology,* **63,** 882-899.

Brandt, D. T., Marion, S., Griffiths, G., Watanabe, T., Kaibuchi, K. & Grosse, R. 2007. Dia1 and Iqgap1 Interact in Cell Migration and Phagocytic Cup Formation. *Journal of Cell Biology,* **178,** 193-200.

Brazma, A., Hingamp, P., Quackenbush, J., Sherlock, G., Spellman, P., Stoeckert, C., Aach, J., Ansorge, W., Ball, C. A., Causton, H. C., Gaasterland, T., Glenisson, P., Holstege, F. C., Kim, I. F., Markowitz, V., Matese, J. C., Parkinson, H., Robinson, A., Sarkans, U., Schulze-Kremer, S., Stewart, J., Taylor, R., Vilo, J. & Vingron, M. 2001. Minimum Information About a Microarray Experiment (Miame)-toward Standards for Microarray Data. *Nature Genetics,* **29,** 365-371.

Breitner, J. C., Baker, L. D., Montine, T. J., Meinert, C. L., Lyketsos, C. G., Ashe, K. H., Brandt, J., Craft, S., Evans, D. E., Green, R. C., Ismail, M. S., Martin, B. K., Mullan, M. J., Sabbagh, M. & Tariot, P. N. 2011. Extended Results of the Alzheimer's Disease Anti-Inflammatory Prevention Trial. *Alzheimer's & Dementia: The Journal of the Alzheimer's Association,* **7,** 402-411.

Brink, B. P., Veerhuis, R., Breij, E. C., van der Valk, P., Dijkstra, C. D. & Bo, L. 2005. The Pathology of Multiple Sclerosis Is Location-Dependent: No Significant Complement Activation Is Detected in Purely Cortical Lesions. *Journal of Neuropathology and Experimental Neurology,* **64,** 147-155.

Brooks, E. M., Sheflin, L. G. & Spaulding, S. W. 1995. Secondary Structure in the 3' Utr of Egf and the Choice of Reverse Transcriptases Affect the Detection of Message Diversity by Rt-Pcr. *BioTechniques,* **19,** 806-812, 814-815.

Brooks, G. A., Dubouchaud, H., Brown, M., Sicurello, J. P. & Butz, C. E. 1999. Role of Mitochondrial Lactate Dehydrogenase and Lactate Oxidation in the Intracellular Lactate Shuttle. *Proceedings of the National Academy of Sciences of the United States of America,* **96,** 1129-1134.

Brotherston, J. G., Renwick, C. C., Stamp, J. T., Zlotnik, I. & Pattison, I. H. 1968. Spread of Scrapie by Contact to Goats and Sheep. *Journal of Comparative Pathology,* **78,** 9-17.

Brown, A. R., Rebus, S., McKimmie, C. S., Robertson, K., Williams, A. & Fazakerley, J. K. 2005. Gene Expression Profiling of the Preclinical Scrapie-Infected Hippocampus. *Biochemical and Biophysical Research Communications,* **334,** 86-95.

Brown, A. R., Webb, J., Rebus, S., Walker, R., Williams, A. & Fazakerley, J. K. 2003. Inducible Cytokine Gene Expression in the Brain in the Me7/Cv Mouse Model of Scrapie Is Highly Restricted, Is at a Strikingly Low Level Relative to the Degree of Gliosis and Occurs Only Late in Disease. *Journal of General Virology,* **84,** 2605-2611.

Brown, A. R., Webb, J., Rebus, S., Williams, A. & Fazakerley, J. K. 2004. Identification of up-Regulated Genes by Array Analysis in Scrapie-Infected Mouse Brains. *Neuropathology and Applied Neurobiology,* **30,** 555-567.

Brown, D., Belichenko, P., Sales, J., Jeffrey, M. & Fraser, J. R. 2001. Early Loss of Dendritic Spines in Murine Scrapie Revealed by Confocal Analysis. *Neuroreport,* **12,** 179-183.

Brown, D. R., Schmidt, B. & Kretzschmar, H. A. 1996. Role of Microglia and Host Prion Protein in Neurotoxicity of a Prion Protein Fragment. *Nature,* **380,** 345-347.

Brown, D. R., Wong, B. S., Hafiz, F., Clive, C., Haswell, S. J. & Jones, I. M. 1999a. Normal Prion Protein Has an Activity Like That of Superoxide Dismutase. *Biochemical Journal,* **344 Pt 1,** 1-5.

Brown, G. C. & Neher, J. J. 2012. Eaten Alive! Cell Death by Primary Phagocytosis: 'Phagoptosis'. *Trends in Biochemical Sciences,* **37,** 325-332.

Brown, H. C., Castano, A., Fearn, S., Townsend, M., Edwards, G., Streuli, C. & Perry, V. H. 1997. Adhesion Molecules Involved in Macrophage Responses to Wallerian Degeneration in the Murine Peripheral Nervous System. *European Journal of Neuroscience,* **9,** 2057-2063.

Brown, K. L., Gossner, A., Mok, S. & Mabbott, N. A. 2011. The Effects of Host Age on the Transport of Complement-Bound Complexes to the Spleen and the Pathogenesis of Intravenous Scrapie Infection. *Journal of Virology,* **86,** 25-35.

Brown, K. L., Stewart, K., Ritchie, D. L., Mabbott, N. A., Williams, A., Fraser, H., Morrison, W. I. & Bruce, M. E. 1999b. Scrapie Replication in Lymphoid Tissues Depends on Prion Protein-Expressing Follicular Dendritic Cells. *Nature Medicine,* **5,** 1308-1312.

Brown, K. L., Wathne, G. J., Sales, J., Bruce, M. E. & Mabbott, N. A. 2009. The Effects of Host Age on Follicular Dendritic Cell Status Dramatically Impair Scrapie Agent Neuroinvasion in Aged Mice. *Journal of Immunology,* **153,** 5199-5207.

Brown, S., Heinisch, I., Ross, E., Shaw, K., Buckley, C. D. & Savill, J. 2002. Apoptosis Disables Cd31-Mediated Cell Detachment from Phagocytes Promoting Binding and Engulfment. *Nature,* **418,** 200-203.

Bruce, M., Chree, A., McConnell, I., Foster, J., Pearson, G. & Fraser, H. 1994. Transmission of Bovine Spongiform Encephalopathy and Scrapie to Mice: Strain Variation and the Species Barrier. *Philosophical Transactions of the Royal Society of London. Series B: Biological Sciences,* **343,** 405-411.

Bruce, M. E. 1993. Scrapie Strain Variation and Mutation. *British Medical Bulletin,* **49,** 822-838.

Bruce, M. E. 2003. Tse Strain Variation: An Investigation into Prion Disease Diversity. *British Medical Bulletin,* **66,** 99-108.

Bruce, M. E., Boyle, A., Cousens, S., McConnell, I., Foster, J., Goldmann, W. & Fraser, H. 2002. Strain Characterization of Natural Sheep Scrapie and Comparison with Bse. *Journal of General Virology,* **83,** 695-704.

Bruce, M. E., McConnell, I., Fraser, H. & Dickinson, A. G. 1991. The Disease Characteristics of Different Strains of Scrapie in Sinc Congenic Mouse Lines: Implications for the Nature of the Agent and Host Control of Pathogenesis. *The Journal of General Virology,* **72 (Pt 3),** 595-603.

Bruce, M. E., Will, R. G., Ironside, J. W., McConnell, I., Drummond, D., Suttie, A., McCardle, L., Chree, A., Hope, J., Birkett, C., Cousens, S., Fraser, H. & Bostock, C. J. 1997. Transmissions to Mice Indicate That 'New Variant' Cjd Is Caused by the Bse Agent. *Nature,* **389,** 498-501.

Büeler, H., Aguzzi, A., Sailer, A., Greiner, R. A., Autenried, P., Aguet, M. & Weissmann, C. 1993. Mice Devoid of Prp Are Resistant to Scrapie. *Cell,* **73,** 1339-1347.

Burgess, A. W. 1989. Epidermal Growth Factor and Transforming Growth Factor Alpha. *British Medical Bulletin,* **45,** 401-424.

Burrell, K., Hill, R. P. & Zadeh, G. 2012. High-Resolution in-Vivo Analysis of Normal Brain Response to Cranial Irradiation. *PloS One,* **7,** e38366.

Butovsky, O., Jedrychowski, M. P., Moore, C. S., Cialic, R., Lanser, A. J., Gabriely, G., Koeglsperger, T., Dake, B., Wu, P. M., Doykan, C. E., Fanek, Z., Liu, L., Chen, Z., Rothstein, J. D., Ransohoff, R. M., Gygi, S. P., Antel, J. P. & Weiner, H. L. 2014. Identification of a Unique Tgf-Beta-Dependent Molecular and Functional Signature in Microglia. *Nature Neuroscience,* **17,** 131-143.

Butovsky, O., Siddiqui, S., Gabriely, G., Lanser, A. J., Dake, B., Murugaiyan, G., Doykan, C. E., Wu, P. M., Gali, R. R., Iyer, L. K., Lawson, R., Berry, J., Krichevsky, A. M., Cudkowicz, M. E. & Weiner, H. L. 2012. Modulating Inflammatory Monocytes with a Unique Microrna Gene Signature Ameliorates Murine Als. *Journal of Clinical Investigation,* **122,** 3063-3087.

Butte, A. J. & Kohane, I. S. Mutual Information Relevance Networks: Functional Genomic Clustering Using Pairwise Entropy Measurements. Pacific Symposium on Biocomputing, 2000. 418-429.

Buttini, M. & Boddeke, H. 1995. Peripheral Lipopolysaccharide Stimulation Induces Interleukin-1β Messenger Rna in Rat Brain Microglial Cells. *Neuroscience,* **65,** 523-530.

Caldeira, C., Oliveira, A. F., Cunha, C., Vaz, A. R., Falcao, A. S., Fernandes, A. & Brites, D. 2014. Microglia Change from a Reactive to an Age-Like Phenotype with the Time in Culture. *Frontiers in Cellular Neuroscience,* **8,** 152.

Campanella, G. S., Tager, A. M., El Khoury, J. K., Thomas, S. Y., Abrazinski, T. A., Manice, L. A., Colvin, R. A. & Luster, A. D. 2008. Chemokine Receptor Cxcr3 and Its Ligands Cxcl9 and Cxcl10 Are Required for the Development of Murine Cerebral Malaria. *Proceedings of the National Academy of Sciences of the United States of America,* **105,** 4814-4819.

Cancellotti, E., Bradford, B. M., Tuzi, N. L., Hickey, R. D., Brown, D., Brown, K. L., Barron, R. M., Kisielewski, D., Piccardo, P. & Manson, J. C. 2010. Glycosylation of Prpc Determines Timing of Neuroinvasion and Targeting in the Brain Following Transmissible Spongiform Encephalopathy Infection by a Peripheral Route. *Journal of Virology,* **84,** 3464-3475.

Capani, F., Ellisman, M. H. & Martone, M. E. 2001. Filamentous Actin Is Concentrated in Specific Subpopulations of Neuronal and Glial Structures in Rat Central Nervous System. *Brain Research,* **923,** 1-11.

Cardona, A. E., Huang, D., Sasse, M. E. & Ransohoff, R. M. 2006a. Isolation of Murine Microglial Cells for Rna Analysis or Flow Cytometry. *Nature Protocols,* **1,** 1947-1951.

Cardona, A. E., Pioro, E. P., Sasse, M. E., Kostenko, V., Cardona, S. M., Dijkstra, I. M., Huang, D., Kidd, G., Dombrowski, S., Dutta, R., Lee, J. C., Cook, D. N., Jung, S., Lira, S. A., Littman, D. R. & Ransohoff, R. M. 2006b. Control of Microglial Neurotoxicity by the Fractalkine Receptor. *Nature Neuroscience,* **9,** 917-924.

Carlson, G. A., Ebeling, C., Yang, S. L., Telling, G., Torchia, M., Groth, D., Westaway, D., DeArmond, S. J. & Prusiner, S. B. 1994. Prion Isolate Specified Allotypic Interactions between the Cellular and Scrapie Prion Proteins in Congenic and Transgenic Mice. *Proceedings of the National Academy of Sciences of the United States of America,* **91,** 5690-5694.

Carrillo-Vico, A., Calvo, J. R., Abreu, P., Lardone, P. J., Garcia-Maurino, S., Reiter, R. J. & Guerrero, J. M. 2004. Evidence of Melatonin Synthesis by Human Lymphocytes and Its Physiological Significance: Possible Role as Intracrine, Autocrine, and/or Paracrine Substance. *FASEB Journal,* **18,** 537-539.

Cattaneo, E. & McKay, R. 1990. Proliferation and Differentiation of Neuronal Stem Cells Regulated by Nerve Growth Factor. *Nature,* **347,** 762-765.

Caughey, B., Raymond, G. J., Ernst, D. & Race, R. E. 1991. N-Terminal Truncation of the Scrapie-Associated Form of Prp by Lysosomal Protease(S): Implications Regarding the Site of Conversion of Prp to the Protease-Resistant State. *Journal of Virology,* **65,** 6597-6603.

Cerejeira, J., Firmino, H., Vaz-Serra, A. & Mukaetova-Ladinska, E. B. 2010. The Neuroinflammatory Hypothesis of Delirium. *Acta Neuropathologica,* **119,** 737-754.

Cerletti, U. 1902. Contributo Sperimentale Alla Conoscenza Dei Processi Di Fagocitosi Nelle Sostanza Cerebrale (Experimental Contribution to the Knowledge of the Processes of Phagocytosis in the Brain Substance). *Annali dell'Istituto psichiatrico. della R. università. di Roma,* **1,** 65-73.

Cerletti, U. 1903. Sulla Neuronofagia E Sopra Alcuni Rapporti Normali E Patologici Tra Elementi Nervosa Ed Elementi No-Nervosi (on Neuronophagia and Reports of Normal and Pathological Relationships between Elements of Nervous and Non-Nervous Elements). *Annali dell'Istituto psichiatrico. della R. università. di Roma,* **91**.

Cerletti, U. 1905. Sopra Alcuni Rapporti Tra Le "Cellule a Bastoncello" E Gli Elementi Nervosi Nella Paralisis Progressive (on Some Relationships between the "Rod Cells" and the Nervous Elements in the Progressive Paralysis). *Rivista sperimentale di freniatria* **31** 483-495.

Chamak, B., Dobbertin, A. & Mallat, M. 1995. Immunohistochemical Detection of Thrombospondin in Microglia in the Developing Rat Brain. *Neuroscience,* **69,** 177-187.

Chamak, B., Morandi, V. & Mallat, M. 1994. Brain Macrophages Stimulate Neurite Growth and Regeneration by Secreting Thrombospondin. *Journal of Neuroscience Research,* **38,** 221-233.

Chao, C. C., Hu, S., Molitor, T. W., Shaskan, E. G. & Peterson, P. K. 1992. Activated Microglia Mediate Neuronal Cell Injury Via a Nitric Oxide Mechanism. *Journal of Immunology,* **149,** 2736-2741.

Chelle, P. L. 1942. Un Cas De Tremblante Chez La Chèvre. *Bulletin de l'Académie Vétérinaire de France,* **15,** 294-295.

Chen, Z., Jalabi, W., Hu, W., Park, H. J., Gale, J. T., Kidd, G. J., Bernatowicz, R., Gossman, Z. C., Chen, J. T., Dutta, R. & Trapp, B. D. 2014. Microglial Displacement of Inhibitory Synapses Provides Neuroprotection in the Adult Brain. *Nat Commun,* **5,** 4486.

Chmurzyńska, A. 2006. The Multigene Family of Fatty Acid-Binding Proteins (Fabps): Function, Structure and Polymorphism. *Journal of Applied Genetics,* **47,** 39-48.

Cho, H. J. 1976. Is the Scrapie Agent a Virus? *Nature,* **262,** 411-412.

Cho, H. J. & Greig, A. S. 1975. Isolation of 14-Nm Virus-Like Particles from Mouse Brain Infected with Scrapie Agent. *Nature,* **257,** 685-686.

Chung, W. S., Clarke, L. E., Wang, G. X., Stafford, B. K., Sher, A., Chakraborty, C., Joung, J., Foo, L. C., Thompson, A., Chen, C., Smith, S. J. & Barres, B. A. 2013. Astrocytes Mediate Synapse Elimination through Megf10 and Mertk Pathways. *Nature,* **504,** 394-400.

Clarkson, B. D., Heninger, E., Harris, M. G., Lee, J., Sandor, M. & Fabry, Z. 2012. Innate-Adaptive Crosstalk: How Dendritic Cells Shape Immune Responses in the Cns. *Advances in Experimental Medicine and Biology,* **946,** 309-333.

Clausen, B. H., Lambertsen, K. L., Babcock, A. A., Holm, T. H., Dagnaes-Hansen, F. & Finsen, B. 2008. Interleukin-1beta and Tumor Necrosis Factor-Alpha Are Expressed by Different Subsets of Microglia and Macrophages after Ischemic Stroke in Mice. *Journal of Neuroinflammation,* **5,** 46.

Colby, D. W., Wain, R., Baskakov, I. V., Legname, G., Palmer, C. G., Nguyen, H. O., Lemus, A., Cohen, F. E., DeArmond, S. J. & Prusiner, S. B. 2010. Protease-Sensitive Synthetic Prions. *PLoS Pathogens,* **6,** 1000736.

Colling, S. B., Khana, M., Collinge, J. & Jefferys, J. G. 1997. Mossy Fibre Reorganization in the Hippocampus of Prion Protein Null Mice. *Brain Research,* **755,** 28-35.

Collinge, J., Whittington, M. A., Sidle, K. C., Smith, C. J., Palmer, M. S., Clarke, A. R. & Jefferys, J. G. 1994. Prion Protein Is Necessary for Normal Synaptic Function. *Nature,* **370,** 295-297.

Colton, C. A. & Gilbert, D. L. 1987. Production of Superoxide Anions by a Cns Macrophage, the Microglia. *FEBS Letters,* **223,** 284-288.

Comber, T. 1772. *Real Improvements in Agriculture [Electronic Resource] : (on the Principles of A. Young, Esq;) Recommended to Accompany Improvements of Rents; in a Letter to Reade Peacock, ... To Which Is Added, a Letter to Dr. Hunter, ... Concerning the Rickets in Sheep. By T. Comber*, London : Printed for W. Nicoll, 1772., Page: 73-83.

Combrinck, M. I., Perry, V. H. & Cunningham, C. 2002. Peripheral Infection Evokes Exaggerated Sickness Behaviour in Pre-Clinical Murine Prion Disease. *Neuroscience,* **112,** 7-11.

Combs, C. K., Johnson, D. E., Karlo, J. C., Cannady, S. B. & Landreth, G. E. 2000. Inflammatory Mechanisms in Alzheimer's Disease: Inhibition of B-Amyloid-Stimulated Proinflammatory Responses and Neurotoxicity by Pparγ Agonists. *The Journal of Neuroscience,* **20,** 558-567.

Concepcion, G. P., David, M. P. & Padlan, E. A. 2005. Why Don't Humans Get Scrapie from Eating Sheep? A Possible Explanation Based on Secondary Structure Predictions. *Medical Hypotheses,* **64,** 919-924.

Conde, J. R. & Streit, W. J. 2006. Effect of Aging on the Microglial Response to Peripheral Nerve Injury. *Neurobiology of Aging,* **27,** 1451-1461.

Cosseddu, G. M., Nonno, R., Vaccari, G., Bucalossi, C., Fernandez-Borges, N., Di Bari, M. A., Castilla, J. & Agrimi, U. 2011. Ultra-Efficient Prp(Sc) Amplification Highlights Potentialities and Pitfalls of Pmca Technology. *PLoS Pathogens,* **7,** e1002370.

Cox, G. M., Kithcart, A. P., Pitt, D., Guan, Z., Alexander, J., Williams, J. L., Shawler, T., Dagia, N. M., Popovich, P. G., Satoskar, A. R. & Whitacre, C. C. 2013. Macrophage Migration Inhibitory Factor Potentiates Autoimmune-Mediated Neuroinflammation. *Journal of Immunology,* **24,** 24.

Cramer, P. E., Cirrito, J. R., Wesson, D. W., Lee, C. Y. D., Karlo, J. C., Zinn, A. E., Casali, B. T., Restivo, J. L., Goebel, W. D., James, M. J., Brunden, K. R., Wilson, D. A. & Landreth, G. E. 2012. Apoe-Directed Therapeutics Rapidly Clear B-Amyloid and Reverse Deficits in Ad Mouse Models. *Science,* **335,** 1503-1506.

Cruttwell, R. 1795. *Letters and Papers on Agriculture, Planting, &C. Selected from the Correspondence of the Bath and West of England Society.Vol.Vii*, Page: 72-73.

Cunningham, C., Boche, D. & Perry, V. H. 2002. Transforming Growth Factor B1, the Dominant Cytokine in Murine Prion Disease: Influence on Inflammatory Cytokine Synthesis and Alteration of Vascular Extracellular Matrix. *Neuropathology and Applied Neurobiology,* **28,** 107-119.

Cunningham, C., Campion, S., Lunnon, K., Murray, C. L., Woods, J. F., Deacon, R. M., Rawlins, J. N. & Perry, V. H. 2009. Systemic Inflammation Induces Acute Behavioral and Cognitive Changes and Accelerates Neurodegenerative Disease. *Biological Psychiatry,* **65,** 304-312.

Cunningham, C., Deacon, R., Wells, H., Boche, D., Waters, S., Diniz, C. P., Scott, H., Rawlins, J. N. P. & Perry, V. H. 2003. Synaptic Changes Characterize Early Behavioural Signs in the Me7 Model of Murine Prion Disease. *The European Journal of Neuroscience,* **17,** 2147-2155.

Cunningham, C., Wilcockson, D. C., Boche, D. & Perry, V. H. 2005a. Comparison of Inflammatory and Acute-Phase Responses in the Brain and Peripheral Organs of the Me7 Model of Prion Disease. *Journal of Virology,* **79,** 5174-5184.

Cunningham, C., Wilcockson, D. C., Campion, S., Lunnon, K. & Perry, V. H. 2005b. Central and Systemic Endotoxin Challenges Exacerbate the Local Inflammatory Response and Increase Neuronal Death During Chronic Neurodegeneration. *Journal of Neuroscience,* **25,** 9275-9284.

Cunningham, C. L., Martinez-Cerdeno, V. & Noctor, S. C. 2013. Microglia Regulate the Number of Neural Precursor Cells in the Developing Cerebral Cortex. *Journal of Neuroscience,* **33,** 4216-4233.

Dagleish, M. P., Martin, S., Steele, P., Finlayson, J., Siso, S., Hamilton, S., Chianini, F., Reid, H. W., Gonzalez, L. & Jeffrey, M. 2008. Experimental Transmission of Bovine Spongiform Encephalopathy to European Red Deer (Cervus Elaphus Elaphus). *BMC Veterinary Research,* **4,** 17.

Dana, A. & Tuller, T. 2012. Determinants of Translation Elongation Speed and Ribosomal Profiling Biases in Mouse Embryonic Stem Cells. *PLoS Computational Biology,* **8,** e1002755.

Daneman, R., Zhou, L., Kebede, A. A. & Barres, B. A. 2010. Pericytes Are Required for Blood-Brain Barrier Integrity During Embryogenesis. *Nature,* **468,** 562-566.

Dantzer, R. 2001. Cytokine-Induced Sickness Behavior: Mechanisms and Implications. *Annals of the New York Academy of Sciences,* **933,** 222-234.

Dantzer, R. 2004. Cytokine-Induced Sickness Behaviour: A Neuroimmune Response to Activation of Innate Immunity. *European Journal of Pharmacology,* **500,** 399-411.

Davalos, D., Grutzendler, J., Yang, G., Kim, J. V., Zuo, Y., Jung, S., Littman, D. R., Dustin, M. L. & Gan, W. B. 2005. Atp Mediates Rapid Microglial Response to Local Brain Injury in Vivo. *Nature Neuroscience,* **8,** 752-758.

Dawson, M., Hoinville, L. J., Hosie, B. D. & Hunter, N. 1998. Guidance on the Use of Prp Genotyping as an Aid to the Control of Clinical Scrapie. Scrapie Information Group. *Veterinary Record,* **142,** 623-625.

de Haas, A. H., Boddeke, H. W. & Biber, K. 2008. Region-Specific Expression of Immunoregulatory Proteins on Microglia in the Healthy Cns. *Glia,* **56,** 888-894.

de Haas, A. H., Boddeke, H. W., Brouwer, N. & Biber, K. 2007. Optimized Isolation Enables Ex Vivo Analysis of Microglia from Various Central Nervous System Regions. *Glia,* **55,** 1374-1384.

DeArmond, S. J. 1993. Alzheimer's Disease and Creutzfeldt-Jakob Disease: Overlap of Pathogenic Mechanisms. *Current Opinion in Neurology,* **6,** 872-881.

DeArmond, S. J., Sánchez, H., Yehiely, F., Qiu, Y., Ninchak-Casey, A., Daggett, V., Camerino, A. P., Cayetano, J., Rogers, M., Groth, D., Torchia, M., Tremblay, P., Scott, M. R., Cohen, F. E. & Prusiner, S. B. 1997. Selective Neuronal Targeting in Prion Disease. *Neuron,* **19,** 1337-1348.

DeArmond, S. J., Yang, S. L., Cayetano-Canlas, J., Groth, D. & Prusiner, S. B. 1994. The Neuropathological Phenotype in Transgenic Mice Expressing Different Prion Protein Constructs. *Philosophical Transactions of the Royal Society of London. Series B: Biological Sciences,* **343,** 415-423.

Deleault, N. R., Harris, B. T., Rees, J. R. & Supattapone, S. 2007. Formation of Native Prions from Minimal Components in Vitro. *Proceedings of the National Academy of Sciences of the United States of America,* **104,** 9741-9746.

Desplats, P., Lee, H. J., Bae, E. J., Patrick, C., Rockenstein, E., Crews, L., Spencer, B., Masliah, E. & Lee, S. J. 2009. Inclusion Formation and Neuronal Cell Death through Neuron-to-Neuron Transmission of Alpha-Synuclein. *Proceedings of the National Academy of Sciences of the United States of America,* **106,** 13010-13015.

Dickinson, A. G. 1976. Scrapie in Sheep and Goats. *Frontiers of Biology,* **44,** 209-241.

Dickinson, A. G., Fraser, H., Meikle, V. M. & Outram, G. W. 1972. Competition between Different Scrapie Agents in Mice. *Nature: New Biology,* **237,** 244-245.

Dickinson, A. G. & Mackay, J. M. 1964. Genetical Control of the Incubation Period in Mice of the Neurological Disease, Scrapie. *Heredity,* **19,** 279-288.

Dickinson, A. G. & Meikle, V. M. 1971. Host-Genotype and Agent Effects in Scrapie Incubation: Change in Allelic Interaction with Different Strains of Agent. *Molecular and General Genetics,* **112,** 73-79.

Dickinson, A. G., Meikle, V. M. & Fraser, H. 1968. Identification of a Gene Which Controls the Incubation Period of Some Strains of Scrapie Agent in Mice. *Journal of Comparative Pathology,* **78,** 293-299.

Dickinson, A. G. & Outram, G. W. 1988. Genetic Aspects of Unconventional Virus Infections: The Basis of the Virino Hypothesis. *Ciba Foundation Symposium,* **135,** 63-83.

Dietrich, M. O., Andrews, Z. B. & Horvath, T. L. 2008. Exercise-Induced Synaptogenesis in the Hippocampus Is Dependent on Ucp2-Regulated Mitochondrial Adaptation. *Journal of Neuroscience,* **28,** 10766-10771.

Diez, M., Koistinaho, J., Dearmond, S. J., Groth, D., Prusiner, S. B. & Hokfelt, T. 1997. Marked Decrease of Neuropeptide Y Y2 Receptor Binding Sites in the Hippocampus in Murine Prion Disease. *Proceedings of the National Academy of Sciences of the United States of America,* **94,** 13267-13272.

Dilger, R. N. & Johnson, R. W. 2008. Aging, Microglial Cell Priming, and the Discordant Central Inflammatory Response to Signals from the Peripheral Immune System. *Journal of Leukocyte Biology,* **84,** 932-939.

Ding, Y., Chen, D., Tarcsafalvi, A., Su, R., Qin, L. & Bromberg, J. S. 2003. Suppressor of Cytokine Signaling 1 Inhibits Il-10-Mediated Immune Responses. *Journal of Immunology,* **170,** 1383-1391.

Dohgu, S., Yamauchi, A., Takata, F., Naito, M., Tsuruo, T., Higuchi, S., Sawada, Y. & Kataoka, Y. 2004. Transforming Growth Factor-Beta1 Upregulates the Tight Junction and P-Glycoprotein of Brain Microvascular Endothelial Cells. *Cellular and Molecular Neurobiology,* **24,** 491-497.

Dongen, V. 2000. Performance Criteria for Graph Clustering and Markov Cluster Experiments. *CWI (Centre for Mathematics and Computer Science)***,** INS-R0012.

Donnelly, D. J., Gensel, J. C., Ankeny, D. P., van Rooijen, N. & Popovich, P. G. 2009. An Efficient and Reproducible Method for Quantifying Macrophages in Different Experimental Models of Central Nervous System Pathology. *Journal of Neuroscience Methods,* **181,** 36-44.

Doyle, J. P., Dougherty, J. D., Heiman, M., Schmidt, E. F., Stevens, T. R., Ma, G., Bupp, S., Shrestha, P., Shah, R. D., Doughty, M. L., Gong, S., Greengard, P. & Heintz, N. 2008. Application of a Translational Profiling Approach for the Comparative Analysis of Cns Cell Types. *Cell,* **135,** 749-762.

Drake, C., Boutin, H., Jones, M. S., Denes, A., McColl, B. W., Selvarajah, J. R., Hulme, S., Georgiou, R. F., Hinz, R., Gerhard, A., Vail, A., Prenant, C., Julyan, P., Maroy, R., Brown, G., Smigova, A., Herholz, K., Kassiou, M., Crossman, D., Francis, S., Proctor, S. D., Russell, J. C., Hopkins, S. J., Tyrrell, P. J., Rothwell, N. J. & Allan, S. M. 2011. Brain Inflammation Is Induced by Co-Morbidities and Risk Factors for Stroke. *Brain, Behavior, and Immunity,* **25,** 1113-1122.

Drew, P. D. & Chavis, J. A. 2000. Female Sex Steroids: Effects Upon Microglial Cell Activation. *Journal of Neuroimmunology,* **111,** 77-85.

Dron, M., Moudjou, M., Chapuis, J., Salamat, M. K., Bernard, J., Cronier, S., Langevin, C. & Laude, H. 2010. Endogenous Proteolytic Cleavage of Disease-Associated Prion Protein to Produce C2 Fragments Is Strongly Cell- and Tissue-Dependent. *Journal of Biological Chemistry,* **285,** 10252-10264.

Duggan, D. J., Bittner, M., Chen, Y., Meltzer, P. & Trent, J. M. 1999. Expression Profiling Using Cdna Microarrays. *Nature Genetics,* **21,** 10-14.

Dujardin, S., Lecolle, K., Caillierez, R., Begard, S., Zommer, N., Lachaud, C., Carrier, S., Dufour, N., Auregan, G., Winderickx, J., Hantraye, P., Deglon, N., Colin, M. & Buee, L. 2014. Neuron-to-Neuron Wild-Type Tau Protein Transfer through a Trans-Synaptic Mechanism: Relevance to Sporadic Tauopathies. *Acta Neuropathol Commun,* **2,** 14.

Dunn, L. C., GrüNeberg, H. & Snell, G. D. 1940. Report of the Committee on Mouse Genetics Nomenclature. *The Journal of Heredity,* **31,** 505-506.

Duran-Aniotz, C., Morales, R., Moreno-Gonzalez, I., Hu, P. P. & Soto, C. 2013. Brains from Non-Alzheimer's Individuals Containing Amyloid Deposits Accelerate Abeta Deposition in Vivo. *Acta Neuropathol Commun,* **1,** 76.

Edgington, E. S. 1964. Randomization Tests. *Journal of Psychology,* **57,** 445.

Edri, S. & Tuller, T. 2014. Quantifying the Effect of Ribosomal Density on Mrna Stability. *PloS One,* **9,** e102308.

Eigen, M. & Schuster, P. 1977. The Hypercycle. A Principle of Natural Self-Organization. Part A: Emergence of the Hypercycle. *Naturwissenschaften,* **64,** 541-565.

Eitzen, U. V., Egensperger, R., Kösel, S., Grasbon-Frodl, E. M., Imai, Y., Bise, K., Kohsaka, S., Mehraein, P. & Graeber, M. B. 1998. Microglia and the Development of Spongiform Change in Creutzfeldt-Jakob Disease. *Journal of Neuropathology and Experimental Neurology,* **57,** 246-256.

Ekdahl, C. T., Claasen, J. H., Bonde, S., Kokaia, Z. & Lindvall, O. 2003. Inflammation Is Detrimental for Neurogenesis in Adult Brain. *Proceedings of the National Academy of Sciences of the United States of America,* **100,** 13632-13637.

Eklund, C. M., Kennedy, R. C. & Hadlow, W. J. 1967. Pathogenesis of Scrapie Virus Infection in the Mouse. *Journal of Infectious Diseases,* **117,** 15-22.

Elishmereni, M. & Levi-Schaffer, F. 2011. Cd48: A Co-Stimulatory Receptor of Immunity. *International Journal of Biochemistry and Cell Biology,* **43,** 25-28.

Elkabes, S., DiCicco-Bloom, E. M. & Black, I. B. 1996. Brain Microglia/Macrophages Express Neurotrophins That Selectively Regulate Microglial Proliferation and Function. *Journal of Neuroscience,* **16,** 2508-2521.

Elmore, M. R., Najafi, A. R., Koike, M. A., Dagher, N. N., Spangenberg, E. E., Rice, R. A., Kitazawa, M., Matusow, B., Nguyen, H., West, B. L. & Green, K. N. 2014. Colony-Stimulating Factor 1 Receptor Signaling Is Necessary for Microglia Viability, Unmasking a Microglia Progenitor Cell in the Adult Brain. *Neuron,* **82,** 380-397.

Espey, M. G., Chernyshev, O. N., Reinhard, J. F., Jr., Namboodiri, M. A. & Colton, C. A. 1997. Activated Human Microglia Produce the Excitotoxin Quinolinic Acid. *Neuroreport,* **8,** 431-434.

European Commission 2003. Commission Regulation (Ec) No 1915/2003 of 30 October 2003 Amending Annexes Vii, Viii and Ix to Regulation (Ec) No 999/2001 of the European Parliament and of the Council as Regards the Trade and Import of Ovine and Caprine Animals and the Measures Following the Confirmation of Transmissible Spongiform Encephalopathies in Bovine, Ovine and Caprine Animals (Text with Eea Relevance). *Official Journal of the European Union,* **L 283,** 29–33.

Fadok, V. A., Bratton, D. L., Konowal, A., Freed, P. W., Westcott, J. Y. & Henson, P. M. 1998. Macrophages That Have Ingested Apoptotic Cells in Vitro Inhibit Proinflammatory Cytokine Production through Autocrine/Paracrine Mechanisms Involving Tgf-Beta, Pge2, and Paf. *Journal of Clinical Investigation,* **101,** 890-898.

Fallon, J., Reid, S., Kinyamu, R., Opole, I., Opole, R., Baratta, J., Korc, M., Endo, T. L., Duong, A., Nguyen, G., Karkehabadhi, M., Twardzik, D., Patel, S. & Loughlin, S. 2000. In Vivo Induction of Massive Proliferation, Directed Migration, and Differentiation of Neural Cells in the Adult Mammalian Brain. *Proceedings of the National Academy of Sciences of the United States of America,* **97,** 14686-14691.

Feinberg, A. P. & Vogelstein, B. 1983. A Technique for Radiolabeling DNA Restriction Endonuclease Fragments to High Specific Activity. *Analytical Biochemistry,* **132,** 6-13.

Felsenstein, J. 1985. Confidence Limits on Phylogenies: An Approach Using the Bootstrap. *Evolution,* **39,** 783-791.

Fernandes, A. M., Landeira-Fernandez, A. M., Souza-Santos, P., Carvalho-Alves, P. C. & Castilho, R. F. 2008. Quinolinate-Induced Rat Striatal Excitotoxicity Impairs

Endoplasmic Reticulum Ca2+-Atpase Function. *Neurochemical Research,* **33,** 1749-1758.

Fernandez-Borja, M., Janssen, L., Verwoerd, D., Hordijk, P. & Neefjes, J. 2005. Rhob Regulates Endosome Transport by Promoting Actin Assembly on Endosomal Membranes through Dia1. *Journal of Cell Science,* **118,** 2661-2670.

Field, R., Campion, S., Warren, C., Murray, C. & Cunningham, C. 2010. Systemic Challenge with the Tlr3 Agonist Poly I:C Induces Amplified Ifnalpha/Beta and Il-1beta Responses in the Diseased Brain and Exacerbates Chronic Neurodegeneration. *Brain, Behavior, and Immunity,* **24,** 996-1007.

Flanary, B. E., Sammons, N. W., Nguyen, C., Walker, D. & Streit, W. J. 2007. Evidence That Aging and Amyloid Promote Microglial Cell Senescence. *Rejuvenation Res,* **10,** 61-74.

Flanary, B. E. & Streit, W. J. 2005. Effects of Axotomy on Telomere Length, Telomerase Activity, and Protein in Activated Microglia. *Journal of Neuroscience Research,* **82,** 160-171.

Fleige, G., Nolte, C., Synowitz, M., Seeberger, F., Kettenmann, H. & Zimmer, C. 2001. Magnetic Labeling of Activated Microglia in Experimental Gliomas. *Neoplasia,* **3,** 489-499.

Fodor, S. P., Read, J. L., Pirrung, M. C., Stryer, L., Lu, A. T. & Solas, D. 1991. Light-Directed, Spatially Addressable Parallel Chemical Synthesis. *Science,* **251,** 767-773.

Ford, M. J., Burton, L. J., Li, H., Graham, C. H., Frobert, Y., Grassi, J., Hall, S. M. & Morris, R. J. 2002. A Marked Disparity between the Expression of Prion Protein and Its Message by Neurones of the Cns. *Neuroscience,* **111,** 533-551.

Franchi, L., Eigenbrod, T., Munoz-Planillo, R. & Nunez, G. 2009. The Inflammasome: A Caspase-1-Activation Platform That Regulates Immune Responses and Disease Pathogenesis. *Nature Immunology,* **10,** 241-247.

Franke, H., Schepper, C., Illes, P. & Krugel, U. 2007. Involvement of P2x and P2y Receptors in Microglial Activation in Vivo. *Purinergic Signal,* **3,** 435-445.

Fraser, H., Brown, K. L., Stewart, K., McConnell, I., McBride, P. & Williams, A. 1996. Replication of Scrapie in Spleens of Scid Mice Follows Reconstitution with Wild-Type Mouse Bone Marrow. *Journal of General Virology,* **77** 1935-1940.

Fraser, H. & Dickinson, A. G. 1967. Distribution of Experimentally Induced Scrapie Lesions in the Brain. *Nature,* **216,** 1310-1311.

Fraser, H. & Dickinson, A. G. 1968. The Sequential Development of the Brain Lesion of Scrapie in Three Strains of Mice. *Journal of Comparative Pathology,* **78,** 301-311.

Fraser, H. & Dickinson, A. G. 1985. Targeting of Scrapie Lesions and Spread of Agent Via the Retino-Tectal Projection. *Brain Research,* **346,** 32-41.

Freeman, T. C., Goldovsky, L., Brosch, M., van Dongen, S., Mazière, P., Grocock, R. J., Freilich, S., Thornton, J. & Enright, A. J. 2007. Construction, Visualisation, and Clustering of Transcription Networks from Microarray Expression Data. *PLoS Computational Biology,* **3,** 2032-2042.

Freire-de-Lima, C. G., Nascimento, D. O., Soares, M. B., Bozza, P. T., Castro-Faria-Neto, H. C., de Mello, F. G., DosReis, G. A. & Lopes, M. F. 2000. Uptake of Apoptotic Cells Drives the Growth of a Pathogenic Trypanosome in Macrophages. *Nature,* **403,** 199-203.

Fricker, M., Neher, J. J., Zhao, J. W., Thery, C., Tolkovsky, A. M. & Brown, G. C. 2012. Mfg-E8 Mediates Primary Phagocytosis of Viable Neurons During Neuroinflammation. *Journal of Neuroscience,* **32,** 2657-2666.

Frigg, R., Wenzel, A., Samardzija, M., Oesch, B., Wariwoda, H., Navarini, A. A., Seeliger, M. W., Tanimoto, N., Reme, C. & Grimm, C. 2006. The Prion Protein Is Neuroprotective against Retinal Degeneration in Vivo. *Experimental Eye Research,* **83,** 1350-1358.

Fuhrmann, M., Bittner, T., Jung, C. K., Burgold, S., Page, R. M., Mitteregger, G., Haass, C., LaFerla, F. M., Kretzschmar, H. & Herms, J. 2010. Microglial Cx3cr1 Knockout Prevents Neuron Loss in a Mouse Model of Alzheimer's Disease. *Nature Neuroscience,* **13,** 411-413.

Fukuda, S., Abematsu, M., Mori, H., Yanagisawa, M., Kagawa, T., Nakashima, K., Yoshimura, A. & Taga, T. 2007. Potentiation of Astrogliogenesis by Stat3-Mediated Activation of Bone Morphogenetic Protein-Smad Signaling in Neural Stem Cells. *Molecular and Cellular Biology,* **27,** 4931-4937.

Galea, I., Palin, K., Newman, T. A., Van Rooijen, N., Perry, V. H. & Boche, D. 2005. Mannose Receptor Expression Specifically Reveals Perivascular Macrophages in Normal, Injured, and Diseased Mouse Brain. *Glia,* **49,** 375-384.

Gallaher, Z. R., Ryu, V., Herzog, T., Ritter, R. C. & Czaja, K. 2012. Changes in Microglial Activation within the Hindbrain, Nodose Ganglia, and the Spinal Cord Following Subdiaphragmatic Vagotomy. *Neuroscience Letters,* **513,** 31-36.

Gao, L., Hidalgo-Figueroa, M., Escudero, L. M., Diaz-Martin, J., Lopez-Barneo, J. & Pascual, A. 2013. Age-Mediated Transcriptomic Changes in Adult Mouse Substantia Nigra. *PloS One,* **8,** e62456.

Garcia, C. M., Darland, D. C., Massingham, L. J. & D'Amore, P. A. 2004. Endothelial Cell-Astrocyte Interactions and Tgf Beta Are Required for Induction of Blood-Neural Barrier Properties. *Brain Research: Developmental Brain Research,* **152,** 25-38.

Gath, J., Bousset, L., Habenstein, B., Melki, R., Bockmann, A. & Meier, B. H. 2014. Unlike Twins: An Nmr Comparison of Two Alpha-Synuclein Polymorphs Featuring Different Toxicity. *PloS One,* **9,** e90659.

Gatti, S. & Bartfai, T. 1993. Induction of Tumor Necrosis Factor-A Mrna in the Brain after Peripheral Endotoxin Treatment: Comparison with Interleukin-1 Family and Interleukin-6. *Brain Research,* **624,** 291-294.

Gehlenborg, N., Hwang, D., Lee, I. Y., Yoo, H., Baxter, D., Petritis, B., Pitstick, R., Marzolf, B., Dearmond, S. J., Carlson, G. A. & Hood, L. 2009. The Prion Disease Database: A Comprehensive Transcriptome Resource for Systems Biology Research in Prion Diseases. *Database,* **17,** 17.

Gehrmann, J., Matsumoto, Y. & Kreutzberg, G. W. 1995. Microglia: Intrinsic Immuneffector Cell of the Brain. *Brain Research Reviews,* **20,** 269-287.

Geissmann, F., Jung, S. & Littman, D. R. 2003. Blood Monocytes Consist of Two Principal Subsets with Distinct Migratory Properties. *Immunity,* **19,** 71-82.

Gerber, J. S. & Mosser, D. M. 2001. Reversing Lipopolysaccharide Toxicity by Ligating the Macrophage Fc Gamma Receptors. *Journal of Immunology,* **166,** 6861-6868.

Getts, D. R., Terry, R. L., Getts, M. T., Müller, M., Rana, S., Shrestha, B., Radford, J., Van Rooijen, N., Campbell, I. L. & King, N. J. C. 2008. Ly6c+ "Inflammatory Monocytes" Are Microglial Precursors Recruited in a Pathogenic Manner in West Nile Virus Encephalitis. *The Journal of Experimental Medicine,* **205,** 2319-2337.

Gibbons, R. A. & Hunter, G. D. 1967. Nature of the Scrapie Agent. *Nature,* **215,** 1041-1043.

Gibbs, C. J. & Gajdusek, D. C. 1972. Transmission of Scrapie to the Cynomolgus Monkey (Macaca Fascicularis). *Nature,* **236,** 73-74.

Gibbs, C. J., Jr., Amyx, H. L., Bacote, A., Masters, C. L. & Gajdusek, D. C. 1980. Oral Transmission of Kuru, Creutzfeldt-Jakob Disease, and Scrapie to Nonhuman Primates. *Journal of Infectious Diseases,* **142,** 205-208.

Giese, A., Brown, D. R., Groschup, M. H., Feldmann, C., Haist, I. & Kretzschmar, H. A. 1998. Role of Microglia in Neuronal Cell Death in Prion Disease. *Brain Pathology,* **8,** 449-457.

Giese, A., Groschup, M. H., Hess, B. & Kretzschmar, H. A. 1995. Neuronal Cell Death in Scrapie-Infected Mice Is Due to Apoptosis. *Brain Pathology,* **5,** 213-221.

Gil, M. P., Bohn, E., O'Guin, A. K., Ramana, C. V., Levine, B., Stark, G. R., Virgin, H. W. & Schreiber, R. D. 2001. Biologic Consequences of Stat1-Independent Ifn Signaling. *Proceedings of the National Academy of Sciences of the United States of America,* **98,** 6680-6685.

Ginhoux, F., Greter, M., Leboeuf, M., Nandi, S., See, P., Gokhan, S., Mehler, M. F., Conway, S. J., Ng, L. G., Stanley, E. R., Samokhvalov, I. M. & Merad, M. 2010. Fate Mapping Analysis Reveals That Adult Microglia Derive from Primitive Macrophages. *Science,* **330,** 841-845.

Gitik, M., Liraz-Zaltsman, S., Oldenborg, P. A., Reichert, F. & Rotshenker, S. 2011. Myelin Down-Regulates Myelin Phagocytosis by Microglia and Macrophages through Interactions between Cd47 on Myelin and Sirpalpha (Signal Regulatory Protein-Alpha) on Phagocytes. *Journal of Neuroinflammation,* **8,** 24.

Godbout, J. P., Chen, J., Abraham, J., Richwine, A. F., Berg, B. M., Kelley, K. W. & Johnson, R. W. 2005. Exaggerated Neuroinflammation and Sickness Behavior in Aged Mice after Activation of the Peripheral Innate Immune System. *Federation of American Societies for Experimental Biology Journal*, **19,** 1329-1331.

Godsave, S. F., Wille, H., Pierson, J., Prusiner, S. B. & Peters, P. J. 2013. Plasma Membrane Invaginations Containing Clusters of Full-Length Prpsc Are an Early Form of Prion-Associated Neuropathology in Vivo. *Neurobiology of Aging,* **34,** 1621-1631.

Gomez-Nicola, D., Fransen, N. L., Suzzi, S. & Perry, V. H. 2013. Regulation of Microglial Proliferation During Chronic Neurodegeneration. *Journal of Neuroscience,* **33,** 2481-2493.

Gomez-Nicola, D., Schetters, S. T. & Hugh Perry, V. 2014. Differential Role of Ccr2 in the Dynamics of Microglia and Perivascular Macrophages During Prion Disease. *Glia*, **62,** 1041-1052.

Gordon, W. S., Brownlee, A. & Wilson, D. R. 1940. Studies in Louping-Ill, Tick-Borne Fever and Scrapie, in Proceedings: 3rd International Congress of Microbiology, (New York). *NY)*, **3,** 362-363.

Goshen, I., Kreisel, T., Ben-Menachem-Zidon, O., Licht, T., Weidenfeld, J., Ben-Hur, T. & Yirmiya, R. 2007. Brain Interleukin-1 Mediates Chronic Stress-Induced Depression in Mice Via Adrenocortical Activation and Hippocampal Neurogenesis Suppression. *Molecular Psychiatry,* **13,** 717-728.

Grathwohl, S., Kälin, R., Bolmont, T., Radde, R., Odenthal, J., Mazzella, M., Käser, S., Mathews, P. M., Eldh, T., Wolburg, H., Kohsaka, S., Heppner, F. L. & Jucker, M. 2009. Formation and Maintenance of [Beta]-Amyloid Plaques in the Absence of Microglia. *Alzheimer's and Dementia,* **5,** 439-440.

Gray, B. C., Siskova, Z., Perry, V. H. & O'Connor, V. 2009. Selective Presynaptic Degeneration in the Synaptopathy Associated with Me7-Induced Hippocampal Pathology. *Neurobiology of Disease,* **35,** 63-74.

Green, R. P., Cohn, S. M., Sacchettini, J. C., Jackson, K. E. & Gordon, J. I. 1992. The Mouse Intestinal Fatty Acid Binding Protein Gene: Nucleotide Sequence, Pattern of Developmental and Regional Expression, and Proposed Structure of Its Protein Product. *DNA and Cell Biology,* **11,** 31-41.

Greenlee, J. J., Nicholson, E. M., Smith, J. D., Kunkle, R. A. & Hamir, A. N. 2012. Susceptibility of Cattle to the Agent of Chronic Wasting Disease from Elk after Intracranial Inoculation. *Journal of Veterinary Diagnostic Investigation,* **24,** 1087-1093.

Greenlee, J. J., Smith, J. D. & Kunkle, R. A. 2011. White-Tailed Deer Are Susceptible to the Agent of Sheep Scrapie by Intracerebral Inoculation. *Veterinary Research,* **42,** 107.

Greig, J. R. 1940. Scrapie: Observations on the Transmission of the Disease by Mediate Contact. *Veterinary Journal 1,* **96,** 203-206.

Griffin, W. S., Sheng, J. G., Roberts, G. W. & Mrak, R. E. 1995. Interleukin-1 Expression in Different Plaque Types in Alzheimer's Disease: Significance in Plaque Evolution. *Journal of Neuropathology and Experimental Neurology,* **54,** 276-281.

Griffith, J. S. 1967. Nature of the Scrapie Agent: Self-Replication and Scrapie. *Nature,* **215,** 1043-1044.

Guillemin, G. J., Smythe, G., Takikawa, O. & Brew, B. J. 2005. Expression of Indoleamine 2,3-Dioxygenase and Production of Quinolinic Acid by Human Microglia, Astrocytes, and Neurons. *Glia,* **49,** 15-23.

Guillerme-Bosselut, F., Forestier, L., Jayat-Vignoles, C., Vilotte, J. L., Popa, I., Portoukalian, J., Le Dur, A., Laude, H., Julien, R. & Gallet, P. F. 2009. Glycosylation-Related Gene Expression Profiling in the Brain and Spleen of Scrapie-Affected Mouse. *Glycobiology,* **19,** 879-889.

Guiroy, D. C., Wakayama, I., Liberski, P. P. & Gajdusek, D. C. 1994. Relationship of Microglia and Scrapie Amyloid-Immunoreactive Plaques in Kuru, Creutzfeldt-Jakob Disease and Gerstmann-Sträussler Syndrome. *Acta Neuropathologica,* **87,** 526-530.

Guo, J. L., Covell, D. J., Daniels, J. P., Iba, M., Stieber, A., Zhang, B., Riddle, D. M., Kwong, L. K., Xu, Y., Trojanowski, J. Q. & Lee, V. M. 2013. Distinct Alpha-Synuclein Strains Differentially Promote Tau Inclusions in Neurons. *Cell,* **154,** 103-117.

Guo, J. L. & Lee, V. M. 2013. Neurofibrillary Tangle-Like Tau Pathology Induced by Synthetic Tau Fibrils in Primary Neurons over-Expressing Mutant Tau. *FEBS Letters,* **587,** 717-723.

Gurtan, A. M. & D'Andrea, A. D. 2006. Dedicated to the Core: Understanding the Fanconi Anemia Complex. *DNA Repair,* **5,** 1119-1125.

Haig, D. A. & Clarke, M. C. 1971. Multiplication of the Scrapie Agent. *Nature,* **234,** 106-107.

Hakem, A., Sanchez-Sweatman, O., You-Ten, A., Duncan, G., Wakeham, A., Khokha, R. & Mak, T. W. 2005. Rhoc Is Dispensable for Embryogenesis and Tumor Initiation but Essential for Metastasis. *Genes & Development,* **19,** 1974-1979.

Halfmann, R., Jarosz, D. F., Jones, S. K., Chang, A., Lancaster, A. K. & Lindquist, S. 2012. Prions Are a Common Mechanism for Phenotypic Inheritance in Wild Yeasts. *Nature,* **482,** 363-368.

Hamir, A. N., Kunkle, R. A., Cutlip, R. C., Miller, J. M., O'Rourke, K. I., Williams, E. S., Miller, M. W., Stack, M. J., Chaplin, M. J. & Richt, J. A. 2005. Experimental Transmission of Chronic Wasting Disease Agent from Mule Deer to Cattle by the Intracerebral Route. *Journal of Veterinary Diagnostic Investigation,* **17,** 276-281.

Hamir, A. N., Kunkle, R. A., Cutlip, R. C., Miller, J. M., Williams, E. S. & Richt, J. A. 2006. Transmission of Chronic Wasting Disease of Mule Deer to Suffolk Sheep Following

Intracerebral Inoculation. *Journal of Veterinary Diagnostic Investigation,* **18,** 558-565.

Hamir, A. N., Miller, J. M., Cutlip, R. C., Kunkle, R. A., Jenny, A. L., Stack, M. J., Chaplin, M. J. & Richt, J. A. 2004. Transmission of Sheep Scrapie to Elk (Cervus Elaphus Nelsoni) by Intracerebral Inoculation: Final Outcome of the Experiment. *Journal of Veterinary Diagnostic Investigation,* **16,** 316-321.

Hamir, A. N., Miller, J. M., Kunkle, R. A., Hall, S. M. & Richt, J. A. 2007. Susceptibility of Cattle to First-Passage Intracerebral Inoculation with Chronic Wasting Disease Agent from White-Tailed Deer. *Veterinary Pathology,* **44,** 487-493.

Hanisch, U.-K. & Gertig, U. 2014. Microglial Diversity by Responses and Responders. *Frontiers in Cellular Neuroscience,* **8,** 1-9.

Hanisch, U. K. 2013. Functional Diversity of Microglia - How Heterogeneous Are They to Begin With? *Frontiers in Cellular Neuroscience,* **7,** 1-18.

Harrington, D. P. & Fleming, T. R. 1982. A Class of Rank Test Procedures for Censored Survival Data. *Biometrika,* **69,** 553-566.

Hart, A. D., Wyttenbach, A., Perry, V. H. & Teeling, J. L. 2012. Age Related Changes in Microglial Phenotype Vary between Cns Regions: Grey Versus White Matter Differences. *Brain, Behavior, and Immunity,* **26,** 754-765.

Hart, B. L. 1988. Biological Basis of the Behavior of Sick Animals. *Neuroscience and Biobehavioral Reviews,* **12,** 123-137.

Haynes, S. E., Hollopeter, G., Yang, G., Kurpius, D., Dailey, M. E., Gan, W. B. & Julius, D. 2006. The P2y12 Receptor Regulates Microglial Activation by Extracellular Nucleotides. *Nature Neuroscience,* **9,** 1512-1519.

Heiman, M., Schaefer, A., Gong, S., Peterson, J. D., Day, M., Ramsey, K. E., Suarez-Farinas, M., Schwarz, C., Stephan, D. A., Surmeier, D. J., Greengard, P. & Heintz, N. 2008. A Translational Profiling Approach for the Molecular Characterization of Cns Cell Types. *Cell,* **135,** 738-748.

Heldin, C. H., Miyazono, K. & ten Dijke, P. 1997. Tgf-Beta Signalling from Cell Membrane to Nucleus through Smad Proteins. *Nature,* **390,** 465-471.

Heller-Stilb, B., van Roeyen, C., Rascher, K., Hartwig, H. G., Huth, A., Seeliger, M. W., Warskulat, U. & Haussinger, D. 2002. Disruption of the Taurine Transporter Gene (Taut) Leads to Retinal Degeneration in Mice. *FASEB Journal,* **16,** 231-233.

Henry, C. J., Huang, Y., Wynne, A. M. & Godbout, J. P. 2009. Peripheral Lipopolysaccharide (Lps) Challenge Promotes Microglial Hyperactivity in Aged Mice That Is Associated with Exaggerated Induction of Both Pro-Inflammatory Il-1beta and Anti-Inflammatory Il-10 Cytokines. *Brain, Behavior, and Immunity,* **23,** 309-317.

Heyes, M. P., Achim, C. L., Wiley, C. A., Major, E. O., Saito, K. & Markey, S. P. 1996. Human Microglia Convert L-Tryptophan into the Neurotoxin Quinolinic Acid. *Biochemical Journal,* **320** 595-597.

Hibbs, J. B. 2002. Infection and Nitric Oxide. *The Journal of Infectious Diseases,* **185,** S9-17.

Hickey, W. F. & Kimura, H. 1988. Perivascular Microglial Cells of the Cns Are Bone Marrow-Derived and Present Antigen in Vivo. *Science,* **239,** 290-292.

Hilton, K. J., Cunningham, C., Reynolds, R. A. & Perry, V. H. 2013. Early Hippocampal Synaptic Loss Precedes Neuronal Loss and Associates with Early Behavioural Deficits in Three Distinct Strains of Prion Disease. *PloS One,* **8,** e68062.

Hines, D. J., Hines, R. M., Mulligan, S. J. & Macvicar, B. A. 2009. Microglia Processes Block the Spread of Damage in the Brain and Require Functional Chloride Channels. *Glia,* **57,** 1610-1618.

Hoebe, K., Du, X., Georgel, P., Janssen, E., Tabeta, K., Kim, S. O., Goode, J., Lin, P., Mann, N., Mudd, S., Crozat, K., Sovath, S., Han, J. & Beutler, B. 2003. Identification of Lps2 as a Key Transducer of Myd88-Independent Tir Signalling. *Nature,* **424,** 743-748.

Hoeck, J. D., Jandke, A., Blake, S. M., Nye, E., Spencer-Dene, B., Brandner, S. & Behrens, A. 2010. Fbw7 Controls Neural Stem Cell Differentiation and Progenitor Apoptosis Via Notch and C-Jun. *Nature Neuroscience,* **13,** 1365-1372.

Hoek, R. M., Ruuls, S. R., Murphy, C. A., Wright, G. J., Goddard, R., Zurawski, S. M., Blom, B., Homola, M. E., Streit, W. J., Brown, M. H., Barclay, A. N. & Sedgwick, J. D. 2000. Down-Regulation of the Macrophage Lineage through Interaction with Ox2 (Cd200). *Science,* **290,** 1768-1771.

Holman, H. H. & Pattison, I. H. 1943. Further Evidence on the Significance of Vacuolated Nerve Cells in the Medulla Oblongata of Sheep Affected with Scrapie. *Journal of Comparative Pathology and Therapeutics,* **53,** 231-236.

Hsieh, C. L., Kim, C. C., Ryba, B. E., Niemi, E. C., Bando, J. K., Locksley, R. M., Liu, J., Nakamura, M. C. & Seaman, W. E. 2013. Traumatic Brain Injury Induces Macrophage Subsets in the Brain. *European Journal of Immunology,* **43,** 2010-2022.

Huang, C., Xia, P. Y. & Zhou, H. 2010. Sustained Expression of Tdp-43 and Fus in Motor Neurons in Rodent's Lifetime. *International Journal of Biological Sciences,* **6,** 396-406.

Hughes, M. M., Field, R. H., Perry, V. H., Murray, C. L. & Cunningham, C. 2010. Microglia in the Degenerating Brain Are Capable of Phagocytosis of Beads and of Apoptotic Cells, but Do Not Efficiently Remove Prp(Sc), Even Upon Lps Stimulation. *Glia,* **58,** 2017-2030.

Hughes, P. M., Botham, M. S., Frentzel, S., Mir, A. & Perry, V. H. 2002. Expression of Fractalkine (Cx3cl1) and Its Receptor, Cx3cr1, During Acute and Chronic Inflammation in the Rodent Cns. *Glia,* **37,** 314-327.

Hughes, V. 2012. Microglia: The Constant Gardeners. *Nature,* **485,** 570-572.

Hunter, G. D., Gibbons, R. A., Kimberlin, R. H. & Millson, G. C. 1969. Further Studies of the Infectivity and Stability of Extracts and Homogenates Derived from Scrapie Affected Mouse Brains. *Journal of Comparative Pathology,* **79,** 101-108.

Hunter, G. D., Kimberlin, R. H., Millson, G. C. & Gibbons, R. A. 1971. An Experimental Examination of the Scrapie Agent in Cell Membrane Mixtures: I. Stability and Physicochemical Properties of the Scrapie Agent. *Journal of Comparative Pathology,* **81,** 23-32.

Hunter, G. D. & Millson, G. C. 1967. Attempts to Release the Scrapie Agent from Tissue Debris. *Journal of Comparative Pathology,* **77,** 301-307.

Hunter, N., Goldmann, W., Foster, J. D., Cairns, D. & Smith, G. 1997a. Natural Scrapie and Prp Genotype: Case-Control Studies in British Sheep. *Veterinary Record,* **141,** 137-140.

Hunter, N., Moore, L., Hosie, B. D., Dingwall, W. S. & Greig, A. 1997b. Association between Natural Scrapie and Prp Genotype in a Flock of Suffolk Sheep in Scotland. *Veterinary Record,* **140,** 59-63.

Huynh, M. L., Fadok, V. A. & Henson, P. M. 2002. Phosphatidylserine-Dependent Ingestion of Apoptotic Cells Promotes Tgf-Beta1 Secretion and the Resolution of Inflammation. *Journal of Clinical Investigation,* **109,** 41-50.

Hwang, D., Lee, I. Y., Yoo, H., Gehlenborg, N., Cho, J.-H., Petritis, B., Baxter, D., Pitstick, R., Young, R., Spicer, D., Price, N. D., Hohmann, J. G., DeArmond, S. J., Carlson, G. A. & Hood, L. E. 2009. A Systems Approach to Prion Disease. *Molecular Systems Biology,* **5,** 252.

Hynes, R. O. 1992. Integrins: Versatility, Modulation, and Signaling in Cell Adhesion. *Cell,* **69,** 11-25.

Iken, S., Bachy, V., Gourdain, P., Lim, A., Gregoire, S., Chaigneau, T., Aucouturier, P. & Carnaud, C. 2011. Th2-Polarised Prp-Specific Transgenic T-Cells Confer Partial Protection against Murine Scrapie. *PLoS Pathogens,* **7,** e1002216.

Inoue, E., Deguchi-Tawarada, M., Togawa, A., Matsui, C., Arita, K., Katahira-Tayama, S., Sato, T., Yamauchi, E., Oda, Y. & Takai, Y. 2009. Synaptic Activity Prompts Gamma-Secretase-Mediated Cleavage of Epha4 and Dendritic Spine Formation. *Journal of Cell Biology,* **185,** 551-564.

Inui, M., Manfrin, A., Mamidi, A., Martello, G., Morsut, L., Soligo, S., Enzo, E., Moro, S., Polo, S., Dupont, S., Cordenonsi, M. & Piccolo, S. 2011. Usp15 Is a Deubiquitylating Enzyme for Receptor-Activated Smads. *Nature Cell Biology,* **13,** 1368-1375.

Irizarry, R. A., Hobbs, B., Collin, F., Beazer-Barclay, Y. D., Antonellis, K. J., Scherf, U. & Speed, T. P. 2003. Exploration, Normalization, and Summaries of High Density Oligonucleotide Array Probe Level Data. *Biostatistics (Oxford, England),* **4,** 249-264.

Ishibashi, D., Atarashi, R., Fuse, T., Nakagaki, T., Yamaguchi, N., Satoh, K., Honda, K. & Nishida, N. 2012. Protective Role of Interferon Regulatory Factor 3-Mediated Signaling against Prion Infection. *Journal of Virology,* **86,** 4947-4955.

Ishikura, N., Clever, J. L., Bouzamondo-Bernstein, E., Samayoa, E., Prusiner, S. B., Huang, E. J. & DeArmond, S. J. 2005. Notch-1 Activation and Dendritic Atrophy in Prion Disease. *Proceedings of the National Academy of Sciences of the United States of America,* **102,** 886-891.

Islam, R., Yang, L., Sah, M., Kannan, K., Anamani, D., Vijayan, C., Kwok, J., Cantino, M. E., Beal, M. F. & Fridell, Y. W. 2012. A Neuroprotective Role of the Human Uncoupling Protein 2 (Hucp2) in a Drosophila Parkinson's Disease Model. *Neurobiology of Disease,* **46,** 137-146.

Jamieson, E., Jeffrey, M., Ironside, J. W. & Fraser, J. R. 2001. Apoptosis and Dendritic Dysfunction Precede Prion Protein Accumulation in 87v Scrapie. *Neuroreport,* **12,** 2147-2153.

Jantzen, P. T., Connor, K. E., DiCarlo, G., Wenk, G. L., Wallace, J. L., Rojiani, A. M., Coppola, D., Morgan, D. & Gordon, M. N. 2002. Microglial Activation and Beta -Amyloid Deposit Reduction Caused by a Nitric Oxide-Releasing Nonsteroidal Anti-Inflammatory Drug in Amyloid Precursor Protein Plus Presenilin-1 Transgenic Mice. *Journal of Neuroscience,* **22,** 2246-2254.

Jeffrey, M., Goodsir, C. M., Bruce, M. E., McBride, P. A. & Fraser, J. R. 1997. In Vivo Toxicity of Prion Protein in Murine Scrapie: Ultrastructural and Immunogold Studies. *Neuropathology and Applied Neurobiology,* **23,** 93-101.

Jeffrey, M., Halliday, W. G., Bell, J., Johnston, A. R., MacLeod, N. K., Ingham, C., Sayers, A. R., Brown, D. A. & Fraser, J. R. 2000. Synapse Loss Associated with Abnormal Prp Precedes Neuronal Degeneration in the Scrapie-Infected Murine Hippocampus. *Neuropathology and Applied Neurobiology,* **26,** 41-54.

Jeffrey, M., Martin, S., Barr, J., Chong, A. & Fraser, J. R. 2001. Onset of Accumulation of Prpresin Murine Me7 Scrapie in Relation to Pathological and Prp Immunohistochemical Changes. *Journal of Comparative Pathology,* **124,** 20-28.

Jeffrey, M. & Wells, G. A. 1988. Spongiform Encephalopathy in a Nyala (Tragelaphus Angasi). *Veterinary Pathology,* **25,** 398-399.

Jenmalm, M. C., Cherwinski, H., Bowman, E. P., Phillips, J. H. & Sedgwick, J. D. 2006. Regulation of Myeloid Cell Function through the Cd200 Receptor. *Journal of Immunology,* **176,** 191-199.

Jensen, L. J., Kuhn, M., Stark, M., Chaffron, S., Creevey, C., Muller, J., Doerks, T., Julien, P., Roth, A., Simonovic, M., Bork, P. & von Mering, C. 2009. String 8--a Global View on Proteins and Their Functional Interactions in 630 Organisms. *Nucleic Acids Research,* **37,** D412-416.

Jeong, H. K., Ji, K. M., Kim, B., Kim, J., Jou, I. & Joe, E. H. 2010. Inflammatory Responses Are Not Sufficient to Cause Delayed Neuronal Death in Atp-Induced Acute Brain Injury. *PloS One,* **5,** e13756.

Ji, K., Akgul, G., Wollmuth, L. P. & Tsirka, S. E. 2013. Microglia Actively Regulate the Number of Functional Synapses. *PloS One,* **8,** e56293.

Johnston, A. R., Fraser, J. R., Jeffrey, M. & MacLeod, N. 1998. Synaptic Plasticity in the Ca1 Area of the Hippocampus of Scrapie-Infected Mice. *Neurobiology of Disease,* **5,** 188-195.

Joly, S., Francke, M., Ulbricht, E., Beck, S., Seeliger, M., Hirrlinger, P., Hirrlinger, J., Lang, K. S., Zinkernagel, M., Odermatt, B., Samardzija, M., Reichenbach, A., Grimm, C. & Reme, C. E. 2009. Cooperative Phagocytes: Resident Microglia and Bone Marrow Immigrants Remove Dead Photoreceptors in Retinal Lesions. *American Journal of Pathology,* **174,** 2310-2323.

Jucker, M. & Walker, L. C. 2013. Self-Propagation of Pathogenic Protein Aggregates in Neurodegenerative Diseases. *Nature,* **501,** 45-51.

Jutila, M. A., Kroese, F. G., Jutila, K. L., Stall, A. M., Fiering, S., Herzenberg, L. A., Berg, E. L. & Butcher, E. C. 1988. Ly-6c Is a Monocyte/Macrophage and Endothelial Cell Differentiation Antigen Regulated by Interferon-Gamma. *European Journal of Immunology,* **18,** 1819-1826.

Kakkar, R., Hei, H., Dobner, S. & Lee, R. T. 2012. Interleukin 33 as a Mechanically Responsive Cytokine Secreted by Living Cells. *Journal of Biological Chemistry,* **287,** 6941-6948.

Kascsak, R. J., Rubenstein, R., Merz, P. A., Carp, R. I., Wisniewski, H. M. & Diringer, H. 1985. Biochemical Differences among Scrapie-Associated Fibrils Support the Biological Diversity of Scrapie Agents. *Journal of General Virology,* **66 (Pt 8),** 1715-1722.

Kastin, A. J., Akerstrom, V. & Pan, W. 2003. Circulating Tgf-Beta1 Does Not Cross the Intact Blood-Brain Barrier. *Journal of Molecular Neuroscience,* **21,** 43-48.

Kauffmann, A., Gentleman, R. & Huber, W. 2009. Arrayqualitymetrics--a Bioconductor Package for Quality Assessment of Microarray Data. *Bioinformatics (Oxford, England),* **25,** 415-416.

Kauppinen, T. M., Higashi, Y., Suh, S. W., Escartin, C., Nagasawa, K. & Swanson, R. A. 2008. Zinc Triggers Microglial Activation. *Journal of Neuroscience,* **28,** 5827-5835.

Kawai, T., Adachi, O., Ogawa, T., Takeda, K. & Akira, S. 1999. Unresponsiveness of Myd88-Deficient Mice to Endotoxin. *Immunity,* **11,** 115-122.

Kayed, R., Canto, I., Breydo, L., Rasool, S., Lukacsovich, T., Wu, J., Albay, R., 3rd, Pensalfini, A., Yeung, S., Head, E., Marsh, J. L. & Glabe, C. 2010. Conformation Dependent Monoclonal Antibodies Distinguish Different Replicating Strains or Conformers of Prefibrillar Abeta Oligomers. *Molecular Neurodegeneration,* **5,** 57.

Kearns, A. E., Donohue, M. M., Sanyal, B. & Demay, M. B. 2001. Cloning and Characterization of a Novel Protein Kinase That Impairs Osteoblast Differentiation in Vitro. *Journal of Biological Chemistry,* **276,** 42213-42218.

Keeler, C. E. 1924. The Inheritance of a Retinal Abnormality in White Mice. *Proceedings of the National Academy of Sciences of the United States of America,* **10,** 329-333.

Keeler, C. E. 1931. *The Laboratory Mouse; Its Origin, Heredity, and Culture, by Clyde E. Keeler,* Cambridge, Harvard university press, Page: 32.

Kennedy, D. W. & Abkowitz, J. L. 1998. Mature Monocytic Cells Enter Tissues and Engraft. *Proceedings of the National Academy of Sciences,* **95,** 14944-14949.

Kent, S., Bluthe, R. M., Dantzer, R., Hardwick, A. J., Kelley, K. W., Rothwell, N. J. & Vannice, J. L. 1992. Different Receptor Mechanisms Mediate the Pyrogenic and Behavioral Effects of Interleukin 1. *Proceedings of the National Academy of Sciences of the United States of America,* **89,** 9117-9120.

Kettenmann, H., Kirchhoff, F. & Verkhratsky, A. 2013. Microglia: New Roles for the Synaptic Stripper. *Neuron,* **77,** 10-18.

Kierdorf, K., Erny, D., Goldmann, T., Sander, V., Schulz, C., Perdiguero, E. G., Wieghofer, P., Heinrich, A., Riemke, P., Holscher, C., Muller, D. N., Luckow, B., Brocker, T., Debowski, K., Fritz, G., Opdenakker, G., Diefenbach, A., Biber, K., Heikenwalder, M., Geissmann, F., Rosenbauer, F. & Prinz, M. 2013. Microglia Emerge from Erythromyeloid Precursors Via Pu.1- and Irf8-Dependent Pathways. *Nature Neuroscience,* **16,** 273-280.

Kigerl, K. A., Gensel, J. C., Ankeny, D. P., Alexander, J. K., Donnelly, D. J. & Popovich, P. G. 2009. Identification of Two Distinct Macrophage Subsets with Divergent Effects Causing Either Neurotoxicity or Regeneration in the Injured Mouse Spinal Cord. *Journal of Neuroscience,* **29,** 13435-13444.

Kim, C., Cho, E. D., Kim, H. K., You, S., Lee, H. J., Hwang, D. & Lee, S. J. 2014. Beta1-Integrin-Dependent Migration of Microglia in Response to Neuron-Released Alpha-Synuclein. *Experimental and Molecular Medicine,* **46,** e91.

Kim, H. O., Snyder, G. P., Blazey, T. M., Race, R. E., Chesebro, B. & Skinner, P. J. 2008. Prion Disease Induced Alterations in Gene Expression in Spleen and Brain Prior to Clinical Symptoms. *Advances and Applications in Bioinformatics and Chemistry,* **1,** 29-50.

Kim, J. I., Cali, I., Surewicz, K., Kong, Q., Raymond, G. J., Atarashi, R., Race, B., Qing, L., Gambetti, P., Caughey, B. & Surewicz, W. K. 2010. Mammalian Prions Generated from Bacterially Expressed Prion Protein in the Absence of Any Mammalian Cofactors. *Journal of Biological Chemistry,* **285,** 14083-14087.

Kim, J. I., Jin, J. K., Choi, E. K., Spinner, D., Rubenstein, R., Carp, R. I. & Kim, Y. S. 2007. Increased Expression and Localization of Cyclooxygenase-2 in Astrocytes of Scrapie-Infected Mice. *Journal of Neuroimmunology,* **187,** 74-82.

Kim, M. H., Choi, J., Yang, J., Chung, W., Kim, J. H., Paik, S. K., Kim, K., Han, S., Won, H., Bae, Y. S., Cho, S. H., Seo, J., Bae, Y. C., Choi, S. Y. & Kim, E. 2009. Enhanced Nmda Receptor-Mediated Synaptic Transmission, Enhanced Long-Term Potentiation, and Impaired Learning and Memory in Mice Lacking Irsp53. *Journal of Neuroscience,* **29,** 1586-1595.

Kim, S., Elkon, K. B. & Ma, X. 2004. Transcriptional Suppression of Interleukin-12 Gene Expression Following Phagocytosis of Apoptotic Cells. *Immunity,* **21,** 643-653.

Kimberlin, R. H. 1976. The Pathogenesis of Scrapie in Mice. *Slow Virus Diseases of Animals and Man.* Amsterdam: North Holland Publishing Company, Page: 325-357.

Kimberlin, R. H., Cole, S. & Walker, C. A. 1987. Pathogenesis of Scrapie Is Faster When Infection Is Intraspinal Instead of Intracerebral. *Microbial Pathogenesis,* **2,** 405-415.

Kimberlin, R. H., Hall, S. M. & Walker, C. A. 1983. Pathogenesis of Mouse Scrapie. Evidence for Direct Neural Spread of Infection to the Cns after Injection of Sciatic Nerve. *Journal of the Neurological Sciences,* **61,** 315-325.

Kimberlin, R. H., Millson, G. C. & Hunter, G. D. 1971a. An Experimental Examination of the Scrapie Agent in Cell Membrane Mixtures. 3. Studies of the Operational Size. *Journal of Comparative Pathology,* **81,** 383-391.

Kimberlin, R. H., Millson, G. C. & Mackenzie, A. 1971b. Biochemical and Histopathological Changes in the Brains of Mice Inoculated with Scrapie by the Intraperitoneal Route. *Journal of Comparative Pathology,* **81,** 469-477.

Kimberlin, R. H. & Walker, C. A. 1978. Pathogenesis of Mouse Scrapie: Effect of Route of Inoculation on Infectivity Titres and Dose-Response Curves. *Journal of Comparative Pathology,* **88,** 39-47.

Kimberlin, R. H. & Walker, C. A. 1979. Pathogenesis of Mouse Scrapie: Dynamics of Agent Replication in Spleen, Spinal Cord and Brain after Infection by Different Routes. *Journal of Comparative Pathology,* **89,** 551-562.

Kimberlin, R. H. & Walker, C. A. 1980. Pathogenesis of Mouse Scrapie: Evidence for Neural Spread of Infection to the Cns. *The Journal of General Virology,* **51,** 183-187.

Kimberlin, R. H. & Walker, C. A. 1986. Pathogenesis of Scrapie (Strain 263k) in Hamsters Infected Intracerebrally, Intraperitoneally or Intraocularly. *Journal of General Virology,* **67** 255-263.

Kitazawa, M., Oddo, S., Yamasaki, T. R., Green, K. N. & LaFerla, F. M. 2005. Lipopolysaccharide-Induced Inflammation Exacerbates Tau Pathology by a Cyclin-Dependent Kinase 5-Mediated Pathway in a Transgenic Model of Alzheimer's Disease. *Journal of Neuroscience,* **25,** 8843-8853.

Kitzing, T. M., Wang, Y., Pertz, O., Copeland, J. W. & Grosse, R. 2010. Formin-Like 2 Drives Amoeboid Invasive Cell Motility Downstream of Rhoc. *Oncogene,* **29,** 2441-2448.

Kiyota, T., Ingraham, K. L., Swan, R. J., Jacobsen, M. T., Andrews, S. J. & Ikezu, T. 2012. Aav Serotype 2/1-Mediated Gene Delivery of Anti-Inflammatory Interleukin-10 Enhances Neurogenesis and Cognitive Function in App+Ps1 Mice. *Gene Therapy,* **19,** 724-733.

Kiyota, T., Okuyama, S., Swan, R. J., Jacobsen, M. T., Gendelman, H. E. & Ikezu, T. 2010. Cns Expression of Anti-Inflammatory Cytokine Interleukin-4 Attenuates Alzheimer's Disease-Like Pathogenesis in App+Ps1 Bigenic Mice. *The FASEB Journal,* **24,** 3093-3102.

Klein, R. S., Lin, E., Zhang, B., Luster, A. D., Tollett, J., Samuel, M. A., Engle, M. & Diamond, M. S. 2005. Neuronal Cxcl10 Directs Cd8+ T-Cell Recruitment and Control of West Nile Virus Encephalitis. *Journal of Virology,* **79,** 11457-11466.

Kluger, M. J. 1979. Temperature Regulation, Fever, and Disease. *International Review of Physiology,* **20,** 209-251.

Kocisko, D. A., Come, J. H., Priola, S. A., Chesebro, B., Raymond, G. J., Lansbury, P. T. & Caughey, B. 1994. Cell-Free Formation of Protease-Resistant Prion Protein. *Nature,* **370,** 471-474.

Kohman, R. A., Bhattacharya, T. K., Kilby, C., Bucko, P. & Rhodes, J. S. 2013. Effects of Minocycline on Spatial Learning, Hippocampal Neurogenesis and Microglia in Aged and Adult Mice. *Behavioural Brain Research,* **242,** 17-24.

Kong, Q., Huang, S., Zou, W., Vanegas, D., Wang, M., Wu, D., Yuan, J., Zheng, M., Bai, H., Deng, H., Chen, K., Jenny, A. L., O'Rourke, K., Belay, E. D., Schonberger, L. B., Petersen, R. B., Sy, M. S., Chen, S. G. & Gambetti, P. 2005. Chronic Wasting Disease of Elk: Transmissibility to Humans Examined by Transgenic Mouse Models. *Journal of Neuroscience,* **25,** 7944-7949.

Konold, T., Spiropoulos, J., Chaplin, M. J., Stack, M. J., Hawkins, S. A. C., Wilesmith, J. W. & Wells, G. A. H. 2013. Unsuccessful Oral Transmission of Scrapie from British Sheep to Cattle. *Veterinary Record***,** 118.

Konsman, J. P., Kelley, K. & Dantzer, R. 1999. Temporal and Spatial Relationships between Lipopolysaccharide-Induced Expression of Fos, Interleukin-1 B and Inducible Nitric Oxide Synthase in Rat Brain. *Neuroscience,* **89,** 535-548.

Kovac, A., Erickson, M. A. & Banks, W. A. 2011. Brain Microvascular Pericytes Are Immunoactive in Culture: Cytokine, Chemokine, Nitric Oxide, and Lrp-1 Expression in Response to Lipopolysaccharide. *Journal of Neuroinflammation,* **8,** 139.

Kozai, T. D., Vazquez, A. L., Weaver, C. L., Kim, S. G. & Cui, X. T. 2012. In Vivo Two-Photon Microscopy Reveals Immediate Microglial Reaction to Implantation of Microelectrode through Extension of Processes. *J Neural Eng,* **9,** 066001.

Kreutzberg, G. W., Graeber, M. B. & Streit, W. J. 1989. Neuron-Glial Relationship During Regeneration of Motorneurons. *Metabolic Brain Disease,* **4,** 81-85.

Krieglstein, K., Henheik, P., Farkas, L., Jaszai, J., Galter, D., Krohn, K. & Unsicker, K. 1998. Glial Cell Line-Derived Neurotrophic Factor Requires Transforming Growth Factor-Beta for Exerting Its Full Neurotrophic Potential on Peripheral and Cns Neurons. *Journal of Neuroscience,* **18,** 9822-9834.

Kristensson, K., Feuerstein, B., Taraboulos, A., Hyun, W. C., Prusiner, S. B. & DeArmond, S. J. 1993. Scrapie Prions Alter Receptor-Mediated Calcium Responses in Cultured Cells. *Neurology,* **43,** 2335-2341.

Krupenko, S. A. & Oleinik, N. V. 2002. 10-Formyltetrahydrofolate Dehydrogenase, One of the Major Folate Enzymes, Is Down-Regulated in Tumor Tissues and Possesses Suppressor Effects on Cancer Cells. *Cell Growth and Differentiation,* **13,** 227-236.

Kubota, Y., Takubo, K., Shimizu, T., Ohno, H., Kishi, K., Shibuya, M., Saya, H. & Suda, T. 2009. M-Csf Inhibition Selectively Targets Pathological Angiogenesis and Lymphangiogenesis. *Journal of Experimental Medicine,* **206,** 1089-1102.

Kullberg, S., Aldskogius, H. & Ulfhake, B. 2001. Microglial Activation, Emergence of Ed1-Expressing Cells and Clusterin Upregulation in the Aging Rat Cns, with Special Reference to the Spinal Cord. *Brain Research,* **899,** 169-186.

Kutzbach, C. & Stokstad, E. L. R. 1971. [199] 10-Formyl Tetrahydrofolate: Nadp Oxidoreductase. *In:* Donald, B. M. & Lemuel, D. W. (eds.) *Methods in Enzymology.* Academic Press, Page: 793-798.

Ladeby, R., Wirenfeldt, M., Garcia-Ovejero, D., Fenger, C., Dissing-Olesen, L., Dalmau, I. & Finsen, B. 2005. Microglial Cell Population Dynamics in the Injured Adult Central Nervous System. *Brain Research: Brain Research Reviews,* **48,** 196-206.

Lai, A. Y., Dhami, K. S., Dibal, C. D. & Todd, K. G. 2011. Neonatal Rat Microglia Derived from Different Brain Regions Have Distinct Activation Responses. *Neuron Glia Biology,* **7,** 5-16.

Lai, A. Y., Dibal, C. D., Armitage, G. A., Winship, I. R. & Todd, K. G. 2013. Distinct Activation Profiles in Microglia of Different Ages: A Systematic Study in Isolated Embryonic to Aged Microglial Cultures. *Neuroscience,* **254,** 185-195.

Lancet, T. 1926. Obituary (Sir Stewart Stockman, M.R.C.V.S.). *The Lancet,* **207,** 1171-1174.

Lander, H. M., Tauras, J. M., Ogiste, J. S., Hori, O., Moss, R. A. & Schmidt, A. M. 1997. Activation of the Receptor for Advanced Glycation End Products Triggers a P21(Ras)-Dependent Mitogen-Activated Protein Kinase Pathway Regulated by Oxidant Stress. *Journal of Biological Chemistry,* **272,** 17810-17814.

Landriscina, M., Bagala, C., Mandinova, A., Soldi, R., Micucci, I., Bellum, S., Prudovsky, I. & Maciag, T. 2001. Copper Induces the Assembly of a Multiprotein Aggregate Implicated in the Release of Fibroblast Growth Factor 1 in Response to Stress. *Journal of Biological Chemistry,* **276,** 25549-25557.

Langevin, C., Andreoletti, O., Le Dur, A., Laude, H. & Beringue, V. 2011. Marked Influence of the Route of Infection on Prion Strain Apparent Phenotype in a Scrapie Transgenic Mouse Model. *Neurobiology of Disease,* **41,** 219-225.

Langford-Smith, A., Wilkinson, F. L., Langford-Smith, K. J., Holley, R. J., Sergijenko, A., Howe, S. J., Bennett, W. R., Jones, S. A., Wraith, J., Merry, C. L., Wynn, R. F. & Bigger, B. W. 2012. Hematopoietic Stem Cell and Gene Therapy Corrects Primary Neuropathology and Behavior in Mucopolysaccharidosis Iiia Mice. *Molecular Therapy,* **20,** 1610-1621.

Langston, J. W., Ballard, P., Tetrud, J. W. & Irwin, I. 1983. Chronic Parkinsonism in Humans Due to a Product of Meperidine-Analog Synthesis. *Science,* **219,** 979-980.

Langston, J. W., Forno, L. S., Tetrud, J., Reeves, A. G., Kaplan, J. A. & Karluk, D. 1999. Evidence of Active Nerve Cell Degeneration in the Substantia Nigra of Humans Years after 1-Methyl-4-Phenyl-1,2,3,6-Tetrahydropyridine Exposure. *Annals of Neurology,* **46,** 598-605.

Lashkari, D. A., DeRisi, J. L., McCusker, J. H., Namath, A. F., Gentile, C., Hwang, S. Y., Brown, P. O. & Davis, R. W. 1997. Yeast Microarrays for Genome Wide Parallel Genetic and Gene Expression Analysis. *Proceedings of the National Academy of Sciences of the United States of America,* **94,** 13057-13062.

Lassmann, H., Zimprich, F., Vass, K. & Hickey, W. F. 1991. Microglial Cells Are a Component of the Perivascular Glia Limitans. *Journal of Neuroscience Research,* **28,** 236-243.

Latarjet, R., Muel, B., Haig, D. A., Clarke, M. C. & Alper, T. 1970. Inactivation of the Scrapie Agent by near Monochromatic Ultraviolet Light. *Nature,* **227,** 1341-1343.

Lattin, J. E., Schroder, K., Su, A. I., Walker, J. R., Zhang, J., Wiltshire, T., Saijo, K., Glass, C. K., Hume, D. A., Kellie, S. & Sweet, M. J. 2008. Expression Analysis of G Protein-Coupled Receptors in Mouse Macrophages. *Immunome Research,* **4,** 1745-7580.

Lawson, L. J., Frost, L., Risbridger, J., Fearn, S. & Perry, V. H. 1994. Quantification of the Mononuclear Phagocyte Response to Wallerian Degeneration of the Optic Nerve. *Journal of Neurocytology,* **23,** 729-744.

Lawson, L. J., Perry, V. H., Dri, P. & Gordon, S. 1990. Heterogeneity in the Distribution and Morphology of Microglia in the Normal Adult Mouse Brain. *Neuroscience,* **39,** 151-170.

Lawson, L. J., Perry, V. H. & Gordon, S. 1992. Turnover of Resident Microglia in the Normal Adult Mouse Brain. *Neuroscience,* **48,** 405-415.

Laye, S., Parnet, P., Goujon, E. & Dantzer, R. 1994. Peripheral Administration of Lipopolysaccharide Induces the Expression of Cytokine Transcripts in the Brain and Pituitary of Mice. *Brain Research: Molecular Brain Research,* **27,** 157-162.

Lee, C. K., Weindruch, R. & Prolla, T. A. 2000. Gene-Expression Profile of the Ageing Brain in Mice. *Nature Genetics,* **25,** 294-297.

Lee, Y. J., Jin, J. K., Jeong, B. H., Carp, R. I. & Kim, Y. S. 2006. Increased Expression of Glial Cell Line-Derived Neurotrophic Factor (Gdnf) in the Brains of Scrapie-Infected Mice. *Neuroscience Letters,* **410,** 178-182.

Legname, G., Baskakov, I. V., Nguyen, H. O., Riesner, D., Cohen, F. E., DeArmond, S. J. & Prusiner, S. B. 2004. Synthetic Mammalian Prions. *Science,* **305,** 673-676.

Legname, G., Nguyen, H. O., Baskakov, I. V., Cohen, F. E., Dearmond, S. J. & Prusiner, S. B. 2005. Strain-Specified Characteristics of Mouse Synthetic Prions. *Proceedings of the National Academy of Sciences of the United States of America,* **102,** 2168-2173.

Lehmann, J. M., Lenhard, J. M., Oliver, B. B., Ringold, G. M. & Kliewer, S. A. 1997. Peroxisome Proliferator-Activated Receptors A and Γ Are Activated by Indomethacin and Other Non-Steroidal Anti-Inflammatory Drugs. *Journal of Biological Chemistry,* **272,** 3406-3410.

Lemstra, A. W., Groen in't Woud, J. C. M., Hoozemans, J. J. M., van Haastert, E. S., Rozemuller, A. J. M., Eikelenboom, P. & van Gool, W. A. 2007. Microglia Activation in Sepsis: A Case-Control Study. *Journal of Neuroinflammation,* **4,** 4-4.

Lenz, K. M., Nugent, B. M., Haliyur, R. & McCarthy, M. M. 2013. Microglia Are Essential to Masculinization of Brain and Behavior. *Journal of Neuroscience,* **33,** 2761-2772.

Leopold, J. G. 1759. *Nützliche Und Auf Die Erfahrung Gegründete Einleitung Zu Der Landwirthschaft: Fünf Theile. Mit Kupfer Und Baurissen*, Günther, Page: 348.

Levi, G., Minghetti, L. & Aloisi, F. 1998. Regulation of Prostanoid Synthesis in Microglial Cells and Effects of Prostaglandin E2 on Microglial Functions. *Biochimie,* **80,** 899-904.

Lewicki, H., Tishon, A., Homann, D., Mazarguil, H., Laval, F., Asensio, V. C., Campbell, I. L., DeArmond, S., Coon, B., Teng, C., Gairin, J. E. & Oldstone, M. B. A. 2003. T Cells Infiltrate the Brain in Murine and Human Transmissible Spongiform Encephalopathies. *Journal of Virology,* **77,** 3799-3808.

Lewin, P. 1972. Scrapie : An Infective Peptide ? *The Lancet,* **299,** 748.

Leymarie, F. & Levine, M. D. 1992. Fast Raster Scan Distance Propagation on the Discrete Rectangular Lattice. *CVGIP: Image Underst.,* **55,** 84-94.

Li, J., Wang, J. J., Peng, Q., Chen, C., Humphrey, M. B., Heinecke, J. & Zhang, S. X. 2012. Macrophage Metalloelastase (Mmp-12) Deficiency Mitigates Retinal Inflammation and Pathological Angiogenesis in Ischemic Retinopathy. *PloS One,* **7,** e52699.

Liang, K. J., Lee, J. E., Wang, Y. D., Ma, W., Fontainhas, A. M., Fariss, R. N. & Wong, W. T. 2009. Regulation of Dynamic Behavior of Retinal Microglia by Cx3cr1 Signaling. *Investigative Ophthalmology and Visual Science,* **50,** 4444-4451.

Lim, G. P., Yang, F., Chu, T., Chen, P., Beech, W., Teter, B., Tran, T., Ubeda, O., Ashe, K. H., Frautschy, S. A. & Cole, G. M. 2000. Ibuprofen Suppresses Plaque Pathology and

Inflammation in a Mouse Model for Alzheimer's Disease. *Journal of Neuroscience,* **20,** 5709-5714.

Lim, S. H., Park, E., You, B., Jung, Y., Park, A. R., Park, S. G. & Lee, J. R. 2013. Neuronal Synapse Formation Induced by Microglia and Interleukin 10. *PloS One,* **8,** e81218.

Linsley, P. S. & Ledbetter, J. A. 1993. The Role of the Cd28 Receptor During T Cell Responses to Antigen. *Annual Review of Immunology,* **11,** 191-212.

Liu, B., Chen, H., Johns, T. G. & Neufeld, A. H. 2006. Epidermal Growth Factor Receptor Activation: An Upstream Signal for Transition of Quiescent Astrocytes into Reactive Astrocytes after Neural Injury. *Journal of Neuroscience,* **26,** 7532-7540.

Liu, B. S., Janssen, H. L. & Boonstra, A. 2012. Type I and Iii Interferons Enhance Il-10r Expression on Human Monocytes and Macrophages, Resulting in Il-10-Mediated Suppression of Tlr-Induced Il-12. *European Journal of Immunology,* **11,** 201142360.

Liu, Y., Wong, T. P., Aarts, M., Rooyakkers, A., Liu, L., Lai, T. W., Wu, D. C., Lu, J., Tymianski, M., Craig, A. M. & Wang, Y. T. 2007. Nmda Receptor Subunits Have Differential Roles in Mediating Excitotoxic Neuronal Death Both in Vitro and in Vivo. *Journal of Neuroscience,* **27,** 2846-2857.

Lodge, P. A. & Sriram, S. 1996. Regulation of Microglial Activation by Tgf-Beta, Il-10, and Csf-1. *Journal of Leukocyte Biology,* **60,** 502-508.

Loeuillet, C., Boelle, P. Y., Lemaire-Vieille, C., Baldazza, M., Naquet, P., Chambon, P., Cesbron-Delauw, M. F., Valleron, A. J., Gagnon, J. & Cesbron, J. Y. 2010. Sex Effect in Mouse and Human Prion Disease. *Journal of Infectious Diseases,* **202,** 648-654.

Loke, P. n. & Allison, J. P. 2003. Pd-L1 and Pd-L2 Are Differentially Regulated by Th1 and Th2 Cells. *Proceedings of the National Academy of Sciences of the United States of America,* **100,** 5336-5341.

London, A., Itskovich, E., Benhar, I., Kalchenko, V., Mack, M., Jung, S. & Schwartz, M. 2011. Neuroprotection and Progenitor Cell Renewal in the Injured Adult Murine Retina Requires Healing Monocyte-Derived Macrophages. *Journal of Experimental Medicine,* **208,** 23-39.

Lu, X. & Richardson, P. M. 1991. Inflammation near the Nerve Cell Body Enhances Axonal Regeneration. *Journal of Neuroscience,* **11,** 972-978.

Lucassen, P. J., Williams, A., Chung, W. C. & Fraser, H. 1995. Detection of Apoptosis in Murine Scrapie. *Neuroscience Letters,* **198,** 185-188.

M'Fadyean, J. 1918. Scrapie. *Journal of Comparative Pathology and Therapeutics,* **31,** 102-131.

M'Gowan, J. P. 1918. Scrapie. *Journal of Comparative Pathology and Therapeutics,* **31,** 278-290.

Macdowell, E. C., Allen, E. & Macdowell, C. G. 1927. The Prenatal Growth of the Mouse. *Journal of General Physiology,* **11,** 57-70.

MacLullich, A. M. J., Beaglehole, A., Hall, R. J. & Meagher, D. J. 2009. Delirium and Long-Term Cognitive Impairment. *International Review of Psychiatry,* **21,** 30-42.

Mahal, S. P., Browning, S., Li, J., Suponitsky-Kroyter, I. & Weissmann, C. 2010. Transfer of a Prion Strain to Different Hosts Leads to Emergence of Strain Variants. *Proceedings of the National Academy of Sciences of the United States of America,* **107,** 22653-22658.

Majer, A., Medina, S. J., Niu, Y., Abrenica, B., Manguiat, K. J., Frost, K. L., Philipson, C. S., Sorensen, D. L. & Booth, S. A. 2012. Early Mechanisms of Pathobiology Are Revealed by Transcriptional Temporal Dynamics in Hippocampal Ca1 Neurons of Prion Infected Mice. *PLoS Pathogens,* **8,** e1003002.

Makarava, N., Kovacs, G. G., Bocharova, O., Savtchenko, R., Alexeeva, I., Budka, H., Rohwer, R. G. & Baskakov, I. V. 2010. Recombinant Prion Protein Induces a New Transmissible Prion Disease in Wild-Type Animals. *Acta Neuropathologica,* **119,** 177-187.

Manson, J. C., Clarke, A. R., Hooper, M. L., Aitchison, L., McConnell, I. & Hope, J. 1994a. 129/Ola Mice Carrying a Null Mutation in Prp That Abolishes Mrna Production Are Developmentally Normal. *Molecular Neurobiology,* **8,** 121-127.

Manson, J. C., Clarke, A. R., McBride, P. A., McConnell, I. & Hope, J. 1994b. Prp Gene Dosage Determines the Timing but Not the Final Intensity or Distribution of Lesions in Scrapie Pathology. *Neurodegeneration: A Journal for Neurodegenerative Disorders, Neuroprotection, and Neuroregeneration,* **3,** 331-340.

Mantovani, A., Sica, A. & Locati, M. 2007. New Vistas on Macrophage Differentiation and Activation. *European Journal of Immunology,* **37,** 14-16.

Mantovani, A., Sica, A., Sozzani, S., Allavena, P., Vecchi, A. & Locati, M. 2004. The Chemokine System in Diverse Forms of Macrophage Activation and Polarization. *Trends in Immunology,* **25,** 677-686.

Manuelidis, L., Fritch, W. & Xi, Y.-G. 1997. Evolution of a Strain of Cjd That Induces Bse-Like Plaques. *Science,* **277,** 94-98.

Marella, M. & Chabry, J. 2004. Neurons and Astrocytes Respond to Prion Infection by Inducing Microglia Recruitment. *Journal of Neuroscience,* **24,** 620-627.

Marella, M., Gaggioli, C., Batoz, M., Deckert, M., Tartare-Deckert, S. & Chabry, J. 2005. Pathological Prion Protein Exposure Switches on Neuronal Mitogen-Activated Protein Kinase Pathway Resulting in Microglia Recruitment. *Journal of Biological Chemistry,* **280,** 1529-1534.

Marín-Teva, J. L., Dusart, I., Colin, C., Gervais, A., Van Rooijen, N. & Mallat, M. 2004. Microglia Promote the Death of Developing Purkinje Cells. *Neuron,* **41,** 535-547.

Martin, D. P., Schmidt, R. E., DiStefano, P. S., Lowry, O. H., Carter, J. G. & Johnson, E. M., Jr. 1988. Inhibitors of Protein Synthesis and Rna Synthesis Prevent Neuronal Death Caused by Nerve Growth Factor Deprivation. *Journal of Cell Biology,* **106,** 829-844.

Martinez, F. O., Helming, L. & Gordon, S. 2009. Alternative Activation of Macrophages: An Immunologic Functional Perspective. *Annual Review of Immunology,* **27,** 451-483.

Martinez, F. O., Sica, A., Mantovani, A. & Locati, M. 2008. Macrophage Activation and Polarization. *Frontiers in Bioscience,* **13,** 453-461.

Martinon, F. & Tschopp, J. 2007. Inflammatory Caspases and Inflammasomes: Master Switches of Inflammation. *Cell Death and Differentiation,* **14,** 10-22.

Massengale, M., Wagers, A. J., Vogel, H. & Weissman, I. L. 2005. Hematopoietic Cells Maintain Hematopoietic Fates Upon Entering the Brain. *Journal of Experimental Medicine,* **201,** 1579-1589.

McClintick, J. N., Jerome, R. E., Nicholson, C. R., Crabb, D. W. & Edenberg, H. J. 2003. Reproducibility of Oligonucleotide Arrays Using Small Samples. *BMC Genomics,* **4,** 4-4.

McGeer, E. G. & McGeer, P. L. 1999. Brain Inflammation in Alzheimer Disease and the Therapeutic Implications. *Current Pharmaceutical Design,* **5,** 821-836.

McGeer, P. L., Kawamata, T., Walker, D. G., Akiyama, H., Tooyama, I. & McGeer, E. G. 1993. Microglia in Degenerative Neurological Disease. *Glia,* **7,** 84-92.

McGeer, P. L. & McGeer, E. G. 2008. Glial Reactions in Parkinson's Disease. *Movement Disorders,* **23,** 474-483.

McGeer, P. L., Schwab, C., Parent, A. & Doudet, D. 2003. Presence of Reactive Microglia in Monkey Substantia Nigra Years after 1-Methyl-4-Phenyl-1,2,3,6-Tetrahydropyridine Administration. *Annals of Neurology,* **54,** 599-604.

McKercher, S. R., Torbett, B. E., Anderson, K. L., Henkel, G. W., Vestal, D. J., Baribault, H., Klemsz, M., Feeney, A. J., Wu, G. E., Paige, C. J. & Maki, R. A. 1996. Targeted Disruption of the Pu.1 Gene Results in Multiple Hematopoietic Abnormalities. *EMBO Journal,* **15,** 5647-5658.

McKinley, M. P., Bolton, D. C. & Prusiner, S. B. 1983. A Protease-Resistant Protein Is a Structural Component of the Scrapie Prion. *Cell,* **35,** 57-62.

McLean, A. R. & Bostock, C. J. 2000. Scrapie Infections Initiated at Varying Doses: An Analysis of 117 Titration Experiments. *Philosophical Transactions of the Royal Society of London. Series B: Biological Sciences,* **355,** 1043-1050.

Mechnikov, I. 1908. *Nobel Lecture: On the Present State of the Question of Immunity in Infectious Diseases* [Online]. Stockholm: Nobelprize.org. Nobel Media AB 2013. Available:

http://www.nobelprize.org/nobel_prizes/medicine/laureates/1908/mechnikov-lecture.html [Accessed Web. 25 Feb 2014.

Meda, L., Cassatella, M. A., Szendrei, G. I., Otvos, L., Jr., Baron, P., Villalba, M., Ferrari, D. & Rossi, F. 1995. Activation of Microglial Cells by Beta-Amyloid Protein and Interferon-Gamma. *Nature,* **374,** 647-650.

Mehrotra, P., Riley, J. P., Patel, R., Li, F., Voss, L. & Goenka, S. 2011. Parp-14 Functions as a Transcriptional Switch for Stat6-Dependent Gene Activation. *Journal of Biological Chemistry,* **286,** 1767-1776.

Miele, G., Jeffrey, M., Turnbull, D., Manson, J. & Clinton, M. 2002. Ablation of Cellular Prion Protein Expression Affects Mitochondrial Numbers and Morphology. *Biochemical and Biophysical Research Communications,* **291,** 372-377.

Mildner, A., Schmidt, H., Nitsche, M., Merkler, D., Hanisch, U.-K., Mack, M., Heikenwalder, M., Bruck, W., Priller, J. & Prinz, M. 2007. Microglia in the Adult Brain Arise from Ly-6chiccr2+ Monocytes Only under Defined Host Conditions. *Nature Neuroscience,* **10,** 1544-1553.

Miller, M. W., Williams, E. S., Hobbs, N. T. & Wolfe, L. L. 2004. Environmental Sources of Prion Transmission in Mule Deer. *Emerging Infectious Diseases,* **10,** 1003-1006.

Miller, N. E. 1964. Some Psychophysiological Studies of Motivation and of the Behavioral-Effects of Illness. *Bulletin of the British Psychological Society,* **17,** 1-20.

Millson, G. C., Hunter, G. D. & Kimberlin, R. H. 1971. An Experimental Examination of the Scrapie Agent in Cell Membrane Mixtures: Ii. The Associations of Scrapie Activity with Membrane Fractions. *Journal of Comparative Pathology,* **81,** 255-265.

Millson, G. C., Kimberlin, R. H., Jane Manning, E. & Collis, S. C. 1979. Early Distribution of Radioactive Liposomes and Scrapie Infectivity in Mouse Tissues Following Administration by Different Routes. *Veterinary Microbiology,* **4,** 89-99.

Minghetti, l. 2004. Cyclooxygenase-2 (Cox-2) in Inflammatory and Degenerative Brain Diseases. *Journal of Neuropathology & Experimental Neurology,* **63,** 901-910.

Minghetti, L. & Levi, G. 1998. Microglia as Effector Cells in Brain Damage and Repair: Focus on Prostanoids and Nitric Oxide. *Progress in Neurobiology,* **54,** 99-125.

Minghetti, L. & Pocchiari, M. 2007. Cyclooxygenase-2, Prostaglandin E2, and Microglial Activation in Prion Diseases. *International Review of Neurobiology,* **82,** 265-275.

Minin, A. A., Kulik, A. V., Gyoeva, F. K., Li, Y., Goshima, G. & Gelfand, V. I. 2006. Regulation of Mitochondria Distribution by Rhoa and Formins. *Journal of Cell Science,* **119,** 659-670.

Mironov, A., Jr., Latawiec, D., Wille, H., Bouzamondo-Bernstein, E., Legname, G., Williamson, R. A., Burton, D., DeArmond, S. J., Prusiner, S. B. & Peters, P. J. 2003. Cytosolic Prion Protein in Neurons. *Journal of Neuroscience,* **23,** 7183-7193.

Miyamoto, A., Wake, H., Moorhouse, A. J. & Nabekura, J. 2013. Microglia and Synapse Interactions: Fine Tuning Neural Circuits and Candidate Molecules. *Frontiers in Cellular Neuroscience,* **7,** 1-6.

Moller, J. C., Klein, M. A., Haas, S., Jones, L. L., Kreutzberg, G. W. & Raivich, G. 1996. Regulation of Thrombospondin in the Regenerating Mouse Facial Motor Nucleus. *Glia,* **17,** 121-132.

Monje, M. L., Toda, H. & Palmer, T. D. 2003. Inflammatory Blockade Restores Adult Hippocampal Neurogenesis. *Science,* **302,** 1760-1765.

Moody, L. R., Herbst, A. J., Yoo, H. S., Vanderloo, J. P. & Aiken, J. M. 2009. Comparative Prion Disease Gene Expression Profiling Using the Prion Disease Mimetic, Cuprizone. *Prion,* **3,** 99-109.

Moore, K. W., de Waal Malefyt, R., Coffman, R. L. & O'Garra, A. 2001. Interleukin-10 and the Interleukin-10 Receptor. *Annual Review of Immunology,* **19,** 683-765.

Moore, R. C., Hope, J., McBride, P. A., McConnell, I., Selfridge, J., Melton, D. W. & Manson, J. C. 1998. Mice with Gene Targetted Prion Protein Alterations Show That Prnp, Sinc and Prni Are Congruent. *Nature Genetics,* **18,** 118-125.

Mosmann, T. R. & Coffman, R. L. 1989. Th1 and Th2 Cells: Different Patterns of Lymphokine Secretion Lead to Different Functional Properties. *Annual Review of Immunology,* **7,** 145-173.

Mosser, D. M. 2003. The Many Faces of Macrophage Activation. *Journal of Leukocyte Biology,* **73,** 209-212.

Mosser, D. M. & Edwards, J. P. 2008. Exploring the Full Spectrum of Macrophage Activation. *Nature Reviews: Immunology,* **8,** 958-969.

Mouihate, A. 2014. Tlr4-Mediated Brain Inflammation Halts Neurogenesis: Impact of Hormonal Replacement Therapy. *Frontiers in Cellular Neuroscience,* **8,** 146.

Mould, D. L., Smith, W. & Dawson, A. M. 1965. Centrifugation Studies on the Infectivities of Cellular Fractions Derived from Mouse Brain Infected with Scrapie (Suffolk Strain). *Journal of General Microbiology,* **40,** 71-79.

Mouta Carreira, C., LaVallee, T. M., Tarantini, F., Jackson, A., Lathrop, J. T., Hampton, B., Burgess, W. H. & Maciag, T. 1998. S100a13 Is Involved in the Regulation of Fibroblast Growth Factor-1 and P40 Synaptotagmin-1 Release in Vitro. *Journal of Biological Chemistry,* **273,** 22224-22231.

Mouton, P. R., Long, J. M., Lei, D. L., Howard, V., Jucker, M., Calhoun, M. E. & Ingram, D. K. 2002. Age and Gender Effects on Microglia and Astrocyte Numbers in Brains of Mice. *Brain Research,* **956,** 30-35.

Mowen, K. A., Tang, J., Zhu, W., Schurter, B. T., Shuai, K., Herschman, H. R. & David, M. 2001. Arginine Methylation of Stat1 Modulates Ifnalpha/Beta-Induced Transcription. *Cell,* **104,** 731-741.

Murray, C., Sanderson, D. J., Barkus, C., Deacon, R. M., Rawlins, J. N., Bannerman, D. M. & Cunningham, C. 2012. Systemic Inflammation Induces Acute Working Memory Deficits in the Primed Brain: Relevance for Delirium. *Neurobiology of Aging,* **33,** 603-616. e603.

Murray, C. L., Skelly, D. T. & Cunningham, C. 2011. Exacerbation of Cns Inflammation and Neurodegeneration by Systemic Lps Treatment Is Independent of Circulating Il-1beta and Il-6. *Journal of Neuroinflammation,* **8,** 50.

Nahrendorf, M., Swirski, F. K., Aikawa, E., Stangenberg, L., Wurdinger, T., Figueiredo, J. L., Libby, P., Weissleder, R. & Pittet, M. J. 2007. The Healing Myocardium Sequentially Mobilizes Two Monocyte Subsets with Divergent and Complementary Functions. *Journal of Experimental Medicine,* **204,** 3037-3047.

Nakagawa, T., Guichard, A., Castro, C. P., Xiao, Y., Rizen, M., Zhang, H. Z., Hu, D., Bang, A., Helms, J., Bier, E. & Derynck, R. 2005. Characterization of a Human Rhomboid Homolog, P100hrho/Rhbdf1, Which Interacts with Tgf-Alpha Family Ligands. *Developmental Dynamics,* **233,** 1315-1331.

Naslavsky, N., Stein, R., Yanai, A., Friedlander, G. & Taraboulos, A. 1997. Characterization of Detergent-Insoluble Complexes Containing the Cellular Prion Protein and Its Scrapie Isoform. *Journal of Biological Chemistry,* **272,** 6324-6331.

Neumann, H., Kotter, M. R. & Franklin, R. J. M. 2009. Debris Clearance by Microglia: An Essential Link between Degeneration and Regeneration. *Brain,* **132,** 288-295.

Neumann, H. & Wekerle, H. 2013. Brain Microglia: Watchdogs with Pedigree. *Nature Neuroscience,* **16,** 253-255.

Neumann, J., Sauerzweig, S., Ronicke, R., Gunzer, F., Dinkel, K., Ullrich, O., Gunzer, M. & Reymann, K. G. 2008. Microglia Cells Protect Neurons by Direct Engulfment of Invading Neutrophil Granulocytes: A New Mechanism of Cns Immune Privilege. *Journal of Neuroscience,* **28,** 5965-5975.

Newsom, D. M., Liggitt, H. D., O'Rourke, K., Zhuang, D., Schneider, D. A. & Harrington, R. D. 2011. Cytokine Antibody Array Analysis in Brain and Periphery of Scrapie-Infected Tg338 Mice. *Comparative Immunology, Microbiology and Infectious Diseases,* **34,** 387-397.

Ng, E. L., Ng, J. J., Liang, F. & Tang, B. L. 2009. Rab22b Is Expressed in the Cns Astroglia Lineage and Plays a Role in Epidermal Growth Factor Receptor Trafficking in A431 Cells. *Journal of Cellular Physiology,* **221,** 716-728.

Nguyen, C., Rocha, D., Granjeaud, S., Baldit, M., Bernard, K., Naquet, P. & Jordan, B. R. 1995a. Differential Gene Expression in the Murine Thymus Assayed by Quantitative Hybridization of Arrayed Cdna Clones. *Genomics,* **29,** 207-216.

Nguyen, J., Baldwin, M. A., Cohen, F. E. & Prusiner, S. B. 1995b. Prion Protein Peptides Induce .Alpha.-Helix To .Beta.-Sheet Conformational Transitions. *Biochemistry,* **34,** 4186-4192.

Nikodemova, M. & Watters, J. J. 2012. Efficient Isolation of Live Microglia with Preserved Phenotypes from Adult Mouse Brain. *Journal of Neuroinflammation,* **9,** 1742-2094.

Nimmerjahn, A., Kirchhoff, F. & Helmchen, F. 2005. Resting Microglial Cells Are Highly Dynamic Surveillants of Brain Parenchyma in Vivo. *Science,* **308,** 1314-1318.

Nissl, F. 1899. Ueber Einige Beziehungen Zwishcen Nerven Zellerkrankungen Und Gliosen Erscheinnungen Bei Verschiedenen Psychosen. In: 24. Wanderversammlung Der Südwestdeutschen Neurologen Und Irrenärzte in Baden-Baden. *Archiv für Psychiatrie und Nervenkrankheiten,* **32,** 657-676.

Njie, E. G., Boelen, E., Stassen, F. R., Steinbusch, H. W., Borchelt, D. R. & Streit, W. J. 2012. Ex Vivo Cultures of Microglia from Young and Aged Rodent Brain Reveal Age-Related Changes in Microglial Function. *Neurobiology of Aging,* **33,** 195-195, e191-112.

Noda, U. 1921. A Study of Nissl's Staebchenzellen in the Cerebral Cortex of General Paresis, Senile Dementia, Epilepsy. Glioma, Tuberculous, Meningitis and Delirium Tremens. *The Journal of Nervous and Mental Disease,* **53,** 161-216.

Norden, D. M., Fenn, A. M., Dugan, A. & Godbout, J. P. 2014. Tgfbeta Produced by Il-10 Redirected Astrocytes Attenuates Microglial Activation. *Glia,* **62,** 881-895.

Norton, W. T. & Poduslo, S. E. 1973. Myelination in Rat Brain: Changes in Myelin Composition During Brain Maturation. *Journal of Neurochemistry,* **21,** 759-773.

O'Connor, J. C., André, C., Wang, Y., Lawson, M. A., Szegedi, S. S., Lestage, J., Castanon, N., Kelley, K. W. & Dantzer, R. 2009. Interferon-Γ and Tumor Necrosis Factor-A Mediate the Upregulation of Indoleamine 2,3-Dioxygenase and the Induction of Depressive-Like Behavior in Mice in Response to Bacillus Calmette-Guérin. *The Journal of Neuroscience,* **29,** 4200-4209.

Oesch, B., Westaway, D., Walchli, M., McKinley, M. P., Kent, S. B., Aebersold, R., Barry, R. A., Tempst, P., Teplow, D. B., Hood, L. E. & et al. 1985. A Cellular Gene Encodes Scrapie Prp 27-30 Protein. *Cell,* **40,** 735-746.

Ohtsuji, M., Katsuoka, F., Kobayashi, A., Aburatani, H., Hayes, J. D. & Yamamoto, M. 2008. Nrf1 and Nrf2 Play Distinct Roles in Activation of Antioxidant Response Element-Dependent Genes. *Journal of Biological Chemistry,* **283,** 33554-33562.

Ong, W. Y., Leong, S. K., Garey, L. J., Tan, K. K. & Zhang, H. F. 1995. A Light and Electron Microscopic Study of Hla-Dr Positive Cells in the Human Cerebral Cortex and Subcortical White Matter. *Journal für Hirnforschung,* **36,** 553-563.

Orre, M., Kamphuis, W., Osborn, L. M., Jansen, A. H., Kooijman, L., Bossers, K. & Hol, E. M. 2014. Isolation of Glia from Alzheimer's Mice Reveals Inflammation and Dysfunction. *Neurobiology of Aging,* **35,** 2746-2760.

Outram, G. W. 1976. The Pathogenesis of Scrapie in Mice. *Frontiers of Biology,* **44,** 325-357.

Outram, G. W., Dickinson, A. G. & Fraser, H. 1973. Developmental Maturation of Susceptibility to Scrapie in Mice. *Nature,* **241,** 536-537.

Pahl, H. L. 1999. Activators and Target Genes of Rel/Nf-Kappab Transcription Factors. *Oncogene,* **18,** 6853-6866.

Palin, K., Cunningham, C., Forse, P., Perry, V. H. & Platt, N. 2008. Systemic Inflammation Switches the Inflammatory Cytokine Profile in Cns Wallerian Degeneration. *Neurobiology of Disease,* **30,** 19-29.

Pandi-Perumal, S. R., Srinivasan, V., Maestroni, G. J., Cardinali, D. P., Poeggeler, B. & Hardeland, R. 2006. Melatonin: Nature's Most Versatile Biological Signal? *FEBS Journal,* **273,** 2813-2838.

Pandi-Perumal, S. R., Trakht, I., Srinivasan, V., Spence, D. W., Maestroni, G. J., Zisapel, N. & Cardinali, D. P. 2008. Physiological Effects of Melatonin: Role of Melatonin Receptors and Signal Transduction Pathways. *Progress in Neurobiology,* **85,** 335-353.

Paolicelli, R. C., Bolasco, G., Pagani, F., Maggi, L., Scianni, M., Panzanelli, P., Giustetto, M., Ferreira, T. A., Guiducci, E., Dumas, L., Ragozzino, D. & Gross, C. T. 2011. Synaptic Pruning by Microglia Is Necessary for Normal Brain Development. *Science (New York, N.Y.),* **333,** 1456-1458.

Papadopoulos, V., Lecanu, L., Brown, R. C., Han, Z. & Yao, Z. X. 2006. Peripheral-Type Benzodiazepine Receptor in Neurosteroid Biosynthesis, Neuropathology and Neurological Disorders. *Neuroscience,* **138,** 749-756.

Pappano, W. N., Scott, I. C., Clark, T. G., Eddy, R. L., Shows, T. B. & Greenspan, D. S. 1998. Coding Sequence and Expression Patterns of Mouse Chordin and Mapping of the Cognate Mouse Chrd and Human Chrd Genes. *Genomics,* **52,** 236-239.

Paradis, E., Clavel, S., Bouillaud, F., Ricquier, D. & Richard, D. 2003. Uncoupling Protein 2: A Novel Player in Neuroprotection. *Trends in Molecular Medicine,* **9,** 522-525.

Parakalan, R., Jiang, B., Nimmi, B., Janani, M., Jayapal, M., Lu, J., Tay, S. S., Ling, E. A. & Dheen, S. T. 2012. Transcriptome Analysis of Amoeboid and Ramified Microglia Isolated from the Corpus Callosum of Rat Brain. *BMC Neuroscience,* **13,** 64.

Parkhurst, C. N., Yang, G., Ninan, I., Savas, J. N., Yates, J. R., 3rd, Lafaille, J. J., Hempstead, B. L., Littman, D. R. & Gan, W. B. 2013. Microglia Promote Learning-Dependent Synapse Formation through Brain-Derived Neurotrophic Factor. *Cell,* **155,** 1596-1609.

Parkinson, H., Kapushesky, M., Shojatalab, M., Abeygunawardena, N., Coulson, R., Farne, A., Holloway, E., Kolesnykov, N., Lilja, P., Lukk, M., Mani, R., Rayner, T., Sharma, A.,

William, E., Sarkans, U. & Brazma, A. 2007. Arrayexpress--a Public Database of Microarray Experiments and Gene Expression Profiles. *Nucleic Acids Research,* **35,** 747-750.

Pascual, O., Casper, K. B., Kubera, C., Zhang, J., Revilla-Sanchez, R., Sul, J. Y., Takano, H., Moss, S. J., McCarthy, K. & Haydon, P. G. 2005. Astrocytic Purinergic Signaling Coordinates Synaptic Networks. *Science,* **310,** 113-116.

Passlick, B., Flieger, D. & Ziegler-Heitbrock, H. W. 1989. Identification and Characterization of a Novel Monocyte Subpopulation in Human Peripheral Blood. *Blood,* **74,** 2527-2534.

Patel, N. K., Pavese, N., Javed, S., Hotton, G. R., Brooks, D. J. & Gill, S. S. 2013. Benefits of Putaminal Gdnf Infusion in Parkinson Disease Are Maintained after Gdnf Cessation. *Neurology,* **81,** 1176-1178.

Patino, M. M., Liu, J. J., Glover, J. R. & Lindquist, S. 1996. Support for the Prion Hypothesis for Inheritance of a Phenotypic Trait in Yeast. *Science,* **273,** 622-626.

Pattison, I. H. 1957. Myopathy in Sheep. *The Lancet,* **269,** 104-105.

Pattison, I. H. 1966. The Relative Susceptibility of Sheep, Goats and Mice to Two Types of the Goat Scrapie Agent. *Research in Veterinary Science,* **7,** 207-212.

Pattison, I. H., Gordon, W. S. & Millson, G. C. 1959. Experimental Production of Scrapie in Goats. *Journal of Comparative Pathology and Therapeutics,* **69,** 300-IN320.

Pattison, I. H. & Jones, K. M. 1967. The Possible Nature of the Transmissible Agent of Scrapie. *Veterinary Record,* **80,** 2-9.

Pattison, I. H. & Millson, G. C. 1961. Scrapie Produced Experimentally in Goats with Special Reference to the Clinical Syndrome. *Journal of Comparative Pathology,* **71,** 101-109.

Pekny, M., Leveen, P., Pekna, M., Eliasson, C., Berthold, C. H., Westermark, B. & Betsholtz, C. 1995. Mice Lacking Glial Fibrillary Acidic Protein Display Astrocytes Devoid of Intermediate Filaments but Develop and Reproduce Normally. *EMBO Journal,* **14,** 1590-1598.

Penfield, W. 1925. Microglia and the Process of Phagocytosis in Gliomas. *American Journal of Pathology,* **1,** 77-U21.

Perez-Asensio, F. J., Perpina, U., Planas, A. M. & Pozas, E. 2013. Interleukin-10 Regulates Progenitor Differentiation and Modulates Neurogenesis in Adult Brain. *Journal of Cell Science,* **126,** 4208-4219.

Perry, V. H., Cunningham, C. & Boche, D. 2002. Atypical Inflammation in the Central Nervous System in Prion Disease. *Current Opinion in Neurology,* **15,** 349-354.

Perry, V. H., Matyszak, M. K. & Fearn, S. 1993. Altered Antigen Expression of Microglia in the Aged Rodent Cns. *Glia,* **7,** 60-67.

Perry, V. H., Nicoll, J. A. R. & Holmes, C. 2010. Microglia in Neurodegenerative Disease. *Nature Reviews Neurology,* **6,** 193-201.

Pestka, S., Krause, C. D., Sarkar, D., Walter, M. R., Shi, Y. & Fisher, P. B. 2004. Interleukin-10 and Related Cytokines and Receptors. *Annual Review of Immunology,* **22,** 929-979.

Peterziel, H., Unsicker, K. & Krieglstein, K. 2002. Tgfβ Induces Gdnf Responsiveness in Neurons by Recruitment of Gfrα1 to the Plasma Membrane. *The Journal of Cell Biology,* **159,** 157-167.

Peyrin, J. M., Lasmezas, C. I., Haik, S., Tagliavini, F., Salmona, M., Williams, A., Richie, D., Deslys, J. P. & Dormont, D. 1999. Microglial Cells Respond to Amyloidogenic Prp Peptide by the Production of Inflammatory Cytokines. *Neuroreport,* **10,** 723-729.

Piccio, L., Rossi, B., Scarpini, E., Laudanna, C., Giagulli, C., Issekutz, A. C., Vestweber, D., Butcher, E. C. & Constantin, G. 2002. Molecular Mechanisms Involved in Lymphocyte Recruitment in Inflamed Brain Microvessels: Critical Roles for P-Selectin Glycoprotein Ligand-1 and Heterotrimeric G(I)-Linked Receptors. *Journal of Immunology,* **168,** 1940-1949.

Picelli, S., Faridani, O. R., Björklund, Å. K., Winberg, G., Sagasser, S. & Sandberg, R. 2014. Full-Length Rna-Seq from Single Cells Using Smart-Seq2. *Nat. Protocols,* **9,** 171-181.

Pinotsi, D., Buell, A. K., Galvagnion, C., Dobson, C. M., Kaminski Schierle, G. S. & Kaminski, C. F. 2014. Direct Observation of Heterogeneous Amyloid Fibril Growth Kinetics Via Two-Color Super-Resolution Microscopy. *Nano Letters,* **14,** 339-345.

Pott Godoy, M. C., Tarelli, R., Ferrari, C. C., Sarchi, M. I. & Pitossi, F. J. 2008. Central and Systemic Il-1 Exacerbates Neurodegeneration and Motor Symptoms in a Model of Parkinson's Disease. *Brain,* **131,** 1880-1894.

Potter, M. 1985. History of the Balb/C Family. *Current Topics in Microbiology and Immunology,* **122,** 1-5.

Priller, J., Prinz, M., Heikenwalder, M., Zeller, N., Schwarz, P., Heppner, F. L. & Aguzzi, A. 2006. Early and Rapid Engraftment of Bone Marrow-Derived Microglia in Scrapie. *Journal of Neuroscience,* **26,** 11753-11762.

Prinz, M., Heikenwalder, M., Schwarz, P., Takeda, K., Akira, S. & Aguzzi, A. 2003. Prion Pathogenesis in the Absence of Toll-Like Receptor Signalling. *EMBO Rep,* **4,** 195-199.

Prusiner, S. B. 1982. Novel Proteinaceous Infectious Particles Cause Scrapie. *Science (New York, N.Y.),* **216,** 136-144.

Prusiner, S. B. 1998. Prions. *Proceedings of the National Academy of Sciences of the United States of America,* **95,** 13363-13383.

Quan, N. & Banks, W. A. 2007. Brain-Immune Communication Pathways. *Brain, Behavior, and Immunity,* **21,** 727-735.

Quan, N., Stern, E. L., Whiteside, M. B. & Herkenham, M. 1999. Induction of Pro-Inflammatory Cytokine Mrnas in the Brain after Peripheral Injection of Subseptic Doses of Lipopolysaccharide in the Rat. *Journal of Neuroimmunology,* **93,** 72-80.

Race, R. E., Priola, S. A., Bessen, R. A., Ernst, D., Dockter, J., Rall, G. F., Mucke, L., Chesebro, B. & Oldstone, M. B. 1995. Neuron-Specific Expression of a Hamster Prion Protein Minigene in Transgenic Mice Induces Susceptibility to Hamster Scrapie Agent. *Neuron,* **15,** 1183-1191.

Radogna, F., Nuccitelli, S., Mengoni, F. & Ghibelli, L. 2009. Neuroprotection by Melatonin on Astrocytoma Cell Death. *Annals of the New York Academy of Sciences,* **1171,** 509-513.

Rafice, S. A., Chauhan, N., Efimov, I., Basran, J. & Raven, E. L. 2009. Oxidation of L-Tryptophan in Biology: A Comparison between Tryptophan 2,3-Dioxygenase and Indoleamine 2,3-Dioxygenase. *Biochemical Society Transactions,* **37,** 408-412.

Raivich, G., Bohatschek, M., Kloss, C. U., Werner, A., Jones, L. L. & Kreutzberg, G. W. 1999. Neuroglial Activation Repertoire in the Injured Brain: Graded Response, Molecular Mechanisms and Cues to Physiological Function. *Brain Research: Brain Research Reviews,* **30,** 77-105.

Ramaswamy, S., Soderstrom, K. E. & Kordower, J. H. 2009. Trophic Factors Therapy in Parkinson's Disease. *In:* Joost Verhaagen, E. M. H. I. H. J. W. A. B. B. G. J. B. & Dick, F. S. (eds.) *Progress in Brain Research.* Elsevier, Page: 201-216.

Ransohoff, R. M. 2007. Microgliosis: The Questions Shape the Answers. *Nature Neuroscience,* **10,** 1507-1509.

Ransohoff, R. M. 2011. Microglia and Monocytes: 'Tis Plain the Twain Meet in the Brain. *Nature Neuroscience,* **14,** 1098-1100.

Raymond, G. J., Bossers, A., Raymond, L. D., O'Rourke, K. I., McHolland, L. E., Bryant, P. K., 3rd, Miller, M. W., Williams, E. S., Smits, M. & Caughey, B. 2000. Evidence of a Molecular Barrier Limiting Susceptibility of Humans, Cattle and Sheep to Chronic Wasting Disease. *EMBO Journal,* **19,** 4425-4430.

Retz, K. C. & Steele, W. J. 1980. Ribosome Turnover in Rat Brain and Liver. *Life Sciences,* **27,** 2601-2604.

Rezaie, P. & Lantos, P. L. 2001. Microglia and the Pathogenesis of Spongiform Encephalopathies. *Brain Research Reviews,* **35,** 55-72.

Ridley, A. J. 2006. Rho Gtpases and Actin Dynamics in Membrane Protrusions and Vesicle Trafficking. *Trends in Cell Biology,* **16,** 522-529.

Riemer, C., Neidhold, S., Burwinkel, M., Schwarz, A., Schultz, J., Kratzschmar, J., Monning, U. & Baier, M. 2004. Gene Expression Profiling of Scrapie-Infected Brain Tissue. *Biochemical and Biophysical Research Communications,* **323,** 556-564.

Riemer, C., Schultz, J., Burwinkel, M., Schwarz, A., Mok, S. W., Gultner, S., Bamme, T., Norley, S., van Landeghem, F., Lu, B., Gerard, C. & Baier, M. 2008. Accelerated Prion Replication in, but Prolonged Survival Times of, Prion-Infected Cxcr3-/- Mice. *Journal of Virology,* **82,** 12464-12471.

Rio-Hortega, P. 1932. *Microglia In: Cytology & Cellular Pathology of the Nervous System*, P.B. Hoeber, Inc., Page: 482-534.

Río-Hortega, P. d. 1920. La Microglia Y Su Transformación En Celulas En Bastoncito Y Cuerpos Granulo-Adiposos. *trabajo del lab de investigacion biologia,* **xviii (18),** 37-82.

Río-Hortega, P. d. 1921. *El Tercer Elemento De Los Centros Nerviosos: Histogénesis Y Evolución Normal; Éxodo Y Distribución Regional De La Microglía,* Madrid, : Sociedad Española de Historia Natural, Page: 213-268.

Robertson, F. 1900. A Microscopic Demonstration of the Normal and Pathological Histology of Mesoglia Cells. *The British Journal of Psychiatry,* **46,** 724-724.

Robinson, C. M., Hale, P. T. & Carlin, J. M. 2006. Nf-Kappa B Activation Contributes to Indoleamine Dioxygenase Transcriptional Synergy Induced by Ifn-Gamma and Tumor Necrosis Factor-Alpha. *Cytokine,* **35,** 53-61.

Rogers, J., Kirby, L. C., Hempelman, S. R., Berry, D. L., McGeer, P. L., Kaszniak, A. W., Zalinski, J., Cofield, M., Mansukhani, L., Willson, P. & et al. 1993. Clinical Trial of Indomethacin in Alzheimer's Disease. *Neurology,* **43,** 1609-1611.

Rogers, J. T., Morganti, J. M., Bachstetter, A. D., Hudson, C. E., Peters, M. M., Grimmig, B. A., Weeber, E. J., Bickford, P. C. & Gemma, C. 2011. Cx3cr1 Deficiency Leads to Impairment of Hippocampal Cognitive Function and Synaptic Plasticity. *Journal of Neuroscience,* **31,** 16241-16250.

Romano, M., Sironi, M., Toniatti, C., Polentarutti, N., Fruscella, P., Ghezzi, P., Faggioni, R., Luini, W., van Hinsbergh, V., Sozzani, S., Bussolino, F., Poli, V., Ciliberto, G. & Mantovani, A. 1997. Role of Il-6 and Its Soluble Receptor in Induction of Chemokines and Leukocyte Recruitment. *Immunity,* **6,** 315-325.

Russell, E. S. 1978. Origins and History of Mouse Inbred Strains: Contributions of Clarence Cook Little. *In:* Herbert, C. M., III (ed.) *Origins of Inbred Mice.* Academic Press, Page: 33-44.

Russell, W. M. S. B. R. L. 1959. *The Principles of Humane Experimental Technique,* London, Methuen, Page: 238.

Saba, R., Gushue, S., Huzarewich, R. L., Manguiat, K., Medina, S., Robertson, C. & Booth, S. A. 2012. Microrna 146a (Mir-146a) Is over-Expressed During Prion Disease and Modulates the Innate Immune Response and the Microglial Activation State. *PloS One,* **7,** 17.

Saborio, G. P., Permanne, B. & Soto, C. 2001. Sensitive Detection of Pathological Prion Protein by Cyclic Amplification of Protein Misfolding. *Nature,* **411,** 810-813.

Saederup, N., Cardona, A. E., Croft, K., Mizutani, M., Cotleur, A. C., Tsou, C. L., Ransohoff, R. M. & Charo, I. F. 2010. Selective Chemokine Receptor Usage by Central Nervous System Myeloid Cells in Ccr2-Red Fluorescent Protein Knock-in Mice. *PloS One,* **5,** 0013693.

Safar, J., Wille, H., Itri, V., Groth, D., Serban, H., Torchia, M., Cohen, F. E. & Prusiner, S. B. 1998. Eight Prion Strains Have Prp(Sc) Molecules with Different Conformations. *Nature Medicine,* **4,** 1157-1165.

Sakai, K., Hasebe, R., Takahashi, Y., Song, C. H., Suzuki, A., Yamasaki, T. & Horiuchi, M. 2013. Absence of Cd14 Delays Progression of Prion Diseases Accompanied by Increased Microglial Activation. *Journal of Virology,* **87,** 13433-13445.

Sallusto, F. & Lanzavecchia, A. 2009. Heterogeneity of Cd4 Memory T Cells: Functional Modules for Tailored Immunity. *European Journal of Immunology,* **39,** 2076-2082.

Samuel, D. & Kroner, A. 2011. Repertoire of Microglial and Macrophage Responses after Spinal Cord Injury. *Nature Reviews: Neuroscience,* **12,** 388-399.

Saravia, F., Beauquis, J., Pietranera, L. & De Nicola, A. F. 2007. Neuroprotective Effects of Estradiol in Hippocampal Neurons and Glia of Middle Age Mice. *Psychoneuroendocrinology,* **32,** 480-492.

Sasaki, A. & Nakazato, Y. 1992. The Identity of Cells Expressing Mhc Class Ii Antigens in Normal and Pathological Human Brain. *Neuropathology and Applied Neurobiology,* **18,** 13-26.

Sasaki, Y., Hoshi, M., Akazawa, C., Nakamura, Y., Tsuzuki, H., Inoue, K. & Kohsaka, S. 2003. Selective Expression of Gi/O-Coupled Atp Receptor P2y12 in Microglia in Rat Brain. *Glia,* **44,** 242-250.

Sasmono, R. T., Ehrnsperger, A., Cronau, S. L., Ravasi, T., Kandane, R., Hickey, M. J., Cook, A. D., Himes, S. R., Hamilton, J. A. & Hume, D. A. 2007. Mouse Neutrophilic Granulocytes Express Mrna Encoding the Macrophage Colony-Stimulating Factor Receptor (Csf-1r) as Well as Many Other Macrophage-Specific Transcripts and Can Transdifferentiate into Macrophages in Vitro in Response to Csf-1. *Journal of Leukocyte Biology,* **82,** 111-123.

Sasmono, R. T., Oceandy, D., Pollard, J. W., Tong, W., Pavli, P., Wainwright, B. J., Ostrowski, M. C., Himes, S. R. & Hume, D. A. 2003. A Macrophage Colony-Stimulating Factor Receptor-Green Fluorescent Protein Transgene Is Expressed Throughout the Mononuclear Phagocyte System of the Mouse. *Blood,* **101,** 1155-1163.

Savill, J. S., Wyllie, A. H., Henson, J. E., Walport, M. J., Henson, P. M. & Haslett, C. 1989. Macrophage Phagocytosis of Aging Neutrophils in Inflammation. Programmed Cell Death in the Neutrophil Leads to Its Recognition by Macrophages. *Journal of Clinical Investigation,* **83,** 865-875.

Schafer, D. P., Lehrman, E. K., Kautzman, A. G., Koyama, R., Mardinly, A. R., Yamasaki, R., Ransohoff, R. M., Greenberg, M. E., Barres, B. A. & Stevens, B. 2012. Microglia Sculpt Postnatal Neural Circuits in an Activity and Complement-Dependent Manner. *Neuron,* **74,** 691-705.

Schafer, D. P., Lehrman, E. K. & Stevens, B. 2013. The "Quad-Partite" Synapse: Microglia-Synapse Interactions in the Developing and Mature Cns. *Glia,* **61,** 24-36.

Schebesch, C., Kodelja, V., Muller, C., Hakij, N., Bisson, S., Orfanos, C. E. & Goerdt, S. 1997. Alternatively Activated Macrophages Actively Inhibit Proliferation of Peripheral Blood Lymphocytes and Cd4+ T Cells in Vitro. *Immunology,* **92,** 478-486.

Schena, M., Shalon, D., Davis, R. W. & Brown, P. O. 1995. Quantitative Monitoring of Gene Expression Patterns with a Complementary DNA Microarray. *Science,* **270,** 467-470.

Schena, M., Shalon, D., Heller, R., Chai, A., Brown, P. O. & Davis, R. W. 1996. Parallel Human Genome Analysis: Microarray-Based Expression Monitoring of 1000 Genes. *Proceedings of the National Academy of Sciences of the United States of America,* **93,** 10614-10619.

Schenkel, A. R., Mamdouh, Z. & Muller, W. A. 2004. Locomotion of Monocytes on Endothelium Is a Critical Step During Extravasation. *Nature Immunology,* **5,** 393-400.

Schiefer, J., Kampe, K., Dodt, H. U., Zieglgansberger, W. & Kreutzberg, G. W. 1999. Microglial Motility in the Rat Facial Nucleus Following Peripheral Axotomy. *Journal of Neurocytology,* **28,** 439-453.

Schilling, E., El Chartouni, C. & Rehli, M. 2009. Allele-Specific DNA Methylation in Mouse Strains Is Mainly Determined by Cis-Acting Sequences. *Genome Research,* **19,** 2028-2035.

Schmitz, J., Owyang, A., Oldham, E., Song, Y., Murphy, E., McClanahan, T. K., Zurawski, G., Moshrefi, M., Qin, J., Li, X., Gorman, D. M., Bazan, J. F. & Kastelein, R. A. 2005. Il-33, an Interleukin-1-Like Cytokine That Signals Via the Il-1 Receptor-Related Protein St2 and Induces T Helper Type 2-Associated Cytokines. *Immunity,* **23,** 479-490.

Schneider, C. A., Rasband, W. S. & Eliceiri, K. W. 2012. Nih Image to Imagej: 25 Years of Image Analysis. *Nat Meth,* **9,** 671-675.

Schober, A., Hertel, R., Arumäe, U., Farkas, L., Jaszai, J., Krieglstein, K., Saarma, M. & Unsicker, K. 1999. Glial Cell Line-Derived Neurotrophic Factor Rescues Target-Deprived Sympathetic Spinal Cord Neurons but Requires Transforming Growth Factor-B as Cofactor in Vivo. *Journal of Neuroscience,* **19,** 2008-2015.

Schuitemaker, A., van der Doef, T. F., Boellaard, R., van der Flier, W. M., Yaqub, M., Windhorst, A. D., Barkhof, F., Jonker, C., Kloet, R. W., Lammertsma, A. A., Scheltens, P. & van Berckel, B. N. 2012. Microglial Activation in Healthy Aging. *Neurobiology of Aging,* **33,** 1067-1072.

Schultz, J., Schwarz, A., Neidhold, S., Burwinkel, M., Riemer, C., Simon, D., Kopf, M., Otto, M. & Baier, M. 2004. Role of Interleukin-1 in Prion Disease-Associated Astrocyte Activation. *American Journal of Pathology,* **165,** 671-678.

Scott, E. W., Simon, M. C., Anastasi, J. & Singh, H. 1994. Requirement of Transcription Factor Pu.1 in the Development of Multiple Hematopoietic Lineages. *Science,* **265,** 1573-1577.

Scott, J. R., Davies, D. & Fraser, H. 1992. Scrapie in the Central Nervous System: Neuroanatomical Spread of Infection and Sinc Control of Pathogenesis. *Journal of General Virology,* **73,** 1637-1644.

Scott, M., Groth, D., Foster, D., Torchia, M., Yang, S.-L., DeArmond, S. J. & Prusiner, S. B. 1993. Propagation of Prions with Artificial Properties in Transgenic Mice Expressing Chimeric Prp Genes. *Cell,* **73,** 979-988.

Sergijenko, A., Langford-Smith, A., Liao, A. Y., Pickford, C. E., McDermott, J., Nowinski, G., Langford-Smith, K. J., Merry, C. L., Jones, S. A., Wraith, J. E., Wynn, R. F., Wilkinson, F. L. & Bigger, B. W. 2013. Myeloid/Microglial Driven Autologous Hematopoietic Stem Cell Gene Therapy Corrects a Neuronopathic Lysosomal Disease. *Molecular Therapy,* **21,** 1938-1949.

Serrats, J., Schiltz, J. C., Garcia-Bueno, B., van Rooijen, N., Reyes, T. M. & Sawchenko, P. E. 2010. Dual Roles for Perivascular Macrophages in Immune-to-Brain Signaling. *Neuron,* **65,** 94-106.

Shalek, A. K., Satija, R., Adiconis, X., Gertner, R. S., Gaublomme, J. T., Raychowdhury, R., Schwartz, S., Yosef, N., Malboeuf, C., Lu, D., Trombetta, J. J., Gennert, D., Gnirke, A., Goren, A., Hacohen, N., Levin, J. Z., Park, H. & Regev, A. 2013. Single-Cell Transcriptomics Reveals Bimodality in Expression and Splicing in Immune Cells. *Nature,* **498,** 236-240.

Shechter, R., London, A., Varol, C., Raposo, C., Cusimano, M., Yovel, G., Rolls, A., Mack, M., Pluchino, S., Martino, G., Jung, S. & Schwartz, M. 2009. Infiltrating Blood-Derived Macrophages Are Vital Cells Playing an Anti-Inflammatory Role in Recovery from Spinal Cord Injury in Mice. *PLoS Medicine,* **6,** e1000113.

Sheffield, L. G. & Berman, N. E. 1998. Microglial Expression of Mhc Class Ii Increases in Normal Aging of Nonhuman Primates. *Neurobiology of Aging,* **19,** 47-55.

Sheng, J. G., Mrak, R. E. & Griffin, W. S. 1997. Glial-Neuronal Interactions in Alzheimer Disease: Progressive Association of Il-1alpha+ Microglia and S100beta+ Astrocytes with Neurofibrillary Tangle Stages. *Journal of Neuropathology and Experimental Neurology,* **56,** 285-290.

Shi, L., Campbell, G., Jones, W. D., Campagne, F., Wen, Z., Walker, S. J., Su, Z., Chu, T. M., Goodsaid, F. M., Pusztai, L., Shaughnessy, J. D., Jr., Oberthuer, A., Thomas, R. S., Paules, R. S., Fielden, M., Barlogie, B., Chen, W., Du, P., Fischer, M., Furlanello, C., Gallas, B. D., Ge, X., Megherbi, D. B., Symmans, W. F., Wang, M. D., Zhang, J., Bitter, H., Brors, B., Bushel, P. R., Bylesjo, M., Chen, M., Cheng, J., Cheng, J., Chou, J.,

Davison, T. S., Delorenzi, M., Deng, Y., Devanarayan, V., Dix, D. J., Dopazo, J., Dorff, K. C., Elloumi, F., Fan, J., Fan, S., Fan, X., Fang, H., Gonzaludo, N., Hess, K. R., Hong, H., Huan, J., Irizarry, R. A., Judson, R., Juraeva, D., Lababidi, S., Lambert, C. G., Li, L., Li, Y., Li, Z., Lin, S. M., Liu, G., Lobenhofer, E. K., Luo, J., Luo, W., McCall, M. N., Nikolsky, Y., Pennello, G. A., Perkins, R. G., Philip, R., Popovici, V., Price, N. D., Qian, F., Scherer, A., Shi, T., Shi, W., Sung, J., Thierry-Mieg, D., Thierry-Mieg, J., Thodima, V., Trygg, J., Vishnuvajjala, L., Wang, S. J., Wu, J., Wu, Y., Xie, Q., Yousef, W. A., Zhang, L., Zhang, X., Zhong, S., Zhou, Y., Zhu, S., Arasappan, D., Bao, W., Lucas, A. B., Berthold, F., Brennan, R. J., Buness, A., Catalano, J. G., Chang, C., Chen, R., Cheng, Y., *et al.* 2010. The Microarray Quality Control (Maqc)-Ii Study of Common Practices for the Development and Validation of Microarray-Based Predictive Models. *Nature Biotechnology,* **28,** 827-838.

Shi, L., Jones, W., Jensen, R., Harris, S., Perkins, R., Goodsaid, F., Guo, L., Croner, L., Boysen, C., Fang, H., Qian, F., Amur, S., Bao, W., Barbacioru, C., Bertholet, V., Cao, X., Chu, T.-M., Collins, P., Fan, X.-h. & Frueh, F. 2008. The Balance of Reproducibility, Sensitivity, and Specificity of Lists of Differentially Expressed Genes in Microarray Studies. *BMC Bioinformatics,* **9,** S10.

Shi, L., Reid, L. H., Jones, W. D., Shippy, R., Warrington, J. A., Baker, S. C., Collins, P. J., de Longueville, F., Kawasaki, E. S., Lee, K. Y., Luo, Y., Sun, Y. A., Willey, J. C., Setterquist, R. A., Fischer, G. M., Tong, W., Dragan, Y. P., Dix, D. J., Frueh, F. W., Goodsaid, F. M., Herman, D., Jensen, R. V., Johnson, C. D., Lobenhofer, E. K., Puri, R. K., Schrf, U., Thierry-Mieg, J., Wang, C., Wilson, M., Wolber, P. K., Zhang, L., Amur, S., Bao, W., Barbacioru, C. C., Lucas, A. B., Bertholet, V., Boysen, C., Bromley, B., Brown, D., Brunner, A., Canales, R., Cao, X. M., Cebula, T. A., Chen, J. J., Cheng, J., Chu, T. M., Chudin, E., Corson, J., Corton, J. C., Croner, L. J., Davies, C., Davison, T. S., Delenstarr, G., Deng, X., Dorris, D., Eklund, A. C., Fan, X. H., Fang, H., Fulmer-Smentek, S., Fuscoe, J. C., Gallagher, K., Ge, W., Guo, L., Guo, X., Hager, J., Haje, P. K., Han, J., Han, T., Harbottle, H. C., Harris, S. C., Hatchwell, E., Hauser, C. A., Hester, S., Hong, H., Hurban, P., Jackson, S. A., Ji, H., Knight, C. R., Kuo, W. P., LeClerc, J. E., Levy, S., Li, Q. Z., Liu, C., Liu, Y., Lombardi, M. J., Ma, Y., Magnuson, S. R., Maqsodi, B., McDaniel, T., Mei, N., Myklebost, O., Ning, B., Novoradovskaya, N., Orr, M. S., Osborn, T. W., Papallo, A., Patterson, T. A., Perkins, R. G., Peters, E. H., Peterson, R., *et al.* 2006. The Microarray Quality Control (Maqc) Project Shows Inter- and Intraplatform Reproducibility of Gene Expression Measurements. *Nature Biotechnology,* **24,** 1151-1161.

Shigemoto-Mogami, Y., Hoshikawa, K., Goldman, J. E., Sekino, Y. & Sato, K. 2014. Microglia Enhance Neurogenesis and Oligodendrogenesis in the Early Postnatal Subventricular Zone. *Journal of Neuroscience,* **34,** 2231-2243.

Shimoda, K., van Deursen, J., Sangster, M. Y., Sarawar, S. R., Carson, R. T., Tripp, R. A., Chu, C., Quelle, F. W., Nosaka, T., Vignali, D. A., Doherty, P. C., Grosveld, G., Paul, W. E. & Ihle, J. N. 1996. Lack of Il-4-Induced Th2 Response and Ige Class Switching in Mice with Disrupted Stat6 Gene. *Nature,* **380,** 630-633.

Shokouhi, B. N., Wong, B. Z., Siddiqui, S., Lieberman, A. R., Campbell, G., Tohyama, K. & Anderson, P. N. 2010. Microglial Responses around Intrinsic Cns Neurons Are Correlated with Axonal Regeneration. *BMC Neuroscience,* **11,** 13.

Shuai, K. & Liu, B. 2003. Regulation of Jak-Stat Signalling in the Immune System. *Nature Reviews: Immunology,* **3,** 900-911.

Sierra, A., Encinas, J. M., Deudero, J. J., Chancey, J. H., Enikolopov, G., Overstreet-Wadiche, L. S., Tsirka, S. E. & Maletic-Savatic, M. 2010. Microglia Shape Adult Hippocampal Neurogenesis through Apoptosis-Coupled Phagocytosis. *Cell Stem Cell,* **7,** 483-495.

Sierra, A., Gottfried-Blackmore, A. C., McEwen, B. S. & Bulloch, K. 2007. Microglia Derived from Aging Mice Exhibit an Altered Inflammatory Profile. *Glia,* **55,** 412-424.

Sigurdsson, B., Palsson, P. & Grimsson, H. 1957. Visna, a Demyelinating Transmissible Disease of Sheep. *Journal of Neuropathology and Experimental Neurology,* **16,** 389-403.

Sigurdsson, B. & Palsson, P. A. 1958. Visna of Sheep; a Slow, Demyelinating Infection. *British Journal of Experimental Pathology,* **39,** 519-528.

Sikorska, B., Liberski, P. P., Giraud, P., Kopp, N. & Brown, P. 2004. Autophagy Is a Part of Ultrastructural Synaptic Pathology in Creutzfeldt-Jakob Disease: A Brain Biopsy Study. *International Journal of Biochemistry and Cell Biology,* **36,** 2563-2573.

Sironi, M., Martinez, F. O., D'Ambrosio, D., Gattorno, M., Polentarutti, N., Locati, M., Gregorio, A., Iellem, A., Cassatella, M. A., Van Damme, J., Sozzani, S., Martini, A., Sinigaglia, F., Vecchi, A. & Mantovani, A. 2006. Differential Regulation of Chemokine Production by Fcgamma Receptor Engagement in Human Monocytes: Association of Ccl1 with a Distinct Form of M2 Monocyte Activation (M2b, Type 2). *Journal of Leukocyte Biology,* **80,** 342-349.

Siskova, Z., Page, A., O'Connor, V. & Perry, V. H. 2009. Degenerating Synaptic Boutons in Prion Disease: Microglia Activation without Synaptic Stripping. *American Journal of Pathology,* **175,** 1610-1621.

Siskova, Z., Reynolds, R. A., O'Connor, V. & Perry, V. H. 2013. Brain Region Specific Pre-Synaptic and Post-Synaptic Degeneration Are Early Components of Neuropathology in Prion Disease. *PloS One,* **8,** 30.

Siskova, Z. & Tremblay, M. E. 2013. Microglia and Synapse: Interactions in Health and Neurodegeneration. *Neural Plasticity,* **2013,** 425845.

Sisó, S., Chianini, F., Eaton, S. L., Witz, J., Hamilton, S., Martin, S., Finlayson, J., Pang, Y., Stewart, P., Steele, P., Dagleish, M. P., Goldmann, W., Reid, H. W., Jeffrey, M. & Gonzalez, L. 2012. Disease Phenotype in Sheep after Infection with Cloned Murine Scrapie Strains. *Prion,* **6,** 174-183.

Siso, S., Puig, B., Varea, R., Vidal, E., Acin, C., Prinz, M., Montrasio, F., Badiola, J., Aguzzi, A., Pumarola, M. & Ferrer, I. 2002. Abnormal Synaptic Protein Expression and Cell Death in Murine Scrapie. *Acta Neuropathologica,* **103,** 615-626.

Skinner, P. J., Abbassi, H., Chesebro, B., Race, R. E., Reilly, C. & Haase, A. T. 2006. Gene Expression Alterations in Brains of Mice Infected with Three Strains of Scrapie. *BMC Genomics,* **7,** 114-114.

Sly, L. M., Krzesicki, R. F., Brashler, J. R., Buhl, A. E., McKinley, D. D., Carter, D. B. & Chin, J. E. 2001. Endogenous Brain Cytokine Mrna and Inflammatory Responses to Lipopolysaccharide Are Elevated in the Tg2576 Transgenic Mouse Model of Alzheimer's Disease. *Brain Research Bulletin,* **56,** 581-588.

Snell, G. D. 1941. *Biology of the Laboratory Mouse,* York U.S.A., Maple Press Company, Page: 242-243.

Snell, G. D. 1978. Congenic Resistant Strains of Mice. *In:* Herbert, C. M., III (ed.) *Origins of Inbred Mice.* Academic Press, Page: 119-156.

Sofroniew, M. V. & Vinters, H. V. 2010. Astrocytes: Biology and Pathology. *Acta Neuropathologica,* **119,** 7-35.

Sogn, C., Puchades, M. & Gundersen, V. 2013. Rare Contacts between Synapses and Microglial Processes Containing High Levels of Iba1 and Actin - a Postembedding Immunogold Study in the Healthy Rat Brain. *European Journal of Neuroscience***,** 2030-2040.

Sollberger, G., Strittmatter, G. E., Kistowska, M., French, L. E. & Beer, H. D. 2012. Caspase-4 Is Required for Activation of Inflammasomes. *Journal of Immunology,* **188,** 1992-2000.

Somerville, R. A., Chong, A., Mulqueen, O. U., Birkett, C. R., Wood, S. C. & Hope, J. 1997. Biochemical Typing of Scrapie Strains. *Nature,* **386,** 564.

Song, D. Y., Yu, H. N., Park, C. R., Lee, J. S., Lee, J. Y., Park, B. G., Woo, R. S., Han, J. T., Cho, B. P. & Baik, T. K. 2013. Down-Regulation of Microglial Activity Attenuates Axotomized Nigral Dopaminergic Neuronal Cell Loss. *BMC Neuroscience,* **14,** 112.

Sparkes, R. S., Simon, M., Cohn, V. H., Fournier, R. E., Lem, J., Klisak, I., Heinzmann, C., Blatt, C., Lucero, M., Mohandas, T. & et al. 1986. Assignment of the Human and Mouse Prion Protein Genes to Homologous Chromosomes. *Proceedings of the National Academy of Sciences of the United States of America,* **83,** 7358-7362.

Spinner, D. S., Cho, I. S., Park, S. Y., Kim, J. I., Meeker, H. C., Ye, X., Lafauci, G., Kerr, D. J., Flory, M. J., Kim, B. S., Kascsak, R. B., Wisniewski, T., Levis, W. R., Schuller-Levis, G. B., Carp, R. I., Park, E. & Kascsak, R. J. 2008. Accelerated Prion Disease Pathogenesis in Toll-Like Receptor 4 Signaling-Mutant Mice. *Journal of Virology,* **82,** 10701-10708.

Spudich, A., Frigg, R., Kilic, E., Kilic, U., Oesch, B., Raeber, A., Bassetti, C. L. & Hermann, D. M. 2005. Aggravation of Ischemic Brain Injury by Prion Protein Deficiency: Role of Erk-1/-2 and Stat-1. *Neurobiology of Disease,* **20,** 442-449.

Stahl, N., Baldwin, M. A., Teplow, D. B., Hood, L., Gibson, B. W., Burlingame, A. L. & Prusiner, S. B. 1993. Structural Studies of the Scrapie Prion Protein Using Mass Spectrometry and Amino Acid Sequencing. *Biochemistry,* **32,** 1991-2002.

Stalder, M., Deller, T., Staufenbiel, M. & Jucker, M. 2001. 3d-Reconstruction of Microglia and Amyloid in App23 Transgenic Mice: No Evidence of Intracellular Amyloid. *Neurobiology of Aging,* **22,** 427-434.

Stalder, M., Phinney, A., Probst, A., Sommer, B., Staufenbiel, M. & Jucker, M. 1999. Association of Microglia with Amyloid Plaques in Brains of App23 Transgenic Mice. *American Journal of Pathology,* **154,** 1673-1684.

Stangegaard, M., Dufva, I. H. & Dufva, M. 2006. Reverse Transcription Using Random Pentadecamer Primers Increases Yield and Quality of Resulting Cdna. *BioTechniques,* **40,** 649-657.

Stanley, E. R., Berg, K. L., Einstein, D. B., Lee, P. S., Pixley, F. J., Wang, Y. & Yeung, Y. G. 1997. Biology and Action of Colony--Stimulating Factor-1. *Molecular Reproduction and Development,* **46,** 4-10.

Stanton, J. B., Knowles, D. P., Call, D. R., Mathison, B. A. & Baszler, T. V. 2009. Limited Transcriptional Response of Ovine Microglia to Prion Accumulation. *Biochemical and Biophysical Research Communications,* **386,** 345-350.

Stefater, J. A., 3rd, Lewkowich, I., Rao, S., Mariggi, G., Carpenter, A. C., Burr, A. R., Fan, J., Ajima, R., Molkentin, J. D., Williams, B. O., Wills-Karp, M., Pollard, J. W., Yamaguchi, T., Ferrara, N., Gerhardt, H. & Lang, R. A. 2011. Regulation of Angiogenesis by a Non-Canonical Wnt-Flt1 Pathway in Myeloid Cells. *Nature,* **474,** 511-515.

Stein, M., Keshav, S., Harris, N. & Gordon, S. 1992. Interleukin 4 Potently Enhances Murine Macrophage Mannose Receptor Activity: A Marker of Alternative Immunologic Macrophage Activation. *Journal of Experimental Medicine,* **176,** 287-292.

Stewart, W. F., Kawas, C., Corrada, M. & Metter, E. J. 1997. Risk of Alzheimer's Disease and Duration of Nsaid Use. *Neurology,* **48,** 626-632.

Stockman, S. 1913. Scrapie: An Obscure Disease of Sheep. *Journal of Comparative Pathology and Therapeutics,* **26,** 317-327.

Stockman, S. 1926. Contribution to the Study of the Disease Known as Scrapie. *Journal of Comparative Pathology and Therapeutics,* **39,** 42-71.

Stohr, J., Condello, C., Watts, J. C., Bloch, L., Oehler, A., Nick, M., DeArmond, S. J., Giles, K., DeGrado, W. F. & Prusiner, S. B. 2014. Distinct Synthetic Abeta Prion Strains Producing Different Amyloid Deposits in Bigenic Mice. *Proceedings of the National Academy of Sciences of the United States of America,* **111,** 10329-10334.

Stohr, J., Watts, J. C., Mensinger, Z. L., Oehler, A., Grillo, S. K., DeArmond, S. J., Prusiner, S. B. & Giles, K. 2012. Purified and Synthetic Alzheimer's Amyloid Beta (Abeta) Prions.

Proceedings of the National Academy of Sciences of the United States of America, **109,** 11025-11030.

Stone, T. W. 2001. Endogenous Neurotoxins from Tryptophan. *Toxicon,* **39,** 61-73.

Stone, T. W. & Perkins, M. N. 1981. Quinolinic Acid: A Potent Endogenous Excitant at Amino Acid Receptors in Cns. *European Journal of Pharmacology,* **72,** 411-412.

Stoner, G. D., Adam-Rodwell, G. & Morse, M. A. 1993. Lung Tumors in Strain a Mice: Application for Studies in Cancer Chemoprevention. *Journal of Cellular Biochemistry. Supplement***,** 95-103.

Streit, W. J. 2002. Microglia as Neuroprotective, Immunocompetent Cells of the Cns. *Glia,* **40,** 133-139.

Streit, W. J., Graeber, M. B. & Kreutzberg, G. W. 1988. Functional Plasticity of Microglia: A Review. *Glia,* **1,** 301-307.

Streit, W. J., Graeber, M. B. & Kreutzberg, G. W. 1989a. Expression of Ia Antigen on Perivascular and Microglial Cells after Sublethal and Lethal Motor Neuron Injury. *Experimental Neurology,* **105,** 115-126.

Streit, W. J., Graeber, M. B. & Kreutzberg, G. W. 1989b. Expression of Ia Antigen on Perivascular and Microglial Cells after Sublethal and Lethal Motor Neuron Injury. *Experimental Neurology,* **105,** 115-126.

Streit, W. J., Graeber, M. B. & Kreutzberg, G. W. 1989c. Peripheral Nerve Lesion Produces Increased Levels of Major Histocompatibility Complex Antigens in the Central Nervous System. *Journal of Neuroimmunology,* **21,** 117-123.

Streit, W. J., Sammons, N. W., Kuhns, A. J. & Sparks, D. L. 2004. Dystrophic Microglia in the Aging Human Brain. *Glia,* **45,** 208-212.

Strong, L. C. 1936. The Establishment of the "a" Strain of Inbred Mice. *Journal of Heredity,* **27,** 21-24.

Su, A. I., Cooke, M. P., Ching, K. A., Hakak, Y., Walker, J. R., Wiltshire, T., Orth, A. P., Vega, R. G., Sapinoso, L. M., Moqrich, A., Patapoutian, A., Hampton, G. M., Schultz, P. G. & Hogenesch, J. B. 2002. Large-Scale Analysis of the Human and Mouse Transcriptomes. *Proceedings of the National Academy of Sciences of the United States of America,* **99,** 4465-4470.

Sun, S. C., Ganchi, P. A., Ballard, D. W. & Greene, W. C. 1993. Nf-Kappa B Controls Expression of Inhibitor I Kappa B Alpha: Evidence for an Inducible Autoregulatory Pathway. *Science,* **259,** 1912-1915.

Sunderkötter, C., Nikolic, T., Dillon, M. J., Van Rooijen, N., Stehling, M., Drevets, D. A. & Leenen, P. J. M. 2004. Subpopulations of Mouse Blood Monocytes Differ in Maturation Stage and Inflammatory Response. *Journal of Immunology (Baltimore, Md.: 1950),* **172,** 4410-4417.

Sunyach, C., Jen, A., Deng, J., Fitzgerald, K. T., Frobert, Y., Grassi, J., McCaffrey, M. W. & Morris, R. 2003. The Mechanism of Internalization of Glycosylphosphatidylinositol-Anchored Prion Protein. *EMBO Journal,* **22,** 3591-3601.

Sykova, E. 2004. Extrasynaptic Volume Transmission and Diffusion Parameters of the Extracellular Space. *Neuroscience,* **129,** 861-876.

Szekely, C. A., Breitner, J. C., Fitzpatrick, A. L., Rea, T. D., Psaty, B. M., Kuller, L. H. & Zandi, P. P. 2008. Nsaid Use and Dementia Risk in the Cardiovascular Health Study: Role of Apoe and Nsaid Type. *Neurology,* **70,** 17-24.

Tahara, K., Kim, H.-D., Jin, J.-J., Maxwell, J. A., Li, L. & Fukuchi, K.-i. 2006. Role of Toll-Like Receptor Signalling in a{Beta} Uptake and Clearance. *Brain,* **129,** 3006-3019.

Takahashi, K., Rochford, C. D. & Neumann, H. 2005. Clearance of Apoptotic Neurons without Inflammation by Microglial Triggering Receptor Expressed on Myeloid Cells-2. *Journal of Experimental Medicine,* **201,** 647-657.

Tamura, H., Dong, H., Zhu, G., Sica, G. L., Flies, D. B., Tamada, K. & Chen, L. 2001. B7-H1 Costimulation Preferentially Enhances Cd28-Independent T-Helper Cell Function. *Blood,* **97,** 1809-1816.

Tanaka, M., Kishi, K., McCarron, R. M. & Miyatake, T. 1993. The Generation of Macrophages from Precursor Cells Incubated with Brain Endothelial Cells--a Release of Csf-1 Like Factor from Endothelial Cells. *Tohoku Journal of Experimental Medicine,* **171,** 211-220.

Tang, F., Barbacioru, C., Nordman, E., Li, B., Xu, N., Bashkirov, V. I., Lao, K. & Surani, M. A. 2010. Rna-Seq Analysis to Capture the Transcriptome Landscape of a Single Cell. *Nature Protocols,* **5,** 516-535.

Tarkowski, E., Blennow, K., Wallin, A. & Tarkowski, A. 1999. Intracerebral Production of Tumor Necrosis Factor-Alpha, a Local Neuroprotective Agent, in Alzheimer Disease and Vascular Dementia. *Journal of Clinical Immunology,* **19,** 223-230.

Tashiro, H., Dohura, K. & Iwaki, T. 1998. Differential Expression of Transforming Growth Factor-Beta Isoforms in Human Prion Diseases. *Neuropathology and Applied Neurobiology,* **24,** 284-292.

Tasker, J. G., Oliet, S. H., Bains, J. S., Brown, C. H. & Stern, J. E. 2012. Glial Regulation of Neuronal Function: From Synapse to Systems Physiology. *Journal of Neuroendocrinology,* **24,** 566-576.

Taylor, D. M., Brown, J. M., Fernie, K. & McConnell, I. 1997. The Effect of Formic Acid on Bse and Scrapie Infectivity in Fixed and Unfixed Brain-Tissue. *Veterinary Microbiology,* **58,** 167-174.

Taylor, P. R., Martinez-Pomares, L., Stacey, M., Lin, H. H., Brown, G. D. & Gordon, S. 2005. Macrophage Receptors and Immune Recognition. *Annual Review of Immunology,* **23,** 901-944.

Tereshchenko, J., Maddalena, A., Bahr, M. & Kugler, S. 2014. Pharmacologically Controlled, Discontinuous Gdnf Gene Therapy Restores Motor Function in a Rat Model of Parkinson's Disease. *Neurobiology of Disease,* **65,** 35-42.

Thackray, A. M., McKenzie, A. N., Klein, M. A., Lauder, A. & Bujdoso, R. 2004. Accelerated Prion Disease in the Absence of Interleukin-10. *Journal of Virology,* **78,** 13697-13707.

Thaler, J. P., Yi, C. X., Schur, E. A., Guyenet, S. J., Hwang, B. H., Dietrich, M. O., Zhao, X., Sarruf, D. A., Izgur, V., Maravilla, K. R., Nguyen, H. T., Fischer, J. D., Matsen, M. E., Wisse, B. E., Morton, G. J., Horvath, T. L., Baskin, D. G., Tschop, M. H. & Schwartz, M. W. 2012. Obesity Is Associated with Hypothalamic Injury in Rodents and Humans. *Journal of Clinical Investigation,* **122,** 153-162.

Theocharidis, A., van Dongen, S., Enright, A. J. & Freeman, T. C. 2009. Network Visualization and Analysis of Gene Expression Data Using Biolayout Express3d. *Nat. Protocols,* **4,** 1535-1550.

Thomson, C. A., McColl, A., Cavanagh, J. & Graham, G. J. 2014. Peripheral Inflammation Is Associated with Remote Global Gene Expression Changes in the Brain. *Journal of Neuroinflammation,* **11,** 73.

Timmes, A. G., Moore, R. A., Fischer, E. R. & Priola, S. A. 2013. Recombinant Prion Protein Refolded with Lipid and Rna Has the Biochemical Hallmarks of a Prion but Lacks in Vivo Infectivity. *PloS One,* **8,** e71081.

Tobler, I., Gaus, S. E., Deboer, T., Achermann, P., Fischer, M., Rulicke, T., Moser, M., Oesch, B., McBride, P. A. & Manson, J. C. 1996. Altered Circadian Activity Rhythms and Sleep in Mice Devoid of Prion Protein. *Nature,* **380,** 639-642.

Torres-Platas, S. G., Comeau, S., Rachalski, A., Bo, G. D., Cruceanu, C., Turecki, G., Giros, B. & Mechawar, N. 2014. Morphometric Characterization of Microglial Phenotypes in Human Cerebral Cortex. *Journal of Neuroinflammation,* **11,** 12.

Tourrière, H., Chebli, K. & Tazi, J. 2002. Mrna Degradation Machines in Eukaryotic Cells. *Biochimie,* **84,** 821-837.

Trapp, B. D., Wujek, J. R., Criste, G. A., Jalabi, W., Yin, X., Kidd, G. J., Stohlman, S. & Ransohoff, R. 2007. Evidence for Synaptic Stripping by Cortical Microglia. *Glia,* **55,** 360-368.

Tremblay, M.-È., Lowery, R. L. & Majewska, A. K. 2010. Microglial Interactions with Synapses Are Modulated by Visual Experience. *PLoS Biology,* **8,** e1000527.

Tremblay, M.-È. & Majewska, A. K. 2011. A Role for Microglia in Synaptic Plasticity? *Communicative & Integrative Biology,* **4,** 220-222.

Tremblay, P., Ball, H. L., Kaneko, K., Groth, D., Hegde, R. S., Cohen, F. E., DeArmond, S. J., Prusiner, S. B. & Safar, J. G. 2004. Mutant Prpsc Conformers Induced by a Synthetic Peptide and Several Prion Strains. *Journal of Virology,* **78,** 2088-2099.

True, H. L. & Lindquist, S. L. 2000. A Yeast Prion Provides a Mechanism for Genetic Variation and Phenotypic Diversity. *Nature,* **407,** 477-483.

Tsukazaki, T., Chiang, T. A., Davison, A. F., Attisano, L. & Wrana, J. L. 1998. Sara, a Fyve Domain Protein That Recruits Smad2 to the Tgfbeta Receptor. *Cell,* **95,** 779-791.

Turtzo, L. C., Lescher, J., Janes, L., Dean, D. D., Budde, M. D. & Frank, J. A. 2014. Macrophagic and Microglial Responses after Focal Traumatic Brain Injury in the Female Rat. *Journal of Neuroinflammation,* **11,** 82.

Tusher, V. G., Tibshirani, R. & Chu, G. 2001. Significance Analysis of Microarrays Applied to the Ionizing Radiation Response. *Proceedings of the National Academy of Sciences of the United States of America,* **98,** 5116-5121.

Ulevitch, R. J. & Tobias, P. S. 1995. Receptor-Dependent Mechanisms of Cell Stimulation by Bacterial Endotoxin. *Annual Review of Immunology,* **13,** 437-457.

van Dam, A.-M., Brouns, M., Louisse, S. & Berkenbosch, F. 1992. Appearance of Interleukin-1 in Macrophages and in Ramified Microglia in the Brain of Endotoxin-Treated Rats: A Pathway for the Induction of Non-Specific Symptoms of Sickness? *Brain Research,* **588,** 291-296.

Van Dam, A. M., Bauer, J., Tilders, F. J. & Berkenbosch, F. 1995. Endotoxin-Induced Appearance of Immunoreactive Interleukin-1 Beta in Ramified Microglia in Rat Brain: A Light and Electron Microscopic Study. *Neuroscience,* **65,** 815-826.

van Gool, W. A., van de Beek, D. & Eikelenboom, P. 2010. Systemic Infection and Delirium: When Cytokines and Acetylcholine Collide. *Lancet,* **375,** 773-775.

Vane, J. R. 1971. Inhibition of Prostaglandin Synthesis as a Mechanism of Action for Aspirin-Like Drugs. *Nature: New Biology,* **231,** 232-235.

Vargas, L. M., Leal, N., Estrada, L. D., Gonzalez, A., Serrano, F., Araya, K., Gysling, K., Inestrosa, N. C., Pasquale, E. B. & Alvarez, A. R. 2014. Epha4 Activation of C-Abl Mediates Synaptic Loss and Ltp Blockade Caused by Amyloid-Beta Oligomers. *PloS One,* **9,** e92309.

Varin, A. & Gordon, S. 2009. Alternative Activation of Macrophages: Immune Function and Cellular Biology. *Immunobiology,* **214,** 630-641.

Varvel, N. H., Grathwohl, S. A., Baumann, F., Liebig, C., Bosch, A., Brawek, B., Thal, D. R., Charo, I. F., Heppner, F. L., Aguzzi, A., Garaschuk, O., Ransohoff, R. M. & Jucker, M. 2012. Microglial Repopulation Model Reveals a Robust Homeostatic Process for Replacing Cns Myeloid Cells. *Proceedings of the National Academy of Sciences of the United States of America,* **109,** 18150-18155.

Vass, K. & Lassmann, H. 1990. Intrathecal Application of Interferon Gamma. Progressive Appearance of Mhc Antigens within the Rat Nervous System. *American Journal of Pathology,* **137,** 789-800.

Vastrik, I., D'Eustachio, P., Schmidt, E., Gopinath, G., Croft, D., de Bono, B., Gillespie, M., Jassal, B., Lewis, S., Matthews, L., Wu, G., Birney, E. & Stein, L. 2007. Reactome: A Knowledge Base of Biologic Pathways and Processes. *Genome Biology,* **8,** R39.

Vasudevan, A., Long, J. E., Crandall, J. E., Rubenstein, J. L. & Bhide, P. G. 2008. Compartment-Specific Transcription Factors Orchestrate Angiogenesis Gradients in the Embryonic Brain. *Nature Neuroscience,* **11,** 429-439.

Ventura, G., Moinard, C., Segaud, F., Le Plenier, S., Cynober, L. & De Bandt, J. P. 2010. Adaptative Response of Nitrogen Metabolism in Early Endotoxemia: Role of Ornithine Aminotransferase. *Amino Acids,* **39,** 1417-1426.

Vinet, J., Weering, H. R., Heinrich, A., Kalin, R. E., Wegner, A., Brouwer, N., Heppner, F. L., Rooijen, N., Boddeke, H. W. & Biber, K. 2012. Neuroprotective Function for Ramified Microglia in Hippocampal Excitotoxicity. *Journal of Neuroinflammation,* **9,** 27.

Virchow, R. 1846. Über Das Granulierte Aussehen Der Wandungen Des Gehirnvenrtikels. *Zeitschrift für Psychiatrie***,** 242-250.

Virchow, R. 1858. *Das Nervensystem, In: Die Cellularpathologie in Ihrer Begründung Auf Physiologische Und Pathologische Gewebelchre (the Cellular Pathology in Its Reasoning on Physiological and Pathological Histology),* Frankfurt, Page: 218-237.

Viselli, S. M., Stanziale, S., Shults, K., Kovacs, W. J. & Olsen, N. J. 1995. Castration Alters Peripheral Immune Function in Normal Male Mice. *Immunology,* **84,** 337-342.

Voll, R. E., Herrmann, M., Roth, E. A., Stach, C., Kalden, J. R. & Girkontaite, I. 1997. Immunosuppressive Effects of Apoptotic Cells. *Nature,* **390,** 350-351.

Vukovic, J., Colditz, M. J., Blackmore, D. G., Ruitenberg, M. J. & Bartlett, P. F. 2012. Microglia Modulate Hippocampal Neural Precursor Activity in Response to Exercise and Aging. *Journal of Neuroscience,* **32,** 6435-6443.

Wake, H., Moorhouse, A. J., Jinno, S., Kohsaka, S. & Nabekura, J. 2009. Resting Microglia Directly Monitor the Functional State of Synapses in Vivo and Determine the Fate of Ischemic Terminals. *The Journal of Neuroscience: The Official Journal of the Society for Neuroscience,* **29,** 3974-3980.

Walsh, D. T., Perry, V. H. & Minghetti, L. 2000. Cyclooxygenase-2 Is Highly Expressed in Microglial-Like Cells in a Murine Model of Prion Disease. *Glia,* **29,** 392-396.

Walsh, D. T. P., Betmouni, S. D. & Perry, V. H. D. 2001. Absence of Detectable Il-1[Beta] Production in Murine Prion Disease: A Model of Chronic Neurodegeneration. [Article]. *Journal of Neuropathology & Experimental Neurology February,* **60,** 173-182.

Wang, F., Wang, X., Yuan, C. G. & Ma, J. 2010. Generating a Prion with Bacterially Expressed Recombinant Prion Protein. *Science,* **327,** 1132-1135.

Wang, F., Zhang, Z., Wang, X., Li, J., Zha, L., Yuan, C. G., Weissmann, C. & Ma, J. 2012. Genetic Informational Rna Is Not Required for Recombinant Prion Infectivity. *Journal of Virology,* **86,** 1874-1876.

Wang, J., Yang, Z., Liu, C., Zhao, Y. & Chen, Y. 2013. Activated Microglia Provide a Neuroprotective Role by Balancing Glial Cell-Line Derived Neurotrophic Factor and Tumor Necrosis Factor-Alpha Secretion after Subacute Cerebral Ischemia. *International Journal of Molecular Medicine,* **31,** 172-178.

Warner, J. R. 1999. The Economics of Ribosome Biosynthesis in Yeast. *Trends in Biochemical Sciences,* **24,** 437-440.

Watts, J. C., Condello, C., Stohr, J., Oehler, A., Lee, J., DeArmond, S. J., Lannfelt, L., Ingelsson, M., Giles, K. & Prusiner, S. B. 2014. Serial Propagation of Distinct Strains of Abeta Prions from Alzheimer's Disease Patients. *Proceedings of the National Academy of Sciences of the United States of America,* **111,** 10323-10328.

Wehinger, J., Gouilleux, F., Groner, B., Finke, J., Mertelsmann, R. & Weber-Nordt, R. M. 1996. Il-10 Induces DNA Binding Activity of Three Stat Proteins (Stat1, Stat3, and Stat5) and Their Distinct Combinatorial Assembly in the Promoters of Selected Genes. *FEBS Letters,* **394,** 365-370.

Weissmann, C., Li, J., Mahal, S. P. & Browning, S. 2011. Prions on the Move. *EMBO Rep,* **12,** 1109-1117.

Wells, G. A., Scott, A. C., Johnson, C. T., Gunning, R. F., Hancock, R. D., Jeffrey, M., Dawson, M. & Bradley, R. 1987. A Novel Progressive Spongiform Encephalopathy in Cattle. *Veterinary Record,* **121,** 419-420.

Westfall, P. H. 1993. *Resampling-Based Multiple Testing: Examples and Methods for P-Value Adjustment,* Hoboken U.S.A., John Wiley & Sons, Page: 1359-64.

Whiting, D., Hsieh, G., Yun, J. J., Banerji, A., Yao, W., Fishbein, M. C., Belperio, J., Strieter, R. M., Bonavida, B. & Ardehali, A. 2004. Chemokine Monokine Induced by Ifn-Gamma/Cxc Chemokine Ligand 9 Stimulates T Lymphocyte Proliferation and Effector Cytokine Production. *Journal of Immunology,* **172,** 7417-7424.

Wilesmith, J. W., Ryan, J. B. & Atkinson, M. J. 1991. Bovine Spongiform Encephalopathy: Epidemiological Studies on the Origin. *Veterinary Record,* **128,** 199-203.

Wilesmith, J. W., Wells, G. A., Cranwell, M. P. & Ryan, J. B. 1988. Bovine Spongiform Encephalopathy: Epidemiological Studies. *Veterinary Record,* **123,** 638-644.

Williams, A., Lucassen, P. J., Ritchie, D. & Bruce, M. 1997. Prp Deposition, Microglial Activation, and Neuronal Apoptosis in Murine Scrapie. *Experimental Neurology,* **144,** 433-438.

Williams, A. E., Lawson, L. J., Perry, V. H. & Fraser, H. 1994. Characterization of the Microglial Response in Murine Scrapie. *Neuropathology and Applied Neurobiology,* **20,** 47-55.

Williams, A. E., Ryder, S. & Blakemore, W. F. 1995. Monocyte Recruitment into the Scrapie-Affected Brain. *Acta Neuropathologica,* **90,** 164-169.

Williams, E. S. & Young, S. 1980. Chronic Wasting Disease of Captive Mule Deer: A Spongiform Encephalopathy. *Journal of Wildlife Diseases,* **16,** 89-98.

Wong, C. H., Abeynaike, L. D., Crack, P. J. & Hickey, M. J. 2011. Divergent Roles of Glutathione Peroxidase-1 (Gpx1) in Regulation of Leukocyte-Endothelial Cell Interactions in the Inflamed Cerebral Microvasculature. *Microcirculation,* **18,** 12-23.

Wu, C., Orozco, C., Boyer, J., Leglise, M., Goodale, J., Batalov, S., Hodge, C. L., Haase, J., Janes, J., Huss, J. W., 3rd & Su, A. I. 2009. Biogps: An Extensible and Customizable Portal for Querying and Organizing Gene Annotation Resources. *Genome Biology,* **10,** 2009-2010.

Wu, D. C., Teismann, P., Tieu, K., Vila, M., Jackson-Lewis, V., Ischiropoulos, H. & Przedborski, S. 2003. Nadph Oxidase Mediates Oxidative Stress in the 1-Methyl-4-Phenyl-1,2,3,6-Tetrahydropyridine Model of Parkinson's Disease. *Proceedings of the National Academy of Sciences of the United States of America,* **100,** 6145-6150.

Wu, J., Yang, S., Luo, H., Zeng, L., Ye, L. & Lu, Y. 2006. Quantitative Evaluation of Monocyte Transmigration into the Brain Following Chemical Opening of the Blood-Brain Barrier in Mice. *Brain Research,* **1098,** 79-85.

Wynn, R. F., Wraith, J. E., Mercer, J., O'Meara, A., Tylee, K., Thornley, M., Church, H. J. & Bigger, B. W. 2009. Improved Metabolic Correction in Patients with Lysosomal Storage Disease Treated with Hematopoietic Stem Cell Transplant Compared with Enzyme Replacement Therapy. *Journal of Pediatrics,* **154,** 609-611.

Wynne, A. M., Henry, C. J., Huang, Y., Cleland, A. & Godbout, J. P. 2010. Protracted Downregulation of Cx3cr1 on Microglia of Aged Mice after Lipopolysaccharide Challenge. *Brain, Behavior, and Immunity,* **24,** 1190-1201.

Xiang, W., Hummel, M., Mitteregger, G., Pace, C., Windl, O., Mansmann, U. & Kretzschmar, H. A. 2007. Transcriptome Analysis Reveals Altered Cholesterol Metabolism During the Neurodegeneration in Mouse Scrapie Model. *Journal of Neurochemistry,* **102,** 834-847.

Xiang, W., Windl, O., Wunsch, G., Dugas, M., Kohlmann, A., Dierkes, N., Westner, I. M. & Kretzschmar, H. A. 2004. Identification of Differentially Expressed Genes in Scrapie-Infected Mouse Brains by Using Global Gene Expression Technology. *Journal of Virology,* **78,** 11051-11060.

Xie, W. L., Shi, Q., Zhang, J., Zhang, B. Y., Gong, H. S., Guo, Y., Wang, S. B., Xu, Y., Wang, K., Chen, C., Liu, Y. & Dong, X. P. 2013. Abnormal Activation of Microglia Accompanied with Disrupted Cx3cr1/Cx3cl1 Pathway in the Brains of the Hamsters Infected with Scrapie Agent 263k. *Journal of Molecular Neuroscience,* **51,** 919-932.

Xu, Y., Tian, C., Wang, S. B., Xie, W. L., Guo, Y., Zhang, J., Shi, Q., Chen, C. & Dong, X. P. 2012. Activation of the Macroautophagic System in Scrapie-Infected Experimental Animals and Human Genetic Prion Diseases. *Autophagy,* **8,** 1604-1620.

Xue, L., Fletcher, G. C. & Tolkovsky, A. M. 1999. Autophagy Is Activated by Apoptotic Signalling in Sympathetic Neurons: An Alternative Mechanism of Death Execution. *Molecular and Cellular Neurosciences,* **14,** 180-198.

Yamada, A., Akimoto, H., Kagawa, S., Guillemin, G. J. & Takikawa, O. 2009. Proinflammatory Cytokine Interferon-Gamma Increases Induction of Indoleamine 2,3-Dioxygenase in Monocytic Cells Primed with Amyloid Beta Peptide 1-42: Implications for the Pathogenesis of Alzheimer's Disease. *Journal of Neurochemistry,* **110,** 791-800.

Yamada, J. & Jinno, S. 2013. Novel Objective Classification of Reactive Microglia Following Hypoglossal Axotomy Using Hierarchical Cluster Analysis. *Journal of Comparative Neurology,* **521,** 1184-1201.

Yamamoto, M., Sato, S., Hemmi, H., Hoshino, K., Kaisho, T., Sanjo, H., Takeuchi, O., Sugiyama, M., Okabe, M., Takeda, K. & Akira, S. 2003. Role of Adaptor Trif in the Myd88-Independent Toll-Like Receptor Signaling Pathway. *Science,* **301,** 640-643.

Zhang, B. & Horvath, S. 2005. A General Framework for Weighted Gene Co-Expression Network Analysis. *Statistical Applications in Genetics and Molecular Biology,* **4,** Article17.

Zhang, G., Bogdanova, N., Gao, T., Song, J. J., Cragg, M. S., Glennie, M. J. & Sheikh, K. A. 2014. Fcgamma Receptor-Mediated Inflammation Inhibits Axon Regeneration. *PloS One,* **9,** e88703.

Zhang, Y., McCartney, A. J., Zolov, S. N., Ferguson, C. J., Meisler, M. H., Sutton, M. A. & Weisman, L. S. 2012. Modulation of Synaptic Function by Vac14, a Protein That Regulates the Phosphoinositides Pi(3,5)P(2) and Pi(5)P. *EMBO Journal,* **31,** 3442-3456.

Zharkikh, A. & Li, W. H. 1995. Estimation of Confidence in Phylogeny: The Complete-and-Partial Bootstrap Technique. *Molecular Phylogenetics and Evolution,* **4,** 44-63.

Zhou, X. M., Xu, G. X. & Zhao, D. M. 2008. In Vitro Effect of Prion Peptide Prp 106-126 on Mouse Macrophages: Possible Role of Macrophages in Transport and Proliferation for Prion Protein. *Microbial Pathogenesis,* **44,** 129-134.

Zhu, P., Hata, R., Cao, F., Gu, F., Hanakawa, Y., Hashimoto, K. & Sakanaka, M. 2008. Ramified Microglial Cells Promote Astrogliogenesis and Maintenance of Neural Stem Cells through Activation of Stat3 Function. *FASEB Journal,* **22,** 3866-3877.

Zlotnik, A. & Spittau, B. 2014. Gdnf Fails to Inhibit Lps-Mediated Activation of Mouse Microglia. *Journal of Neuroimmunology,* **270,** 22-28.

Zlotnik, I. & Rennie, J. C. 1962. The Pathology of the Brain of Mice Inoculated with Tissues from Scrapie Sheep. *Journal of Comparative Pathology,* **72,** 360-365.

Zlotnik, I. & Rennie, J. C. 1963. Further Observations on the Experimental Transmission of Scrapie from Sheep and Goats to Laboratory Mice. *Journal of Comparative Pathology,* **73,** 150-162.

Zlotnik, I. & Rennie, J. C. 1965. Experimental Transmission of Mouse Passaged Scrapie to Goats, Sheep, Rats and Hamsters. *Journal of Comparative Pathology,* **75,** 147-157.

8 Appendices

Appendix 8-1

Appendix 8-1: Origins of Scrapie. Scrapie is a notifiable disease and requires the Animal and Plant Health Agency to be made aware of any animal suspected of being infected. As the disease is infectious and there is no cure a positive identification of Scrapie invariably leads to euthanasia of the infected animal. Genetic screening of sheep made it possible to identify the genotypes most susceptible to infection. European schemes were put in place from 2001 with the aim of significantly reducing the presence of the disease within the national flocks (European Commission, 2003).

Prior to the application of breeding programs, action to disease was taken *post-hoc* in an effort to identify patterns in susceptibility. The result was a considerable period of time in which the disease was considered as nothing more than a singular event. The infection of sheep with the deceptive 'itching' disease, in which sheep rub themselves raw against their enclosure, had been documented in Europe for many centuries. The name 'Scrapie', an adaptation of the Scottish word for scratching, was first attributed to a flock of cross-bred Cheviot and Leicester sheep in a farm near Yetholm within the Scottish Borders in 1853 (Stockman, 1913). This also led to the hypothesis that transmission was vertical from ewe to progeny. The symptoms of sheep with Scrapie-like nervous disorders are claimed to have been recorded even earlier circa 1732 (M'Gowan, 1918) however the descriptions were vague and there were many other diseases of sheep present in Eighteenth century Britain for which the visual symptoms were similar. Indeed the disease, then more widely known in the field as 'Goggles' or 'Rickets' was so little regarded by the British authorities that flock owners could only respond to and not influence the literature of the time (Comber, 1772, Cruttwell, 1795). By contrast the disease was well characterised by the German authorities during the mid-Eighteenth century as 'Trot' and accepted as a horizontally contagious and invariably fatal wasting disease (Figure 1-6).

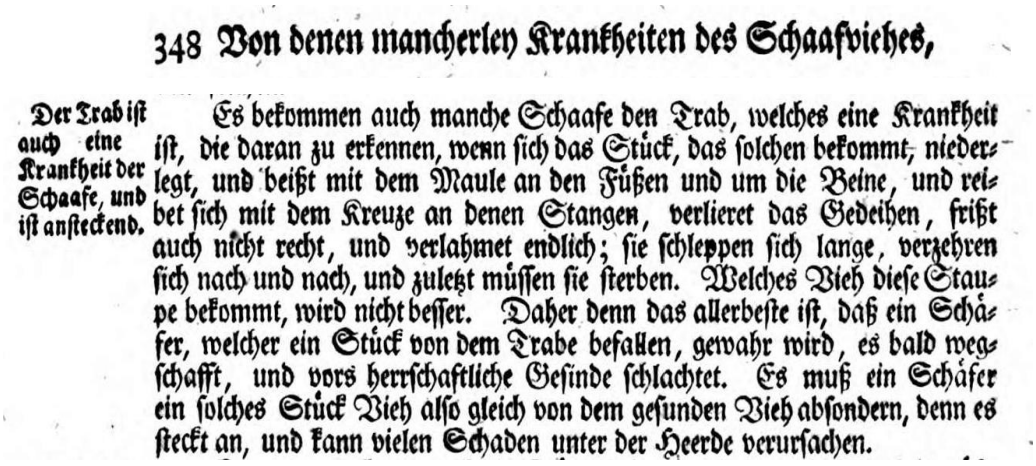

348 Von denen mancherley Krankheiten des Schaafviehes,

Der Trab iſt auch eine Krankheit der Schaafe, und iſt anſteckend.

Es bekommen auch manche Schaafe den Trab, welches eine Krankheit iſt, die daran zu erkennen, wenn ſich das Stück, das ſolchen bekommt, niederlegt, und beißt mit dem Maule an den Füßen und um die Beine, und reibet ſich mit dem Kreuze an denen Stangen, verlieret das Gedeihen, frißt auch nicht recht, und verlahmet endlich; ſie ſchleppen ſich lange, verzehren ſich nach und nach, und zuletzt müſſen ſie ſterben. Welches Vieh dieſe Staupe bekommt, wird nicht beſſer. Daher denn das allerbeſte iſt, daß ein Schäfer, welcher ein Stück von dem Trabe befallen, gewahr wird, es bald wegſchafft, und vors herrſchaftliche Geſinde ſchlachtet. Es muß ein Schäfer ein ſolches Stück Vieh alſo gleich von dem geſunden Vieh abſondern, denn es ſteckt an, und kann vielen Schaden unter der Heerde verurſachen.

Figure 8-1: The first true characterisation of Scrapie can be found in German agricultural literature from 1759 (Leopold, 1759). This extract from the section on diseases of sheep describes both topical and nervous symptoms and recognises the dangers of the transmissible nature of the disease to healthy members of the flock. The volume in which the extract is found is a highly comprehensive guideline for agriculture in the country including land sustainability and the effects of economy. The complete translation for the extract is:

"Of the various Diseases of Sheep, Scrapie is a disease of sheep and is contagious. Scrapie in sheep is* a *disease that can be recognised when the animal that gets the diseases lays down, bites with its mouth* on the *feet and the legs, rubs with the crossbars on* the *enclosure, will lose prosperity, also does not eat right, and finally*; *they drag themselves* along, *gradually lose weight, and at last they invariably die. When an animal gets this distemper, there is no cure. Therefore it is best for the shepherd who sees one of his sheep has fallen to Scrapie, to carry it away for slaughter by non-stately servants. The shepherd must take steps to separate such a case from the healthy, because it is contagious and can cause much harm to the flock"*

*The disease was named 'Trab' in Germany at that time and literally translates to 'Trot' in English.

Ideas were consolidated in the early twentieth century when it was realised that little experimental evidence had been accumulated, incorrect conclusions had been drawn from narrow-minded (*sic*) laboratory observations and there was little regard for the reports made by farmers (M'Fadyean, 1918). A new set of veterinary scientists reviewed the field and realised the disease had an exceptionally long incubation

period and was past-down from the mother; as exemplified by lambs from an infected ewe which would still develop Scrapie even when moved to a new environment days after birth (Stockman, 1926). Post-mortem analysis, principally led by Sir Stewart Stockman (Lancet, 1926) began to piece together the association between Scrapie and nervous tissue damage (Stockman, 1926, Holman and Pattison, 1943). Beginning in the late 1930s, flock analysis studies in Britain finally caught up with what was already known in Germany and documented the horizontal transmissibility of Scrapie infection between unrelated sheep (Gordon *et al.*, 1940, Greig, 1940) and from sheep to goats (Chelle, 1942, Pattison *et al.*, 1959, Pattison and Millson, 1961, Brotherston *et al.*, 1968).

Appendix 8-2

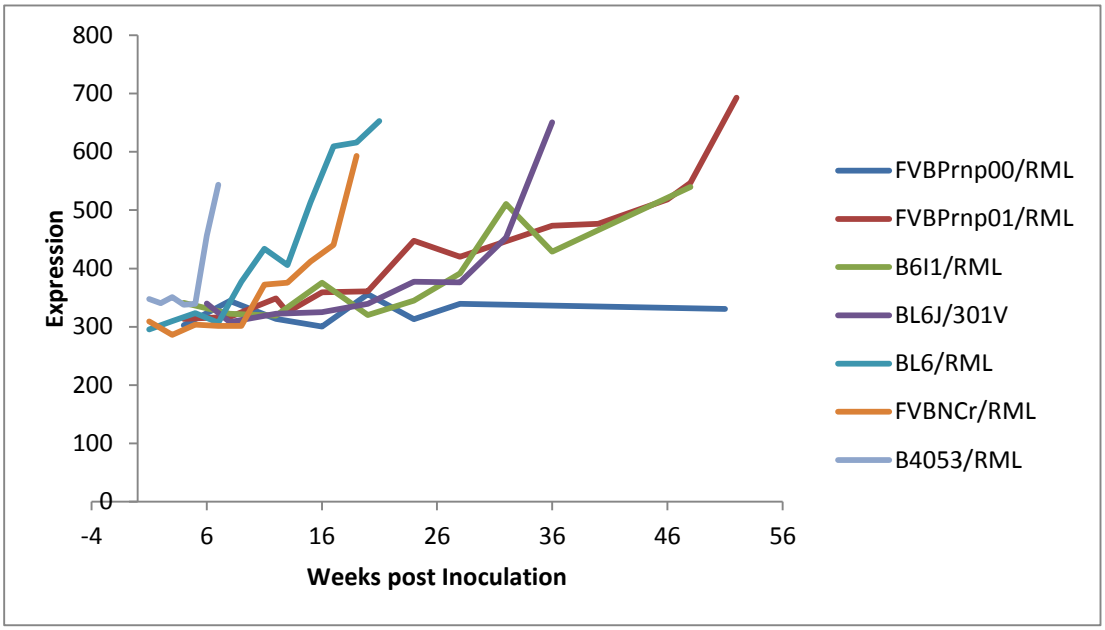

Appendix 8-2: Robust prion disease associated signal in all strains encoded PrP^{C}. The mean expression profile from the 492 disease associated genes identified in this study is very similar in all strains despite pronounced differences in incubation period. A lack of disease in FVB^{PrnP00} null mice serves as confirmation that the signature in all other strains is associated with infection.

Appendix 8-3

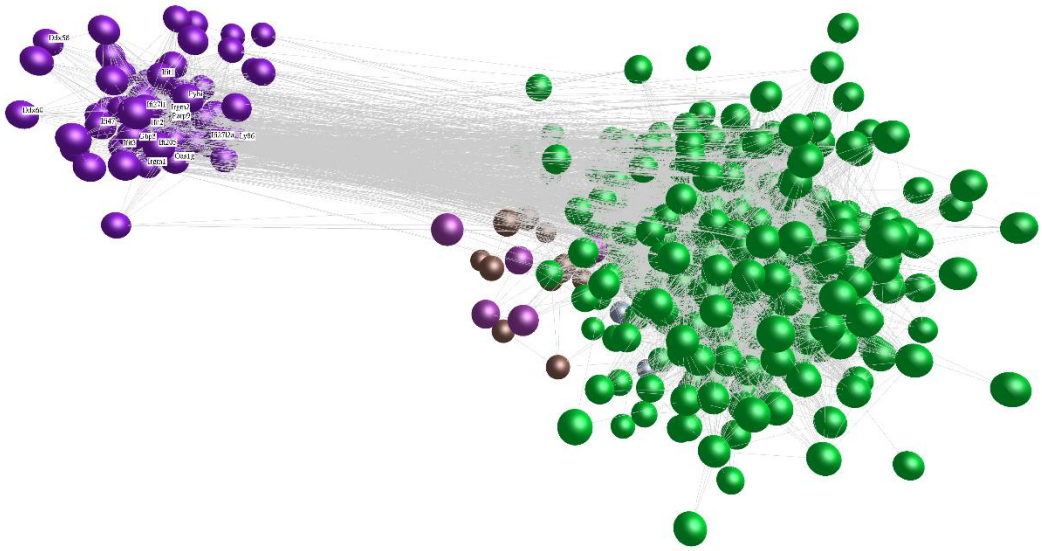

Appendix 8-3: Clusters demonstrate a high level of inter-correlation. The secondary cluster (purple) contains a significant number of interferon response genes. The considerable number of co-expressed (edge linked) genes both within the same cluster and residing in the opposite cluster are evidence of a complex tightly regulated mechanism. Increasing the matrix threshold within BioLayout Express did not allow for further separation of the graph into components indicating the dataset is inseparable using this type of whole brain analysis.

Appendix 8-4

Appendix 8-4: Ontological data for the 492 disease associated genes found in this experiment organised into cell types. Those identified in the original study are highlighted in red. Note that the majority of the red highlighted genes were not associated in the original study with the cell types portrayed here.

Cell Type	Number	Genes
Macrophage Only	315	4632428N05Rik, A830007P12Rik, AA467197, Abi3, Adcy7, Adfp, AF251705, Aif1, Alox5ap, Anxa2, Anxa3, Anxa4, Arhgdib, Arpc1b, Aspg, Axl, B2m, Bcl2a1a, Bcl3, Brd4, C1qa, C1qb, C1qc, C3, C3ar1, C4b, Capg, Casp1, Casp8, Ccl12, Ccl2, Ccl3, Ccl5, Ccl6, Ccl8, Ccl9, Ccr5, Cd14, Cd37, Cd44, Cd48, Cd52, Cd53, Cd68, Cd72, Cd74, Cd84, Cd86, Cebpa, Cebpb, Ch25h, Clec4a3, Clec7a, Clic1, Cln3, Cmtm3, Cmtm6, Cmtm7, Cp, Crispld2, Csf1, Csf1r, Csf2rb, Csf3r, Cst7, Cstb, Ctsa, Ctsb, Ctsc, Ctsd, Ctsh, Ctsl, Ctss, Ctsz, Cxcl10, Cxcl13, Cxcl16, Cyba, Cybb, Ddx58, Ddx60, Dock2, Dtx3l, Ebi3, Edem1, EG667823 (Trim5), Emr1, Epsti1, Fas, Fcer1g, Fcgr1, Fcgr2b, Fcgr3, Fcgr4, Fcrls, Fermt3, Fgd2, Ftl1, Ftl2, Fuca1, Fxyd5, Fyb, Galnt6, Gbp2, Gbp3, Ggta1, Glipr1, Gmfg, Gngt2, Gns, Gpnmb, Gpr183, Gpr34, Gpr65, Gpr84, Gpsm3, Grn, Gusb, H2-Ab1, H2-DMb2, H2-K1, H2-M3, H2-Q7, Havcr2, Hck, Hcls1, Hexa, Hexb, Hfe, Hmox1, Hpgd, Hsd3b7, Hvcn1, Icam1, Ifi204, Ifi205, Ifi27l2a, Ifi30, Ifi35, Ifi44, Ifi47, Ifih1, Ifit1, Ifit2, Ifit3, Ifitm3, Igtp, Iigp1, Ikzf1, Il10rb, Il13ra1, Inpp5d, Irf5, Irf7, Irf8, Irf9, Irgm1, Irgm2, Itgam, Itgax, Itgb2, Itpripl2, Kcnk6, Lag3, Lair1, Lamp2, Laptm5, Lat2, Lcp1, Lcp2, Lgals3bp, Lgals9, Lgmn, Lilrb4, Lpcat2, Lpxn, Lrrc33, Lst1, Ltbr, Ly9, Lyn, Mafb, Man2b1, Man2b2, Mdfic, Mmp12, Mpa2l, Mpeg1, Ms4a6b, Ms4a6d, Ms4a7, Msn, Myd88, Myo1f, Naglu, Naip2, Naip5, Ncf1, Ncf2, Ncf4, Nckap1l, Nek6, Nfe2l2, Nlrc5, Oas1g, Oasl2, OTTMUSG00000000971, P2ry13, P2ry6, Parp12, Parp14, Parp3, Parp9, Phf20l1, Pld4, Plec1, Plek, Plp2, Plxnb2, Pon3, Pros1, Psmb8, Psmb9, Psme1, Psme2, Ptgds2, Ptplad2, Ptpn18, Ptpn6, Ptprc, Pycard, Pyhin1, Rab32, Rab3il1, Renbp, Rmcs5, Rnase4, Rnaset2a, Rnf213, Rrad, Rsad2, Rtp4, S100a11, S100a4, S100a6, S1pr3, Samd9l, Samsn1, Sash3, Scpep1, Selplg, Sema4d, Sepx1, Sfpi1, Sgpl1, Sh3bp2, Shisa5, Siglec5, Siglech, Skap2, Slamf9, Slc11a1, Slc15a3, Slc29a3, Slc39a14, Slc43a3, Slc5a3, Slc7a7, Slfn2, Slfn8, Socs3, Spp1, Sqrdl, Srgn, Stat1, Stat3, Sulf2, Syngr2, Tagln2, Tap2, Tapbp, Tbxas1, Tcn2, Tgfb1, Tgfbr1, Tgfbr2, Tgif1, Tgm2, Thbs2, Tifa, Timp1, Timp2, Tln1, Tlr1, Tlr13, Tlr2, Tm4sf1, Tmem119, Tmem173, Tmem86a, Tnfaip2, Tnfaip8l2, Tnfrsf1a, Tor3a, Trem2, Trim25, Trim30, Trim34, Trim47, Trpt1, Tspo, Tyrobp, Ube1l, Unc93b1, Usp18, Vwa5a, Xaf1
Macrophage & Neuron	7	A2m, Cyb5r3, Glipr2, Gpx1, Lgals1, Lgals3, Olfml3
Astrocyte Only	19	Abhd4, Aldh1l1, Aqp4, Casp12, Chi3l1, Cyp4f14, Decr1, Fgfrl1, Gal3st4, Gm967, Id3, Naprt1, Plcd4, Plscr2, Prelp, Prrx2, Rbp1, Slc25a18, Sox9
Neuron Only	4	Aldh1l2, Hspb8, Sema3d, Serping1

Astrocyte & Neuron	11	Ccdc122, Fxyd1, Kcne1l, Lgi4, Lmcd1, Mlc1, S100a16, Slc14a1, Thbs3, Tsc22d4, Vwa1
Macrophage, Neuron and Astrocyte	27	Cd81, Cotl1, Cyp4v3, Dbi, Ifi27l1, Igfbp2, Itgb5, Ltc4s, Mt1, Mt2, Necap2, Npc2, Oat, Pdlim4, Rab31, Rab7l1, Rhbdf1, Rhoc, S100a13, Sh3glb1, Tmbim1, Tmem176a, Tmem176b, Tspan4, Ucp2, Vamp8, Vim
Macrophage & Astrocyte	28	Cd151, Clec5a, Cybrd1, Dhrs1, Efemp2, Eya4, Galnt4, Gfap, Gstm1, Klk8, Lpcat3, Ly86, Mtmr11, Npl, Nupr1, Pbxip1, Pdpn, Pnpla7, Prdx6, Retsat, S100a1, Sat1, Sh3pxd2b, Tlr3, Trf, Upp1, Vcam1, Zfp91
Oligodendrocyte	8	Tppp3, Tmem98, Pdlim2, Klk6, Galntl2, Dbndd2, Apod, Adamtsl4,
Genric (All CNS cell types)	73	Znrf2, Tax1bp3, Srebf1, Spsb1, Spata13, Slco2b1, Scrg1, Scamp2, Rgs10, Pik3ap1, Phyhd1, Palld, P2rx7, Osmr, Nat2, Mrps6, Lyz2, Lyz1, Lrrfip1, Litaf, Klhl6, Itpkb, Il33, Igsf6, Igf1, Ifitm2, Idh2, Hspb6, H2-DMb1, H2-Aa, Gpr37l1, Golm1, Gbp6, Gba, Fzd9, Fkbp7, Fes, Farp1, Fam129b, Fam102a, F13a1, Ephx1, Entpd1, Emp3, Emp1, Ecm1, E230029C05Rik, Dok1, Ddr1, Dap, D4Ertd22e, Cyth4, Cyp7b1, Cst3, Col16a1, Cnn3, Clu, Cklf, Cebpd, Cd9, Ccdc80, Capn3, Bmp2k, Bdh2, BC026585, Avp, Atp6v0e, Angpt1, Ampd3, Aga, Afp, 5430427O19Rik, 1700112E06Rik
Total:	492	

Appendix 8-5

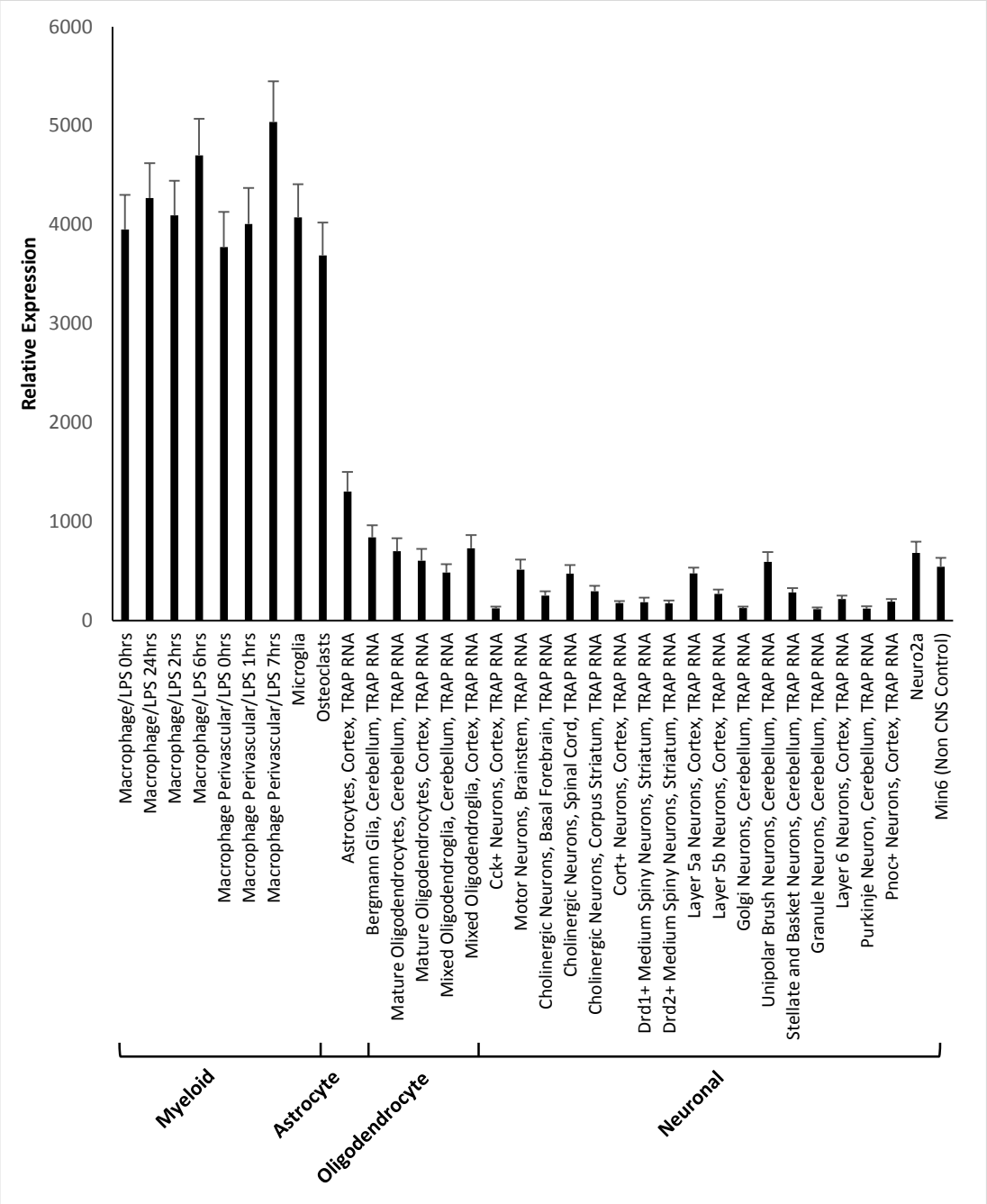

Appendix 8-5: Cross reference of the 333 genes identified in the original study by Hwang et al., (2009) with co-normalised GNFv3, Trap and M0/LPS data within the expression viewer of BioLayout Express3D. Although an immune response was described in the original publication, the majority of differentially expressed genes were attributed to neurons. This figure illustrates clearly the dominant myeloid origin following overlay with brain specific cell populations. Error bars equate to standard error.

Appendix 8-6

Appendix 8-6: The BALB/cJ strain of mouse was first developed in 1912 at The Memorial Hospital, New York by Dr. Halsey J. Bagg using albino fancy mouse stock obtained from a mouse dealer in Ohio. Control was transferred in 1920 to Dr. C. Little and Dr. E.C. MacDowell at the Carnegie Institution of Washington in Cold Spring Harbor, New York. Inbred status was achieved in 1923 reaching filial generation (F) 12 in 1927 (Macdowell *et al.*, 1927). The newly inbred strain was characterised by Dr. Little and Clyde E. Keeler and found to have albino linked retinal degeneration (Keeler, 1924, Keeler, 1931). It was at Cold Spring Harbor that the Bagg strain also led to the development of the "A" (or A/J) strain of mice widely used in cancer and immunology research following a cross with the Cold Spring Harbor albino line in 1921 (Strong, 1936, Stoner *et al.*, 1993).

A breeding sample of the Bagg albino was acquired by Dr. Hermann Joseph Muller at the University of Texas and cared for by Dr George Davis Snell who subsequently maintained the line (Russell, 1978, Potter, 1985). A breeding sample of mice at F26 was taken by Dr George Davis Snell to the Jackson's laboratory in 1935 (Russell, 1978, Snell, 1978). At this point the line was named "Balb" derived from a shortening of Bagg Albino and given the /c substrain designation by Dr Snell to indicate that the genotype at the "colour" locus was c/c (Potter, 1985). The name was formally capitalized in 1940 to "BALB/c" as required by the Committee on 'Standardized Nomenclature for Inbred Strain of Mice' to distinguish between name and mutation characters (Dunn *et al.*, 1940, Snell, 1941).

Dr. Snell gave a breeding colony to Dr. John Paul Scott in 1945 who maintained these mice in The Jackson Laboratory behavioural unit in Hamilton Station, New Jersey. It was this group of mice, at F41, that were used to continue the line following the 1947 Bar Harbor fire which devastated The Jackson Laboratory's main buildings. In 1974 at F136, The Jackson Laboratory attached the /cJ designation to indicate both substrain and laboratory code and supplied the mice to Charles River where the line has since been maintained globally.

Appendix 8-7

Appendix 8-7: The Origin of the mouse-adapted prion strains used in this project. 79A is a Scrapie strain purified by limiting dilutions (cloned) from an SSBP/1 infected goat source into C57BL mice at Compton in 1961. From the same source were derived 139A, 79V and RML. The latter is not a cloned strain but an isolate comprising 79A which can, dependent upon the host, mutate into 139A (Dickinson, 1976). ME7 is derived from a naturally occurring Scrapie case of Suffolk sheep transmitted into C57BL and VM mice at Moredon in 1963. ME7 is not isolated from sources derived from SSBP/1 (Zlotnik and Rennie, 1965) and consequently is unrelated to 79A.

Strain	Origin
79A/V **139A** **RML**	• **Drowsy Goat Scrapie** • Isolated from goats infected with SSBP/1 at Compton (Holman and Pattison, 1943, Pattison, 1957). • Gave rise to Chandler Strain in mice/rat/hamster (Pattison and Millson, 1961) • 3rd pass donated to Rocky Mountain Laboratories as the RML isolate • 21-25th pass transmitted into C57BL – 139A • Drowsy goat source into C57BL gave 79A. VM gave 79V • 4th Chandler hamster pass gave 263K
ME7	• **Suffolk Sheep Scrapie**. • Can be extracted directly. • Transmission made to mice: **M**ouse **E**xperiment **7** at Moredun (Zlotnik and Rennie, 1962, Zlotnik and Rennie, 1963).

Appendix 8-8

Appendix 8-8: Cultured microglia-like cell lines display variance in persistence of infection dependent upon prion strain. A series of *in-vitro* experiments, performed within the Neurobiology Division, The Roslin Institute, suggested killing of neurons is increased in the presence of a prion infected "Scrapie Mouse Brain" (SMB) microglia-like cell line; first isolated and characterised by Haig and Clarke (1971). The *in-vitro* concept of increased neuronal death in the presence of microglia was first published by Bate *et al.* (2004). The unpublished experiments performed in The Roslin Institute were performed in an attempt to further this *in-vitro* work *using* neurons able and unable to express PrP^{C}, thereby confirming that neurotoxicity is neuronal PrP^{C} independent and cell death is instead mediated through a pro-inflammatory cytokine bystander effect. As part of this work SMB cells were infected with a number of different prion strains and demonstrated variability in persistence of infection.

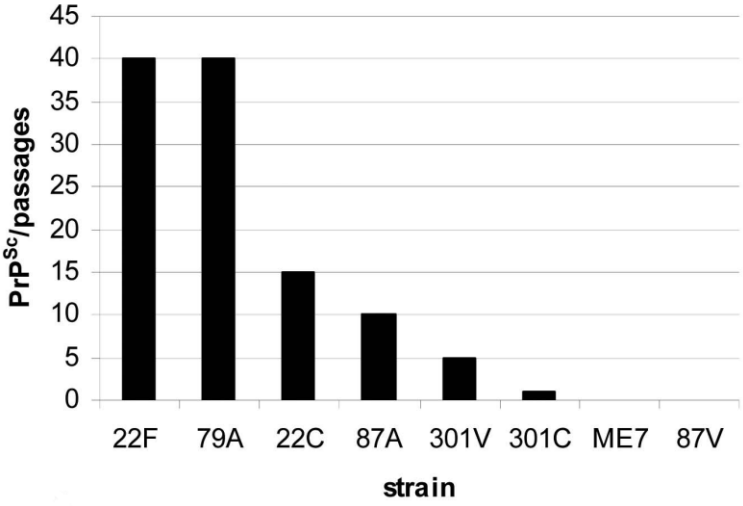

Variability in capacity of differing prion strains to persistently infect cultured SMB microglia-like cell line across multiple passages. Data from 22F passages are from Birkett et al. (2001) the remaining from unpublished work by Dr E Cancellotti, The Roslin Institute & R(D)SVS. Confirmation of infectivity was confirmed with culture filter development with 6H4 or IA8 anti-PrP antibody.

Appendix 8-9

Appendix 8-9: Incubation periods from historic records of wild type mouse strains. Data published by Outram (1976) comprising infection studies of over 4000 mice both i.c. or i.p. with 0.02ml of 10^{-2} w/v infected brain material reveals the incubation periods for 79A into BALB/cJ mice have remained unchanged as per the data sourced (Appendix 8-12) from the Neurobiology Division archives (The Roslin Institute & R(D)SVS, The University of Edinburgh). It is unclear if the sourced archive experimental data was included by Outram who at the time was working in Edinburgh. BALB/cJ mice i.p. infected with ME7 revealed a mixed gender average of 261 days. Incubation periods for BALB/cJ$^{Fms\text{-}EGFP/-}$ and BALB/cJ challenged i.p. with ME7 succumbed in an unexpected average of 313.5 days. * demotes S.E > 2.5 % of the incubation period.

Injection route:	i.c.						i.p.			
Agent group:	22A	ME7					22A	ME7		
Agent:	22A	ME7	79A	22C	58A	87A	22A	ME7	79A	22C
C57BL ♀	453	159	152	177	152	342	601	239	201	234
♂	470	162	157	182	167	351	593	238	207	225
RIII	429	167	136	166		360		248	189	
	432	164	140	175		404*		247	195	
BALB/c	470	172	161	185				266	227	267
	470	169	166	198				256*	232	272

Appendix 8-10

Appendix 8-10: Source of Prion Infected Brain Material used in the BALB/cJ$^{Fms\text{-}EGFP/-}$ and BALB/cJ infections. Brain homogenates (10^{-2} w/v) used in these experiments were produced from the pooling of two frozen brains dissected from C57Bl/6J mice previously infected by intracerebral challenge and taken to terminal. Mice used for normal brain homogenate (10^{-2} w/v) were also from a C57Bl/6J source.

Source Exp. ID	Mouse Strain	Infectious Agent	Animal ID	Gender	Infection Route	Incubation Period	Target Exp.
79A-13Z	C57Bl/6J	79A	B53873	♂	i.c.	176	816A-1A1
79A-13Z	C57Bl/6J	79A	B53874	♂	i.c.	176	816A-1A1
135X-10Z	C57Bl/6J	ME7	B54120	♀	i.c.	166	816B-1A1
135X-10Z	C57Bl/6J	ME7	B54104	♀	i.c.	171	816B-1A1
79A-13Z	C57Bl/6J	79A	B53813	♂	i.c.	162	816D-1A1/1B1
79A-13Z	C57Bl/6J	79A	B53872	♂	i.c.	176	816D-1A1/1B1

Appendix 8-11

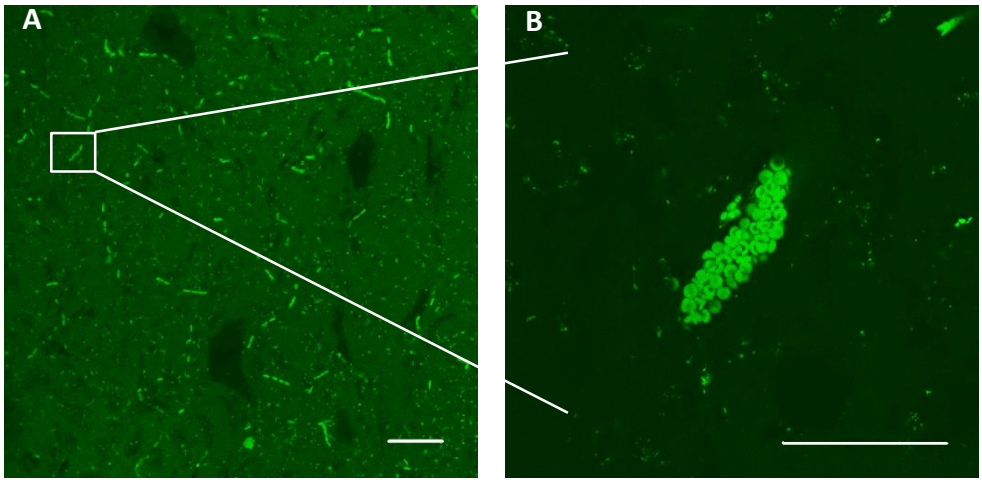

Appendix 8-11: Intense auto fluorescence from blood artefacts severely limited EGFP detection in mouse brain tissue of mice not subjected to saline perfusion. **A:** Auto-fluorescence was detectable in brain as vascular structures containing **B**: non-*Fms-EGFP* expressing (no nuclei) erythrocytes. Scale bars equate to 50 µm.

Appendix 8-12

Appendix 8-12: Historic 79A experiments documented in the Neurobiology Division archives (The Roslin Institute & R(D)SVS, The University of Edinburgh) utilising BALB/cJ mice infected i.p. with 79A mouse-adapted Scrapie at 0.02ml of 10^{-2} w/v. Experiments 816A-1A1 and 816B-1A1 are those documented in this chapter. 521Z-1G is a recently performed aging study using CB20+/+ (congenic BALB/cJ) with a comparable starting age. The remaining 8 experiments were all completed prior to 1975 and show only the control mice infected with 79A alongside further groups with an additional tested variable that rules out their inclusion here. Lesion profiles were constructed using grey matter data from experiments in which lesion scoring information was available. Incubation periods and regional targeting of lesions were similar in all experiments although the superior colliculus does present with some variability. These data show the considerable lack of variation in both the BALB/cJ and 79A stains over a 40 year period. † Experiments documented in this study. * Age at point of inoculation.

Experiment ID	Group Size	Mouse Strain	Incubation Period (days)	SE	Age at Infection (days)
816A-1A1†	9	BALB/cJ$^{Fms\text{-}EGFP/-}$	225	6.3	100
816B-1A1†	8	BALB/cJ	227.9	6.5	100
110A-1A	5	BALB/cJ	235.6	1	28-98
99K-1C	3	BALB/cJ	235	0	21-252
134A-1F	6	BALB/cJ	234.5	4.3	91
134A-1F	6	BALB/cJ	240.7	5.9	51-70
107B-1G	2	BALB/cJ	235	3	49-56
107A-1T	9	BALB/cJ	217.3	1.1	21-168
107A-1D	2	BALB/cJ	236.5	11.5	28-70
107C-1E	5	BALB/cJ	223	5.9	32-42
521Z-1G	12	CB20	260.4	3.4	100

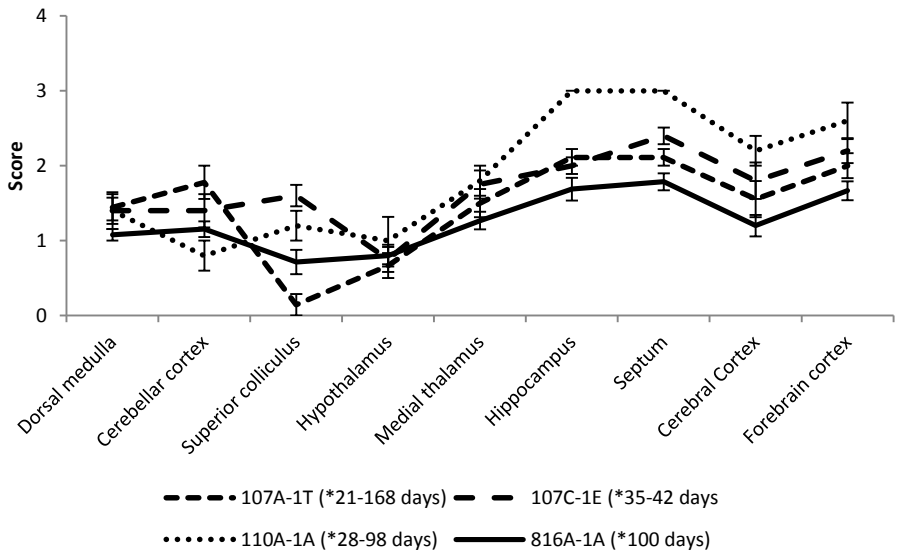

Appendix 8-13

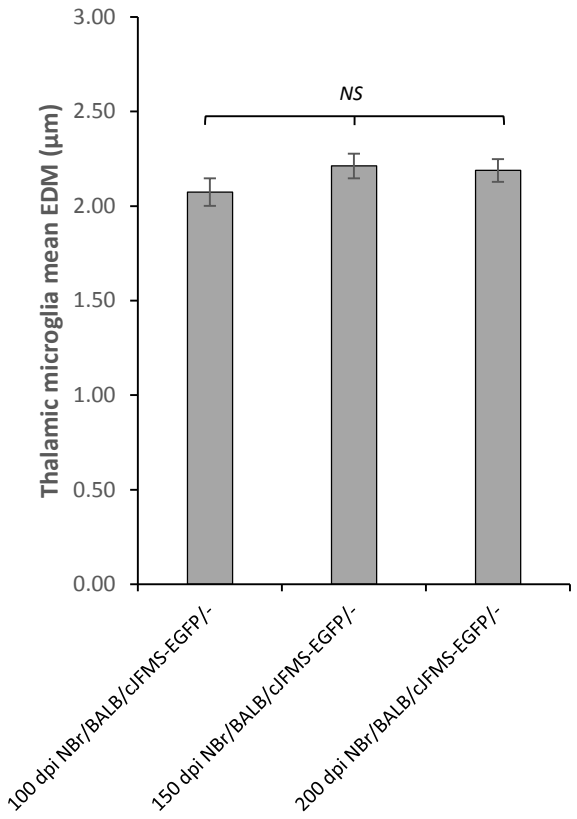

Appendix 8-13: Mean Euclidean distance of thalamic microglia from healthy normal brain inoculated BALB/cJ$^{Fms\text{-}EGFP/-}$ mice. No statistical difference was gained between any tested combinations for these data. Consequently the adoption of a mean value is not a cause of the significant difference observed between the mean value of these data and that gained from 100 and 150 dpi thalamic microglia in 79A infected animals.

Appendix 8-14

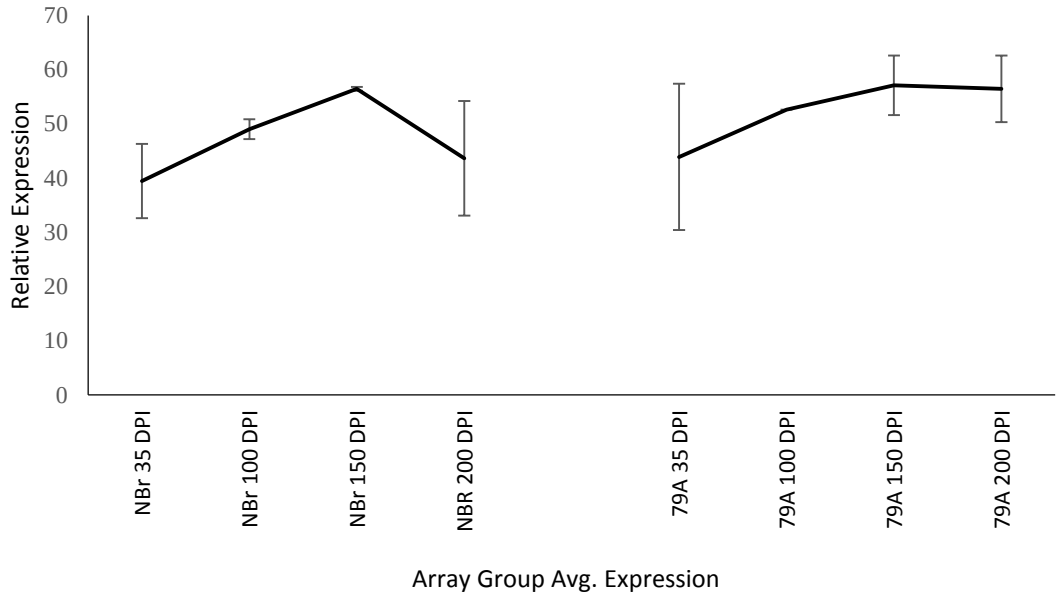

Appendix 8-14: Expression profile of *Myd88*. Rapidly induced during an innate immune response to antigen, the expression levels of Myd88 in this study remain nominal and unchanged in response to disease.